

# TECHNICAL SUPPORT PACKAGE

*for*

TECH BRIEF 68-10528

POROUS IONIZER MATERIALS



*Technology Utilization Division*  
OFFICE OF TECHNOLOGY UTILIZATION  
NATIONAL AERONAUTICS AND SPACE ADMINISTRATION  
*Washington, D.C.*

**NOTICE:** This document was prepared under the sponsorship of the National Aeronautics and Space Administration. Neither the United States Government nor any person acting on behalf of the United States Government assumes any liability resulting from the use of the information contained in this document, or warrants that such use will be free from privately owned rights.

*For Further Information Contact*

**Technology Utilization Office ● Lewis Research Center  
21000 Brookpark Road, Cleveland, Ohio 44135**

---

**For sale by the Clearinghouse for Federal Scientific and Technical Information  
Springfield, Virginia 22151 – CFSTI price \$3.00**

## POROUS IONIZER MATERIALS

### TECHNICAL SUPPORT PACKAGE FOR NASA TECH BRIEF 68-10528

This document describes research conducted to develop techniques for producing composite ionizers of tungsten-tantalum, tungsten-rhenium, and a combination of all three; develop ionizers containing void fractions in excess of 30 percent; testing of materials and processes to evaluate best methods for producing large ionizer bars; and to fabricate and deliver 8 ionizer bars. Fine angular tungsten with Cu flake and Bn particle ionizers were also tested. Ionizers of the first type have reached the development stage; the tungsten, Cu and Bn combination represents a major breakthrough in the state-of-the-art.

Several methods were used to determine particle size of the powders combined with the tungsten and it was concluded that accurate determination is beyond current technology (see Chapter 2, 2-7). The blending of powders was done by motaring, ball milling, or liquid blending. Ball milling was performed both dry and in liquid (benzene) slurry. Liquid blending was done in a standard household unit, using benzyl alcohol as the suspension vehicle and the forces of liquid shear to obtain dispersion of powder agglomerates.

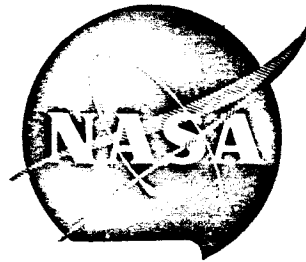
The information in the Technical Support Package comprises the documentation announced in NASA Tech Brief 68-10528, and is provided under the Technology Utilization Program of the National Aeronautics and Space Administration to make available the results of aerospace-related developments considered to have wider technological, scientific or commercial applications. This study derives from NASA's Lewis Research Center. Contract development was carried out by M. LaChance, H. Todd, K. Butler, B. Thompson, and G. Kuskevics of Electro Optical Systems, Inc., a subsidiary of Xerox Corporation.

Additional information regarding porous ionizer materials may be found in Scientific and Technical Reports (STAR) which is a comprehensive abstracting and indexing journal covering worldwide report literature on the science and technology of space and aeronautics. STAR is available to the public on subscription from the Superintendent of Documents, U.S. Government Printing Office.

NASA CR-54707

EOS Report 6650

Summary - Part I



GPO PRICE \$ \_\_\_\_\_

CFSTI PRICE(S) \$ \_\_\_\_\_

Hard copy (HC) 3.75

Microfiche (MF) 1.25

ff 653 July 65

FACILITY FORM 802

N66 35050

(ACCESSION NUMBER)

224

(PAGES)

CR-54707

(NASA CR OR TMX OR AD NUMBER)

(THRU)

(CODE)

(CATEGORY)

## DEVELOPMENT AND TESTING OF POROUS IONIZER MATERIALS

by

M. LaChance, H. Todd, K. Butler, B. Thompson  
and G. Kuskevics

prepared for

NATIONAL AERONAUTICS AND SPACE ADMINISTRATION  
CONTRACT NAS3-7103

**E**  
  
**S**

**ELECTRO-OPTICAL SYSTEMS, INC.**

A Subsidiary of Xerox Corporation

300 N. HALSTEAD ST., PASADENA, CALIFORNIA



54  
NASA CR-54707  
EOS Report 6650  
Summary - Part I

SUMMARY REPORT - PART I

DEVELOPMENT AND TESTING OF POROUS  
IONIZER MATERIALS

by

M. LaChance, H. Todd, K. Butler, B. Thompson and G. Kuskevics

prepared for

NATIONAL AERONAUTICS AND SPACE ADMINISTRATION

September 1, 1966

CONTRACT NAS3-7103

Technical Management  
NASA Lewis Research Center  
Cleveland, Ohio 44135  
Spacecraft Technology Procurement Section  
T. J. Riley and D. L. Lockwood

ELECTRO-OPTICAL SYSTEMS, INC.  
A Subsidiary of Xerox Corp.  
300 North Halstead St., Pasadena, California

# ABSTRACT

35050

This report describes work on Contract NAS3-7103 from February 1965 through May 1966. An additional 7-month effort will be covered in Part II. Two principal types of porous tungsten ionizers were prepared from (1) fine W microspheres, with additions of fine angular Ta or Ta+Re particles, and (2) fine angular W, with additions of Cu flake and BN particles. Ta and BN were added to minimize structural changes in service and to increase useful ionizer life; nonreactive Cu flake was added to increase pore-to-solid ratio and provide desirable pore parameters, with subsequent Cu elimination. Ionizers of type (1) were characterized by relative densities > 70 percent, pore densities up to  $1.4 \times 10^7$ , and greatly extended service lifetimes; type (2) by relative densities < 70 percent, coarser pore structures, excellent thermal stability at 1600 to 1800°C, and economy of fabrication. Evaluation of type (1) ionizers containing iridium was limited to preliminary tests, in which Ir was demonstrated to promote grain growth and pore coarsening. Two W-5Ta-10Re ionizers had neutral fractions ~ 7 and 4X lower (at 5 and 20 mA/cm<sup>2</sup>, respectively) than pure spherical-base tungsten; an ionizer from the W-8Cu-2BN mixture exhibited neutral fractions ~ 13 and 5X lower than the pure-tungsten comparison material. These major reductions in neutral efflux are not directly attributed to the presence of the additive elements, but rather to their beneficial effects on pore parameters. While ionizers of type (1) have reached a development plateau, high-performance low-density ionizers of type (2) represent a major breakthrough having great promise.

## CONTENTS

1.	INTRODUCTION	1-1
2.	EXPERIMENTAL METALS, FABRICATION AND EVALUATION TECHNIQUES	2-1
2.1	Metals	2-1
2.1.1	Metal Source, Grade and Purity	2-1
2.1.2	Particle Size of Powdered Metal Constituents Tungsten Powders	2-1
2.2	Fabrication Techniques	2-7
2.2.1	Classification and Size Analysis of Powders	2-7
2.2.2	Blending of Powders	2-8
2.2.3	Loading of Powders	2-8
2.2.4	Compaction of Metal Powders	2-9
2.2.5	Vacuum Sintering	2-11
2.2.6	Infiltration of Ionizers	2-11
2.2.7	Machining of Infiltrated Ionizers	2-12
2.2.8	Removal of Infiltrant from Ionizers	2-13
2.3	Evaluation Techniques	2-13
2.3.1	Density	2-13
2.3.2	Nitrogen Permeability and Transmission Coefficient	2-14
2.3.3	Metallographic Preparation	2-17
2.3.4	Determination of Pore Parameters	2-17
2.3.5	Accelerated Life Testing	2-20
3.	IONIZERS MADE FROM FINE TUNGSTEN MICROSPHERES WITH ALLOY ADDITIONS OF FINE ANGULAR PARTICLES	3-1
3.1	Ionizers from Fine Ampro Tungsten Microspheres, With and Without Binary Additions of Ta, Re, and Ir	3-1
3.2	Ionizers from Three Size Fractions of Linde Tungsten Microspheres, With and Without Binary Addition of Ta	3-10

## CONTENTS (contd)

3.3	Ionizers from Fine Linde Tungsten Microspheres With Binary (Ta) and Ternary (Ta+Re) Additions	3-26
3.4	Delivery of Small Ionizer Samples to NASA-Lewis	3-32
4.	LOW-DENSITY IONIZERS MADE BY COPPER-FLAKE TECHNIQUE	4-1
4.1	Procedures and Results	4-2
4.2	Effect of Presintering Time on Densification and Pore Structure of Low-Density Ionizers	4-12
4.3	Low-Density Ionizers Stabilized by Addition of Boron Nitride	4-15
5.	ACCELERATED LIFE TESTING OF IONIZERS	5-1
6.	IONIZATION PERFORMANCE TESTING OF SELECTED COMPOSITIONS	6-1
6.1	Test Apparatus	6-1
6.1.1	The Vacuum System	6-1
6.1.2	Ion Source	6-3
6.1.3	Ion Collector	6-3
6.1.4	Neutral Detector	6-3
6.2	Test Procedure	6-6
6.3	Performance Indicator Definition	6-7
6.4	Performance of Ternary Alloy Ionizers	6-10
6.5	Performance of Low-Density Ionizers	6-18
7.	TECHNIQUES AND PROCEDURES DEVELOPED FOR PRODUCING LARGE IONIZER BARS	7-1
7.1	Fabrication Techniques and Procedures	7-1
7.2	Permeability Test Equipment and Procedures	7-5
7.3	Effect of Loading Technique and Vibration on Packing Density	7-7
8.	CONCLUSIONS AND RECOMMENDATIONS	8-1
REFERENCES		
APPENDIX A - PARTICLE SIZE ANALYSIS REPORTS		
APPENDIX B - DENSITY AND N <sub>2</sub> PERMEABILITY DATA FOR EXPERIMENTAL IONIZER BUTTONS		
APPENDIX C - LeRC IONIZER PELLET EVALUATION REPORTS		

## ILLUSTRATIONS

2-1	Hydrostatic Pressing Equipment Used for Compaction of Ionizers	2-10
2-2	Block Diagram of Permeability Apparatus	2-15
2-3	Electrical Circuit Diagram of Permeability Apparatus	2-15
3-1	Densification Rates at 1800°C of Fine Tungsten Microspheres from Two Vendors, Showing Effect of Additives on the Ampro Grade	3-3
3-2	Densification Rates at 2000°C of Fine Tungsten Microspheres from Two Vendors, Showing Effect of Additives on the Ampro Grade	3-4
3-3	Structures of Unalloyed Linde and Ampro Tungsten Microspheres, Vacuum Sintered at 1800°C	3-6
3-4	Structures Showing Effects of Alloy Additions on Ampro Lot U Tungsten Microspheres (0.25-2.5 $\mu$ ), Vacuum Sintered at 2000°C	3-8
3-5	Structures Showing Effects of Alloy Additions on Ampro Lot U Tungsten Microspheres (0.25-2.5 $\mu$ ), Vacuum Sintered at 2000°C	3-9
3-6	Densification Rates at 1800°C of Three Size Fractions of Linde Microspheres with and Without 10 W/oTa Additions, Compared with 0.25-2.5 $\mu$ Ampro Microspheres	3-12
3-7	Densification Rates at 1800°C of Three Size Fractions of Linde Microspheres With and Without 10 W/oTa Additions, Compared with 0.25-2.5 $\mu$ Ampro Microspheres	3-13
3-8	Structures of Unalloyed Linde and Ampro (0.25-2.5 $\mu$ ) Tungsten Microspheres, Vacuum Sintered at 1800°C	3-15
3-9	Structures of Three Fractions of Linde Tungsten Microspheres, Vacuum Sintered at 1800°C	
3-10	Structures of Three Fractions of Linde Tungsten Microspheres, Vacuum Sintered at 1800°C	3-17
3-11	Structures Showing Effect of 10 W/o Submicron Tantalum on Three Size Fractions of Linde Tungsten Microspheres, Vacuum Sintered at 1800°C	3-19

# ILLUSTRATIONS (contd)

3-12	Structures Showing Effect of 10 W/o Submicron Tantalum on Three Size Fractions of Linde Tungsten Microspheres, Vacuum Sintered at 1800°C	3-20
3-13	Infiltrated Structures of (1-4μ)W and (1-4μ)W-10Ta, Before and After Vacuum Sintering	3-22
3-14	Infiltrated Structures of (1-4μ)W and (1-4μ)W-10Ta, Before Vacuum Sintering, Showing 3 Types of Inhomogeneities	3-23
3-15	Sintered W-10W/oTa Containing Relatively Dense Occlusions	3-25
3-16	Microstructures of Ionizers, Made from Various Powder Mixtures, and Sintered at 1800°C for Times Noted	3-16
3-17	Microstructures of Ionizers, Made from Various Powder Mixtures, and Sintered at 1800°C	3-34
4-1	Mixture 1	4-5
4-2	Mixture 2	4-5
4-3	Mixture 3	4-6
4-4	Mixture 4	4-6
4-5	Mixture 5	4-7
4-6	Mixture 6	4-7
4-7	Mixture 7	4-8
4-8	Mixture 8	4-8
4-9	Mixture 9	4-9
4-10	Mixture 10	4-9
4-11	Mixture 11	4-10
4-12	Mixture 12	4-10
4-13	Mixture 13	4-11
4-14	Effect of Presintering Time (at 1040°C) on Sintered Structure of Ionizers, Made from 92 Wt.% of H <sub>2</sub> -Reduced Tungsten Plus 8 Wt.% of Copper Flake	4-16
4-15	Microstructures of Low Density "Shaped Pore" Ionizer Materials, Showing Effect of Boron Nitride Additions	4-19
4-16	Representative Microstructures	4-21
5-1	Change in Density with Heating Time at 1800°C for Various Tungsten Base Ionizers	5-3

## ILLUSTRATIONS (contd)

5-2	Change in N <sub>2</sub> Permeability with Heating Time at 1800°C for Various Tungsten Base Ionizers	5-4
5-3	Change in Density with Heating Time at 1600°C for Various Tungsten-Base Ionizers	5-5
5-4	Change in N <sub>2</sub> Permeability with Heating Time at 1600°C for Various Tungsten-Base Ionizers	5-6
5-5	Change in Density with Heating Time at 1500°C for Various Tungsten Base Ionizers	5-7
5-6	Change in N <sub>2</sub> Permeability with Heating Time at 1500°C for Various Tungsten Base Ionizers	5-8
5-7	Time-Temperature Relationship for Two Types of Porous Tungsten, Indicating the Time Required at Various Temperature Levels for a 50 Percent Decrement in Permeability	5-11
5-8	Time-Temperature Relationship for Six Spherical Tungsten-Base Alloys Indicating the Time Required at Various Temperature Levels for a 10 Percent Decrement in Permeability	5-12
6-1	Schematic of Vacuum Chamber with Ion Source, Neutral Detector, Ion Collector, and Residual Gas Analyzer	6-2
6-2	Residual Gas Analysis with Increasing Ion Beam Current in Diffusion Pumped System with Liquid Nitrogen Liner and Trap	6-2
6-3	Ionizer - Reservoir Assembly with Reusable Heaters	6-4
6-4	Schematic and Circuit Diagram of Ion Accelerator and Neutral Detector	6-5
6-5	Ion Current, Neutral Efflux and Total Flow versus Ionizer Temperature for Porous Tungsten	6-9
6-6	Ion Current Density Versus Ionizer Temperature for W-5 Ta-10Re Alloy Ionizer, IVTXR-10	6-11
6-7	Neutral Fraction Versus Ionizer Temperature for W-5 Ta-10Re Alloy Ionizer, IVTXR-10	6-12
6-8	Neutral Fraction Versus Ion Current Density for W-5Ta-10Re Alloy Ionizer IVTXR-10, Compared with the E3(1-44) Spherical Powder Tungsten Ionizers	6-14
6-9	Ion Current Density Versus Ionizer Temperature for W-5 Ta-10Re Alloy Ionizer, IVTXR-11	6-15

# ILLUSTRATIONS (contd)

6-10	Neutral Fraction Versus Ionizer Temperature for W-5Ta-10Re Alloy Ionizer, IVTXR-11	6-16
6-11	Neutral Fraction Versus Ion Current Density for W-5Ta-10Re Alloy Ionizer IVTXR-11, Compared with the E3(1-4 $\mu$ ) Spherical Powder Tungsten Ionizers	6-17
6-12	Ion Current Density Versus Ionizer Temperature for a 68%-Dense Shaped-Pore Tungsten Ionizer (I-5), Compared with Hughes Iridium Coated Tungsten Ionizer	6-20
6-13	Neutral Fraction vs Ionizer Temperature for a 68%-Dense Shaped-Pore Tungsten Ionizer (I-5)	6-21
6-14	Neutral Fraction vs Ion Current Density for 68% Dense Shaped-Pore Tungsten Ionizer I-5, Compared with the E3(1-4 $\mu$ ) Spherical Powder Tungsten Ionizers, and the Hughes Iridium Coated Tungsten Ionizer	6-22
6-15	Ion Current Density vs Ionizer Temperature for 67% Dense Shaped-Pore Tungsten Ionizer II-2, Compared with Hughes Iridium Coated Tungsten Ionizer	6-23
6-16	Neutral Fraction vs Ionizer Temperature for 67% Dense Shaped-Pore Tungsten Ionizer II-2	6-24
6-17	Neutral Fraction vs. Ion Current Density for 67% Dense Shaped-Pore Tungsten Ionizer II-2, Compared with the E3(1-4 $\mu$ ) Spherical Powder Tungsten Ionizers, and the Hughes Iridium Coated Tungsten Ionizer	6-26
6-18	Ion Current Density vs Ionizer Temperature for 47% Dense Stabilized Shaped-Pore Tungsten Ionizer, VI B-1	6-27
6-19	Neutral Fraction vs Ionizer Temperature for 47% Dense Stabilized Shaped-Pore Tungsten Ionizer, VI B-1	6-28
6-20	Neutral Fraction vs Ion Current Density for 47% Dense Stabilized Shaped-Pore Tungsten Ionizer, VI B-1, Compared with the E3(1-4 $\mu$ ) Spherical Powder Tungsten Ionizers	6-29
6-21	Ion Current Density vs Ionizer Temperature for 61% Dense Stabilized Shaped-Pore Tungsten Ionizer, #57 WB Cu-1	6-30
6-22	Neutral Fraction vs Ionizer Temperature for 61% Dense Stabilized Shaped-Pore Tungsten Ionizer, #57 WB Cu-1	6-31
6-23	Neutral Fraction vs Ion Current Density for 61% Dense Stabilized Shaped Pore Ionizer, #57 WB Cu-1, Compared with the E3(1-4 $\mu$ ) Spherical Powder Tungsten Ionizers	6-33



## ILLUSTRATIONS (contd)

7-1	Ionizer Test-Bar Manufacturing Process Flow-Sheet	7-2
7-2	Block Diagram of Permeability Apparatus	7-6
7-3	Dense Regions in Sintered Pellet, made from 2.5-10 $\mu$ Tungsten Microspheres Which were Packed into Rubber Mold by Vibrating at 40 kc/sec for 60 minutes	7-10

## TABLES

2-I	Metals used in Fabricating Small Experimental Ionizers, with Reference to Source, Grade and Purity	2-2
2-II	Chemical Analyses Data for Metal Powders used in Fabrication of Experimental Ionizers	2-3
2-III	Comparison of Particle Count Data on Ampro Tungsten Microspheres, Performed by Two Different Techniques	2-5
2-IV	Metallograph Preparation of Porous Tungsten, Infiltrated with Copper	2-18
3-I	Various Parameters of Sintered Ionizers, Indicating Effect of Binary Additions to Ampro (0.25-2.5 $\mu$ ) Tungsten Microspheres	3-7
3-II	Sintering Data for Ionizer Pellets, made from 0.25-2.5 $\mu$ Tungsten Microspheres, with Additions of Fine Tantalum and/or Fine Rhenium Powders	3-28
3-III	Pore Parameters for Various Ionizer Compositions	3-30
3-IV	Summary of Pore Parameters for Eight Ionizer Compositions	3-31
3-V	Chemical Analyses Data for Spherical Tungsten-Base Ionizers	3-35
4-I	Sintering Tests on H <sub>2</sub> -Reduced Tungsten Powder-Copper Flake Mixtures	4-4
4-II	Permeability Variance After Bakeout of 92% W + 8% Cu - Bar No. 1	4-13
4-III	Permeability Variance After Bakeout of 92% W + 8% Cu - Bar No. 2	4-14
5-I	Accelerated Life-Test Data, Indicating Effect of Heating on Ionizer Density and Permeability	5-2
5-II	Time Required for 50% or 10% Decrement in N <sub>2</sub> Permeability by Various Ionizer Compositions	5-14
7-I	Effect of Various Packing Techniques on Apparent Density of 2.5-10 $\mu$ Diameter Tungsten Microspheres	7-8

## 1. INTRODUCTION

This research program was conducted with the primary objective of developing improved porous ionizers for use in cesium contact engines. Previous work on tungsten and tungsten-base ionizers indicated that pore structure should be as fine and uniform as possible, consistent with high resistance to change over thousands of hours at ionization temperature.

The research reported herein is a logical sequel to previous ionizer development programs at Electro-Optical Systems. Significant results of these previous programs are summarized in the following paragraphs.

Under Contract NAS 8-2547<sup>1</sup>, the first use of tungsten microspheres as the base material of ionizer construction was instituted and reduced to practice. The use of spherical, rather than angular ( $H_2$ -reduced) tungsten particles, was suggested by the inherent metallurgical advantages of spherical particle form. These advantages include high density of individual particles for efficient transmission of compacting energy; smooth sphericity of particles for good packing uniformity prior to, and during, compaction; uniform strain energy at particle-contact points within the pressed powder mass, as relates directly to uniform densification during subsequent sintering; and minimum total surface free energy of the spheres, which permits relatively slow and controllable sintering to the desired density. Since conventional methods proved inadequate for compacting the tungsten microspheres, a novel isostatic technique was developed.

Spherical tungsten powder was duly shown to have improved thermal stability at the elevated sintering temperatures. Variance in nitrogen permeability within large lots of ionizer buttons was also markedly improved for the spherical-base type. A current density of about

30 mA/cm<sup>2</sup> was achieved with a spherical-base-tungsten ionizer, as compared to 15-20 mA/cm<sup>2</sup> for the angular-base (commercial) type.

A preliminary experiment was conducted, wherein tungsten microspheres were precoated (prior to compaction) with a very thin layer of tantalum. The tantalum was shown to markedly inhibit subsequent grain growth and attendant deterioration of pore structure during sintering at 2000-2200°C. This experiment marked the first use of tantalum as an additive to stabilize the pore structure of tungsten ionizers.

Under Contract NAS 3-2519<sup>2</sup>, tungsten microspheres were classified into 4-8μ, 3-6μ and 1-4μ diameter size fractions. The powder fractions were then used to fabricate an ionizer series having increasingly fine pore structure. Thus the effect of pore refinement on ionizer performance was determined at equivalent levels of ionizer purity and density. Cesium ion current densities to 60 mA/cm<sup>2</sup> were achieved with ionizers made from the 3-6μ and 1-4μ powder fractions. Neutral fractions at 50 mA/cm<sup>2</sup> were 1-3%, representing a considerable improvement over angular powder (commercial) ionizers and over ionizers made from unsized tungsten microspheres. Critical temperature was below Langmuir data for solid tungsten. Neutral fraction vs ionizer temperature curves for the 1-4μ ionizer category showed definite minima and approximated slopes predicted by the Saha-Langmuir equation for a work function of 4.6 - 4.8 eV. Neutral fraction and critical temperature decreased with pore size of the ionizers. Photomicrographs showed that use of 1-4μ microspheres increased the number of pores per unit of ionizing area by a factor of 5.5X, and reduced mean pore size by a factor of 0.4X (compared with use of 1-7μ unsized microspheres). The fine spherical powder ionizers reached much higher current densities with lower neutral fractions than any other tungsten ionizers tested to that time.

Under Contract NAS 3-5248<sup>3</sup>, the thermal stability and, to some degree, the ionization performance of spherical tungsten powder

ionizers were improved by tantalum additions. Two techniques for adding secondary elements were used: blending of angular tantalum particles with 1.7-5 $\mu$  tungsten microspheres, and precoating the tungsten microspheres prior to compaction and sintering. The same tungsten powder base was used for all ionizers. Significant stabilization of sintered density and nitrogen permeability was achieved by 5 and 10 atom percent of Ta particle additions, as indicated by heating at 1800°C and 1600°C in vacuum without cesium. Excellent ionization performance, with current densities up to 85 mA/cm<sup>2</sup>, was measured for a W-10 percent Ta ionizer. Ionizers precoated with 102Å Ta had the finest structures and the highest pore densities (6 million pores/cm<sup>2</sup>). Precoating the tungsten microspheres with rhenium or osmium did not yield the desired combination of finer porosity and greater thermal stability. An ionizer made of microspheres precoated with 45Å of rhenium did not exhibit improved ionization performance. Considering both performance and life expectancy, ionizers made with 5 and 10 percent of tantalum particle additions were indicated to be optimum. For spherical powder ionizers, improved ionization performance correlated with higher pore densities and smaller pore diameters.

The design goals (Phase A) of the present contract are as follows:

1. Pore Size  
0.5 - 1.0 micron diameter pores uniformly distributed over the ionizer surface
2. Pore Density  
More than  $1.0 \times 10^7$  pores per cm<sup>2</sup>
3. Life  
Ionizer material capable of 10,000 hours of operation (at 1100°C to 1400°C with cesium) with changes of less than 1% in density, permeability, and pore size characteristics
4. Emittance  
The value of the total emittance of the surface to be less than 0.3

5. Work Function

4.5 eV or higher

6. Critical Temperature and Current Density

The surface ionization of cesium to take place at 1500°K and less than 1% neutral cesium atoms at a current density of 25 mA per cm<sup>2</sup>

7. Purity

Exclusive of the alloying addition the purity of the ionizer compact should be 99.99+%.

Scope of this contract is summarized as follows:

Phase B      Development of techniques for producing composite ionizers of W-Ta, W-Re, and W-Re-Ta; development of ionizers containing void fractions in excess of 30%.

Phase C      Evaluation and testing of materials and processes to optimize methods for producing large ionizer bars.

Phase D      Fabrication and delivery of 8 large ionizer bars.

At the outset of this research, and based on the three background contracts (previously reviewed), consensus of data indicated that fine accurately sized tungsten microspheres provided the ideal powder base for ionizer fabrication. During the course of this research, however, a new technique was developed which employs an "inert" separator powder blended with tungsten powder. Development of this technique permits the use of low-cost angular tungsten powder, and opens new vistas for additional ionizer improvement.

## 2. EXPERIMENTAL METALS, FABRICATION AND EVALUATION TECHNIQUES

### 2.1 Metals

All data pertinent to the initial metal powders and metals, used in fabricating small experimental ionizers, are presented in this section. Similar data for the large ionizer bars have been included with the LeRC ionizer inspection reports.

#### 2.1.1 Metal Source, Grade and Purity

Various metals and metal powders, used in preparing small experimental ionizers, are listed in Table 2-I. Chemical analyses data are given in Table 2-II for the powder constituents. Complete analyses of all tungsten powders were performed by the Materials Testing Laboratory of Magniflux. Details of MTL's analysis procedures and equipment were reported previously<sup>2</sup>. Analyses data for the minor additive powders, Ta, Re and Cu flake, were supplied by vendors, and are less complete than those for tungsten.

#### 2.1.2 Particle Size of Powdered Metal Constituents

##### Tungsten Powders

One goal of this contract was to classify the tungsten powder base such that 80% of the particles were between 0.5-2.5 $\mu$  in diameter. This was considered necessary in achieving high pore density and small pore diameter of final ionizers.

To procure spherical tungsten powder suitable for classification, seven vendors were contacted by EOS. Of these, five were ruled out as suppliers on the basis of price, quality, inexperience, or inability to assure timely delivery. The two vendors selected were the Linde Division of Union Carbide, and Advanced Materials and Processes Corporation (Ampro); both had previous experience as suppliers on related NASA contracts. All tungsten microspheres used in this research were

TABLE 2-I  
METALS USED IN FABRICATING SMALL EXPERIMENTAL IONIZERS,  
WITH REFERENCE TO SOURCE, GRADE AND PURITY

METAL	VENDOR SOURCE	GRADE	PURITY
Tungsten Powder	Linde Div. of Union Carbide Indianapolis, Indiana	Fine Spherical	See Table 2-II
"	Advanced Mtls. and Processes Palo Alto, California	Fine Spherical	See Table 2-II
"	Lamp Div. of G. E. Cleveland, Ohio	0.8 $\mu$ H <sub>2</sub> Reduced	See Table 2-II
Tantalum Powder	Nat'l. Res. Corp. Newton, Massachusetts	SGQ-4 Capacitor	See Table 2-II
"	Nat'l. Res. Corp. Newton, Massachusetts	QETF-1 "	See Table 2-II
Rhenium Powder	Chase Brass & Copper Waterbury, Connecticut	Grade 1	See Table 2-II
Copper Powder	Crescent Bronze Co. Los Angeles, California	No. 112 Flake	See Table 2-II
IrO <sub>2</sub> Powder	J. Bishop & Co. Malvern, Pennsylvania	-325 mesh	99.95% *
Boron Nitride	Carborundum Co. Los Angeles, California	High Purity Powder	99.9% *
Copper Bar***	American Smelting & Refining South Plainfield, N. J.	ASARCO A-58	>99.95% by diff.**
Iron Wire***	J. T. Baker Chemical Co. Phillipsburg, N. J.	Reagent	Std. Reagent



\* Analyses requested from vendors, but not available.

\*\* Refer to Section 5 of LeRC reports for detailed Ledoux analysis.



\*\*\* For infiltration



TABLE 2 - II  
CHEMICAL ANALYSES DATA FOR METAL POWDERS  
USED IN FABRICATION OF EXPERIMENTAL IONIZERS  
(Impurity contents given in parts per million)

Metal Powder	Vendor	Sub-Group A  B 	Group I					Group II				Group III				Group IV									
			H	Li	Na	K	Cu	Rb	Ag	Be	Mg	Ca	Zn	Sr	Ba	B	Al	In	C	Bi	Tl	Zr	Sn	Hf	Pb
Spherical W	Lindes*	Lot or Grade	--	<10	<20	<10	50	N.D.***	<5	4	1	<10	--	<10	<10	<3	20	<1	16	<10	<5	<10	<5	<30	<5
Spherical W	Ampro*	U	--	<10	<20	30	50	N.D.	10	<1	10	<10	--	<10	<10	5	150	<1	175	<10	<5	<10	<10	<30	<5
H <sub>2</sub> -Reduced W	Gen. Elec.*	U. 80-5407	--	71	66	110	2	348	<1	<1	4	20	--	<1	<10	<3	4	--	30	<10	<5	<10	<3	<60	<3
Capacitor Ta	NRC**	80Q-4	20	--	--	--	<1	--	--	72	<1	--	--	--	--	--	<25	--	40	15	<5	--	<1	--	--
Capacitor Ta	NRC**	QBTF-1	70	--	--	--	<1	--	--	--	<1	--	--	--	--	--	<25	--	41	52	<5	--	<1	--	--
Grade 1 Re	Chase**	449	--	--	--	--	<1	--	--	--	<1	<1	--	--	--	--	<1	--	--	<1	--	--	--	--	--
Copper Flake	Crescent**	112	--	--	--	--	--	--	20	--	2	--	9700	--	--	--	30	--	7900	200	--	--	20	--	20

(CONTINUED)

Metal Powder	Vendor	Sub-Group A  B 	Group V					Group VI			Group VII		Group VIII										Pt	Th	
			N	V	As	Sb	Ta	Bi	O	Cr	Mo	W	Mn	Re	Fe	Co	Ni	Ru	Rh	Pd	Os	Ir			Pt
Spherical W	Lindes*	Lot or Grade	--	<5	<30	<50	<20	<500	<3	1090	<3	<25	Bal.	<1	<200	<10	<5	10	N.D.	N.D.	N.D.	N.D.	N.D.	N.D.	N.D.
Spherical W	Ampro*	U	--	<5	<30	<50	<20	<500	<3	4040	3	<25	Bal.	<1	<200	50	<5	50	N.D.	N.D.	N.D.	N.D.	N.D.	N.D.	N.D.
H <sub>2</sub> -Reduced W	Gen. Elec.*	U. 80-5407	--	2	--	<50	<25	--	<1	--	230	90	Bal.	<1	--	76	<10	<10	<100	<8	<50	<200	<250	<5	<150
Capacitor Ta	NRC**	80Q-4	30	--	--	40	--	Bal.	--	2000	<5	<10	<40	<1	--	10	--	<5	--	--	--	--	--	--	--
Capacitor Ta	NRC**	QBTF-1	29	--	--	<25	--	Bal.	--	5100	3	<10	<40	<1	--	9	--	6	--	--	--	--	--	--	--
Grade 1 Re	Chase**	449	--	--	--	--	--	--	--	--	<1	<1	--	--	--	13	--	<1	--	--	--	--	--	--	--
Copper Flake	Crescent**	112	--	--	--	--	--	--	--	--	--	--	--	5	--	60	--	7	--	--	--	--	--	--	--

Copper Flake  
Bronze

\* Analysis performed by Materials Testing Lab. of Magniflux Corp.

\*\* Analysis supplied by Vendor.

\*\*\* N.D. - Not Detected

sized in a cyclonic air classifier by Ampro.

Attempts to microscopically determine size distribution of tungsten microspheres, predominantly less than  $2.5\mu$  in diameter, were unsuccessful. Failure was mainly due to (1) inability to adequately separate the particles prior to counting, even by a shock-wave dispersion method, and (2) inability to optically resolve the finest particles, particularly when clustered together. This problem was solved by resorting to electron micrography, with subsequent particle counting on the electron micrographs produced. A magnification of 5500 and the equivalent circle technique for particle size analysis were used. Detailed reports by Sloan Research Industries on techniques used, and results derived, are included in Appendix A.

A comparison of particle-size distributions, obtained by microscopic and electron micrographic techniques on Lot U Ampro tungsten powder, is given in Table 2-III. Because of known inherent difficulties in microscopic counting, the results of Table 2-III are not in good agreement. The advantages of the electron micrographic method, on the other hand, appear sufficient to recommend its use for future analyses.

Tabulated data for Ampro Lot U tungsten on page A-5 of Appendix A indicate 81.1% by count of particles in the  $0.25$ - $2.5\mu$  diameter range. This is very close to the classification goal of the contract.

A particle size analysis report on the finest fraction classified from Linde microspheres (and used to produce the best spherical-base ionizers) is included in pages A-14 through A-27 of Appendix A. Tabulated data on page A-16 indicate 78.1% by count of particles in the  $0.25$ - $2.5\mu$  diameter range. This is also very close to the classification goal of the contract.

Particle-size data for the fine,  $H_2$ -reduced tungsten, used to fabricate low-density ionizers (by Cu flake technique), were supplied by General Electric as follows:

TABLE 2-III COMPARISON OF PARTICLE COUNT DATA  
ON AMPRO TUNGSTEN MICROSPHERES, PERFORMED  
BY TWO DIFFERENT TECHNIQUES

Median Diam., $\mu$	Diam Range, $\mu$	Ampro Microspheres (Lot U)			
		Microscopic Count <sup>(a)</sup>		Electron Micro.Count <sup>(b)</sup>	
		No. Count	Increment %	No. Count	Increment %
0.75	0.25-1.24	282	24.8	447	47.5
1.50	1.25-1.74	179	15.7	162	17.2
2.00	1.75-2.24	253	22.2	106	11.3
2.50	2.25-2.74	182	16.1	84	8.9
3.00	2.75-3.24	171	15.0	70	7.4
3.50	3.25-3.74	38	3.4	51	5.4
4.00	3.75-4.24	21	1.8	13	1.4
4.50	4.25-4.74	6	0.5	7	0.8
4.87	4.75-4.99	6	0.5	1	0.1
Totals	0.25-4.99	1138	100.0	941	100.0
<p>(a) Supplied by Ampro with powder</p> <p>(b) Performed at Sloan (see Appendix A)</p>					

<u>Micron Range</u>	<u>Wt. % in Range</u>
0-1	66.5
1-2	22.3
2-3	4.9
3-4	4.3
4-5	2.2
> 5	0.0

Average particle diameter of the G.E. powder was given as  $0.78\mu$ . From the above data, it is clear that a very large percentage by number of particles occurs in the 0-2 $\mu$  range, indicating that this powder is even finer than the classified spherical-powder fractions.

#### Tantalum and Rhenium Powders

Classified tantalum<sup>\*</sup> and rhenium<sup>\*\*</sup> powders, used as additions to the 0.25-2.5 $\mu$  tungsten microspheres, were also submitted to Sloan Research for particle size analyses. Results are given in their report on pages A-28 through A-42 of Appendix A. Briefly, attempts to adequately disperse the Ta and Re particles were not successful. Therefore, the electron micrographs obtained did not permit determination of particle size by the counting method. The tenacity with which the fine Ta and Re particles cling together comes as no surprise, particularly in view of their irregular shapes. The reasoning of Sloan (p. A-31) that the Re particles are firmly attached (as by fusion) seems unlikely in view of previous "sharp" and reliable size fractions obtained by Ampro with the same classifier apparatus. The electron micrographs on pages A-33 through A-42 are included to characterize the powders used. Admittedly, actual particle-count data would be more desirable.

#### Other Powders Used as Minor Additions to Tungsten

These include IrO<sub>2</sub>, copper flake and boron nitride. Consultation with Sloan Research indicated that size distributions of such angular particles could not be determined from electron micrographs

\* NRC Grade SCQ-4, classified by gravity sedimentation at National Res. Corp.  
 \*\* Chase Grade 1, classified by cyclonic air

because of the particle agglomeration problem, encountered previously with fine angular Ta and Re. Thus, determining the size distribution of angular ductile Ta and Re particles, predominately  $< 3\mu$  in diameter, appears to be beyond the capability of current technology.

## 2.2 Fabrication Techniques

### 2.2.1 Classification and Size Analysis of Powders

All tungsten microspheres and angular rhenium powder, used to fabricate experimental ionizers, were classified at Ampro by the cyclonic air method. Details of their classifier apparatus were indicated to be proprietary.

Initial classification of tantalum powders was performed at NRC by the turbidimetric (gravity sedimentation) method. Secondary gravity classification was performed at EOS on the NRC Grade SGQ-4 tantalum, used to fabricate two series of spherical W-Ta-Re compacts. This was done to better assure exclusion of particles over  $3\mu$  in diameter, since such larger particles (admixed with, and diffusing into, 0.25-2.5 $\mu$  tungsten) would result in oversized pores upon sintering.

Secondary classification of tantalum was performed as follows. The starting powder was first submerged in benzyl alcohol and dispersed at high speed in a liquid blender. Separation was accomplished by gravity sedimentation, settling time being calculated by Stoke's law of free fall. The suspension, containing the particles desired, was then siphoned off and the tungsten recovered by filtration, using a Gooch crucible. Initial separation of  $< 2\mu$ -diameter particles produced only a 5.6 weight percent yield. Settling time was therefore decreased by a factor of 0.44 to increase the diameter of particles captured to  $3\mu$ , and to make the separation more feasible economically.

Size analyses of the spherical tungsten powders were performed at Sloan Research, as described in their reports (see Appendix A). Size analyses of angular Ta and Re powder, used as minor additives to tungsten, were attempted by Sloan but severe particle agglomeration was encountered. This problem also precluded size determinations for the other

angular particle additives used.

### 2.2.2 Blending of Powders

Blending of powders was done by mortaring, ball milling, or liquid blending. Ball milling was performed both dry and in liquid (benzene) slurry. Liquid blending was done in a standard household (Waring) unit, using benzyl alcohol as the suspension vehicle and the forces of liquid shear to obtain dispersion of powder agglomerates.

Ball milling of small powder batches (<100gm) was done in suitably sized glass jars, containing 3/8" or 1/2"-diameter hardened-steel ball bearings. The jars were rotated axially in a standard glass-blower's lathe at speeds observed to produce optimum tumbling action of the powders.

Larger batches of powder were blended in a Universal Laboratory Mixer, Model 831. The powders were contained in a 1/4-cubic-foot porcelain jar, and rotated at 50 rpm about a 45° skew axis. Hardened steel bearings of 1/2-inch diameter were included to accelerate and improve homogenization of the mixtures. This ball-mill unit was used in preparing all of the large ionizer bars.

### 2.2.3 Loading of Powders

All powders and powder mixtures were loaded into rubber containers and sealed, prior to compaction. Experiments to determine the effect of vibratory loading were conducted (as described subsequently in Section 7); however, it was found that vibration resulted in segregation of fine particles and nonuniform densification during sintering. Therefore, vibratory loading was not used in preparing ionizers for the test program, and is not recommended for future use.

Powders and powder mixtures for small ionizers (pellet-size) were first dried at least 2 hours under high vacuum, then loaded (within a dry box) into standard laboratory tubing of 5/8-inch diameter. In sequence, the lower end of the tubing was sealed with a metal plug, the powder introduced and packed by repeated tapping of the bottom plug on the dry box floor, and the upper end finally sealed with a second

metal plug. Both plugs were fixed firmly in place simply by tightening wires around the tubing circumference.

Loading of powders and powder mixtures for the large ionizer bars is described subsequently in Section 7.

#### 2.2.4 Compaction of Metal Powders

The rubber-sheathed powders were pressed hydrostatically at up to 60,000 psi under glycerine. The hydrostatic press used is shown in Fig. 2-1. It consists of a glycerine reservoir, an air-actuated pump\*, appropriate valves and gages, and a pressure vessel of high-strength steel. With breach plug seated firmly to seal the chamber, the work space measures 6-1/2-inch diameter x 7-inch height. Effective height of the work space is reduced somewhat, however, by the hemispherical shape of the chamber bottom.

Operation of the press is as follows:

- (1) Immerse rubber-encased powder in the glycerine of high-pressure chamber.
- (2) Install breach plug.
- (3) Open petcock at bottom of vertical air-intake line to blow out water condensate.
- (4) Slowly open air-control valve to the pump and raise level of glycerine until it issues from bleed port in center of breach, expelling all air from system. Close bleed port with threaded plug.
- (5) Again open air-control valve to pump glycerine to desired pressure level (60,000 psi, max).  
Hold at desired pressure if dwell time is desired (not employed in this program).

---

\* Haskell Engineering piston-type pump with pressure step-up ratio of 600-to-1.

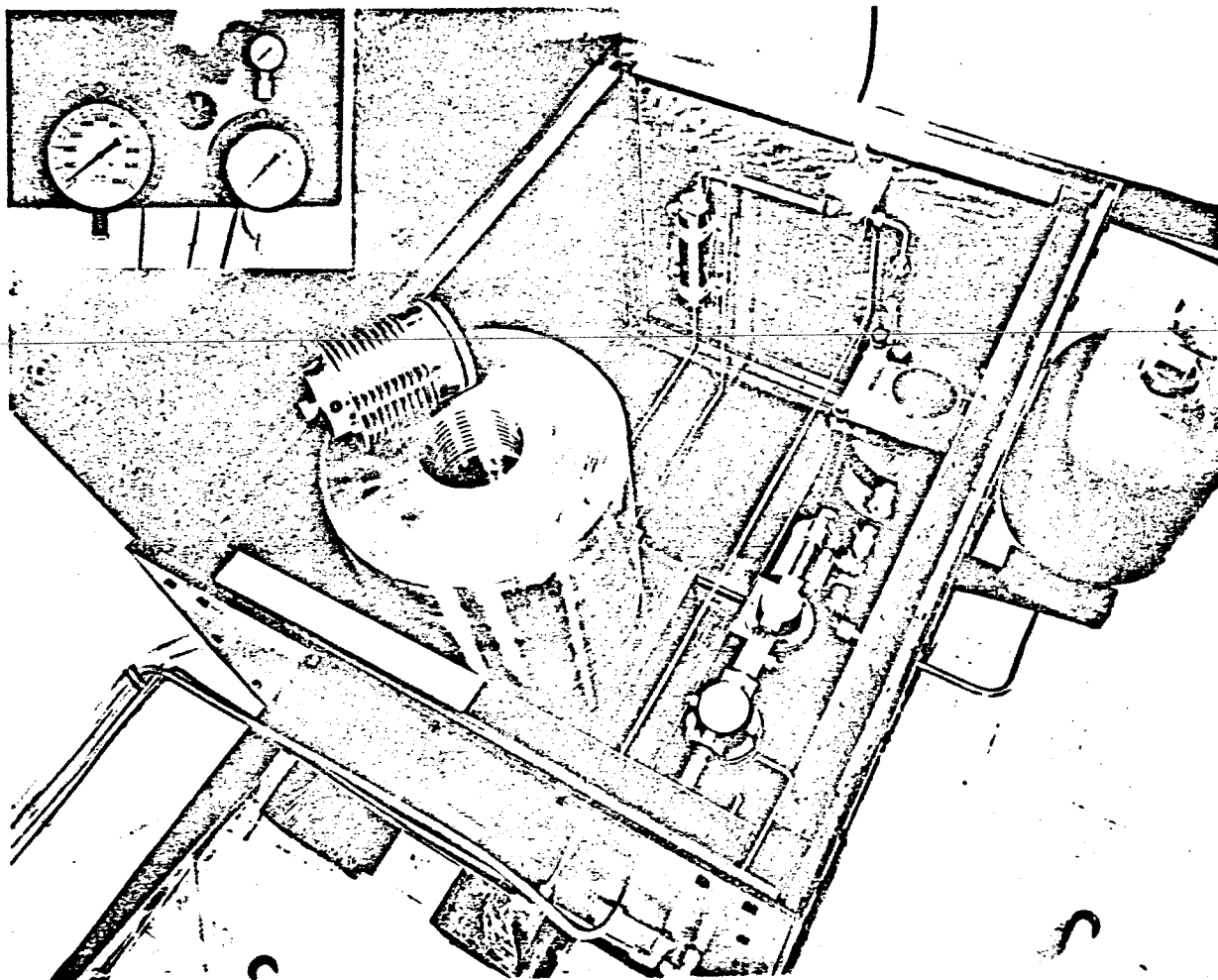


FIG. 2-1 HYDROSTATIC PRESSING EQUIPMENT USED FOR COMPACTION OF IONIZERS



- (6) Close air-control valve to pump, and slowly open valve between pressure chamber and glycerine reservoir, reducing chamber pressure to zero gage.
- (7) Remove plug from bleed port, unscrew breach plug, remove and rinse compact under tap water, and finally extract compact from rubber sheath.

#### 2.2.5 Vacuum Sintering

Sintering was performed in the  $10^{-5}$ -torr pressure range.

Description of the vacuum furnace used is as follows:

Brew, Model 424-C, Serial No. 301

Heating Element: 4-1/2" diam. x 7" height tungsten mesh

Heat Shielding: sheet tungsten

Fore Pump: Welsh Duo-Seal, Model 1997

Diffusion Pump: 6" NRC, Model HS6-1500, Type 162

Pumping Speed: 1500 liters per second

Power Supply: Variable transformer with low-voltage power transformer. 65 KVA capacity- 30 480V

Max. Temperature: 3000°C with pressure of  $5 \times 10^{-5}$  torr

Instrumentation: cold cathode gage in vacuum chamber,  
T.C. gages in both chamber and foreline.

Sample temperatures were monitored with an optical pyrometer. This instrument was checked for accuracy against the melting point of pure iodide titanium, heated slowly within the vacuum chamber proper.

Heating for all sintering was done at such a rate that chamber pressure remained below  $1 \times 10^{-4}$  torr. On an average, about 20 minutes were required to heat from room temperature to 1800°C.

#### 2.2.6 Infiltration of Ionizers

All of the small experimental ionizers were infiltrated with Cu-2Fe alloy at 1150°C to 1200°C, under flowing hydrogen, forming gas ( $85\%N_2$ - $15\%H_2$ ), or argon. Infiltration times of from 1 to 2-1/2 hours were allowed, depending on ionizer thickness and on the ease with which

the infiltration alloy penetrated.

The optimum infiltrant for pure tungsten was W-2Fe alloy. The porous part was placed in contact with the alloy and heated to approximately 1175°C under hydrogen. Factors contributing to the success of the infiltration appeared to be wetting of the tungsten by iron, fluidity of the alloy at the ~100°C of superheat, and the reducing character of hydrogen.

Infiltration of ionizers containing tantalum could not be accomplished reliably under either hydrogen or forming gas, since these gases create a surface condition which inhibits the natural wetting action of the Cu-Fe infiltrant. Therefore, all Ta-containing ionizers were infiltrated under pure argon. In sequence, the ionizers (beneath pieces of Cu-2Fe) were placed in quartz boats within an Inconel tube furnace, evacuated and purged overnight with -60°C dew-point argon, heated at 1200°C for 1-2 hours, and cooled in situ under the argon. Argon flow rate was adjusted to ~1 cfh, being exhausted through a bubble bottle containing vacuum-pump oil.

Infiltration and presintering of the large ionizer bars were performed in a furnace of the following description:

Keith, Model KPR 8 4 12 2150, Serial No. 4015-564

Max. Temperature: 2150°F (1177°C)

Hot-Zone Size: 4" high x 8" wide x ~12" long.

Muffle Material: Inconel

Heating Elements: Silicon carbide globars

Power: 20 KVA- 240V- 86A

Cold Zone: Cooled by water jacket and shielded with flame curtain during periods when loading door was open.

#### 2.2.7 Machining of Infiltrated Ionizers

Machining of small experimental pellets into ionizer buttons was done on a standard lathe, using high-speed steel tool bits. No standards were maintained on feed rate, tool clearances, or angle of attack, these being left to the discretion of experienced machinists.

However, surface grinding of the ionizer buttons was done using the same procedure as in the two previous contracts for consistent surface texture. The circular faces of the buttons were ground using a Norton 37C36-KVK grinding wheel (36 grit silicon carbide, K hardness with vitrified bond). Wheel diameter was 5.82 inch so that, at 3450 rpm, linear velocity at the metal-wheel interface was 87.6 feet per second. Grinding was performed under a water-oil emulsion in 0.001" increments down to the final two passes, where 0.0005" increments were used.

Machining of the large ionizer bars is described subsequently in Section 7.

#### 2.2.8 Removal of Infiltrant from Ionizers

For the small ionizers the infiltrant was removed by simply heating in the Brew furnace (described in Subsection 2.2.5) for 15 minutes at 1500°C, followed by 30 to 45 minutes at 1750°C. Spectrographic analyses indicated that this treatment reduced copper content to below 20 ppm and iron to below 100 ppm.

Removal of infiltrant from the large ionizer bars is described subsequently in Section 7.

### 2.3 Evaluation Techniques

Evaluation techniques and equipment, used on small experimental ionizers, are described in this section. Techniques related to performance testing are described in Section 6; techniques related to the preparation of large ionizer bars are described in Section 7.

#### 2.3.1 Density

All densities were determined on accurately machined buttons, or on pellets sufficiently cylindrical for determination of density from direct weight-to-volume ratios. Where sample geometry is irregular the pycnometer method may be used, with mercury as the immersion fluid. The following formula for calculating absolute density applies:

$$\rho = 13.546 S / (M_1 - M_2)$$

where S is sample weight in air,  $M_1$  is the maximum weight of Hg which can be

held by the pycnometer bottle, and  $M_2$  is the weight of Hg in the pycnometer after immersion of the sample. If P represents the weight of the empty pycnometer, collective weight of pycnometer, residual Hg, and immersed sample =  $P + M_2 + S$ . Then  $P + M_1 + S - (P + M_2 + S) = M_1 - M_2$ , the weight of Hg displaced.

### 2.3.2 Nitrogen Permeability and Transmission Coefficient

The term "nitrogen permeability" is used, throughout this report, synonymously with mass permeability coefficient. This is done as a simplification and to distinguish it from "cesium permeability". Determination of the mass permeability coefficient of porous bodies, with respect to a diffusing gas, is a reliable and simple way of determining fluid-transmitting efficiency. Mass permeability coefficients, in contrast to density values, are extremely sensitive to slight changes in pore structure. Therefore, permeability coefficients have been determined for all ionizer buttons produced under this and previous contracts.

A sketch of the permeability apparatus used at Electro-Optical Systems is included as Fig. 2-2, with the associated electrical circuits shown in Fig. 2-3. A disc-shaped button is clamped in the test fixture within a neoprene "O" ring. Compression exerted by the fixture presses the "O" ring tightly against the cylindrical surface of the button, sealing it so that only the button face surface is exposed to the diffusant gas. Other components of the apparatus consist of a nitrogen tank, drying tower, solenoid gas valve, mercury manometer, and a gas chamber of known volume. The nitrogen pressure between the tank and the solenoid valve (see Fig. 2-2) is first adjusted so that, when the solenoid valve is opened, the mercury in the manometer rises to above the upper electrical contact embedded in the manometer wall. Energizing of the solenoid also admits nitrogen to the gas chamber of known volume and initiates diffusion of nitrogen through the porous sample. The solenoid is then deenergized by releasing the "start button", and the nitrogen pressure begins to decrease by diffusion through the sample.

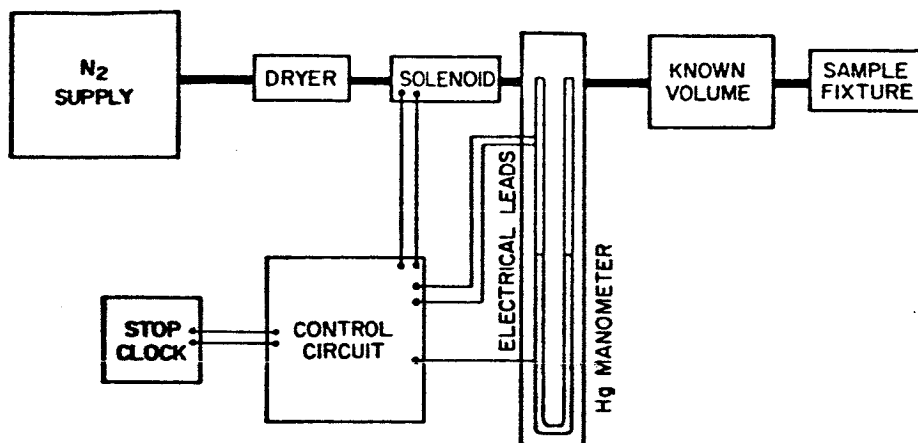
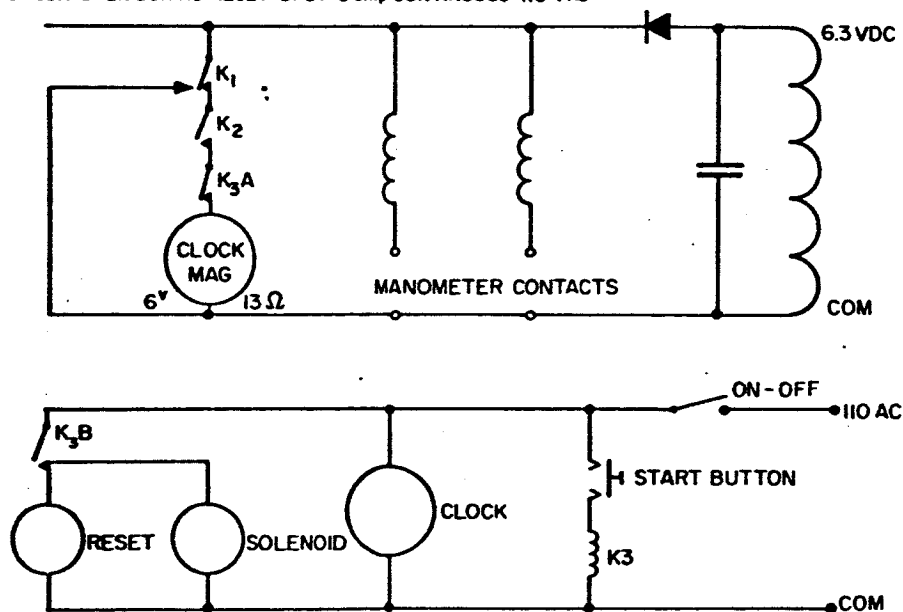


Fig. 2-2 BLOCK DIAGRAM OF PERMEABILITY APPARATUS

1. CLOCK START SPDT } 1 amp 6.3 VDC
2. CLOCK STOP SPDT }
3. CLOCK CIRCUIT OPEN DURING RESET DPDT 3 amp CONTINUOUS 115 VAC



ALL RELAYS SHOWN UNENERGIZED

FIG. 2-3 ELECTRICAL CIRCUIT DIAGRAM OF PERMEABILITY APPARATUS

As the mercury in the manometer breaks from the upper electrical contact, the stop clock is actuated electrically. It continues to run until the mercury breaks from the lower contact, located 25.4 mm below the upper contact. At this instant, the clock stops, recording the time increment " $\delta t$ " required for the known gas volume " $V$ " to undergo a 50.8 mm Hg pressure decrement " $\delta P_{\text{mm}}$ " by diffusion through the porous sample. The " $\delta t$ " value obtained in this way is accurate to within  $\pm 0.01$  second.

Mass permeability coefficient is then calculated by Carman's formula<sup>4</sup>.

$$K = (\delta m) \left( \frac{L}{A} \right) \left( \frac{1}{\delta t} \right) \left( \frac{1}{\Delta P_{\text{mm}}} \right), \text{ gm} \cdot \text{cm}^{-1} \cdot \text{sec}^{-1} \cdot \text{mm Hg}^{-1}$$

where  $\delta m = \frac{\delta P_{\text{mm}} \cdot V \cdot M}{RT}$ , gm of  $N_2$  diffusing in  $\delta t$  seconds

$M$  = gm/mole, molecular weight of  $N_2$

$R$  = ideal gas constant

$T$  =  $^{\circ}\text{K}$ , absolute temperature

$L/A$  =  $\text{cm}^{-1}$ , length/area ratio of test sample

$\Delta P_{\text{mm}}$  = mm Hg, mean differential between gas chamber and atmospheric pressures during  $\delta P_{\text{mm}}$  decrement.

All permeability coefficients reported herein were determined using the following constants:

Diffusant gas,  $N_2$

$M$  = 28.02 gm/mole

$\delta P_{\text{mm}}$  = 50.8 mm Hg  $\approx$  0.06684 atmosphere

$\Delta P_{\text{mm}}$  = 346 mm Hg

$R$  = 82.057  $\text{cm}^3 \cdot \text{atm} \cdot ^{\circ}\text{K}^{-1} \cdot \text{mole}^{-1}$

$T$  = 298 $^{\circ}\text{K}$

$V$  = 74.6  $\text{cm}^3$

$\delta m$  = (5.714)(10) $^{-3}$ gm

or  $\left\{ \begin{array}{l} V = 1051.6 \text{ cm}^3 \\ \delta m = (80.545)(10)^{-3} \text{ gm} \end{array} \right.$

It will be noted that, throughout this report, nitrogen permeability(K) is expressed in units of gm/cm·sec.torr, the natural units of measurement. However, the physical dimension of K is time, and by converting the pressure from torr to dynes/cm<sup>2</sup> (i.e., multiplying by  $7.5 \times 10^{-4}$ ) K will be in seconds. The product of K (in sec) and the coefficient of kinematic viscosity (in cm<sup>2</sup>/sec) is the specific permeability,  $K_s$  (in cm<sup>2</sup>).

Conversion of nitrogen permeability (K) to the dimensionless transmission coefficient (C) is calculated from

$$C = 17.897 K/L, \text{ where } L \text{ is in centimeters.}$$

### 2.3.3 Metallographic Preparation

A detailed outline for metallographic preparation of copper-infiltrated porous tungsten (or tungsten-rich) ionizers is given in Table 2-IV. This procedure provided consistently good delineation of the microstructures. Polishing step IV.B is quite critical and, if continued too long, can give undesirable surface relief. In turn, this leads to pore counts and measurements which are larger than would be obtained on a flat plane of examination.

### 2.3.4 Determination of Pore Parameters

Two different methods of determining pore parameters have been derived over the several years of experimental work, namely, the pore-counting method and the pore-intercept method. Both rely for their accuracy on the same prerequisite, i.e., a high-quality photomicrograph of sufficiently high magnification and of the best possible definition. Both methods have singular advantages and utility, and therefore neither can be eliminated arbitrarily.

In the pore-counting method, an area (usually rectangular) of accurately known size is inscribed on a photomicrograph of accurately known magnification (usually X2000 or higher). Pores totally included within this area are tallied as whole pores; pores intersected by the area boundary lines are tallied as half pores. Calculations of pore parameters are made as follows:

TABLE 2-IV

## METALLOGRAPH PREPARATION OF POROUS TUNGSTEN, INFILTRATED WITH COPPER

- 
- I. Initial Surface Condition - Machined or Machine Ground
- II. Mounting
- A. Bakelite<sup>(a)</sup>
  - B. Pressure, 4200 psi; maximum temperature  $\approx 150^{\circ}\text{C}$
  - C. Hold at above pressure and temperature for about 6 minutes.
- III. Hand Grinding
- A. Wet Papers
    1. 240-grit silicon carbide
    2. 320-grit silicon carbide
    3. 400-grit silicon carbide
    4. 600-grit silicon carbide
  - B. Grind in sequence A, keeping specimen as flat as possible.
- IV. Polishing
- A. Preliminary (to remove most of surface deformation)
    1. Linde A alumina ( $0.3\mu$ ) slurry with  $\text{H}_2\text{O}$  on nylon cloth<sup>(b)</sup>
    2. Wheel speed, 163 rpm; pressure applied, heavy
    3. Polish with hand rotation for the minimum time necessary to remove microscopic scratches.
  - B. Final (to remove residual surface deformation)
    1. Linde B alumina ( $0.05\mu$ ) slurry with modified Murakami's etchant<sup>(d)</sup> on microcloth (c)
    2. Wheel speed, 163 rpm; pressure applied, light
    3. Polish with hand rotation for 5-10 sec. or until grain boundaries become faintly visible.
- V. Differential Oxidation Etch (to provide contrast between tungsten matrix and infiltrant)<sup>(e)</sup>
- A. Heat in air oven at  $140-155^{\circ}\text{C}$  for a minimum of 10 minutes.
  - B. Repeat A until desired contrast is obtained.
- 

(a) Buehler Catalog number 20-3300

(b) Buehler Catalog number 40-7058

(c) Buehler Catalog number 40-7208

(d) 15 gm KOH, 1 gm  $\text{K}_3\text{Fe}(\text{CN})_6$ , 250 ml  $\text{H}_2\text{O}$

(e) Step V unnecessary for noninfiltrated structures



$$\text{No. of Pores/cm}^2 \text{ (at X1 mag.)} = \frac{(\text{Total Pores Counted})(\text{Mag})^2}{(\text{Magnified Area in cm}^2)}$$

$$\text{Diam. of Av Equiv. Cylindrical Pore} = 1128 \sqrt{\frac{\text{Vol. \% of Open Porosity}}{(\text{Pores/cm}^2)}}, \mu$$

$$\text{Av Center Spacing of Pores (square symmetry)} = \frac{10^4}{\sqrt{\text{Pores/cm}^2}}, \mu$$

In the pore-intercept method, a square grid is lined on a photomicrograph of accurately known magnification. Grid spacing is adjusted to be at least 1-1/4 times the average pore spacing, estimated by preliminary approximation. Each grid line must intercept pore and solid regions of the structure in alternating sequence. Lengths of these intercepts are measured, averaged, and divided by the linear magnification of the photomicrograph. Where p and s represent average lengths of the pore and solid intercepts (in microns), pore parameters are calculated as follows:

$$\text{Av Center Spacing of Pores (square symmetry)} = p + s, \text{ microns}$$

$$\text{Diam. of Av Cylindrical Pore} = 2 \sqrt{ps/\pi}, \text{ microns}$$

$$\text{No. of Pores/cm}^2 \text{ (at X1 mag.)} = 10^8 / (p+s)^2$$

For pore structures which are (1) sufficiently coarse such that boundary definition permits accuracy of intercept measurement, and (2) interconnected in the plane of examination to such a degree that perception of individual pores becomes guesswork, the pore-intercept method is markedly superior to the pore-counting method. Thus, the intercept method alone holds promise for pore analysis of low-density (<70%) ionizers, characterized by pore continuity. On the other hand, where pores are (1) so fine as to approach the lower limit of optical lens resolution, with consequent inaccuracy of intercept measurement, and (2) predominately isolated in the plane of examination, the pore-counting method is markedly superior to the pore-intercept method. Thus, the pore-counting method is generally more appropriate for higher density ionizers. Because of the individual limitations and advantages of each method, it has been necessary to use both to comply with the requirements of this contract.

### 2.3.5 Accelerated Life Testing

Accelerated life tests without cesium were conducted on nine different ionizer compositions. Duplicate buttons (0.22" diam. x 0.04" thick) were heated at 1800°C, 1600°C, and 1500°C in time increments of 1, 1, 2 and 4 hours at each temperature. Heating was done in the Brew furnace described previously in Subsection 2.2.5. Pressure was maintained at  $<1 \times 10^{-4}$  torr during heat-up and  $<1 \times 10^{-5}$  while at test temperature. Both density and N<sub>2</sub> permeability of each button were determined after each increment of heating at each temperature. All conditions of heating and measurement were controlled with extreme care. The buttons were positioned on edge in tungsten-lined boats during heating cycles, and were handled throughout the lengthy heat-and-test period by grasping only the button edges in tweezers.

Densities of the buttons were calculated directly from their weight-to-volume ratios. N<sub>2</sub> permeabilities were determined in the apparatus described previously in Subsection 2.3.2. Data derived from these tests are presented and discussed subsequently in Section 5.

### 3. IONIZERS MADE FROM FINE TUNGSTEN MICROSPHERES WITH ALLOY ADDITIONS OF FINE ANGULAR PARTICLES

This section presents data pertaining to three series of ionizer samples. The samples were prepared in the following sequence from:

- (1) fine Ampro tungsten microspheres, with binary additions of angular Ta, Re, and Ir (as  $\text{IrO}_2$ ) particles;
- (2) three size fractions of Linde tungsten microspheres, with 10Wt.% additions of angular Ta particles; and
- (3) fine Linde tungsten microspheres with binary and ternary additions of angular Ta and Ta+Re particles.

Of the foregoing, ionizers of series (1) were not structurally homogeneous, indicating need for improved fabrication techniques. Ionizer series (2) was prepared in order to select the grade and size fraction of tungsten microspheres yielding optimum ionizer structures, as well as to improve fabrication techniques and structural homogeneity. However, structures of all W-10Ta ionizers of series (2) revealed numerous oversized pores. This severe problem was finally corrected in all ionizers of series (3) by using uniformly fine additive particles and improved blending techniques. Full ionizer evaluation was performed on series (3) ionizers because of their superiority and potential. Ionizers of series (1) and (2) were neither life tested nor duplicated for submittal to NASA-Lewis, because of structural inferiority.

#### 3.1 Ionizers from Fine Ampro Tungsten Microspheres, With and Without Binary Additions of Ta, Re, and Ir

Tungsten microspheres, with and without binary additions, were dry blended in glass jars and compacted at 60,000 psi to cylindrical pellet form. Included were tungsten controls of 1.8-4 $\mu$  Linde powder

and 0.25-2.5 $\mu$  Ampro powder, plus the latter with 10W/oTa<sup>(a)</sup>, 10W/oRe<sup>(b)</sup>, and 5W/oIr<sup>(c)</sup> binary additions. The as-pressed pellets were sectioned perpendicular to their cylindrical axes, to yield duplicate sets of samples. One set (series A) was sintered at 1800°C, the other (series B) at 2000°C, with density measurements performed after several increments of sintering time.

Densification rates at 1800°C and 2000°C are plotted in Figs. 3-1 and 3-2, respectively. Here it is seen that the Linde microspheres had higher as-pressed density than the relatively fine Ampro microspheres. This density difference is probably the effect of particle size, although pressed density may also be influenced by particle sphericity. One would normally expect lower pressed density with a finer powder and/or with a powder having the lower degree of sphericity. Referring again to Figs. 3-1 and 3-2, the 1.8-4 $\mu$  Linde powder increased progressively in density at 1800°C and more rapidly at 2000°C. On the other hand, the 0.25-2.5 $\mu$  Ampro powder initially decreased in density (expanded) at both 1800°C and 2000°C. This behavior has been interpreted as the result of absorption of smaller (or non-spherical) particles by the larger particles, with consequent growth of the latter and dimensional expansion of the compact. The magnitudes of these initial expansions were decreased at both 1800°C and 2000°C by adding 10W/oTa, and increased by additions of 10W/oRe and 5W/oIr. An indication of relative dimensional stability may be derived from the following density data:

Composition	Sintered Density After	
	7 hrs. at 1800°C	2 hrs. at 2000°C
Linde 1.8-4 $\mu$ W	82.0 <sup>*</sup> %	81.3 <sup>*</sup> %
Ampro { W-10Ta	75.6	80.3 <sup>*</sup>
W-5Ir	71.8	75.7
0.25-2.5 $\mu$ W	69.7	71.6
W-10Re	66.3	71.9

\* Extrapolated values

- (a) NRC capacitor grade SGQ-4 Ta; W/o indicates weight percentage  
 (b) Chemically reduced Re (colloidal)  
 (c) Added as mortar-ground IrO<sub>2</sub> and vacuum dissociated in situ.

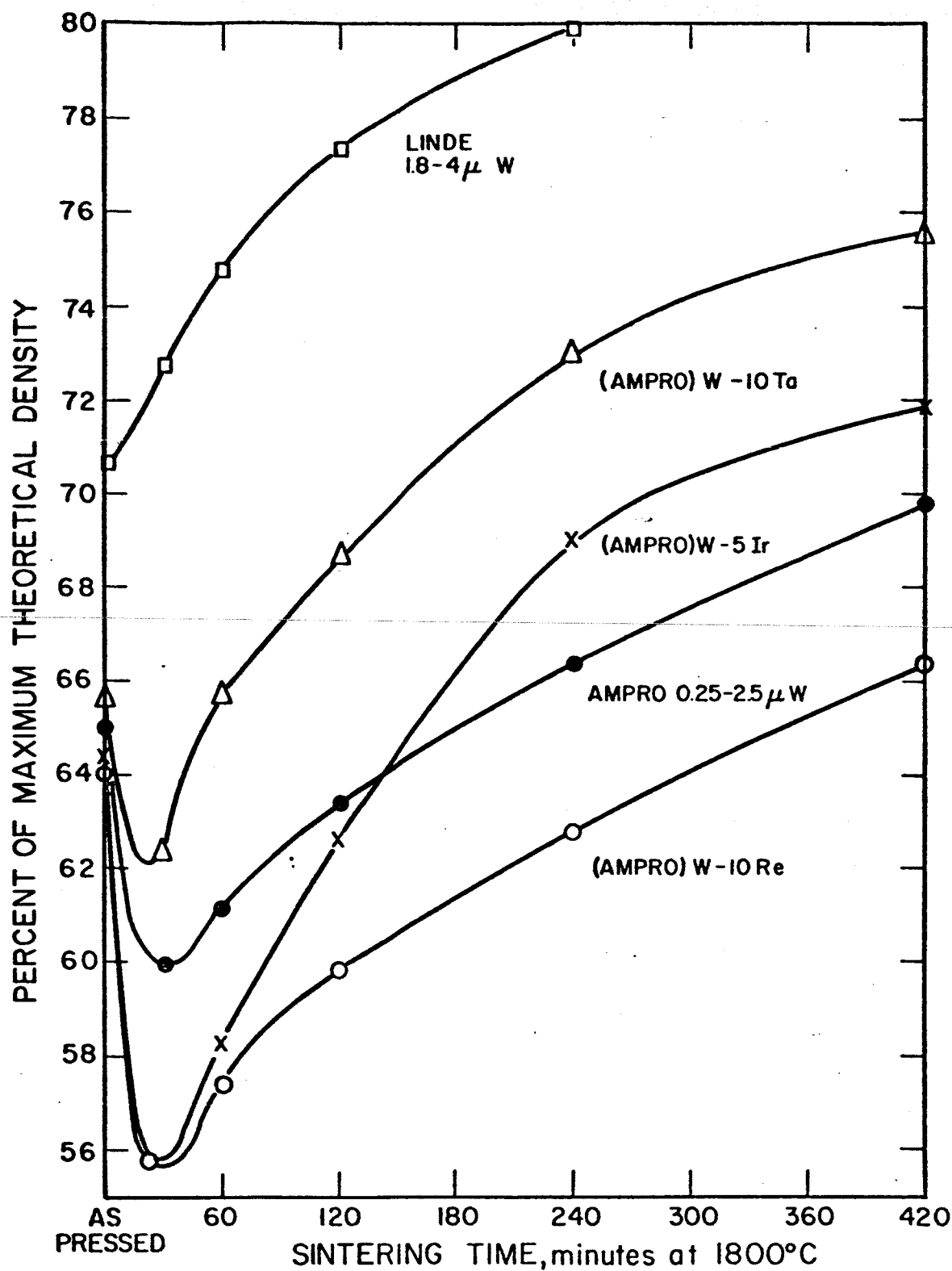


FIG. 3-1 DENSIFICATION RATES AT 1800°C OF FINE TUNGSTEN MICROSPHERES FROM TWO VENDORS, SHOWING EFFECT OF ADDITIVES ON THE AMPRO GRADE

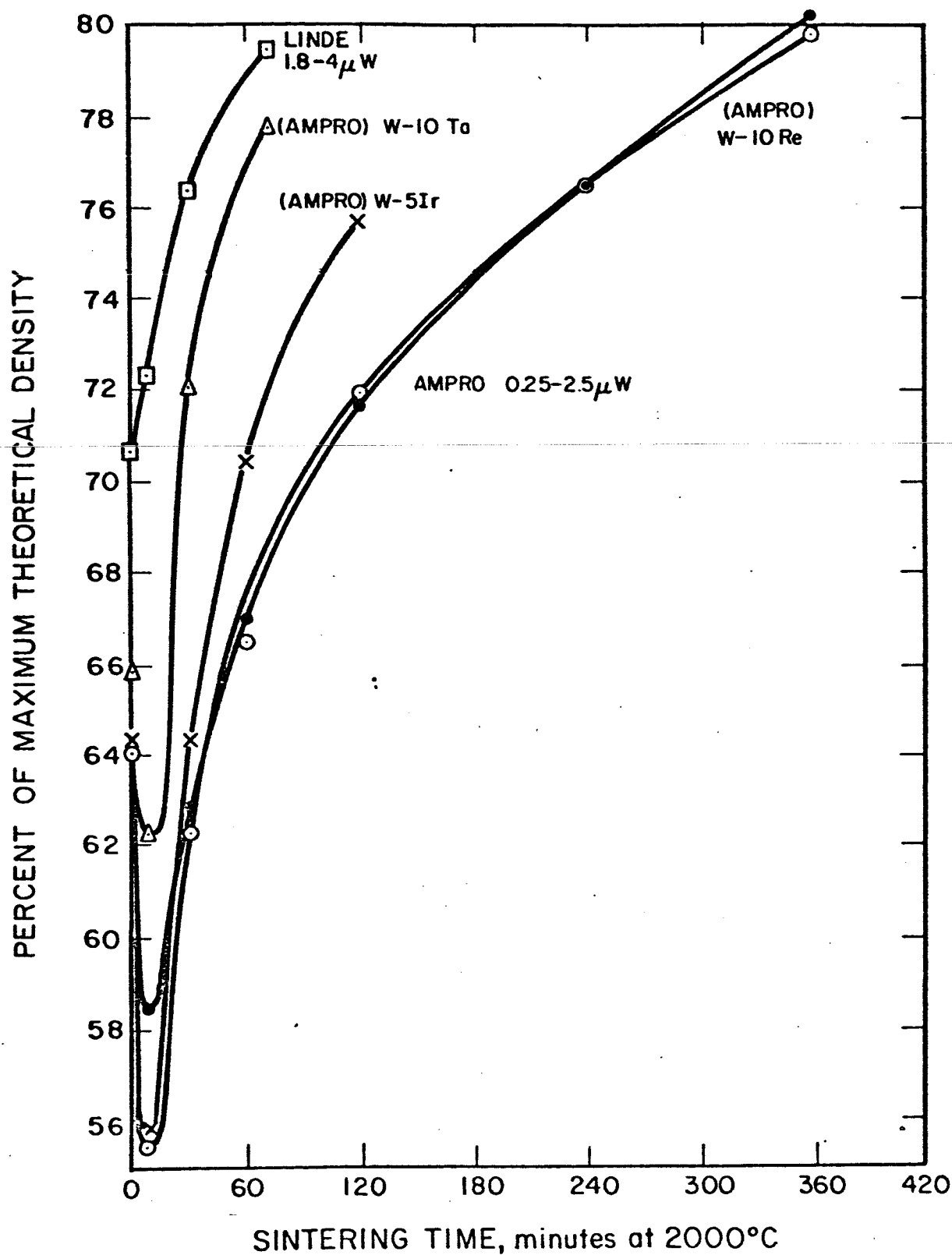
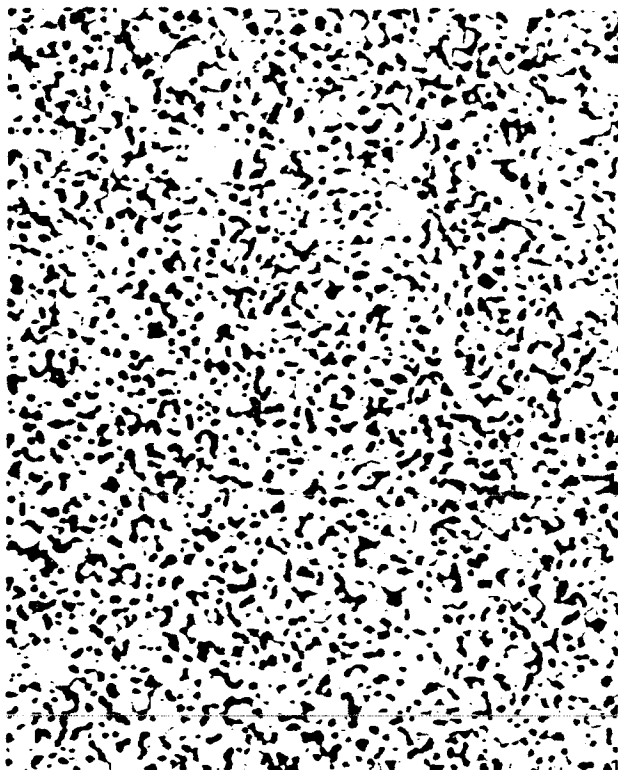


FIG. 3-2 DENSIFICATION RATES AT 2000°C OF FINE TUNGSTEN MICROSPHERES FROM TWO VENDORS, SHOWING EFFECT OF ADDITIVES ON THE AMPRO GRADE

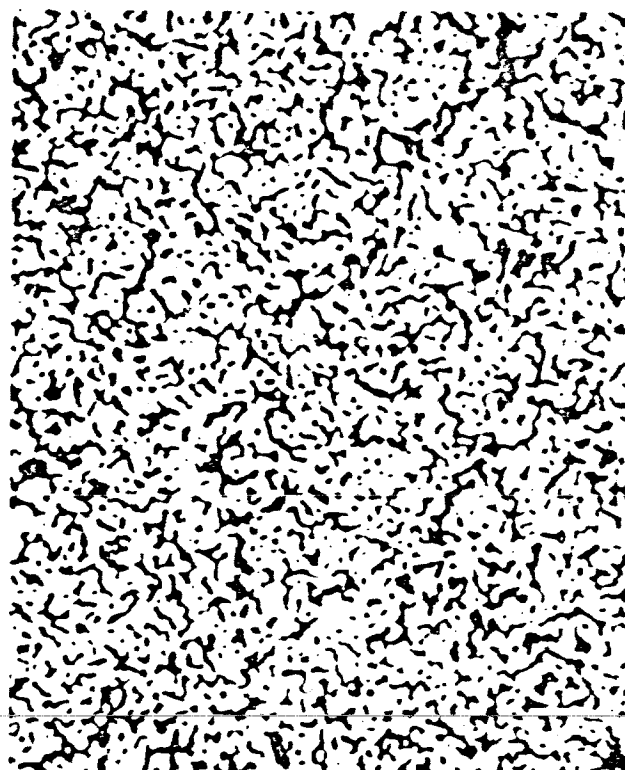
While data on density as a function of sintering time are very useful, it is also necessary to evaluate sintered microstructures. Once excessive grain growth and attendant pore coarsening have occurred during sintering, there is no way to subsequently refine the structure, i.e., to return to one having the high pore density desired. In Fig. 3-3, microstructures of the 1.8-4 $\mu$  Linde and 0.25-2.5 $\mu$  Ampro powder are compared at magnifications of X400 and X2000; sintering conditions, densities and pore parameters are also indicated. The Ampro powder required 7 hours of sintering at 1800 $^{\circ}$  to reach only 70% density, while the Linde powder required only 4 hours to reach 80%. The greater dimensional stability of the Ampro powder is attributed to grain growth (agglomeration) during the initial period of expansion, accompanied by a decrease in specific surface area which, in turn, effected a decrease in subsequent sintering (densification) rate. While pore densities of the two are comparable, average pore size of the Ampro grade is about 25% larger than the Linde grade - this in spite of the fact that the former particles were initially finer. This indicates that (in the absence of a grain growth inhibitor, such as tantalum) the 0.25-2.5 $\mu$  Ampro powder is too fine, and that the 1.8-4 $\mu$  distribution of the Linde powder is closer to optimum.

The pore parameters of series A and B pellets are compared in Table 3-I. Here, pore densities and average pore diameters indicate that the tantalum addition yielded by far the finest pore structure, iridium addition the coarsest structure, and that rhenium addition had no significant affect on structure. Photomicrographs of the four compositions in Table 3-I (2000 $^{\circ}$ C sinter) are shown at X400 in Fig. 3-4 and at X2000 in Fig. 3-5. Figure 3-4 shows the inhomogeneities incurred by inadequate blending of the Ta, IrO<sub>2</sub> and Re additions. Figure 3-5 clearly indicates grain-growth inhibition by Ta and growth promotion by Ir.



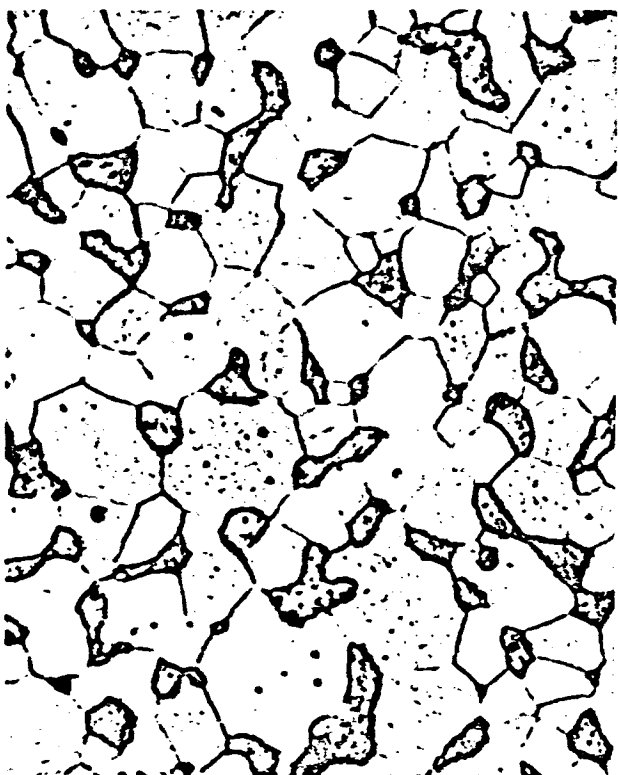
Neg. 2394

(X400)



Neg. 2391

(X400)

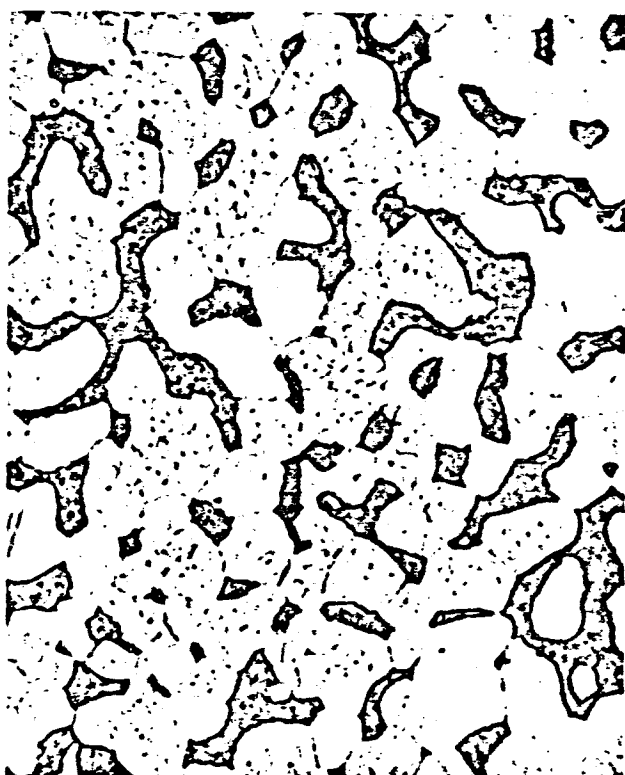


Neg. 2419

Den = 79.90%

(X2000)

Pore Den =  $2.71 \times 10^6/\text{cm}^2$ ;  
Av Pore Diam = 2.98 $\mu$



Neg. 2408

Den = 69.74%

(X2000)

Pore Den =  $2.79 \times 10^6/\text{cm}^2$ ;  
Av Pore Diam = 3.7 $\mu$

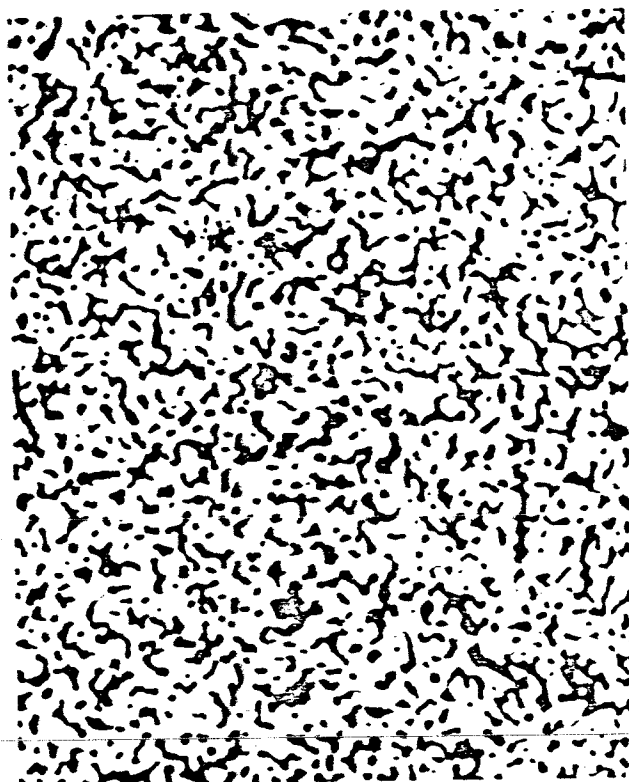
FIG. 3-3 STRUCTURES OF UNALLOYED LINDE AND AMPRO TUNGSTEN MICROSPHERES, VACUUM SINTERED AT 1800°C



TABLE 3-I

VARIOUS PARAMETERS OF SINTERED IONIZERS,  
 INDICATING EFFECT OF BINARY ADDITIONS  
 TO AMPRO (0.25-2.5 $\mu$ ) TUNGSTEN MICROSPHERES

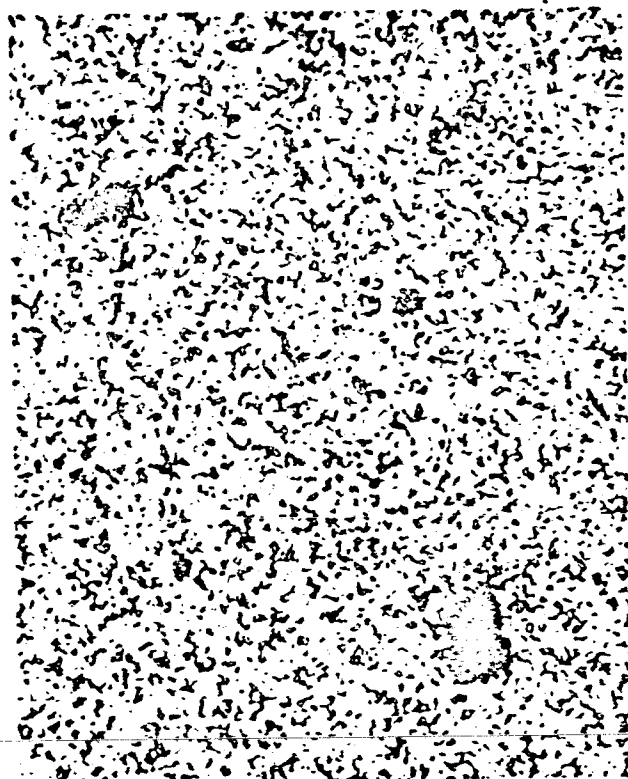
Comp, W/o	No. of Ionizers	Sintering		Av Den, % of theor.	Av N <sub>2</sub> Permeability, gm·cm <sup>-1</sup> ·sec <sup>-1</sup> ·torr <sup>-1</sup>	Pores per cm <sup>2</sup>	Av Pore Diam, $\mu$
		Temp, °C	Time, hrs				
Ampro W (Control)	12	1800	7	69.22	$1.591 \times 10^{-6}$	$2.79 \times 10^6$	3.71
	13	2000	6	80.10	$0.482 \times 10^{-6}$	$1.53 \times 10^6$	3.92
W-10Ta	10	1800	7	76.60	$0.124 \times 10^{-6}$	$5.21 \times 10^6$	2.44
	4	2000	1	78.24	$0.097 \times 10^{-6}$	$5.61 \times 10^6$	2.21
W-5Ir	9	1800	7	72.74	$1.479 \times 10^{-6}$	$1.64 \times 10^6$	4.68
	9	2000	2	76.13	$0.969 \times 10^{-6}$	$1.18 \times 10^6$	5.09
W-10Re	25	1800	7	66.42	$1.638 \times 10^{-6}$	$2.76 \times 10^6$	3.94
	5	2000	6	78.79	$0.641 \times 10^{-6}$	$1.76 \times 10^6$	3.71



Neg. 2429

Den = 80.21%

Tungsten



Neg. 2433

Den = 77.73%

W-10W/oTa



Neg. 2430

Den = 75.67%

W-5W/oIr



Neg. 2431

Den = 79.76%

W-10W/oRe

FIG. 3-4 STRUCTURES SHOWING EFFECTS OF ALLOY ADDITIONS ON AMPRO LOT U TUNGSTEN MICROSPHERES (0.25-2.5 $\mu$ ), VACUUM SINTERED AT 2000°C (X400)



Neg. 2437  $1.53 \times 10^6$  pores/cm<sup>2</sup>  
Den = 80.21%  
Tungsten  
d = 3.92μ



Neg. 2452  $5.61 \times 10^6$  pores/cm<sup>2</sup>  
Den = 77.73%  
W-10W/oTa  
d = 2.21μ



Neg. 2440  $1.18 \times 10^6$  pores/cm<sup>2</sup>  
Den = 75.67%  
W-5W/oIr  
d = 5.09μ



Neg. 2442  $1.76 \times 10^6$  pores/cm<sup>2</sup>  
Den = 79.76%  
W-10W/oRe  
d = 3.71μ

FIG. 3-5 STRUCTURES SHOWING EFFECTS OF ALLOY ADDITIONS ON AMPRO LOT U TUNGSTEN MICROSPHERES (0.25-2.5μ), VACUUM SINTERED AT 2000°C (X2000)

Nitrogen permeability data for series A and B composite ionizers are given in Tables B-I and B-II of Appendix B. Average data from Tables B-I and B-II are retabulated in Table 3-I. Here it may be noted that permeabilities of the W (control), W-5Ir, and W-10Re ionizers are much higher than those of the W-10Ta. This is correlated with the grain-growth and pore-coarsening tendencies of the former compositions, seen in Fig. 3-4. The data of Table 3-I also show that, when tantalum is added to very fine tungsten microspheres, a sintered density of 76.6 percent is too high. In order to retain adequate permeability, a sintered density (for W-Ta alloys) of 75 percent or even lower, is indicated.

Based on these series, there is little doubt that tantalum is a much better binary additive, with respect to the preservation of high pore density and fine pore size, than either iridium or rhenium. In addition, tantalum powder is appreciably cheaper than either iridium or rhenium.

### 3.2 Ionizers from Three Size Fractions of Linde Tungsten Microspheres, With and Without Binary Addition of Ta

Having compared the affects of Ta, Ir and Re binary additions on 0.25-2.5 $\mu$  Ampro tungsten (Section 3.1), it was considered necessary to compare the merit of three Linde tungsten fractions with that of the 0.25-2.5 $\mu$  Ampro tungsten (1) in the unalloyed condition, and (2) with 10W/o of tantalum added, tantalum being the only grain-growth inhibitor of the elements under investigation.

Twenty pounds of Line W microspheres were classified at Ampro. Three fractions, designated "fine" (1.874 lbs), "medium" (5.671 lbs) and "coarse" (12.25 lbs), were derived. The goal of the classification was to capture the largest possible percentage of 0.5-2.5 $\mu$  particles in the "fine" fraction. Subsequent particle size analysis of this fraction indicated 78.1 percent by count of particles in the 0.25-2.5 $\mu$  diameter range, very similar to the fine Ampro powder.

For this experiment, the fine and medium Linde fractions were used, in addition to a blend of 24W/o fine + 76W/o medium fractions. This 1/4-to-3/4 blend ratio equals the fine-to-medium fraction yield ratio, and was selected on the basis of economy. Pellets of tungsten fine, blended, and medium fractions, with 10W/oTa<sup>\*</sup>, were also prepared, together with a 0.25-2.5 $\mu$  Ampro tungsten control sample.

Seven pellets were prepared by identical blending, loading, and pressing techniques. The weighed powders were vacuum-dried, tumbled in glass jars containing hardened-steel ball bearings, dry-box loaded into rubber tubes, and pressed hydrostatically and simultaneously at 60,000 psi. Densities were determined on the as-pressed pellets, and also after vacuum-sintering for 15, 30, 60, 120, 240, and 420 minutes at 1800°C.

Densification rates obtained on the seven pellets are plotted in Fig. 3-6. As indicated, pressed densities of all Linde tungsten-base pellets ranged from 68.0 percent to 71.8 percent, while pressed density of the Ampro tungsten control was 64.7 percent. This difference was noted previously and attributed to a lower degree of sphericity and packing efficiency of the Ampro powder. All fractions of unalloyed Linde powder, starting at a higher pressed density, reached the 78 to 80 percent density range first. Of the unalloyed Linde samples, only the blended fraction showed a tendency to expand - demonstrating again that small high-energy particles are rapidly absorbed by larger adjacent particles to cause expansion of the powder mass. All pellets of Linde tungsten with 10W/oTa expanded initially. The unalloyed Ampro control expanded to a still greater degree.

The curves shown in Fig. 3-6 are replotted in Fig. 3-7 to indicate the percentage change in density as a function of sintering time. In such a plot all curves must originate from the same point, facilitating analysis of the data. The fact that the densification

---

\*"Submicron" capacitor grade QBTF-1 from National Research Corporation.

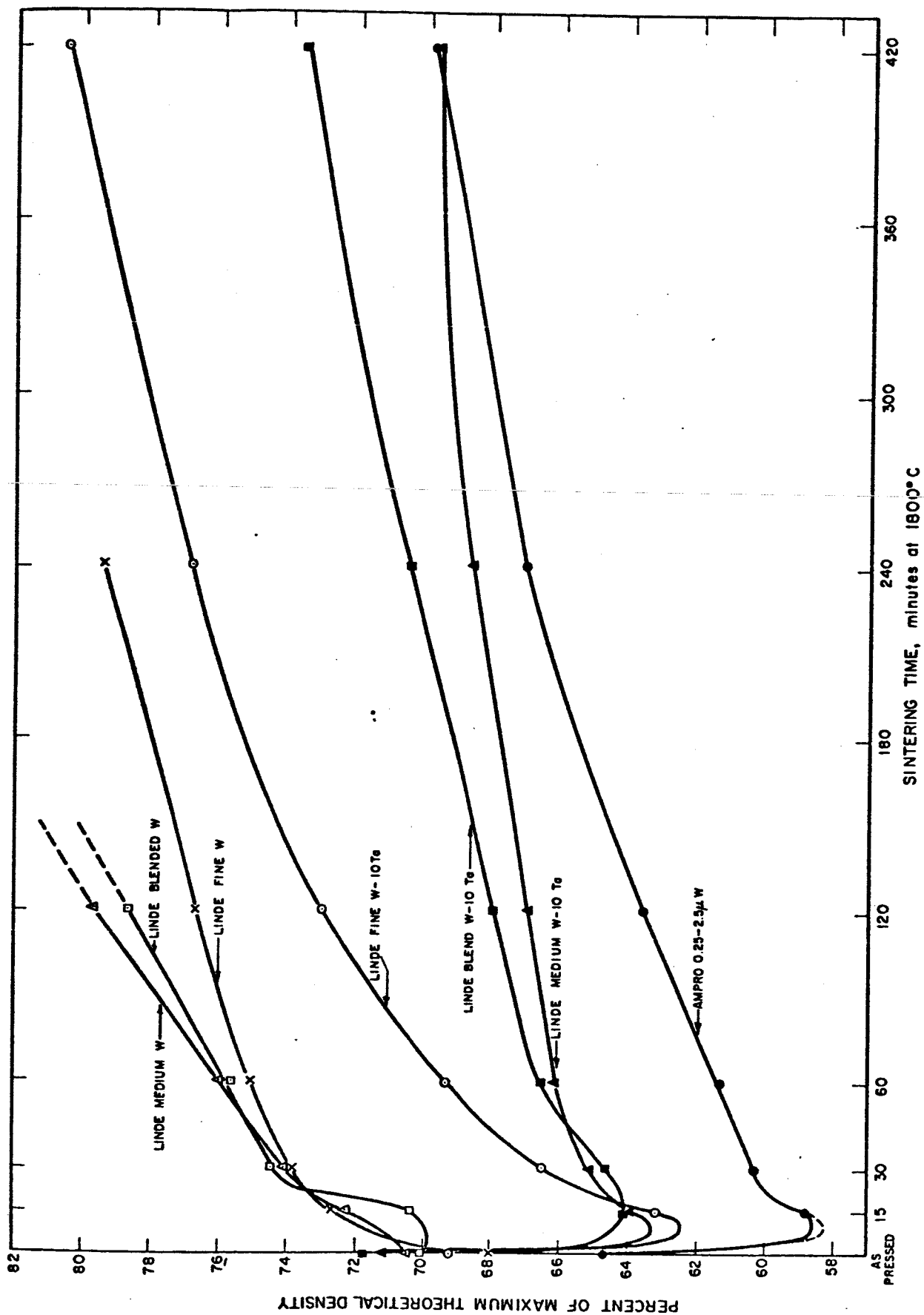


FIG. 3-6 DENSIFICATION RATES AT 1800°C OF THREE SIZE FRACTIONS OF LINDE MICROSPHERES WITH AND WITHOUT 10 W/oTa ADDITIONS, COMPARED WITH 0.25-2.5μ AMPRO MICROSPHERES

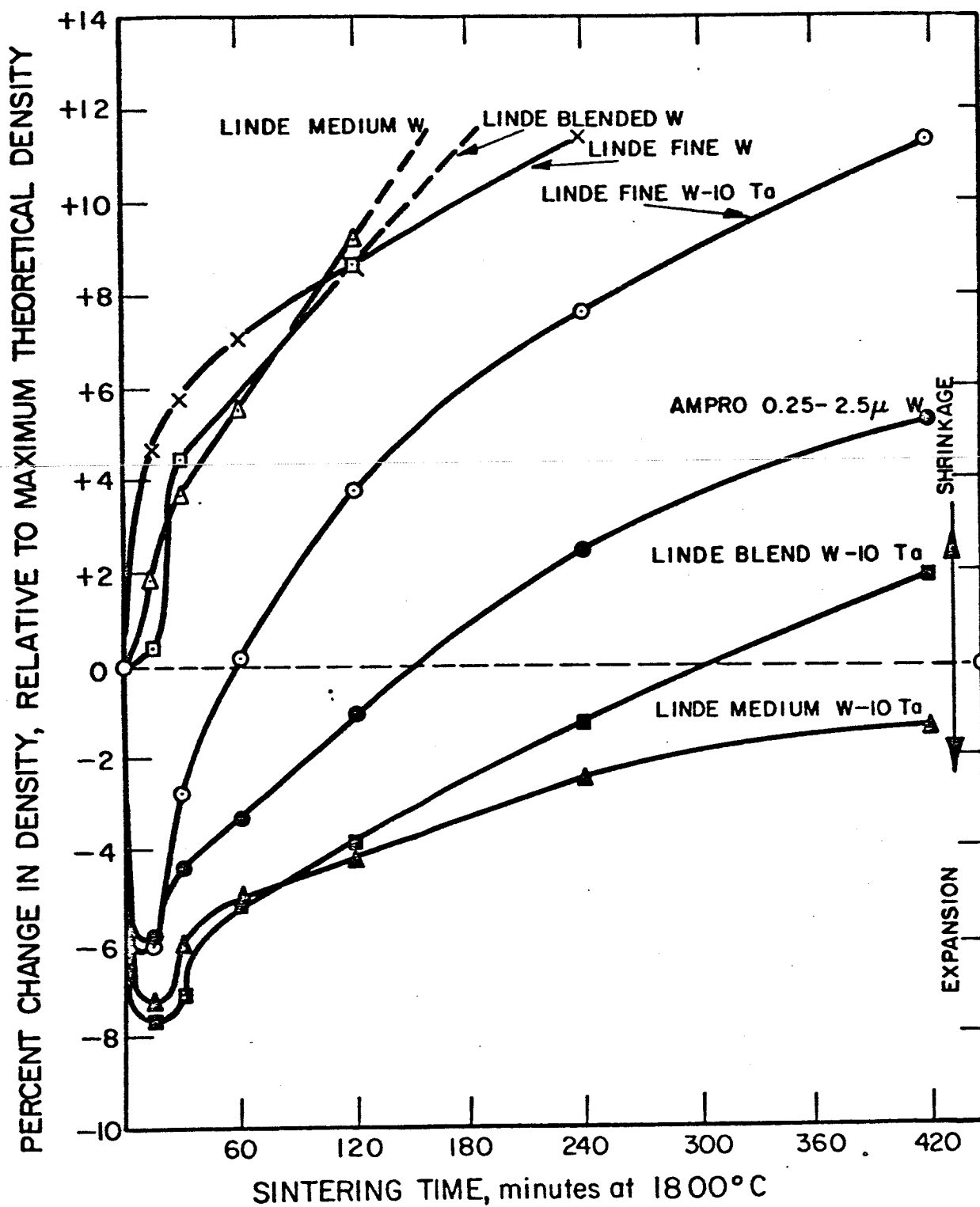


FIG. 3-7 DENSIFICATION RATES AT 1800°C OF THREE SIZE FRACTIONS OF LINDE MICROSPHERES WITH AND WITHOUT 10 W/oTa ADDITIONS, COMPARED WITH 0.25-2.5 $\mu$  AMPRO MICROSPHERES

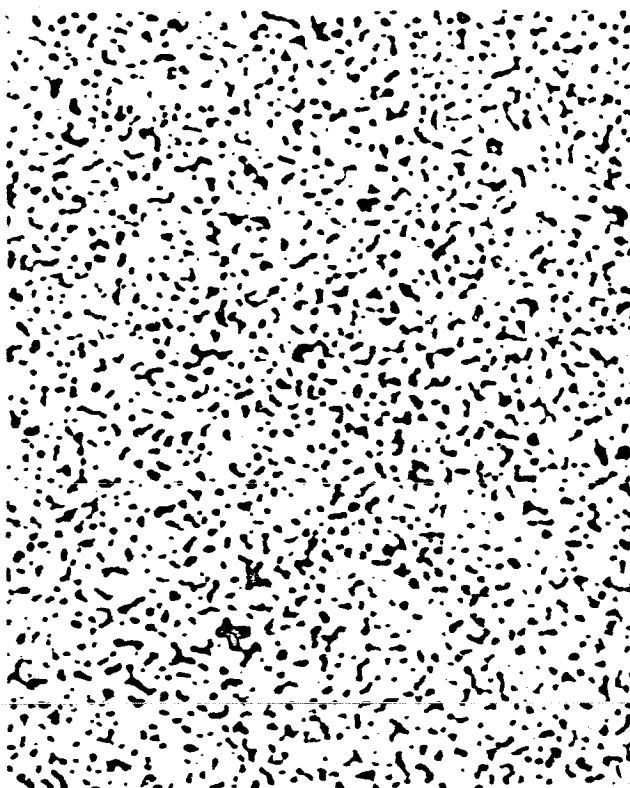
rate of the fine Linde tungsten became slower than that of the medium Linde tungsten indicates that the former underwent early grain growth, with consequent decrease in specific surface area. Apparently, addition of 10W/oTa prevented early grain growth, such that terminal densification rates of the binary alloys are in the order expected (the finest W-base pellet, with largest specific surface, sintering the most rapidly).

Pore structures of the sintered Linde and Ampro (0.25-2.5 $\mu$ ) microspheres are compared in Fig. 3-8. The Linde tungsten reached a density of 79.4 percent in 4 hours at 1800°C; the Ampro grade reached only 69.9 percent in 7 hours at 1800°C, illustrating the greater dimensional stability of the Ampro powder grade. However, Fig. 3-8 indicates that the Linde powder compact retained a 33 percent high pore density and a 31 percent small pore size, despite its higher sintered density. This demonstrates the superior pore-structural stability of the Linde powder grade. The relatively coarse grain and pore structures of the Ampro tungsten are synonymous with low specific surface area which, in turn, was the probable reason for its markedly retarded shrinkage rate. The tendency of Ampro powder to agglomerate and form a relatively coarse pore structure (probably early in sintering) made it a less desirable base powder than the Linde powder for ionizer fabrication.

Pore structures and parameters of the sintered Linde powder series are shown in Fig. 3-9 at X400 and in Fig. 3-10 at X2000. These structures are labeled "fine", "blended", and "medium" fractions, since the particle size of only the fine fraction was determined. The latter was found to be approximately equal in size distribution to 0.25-2.5 $\mu$  Ampro powder. As noted in Figs. 3-9 and 3-10, the "fine" fraction did not yield as high a pore density, or as small a pore size, as did the "blended" and "medium" powder fractions. This fact, plus evidence of grain growth in Fig. 3-10, indicates that particle size of the "fine" fraction was less than optimum in the absence of a stabilizing additive, such as tantalum.



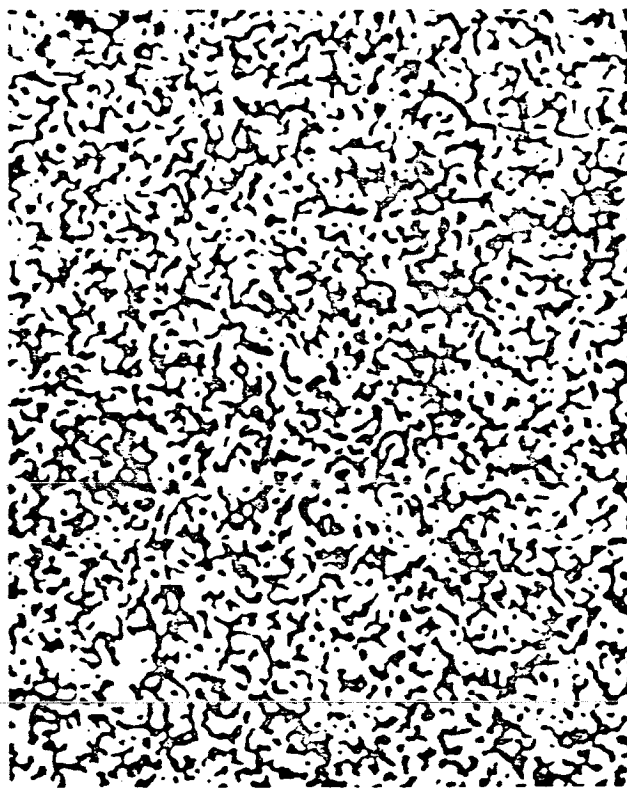
Linde (0.25-2.5 $\mu$ ) W, Sintered 4 hours



Neg. 2457

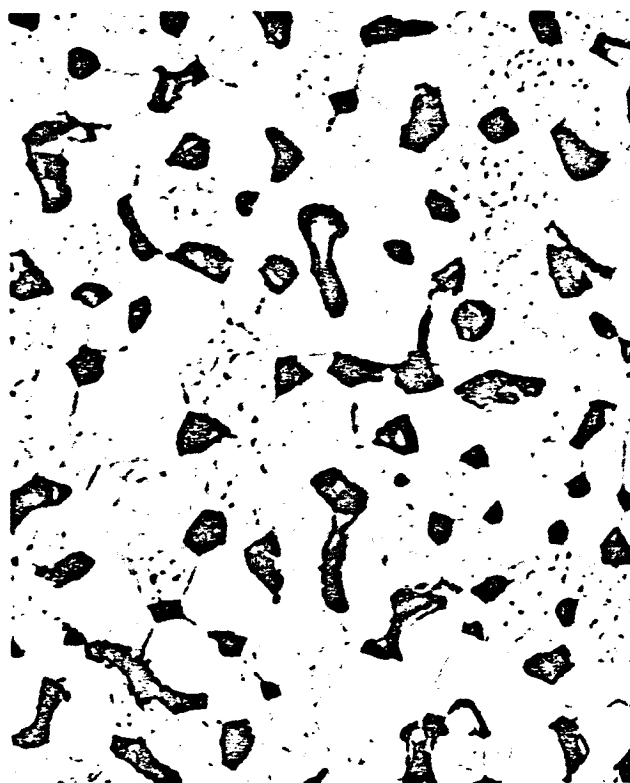
(X400)

Ampro (0.25-2.5 $\mu$ ) W, Sintered 7 hours



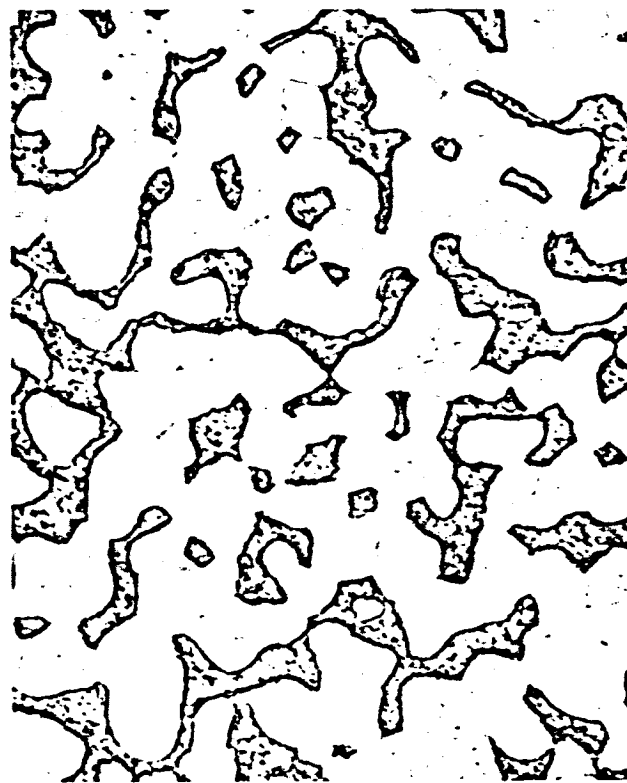
Neg. 2454

(X400)



Neg. 2477      Den = 79.43%      (X2000)

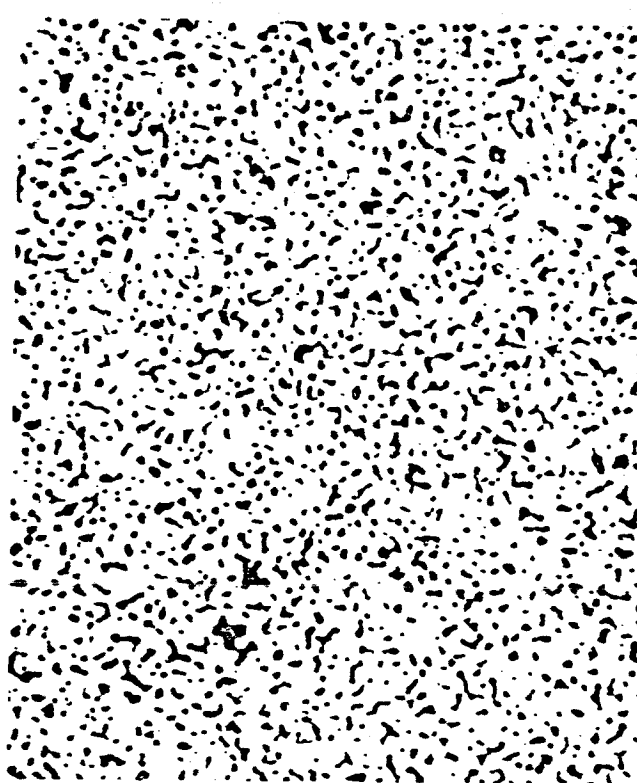
Pore Den =  $3.02 \times 10^6 / \text{cm}^2$   
Av Pore Diam = 2.86 $\mu$



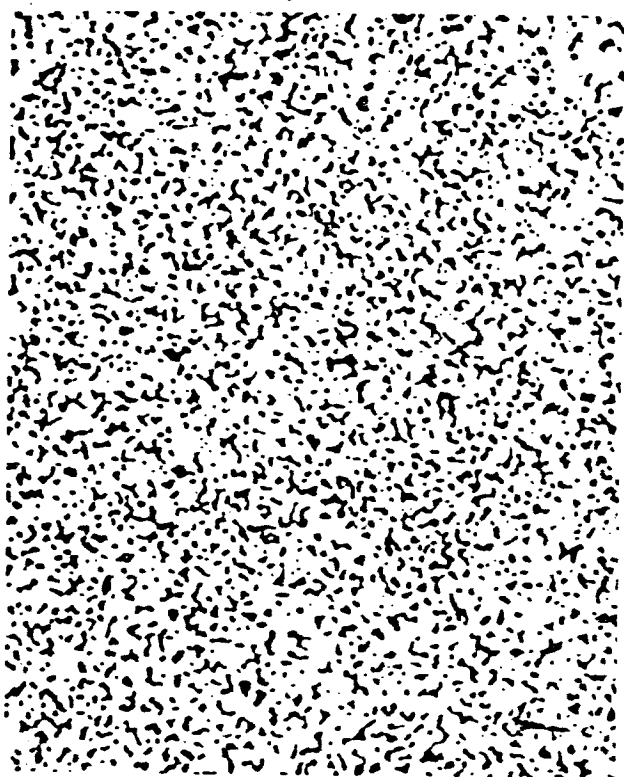
Neg. 2464      Den = 69.90%      (X2000)

Pore Den =  $2.26 \times 10^6 / \text{cm}^2$   
Av Pore Diam = 4.12 $\mu$

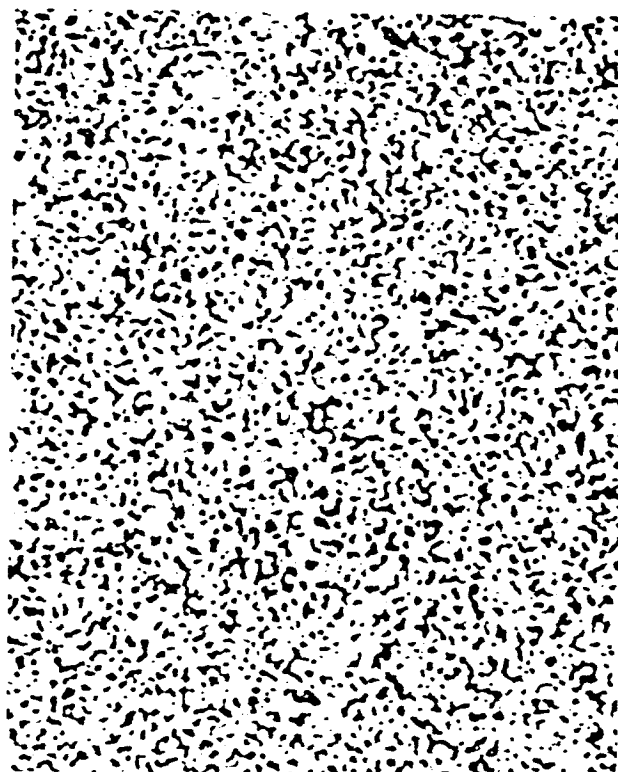
FIG. 3-8 STRUCTURES OF UNALLOYED LINDE AND AMPRO (0.25-2.5 $\mu$ ) TUNGSTEN MICRO-SPHERES, VACUUM SINTERED AT 1800°C



Neg. 2457  $3.02 \times 10^6$  pores/cm<sup>2</sup>  
 Den = 79.43%  $d = 2.86 \mu$   
Fine Fraction, Sintered 4 hours

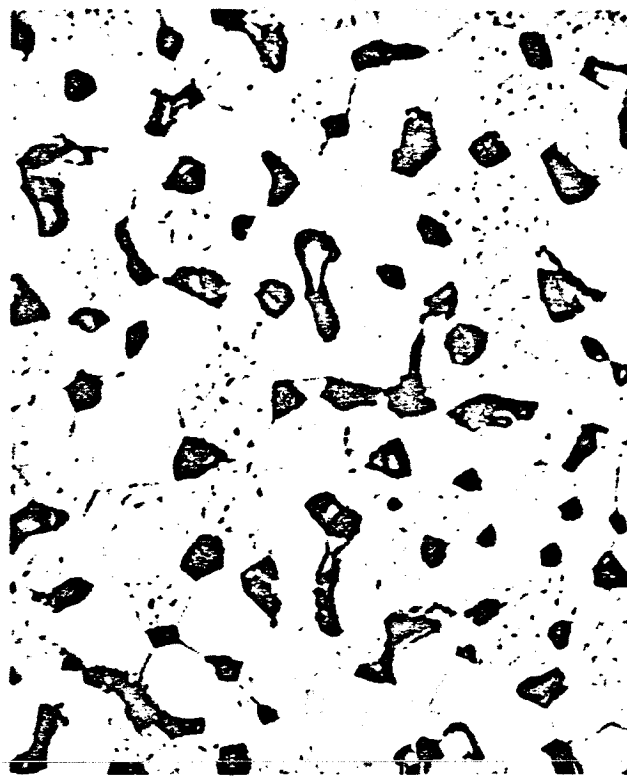


Neg. 2456  $3.96 \times 10^6$  pores/cm<sup>2</sup>  
 Den = 78.70%  $d = 2.56 \mu$   
Blended Fraction, Sintered 2 hours



Neg. 2455  $3.91 \times 10^6$  pores/cm<sup>2</sup>  
 Den = 79.64%  $d = 2.50 \mu$   
Medium Fraction, Sintered 2 hours

FIG. 3-9 STRUCTURES OF THREE FRACTIONS OF LINDE TUNGSTEN MICROSPHERES, VACUUM  
 SINTERED AT 1800°C  
 (X400)



Neg. 2477  $3.02 \times 10^6$  pores/cm<sup>2</sup>  
 Den = 79.43%  $\bar{d} = 2.86\mu$   
Fine Fraction, Sintered 4 hours



Neg. 2473  $3.96 \times 10^6$  pores/cm<sup>2</sup>  
 Den = 78.70%  $\bar{d} = 2.56\mu$   
Blended Fraction, Sintered 2 hours



Neg. 2468  $3.91 \times 10^6$  pores/cm<sup>2</sup>  
 Den = 79.64%  $\bar{d} = 2.50\mu$   
Medium Fraction, Sintered 2 hours

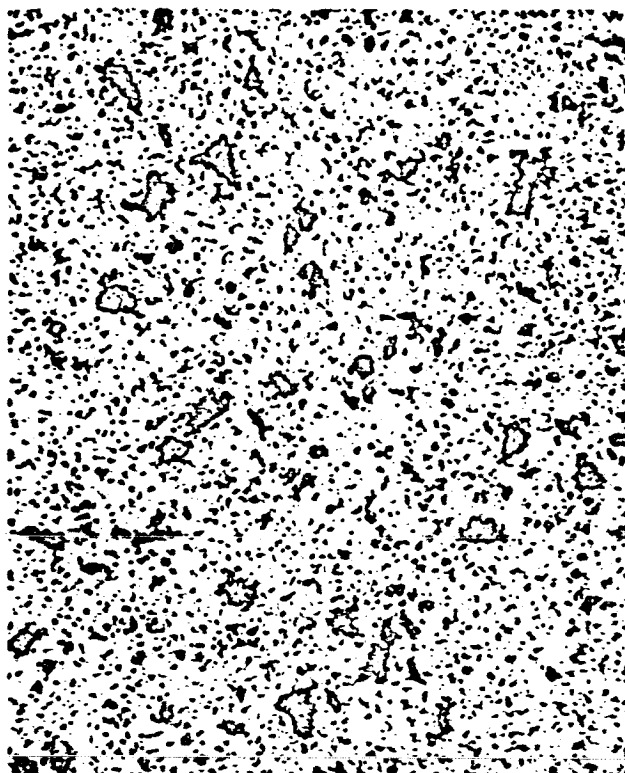
FIG. 3-10 STRUCTURES OF THREE FRACTIONS OF LINDE TUNGSTEN MICROSPHERES, VACUUM SINTERED AT 1800°C (X2000)

Pore structures and parameters of the foregoing Linde-tungsten series, but with 10W/o of NRC QBTF-1 tantalum added, are shown in Fig. 3-11 at X400 and in Fig. 3-12 at X2000. The parameters noted under each micrograph indicate that the finer the tungsten base powder, the denser and finer the pores in the sintered structures. The "fine" W-10Ta shows the highest pore density ( $8.10 \times 10^6$  pores/cm<sup>2</sup>) and smallest average pore size ( $1.68\mu$ ) fabricated at EOS (to that time), again proving strong growth inhibition by Ta. Numerous large voids are also shown in the W-10Ta microstructures of Fig. 3-11. Experiments to improve pore homogeneity of this alloy are described below.

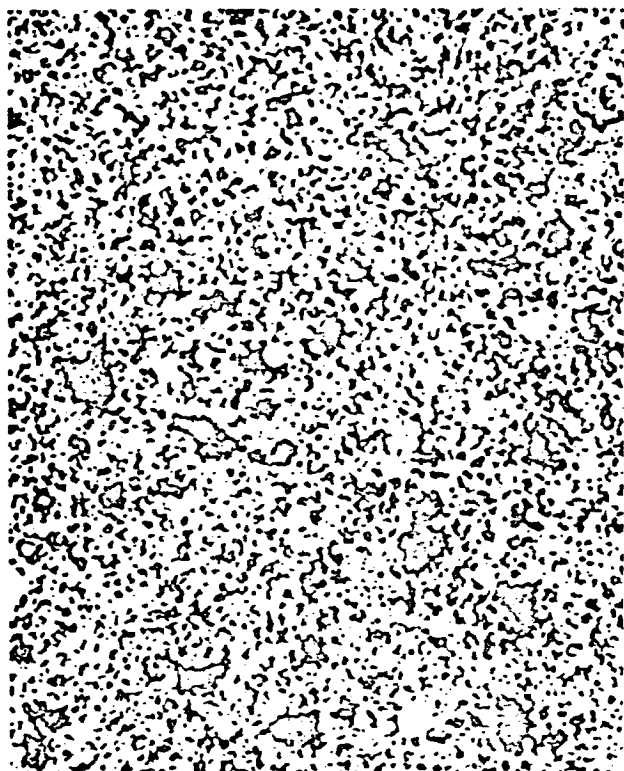
Due to structural homogeneities occurring in alloy ionizers previous to this juncture (see Figs. 3-4 and 3-11), a series of experiments was conducted to determine how homogeneity could be improved. The W-10Ta mixture was selected as the standard for these fabrication experiments.

Using 1-4 $\mu$  tungsten microspheres plus 10W/o of NRC Grade QBTF-1 tantalum, pellets were compacted hydrostatically at 60,000 psi. The pellets were sectioned into two parts, only one of which was sintered. Both the as-pressed and sintered parts were infiltrated with Cu-2Fe at 1200°C under argon. Infiltration of the as-pressed parts was only superficial, indicating a reduction in wettability due to the presence of oxide films on the particles. The relative ease with which the sintered parts were infiltrated indicates that concentration of surface oxides was greatly reduced by diffusion or dissociation during vacuum sintering.

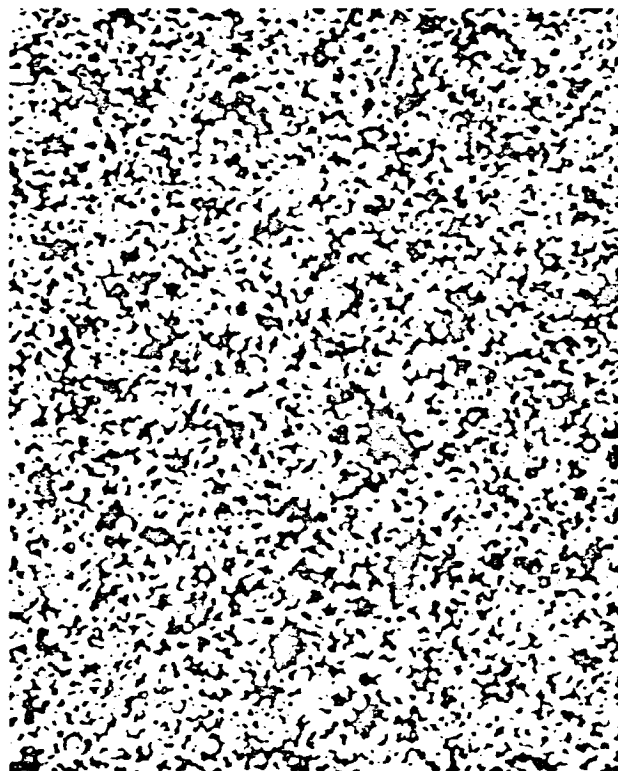
Variables investigated and results obtained are described in the following tabulation:



Neg. 2460  $8.10 \times 10^6$  pores/cm<sup>2</sup>  
 Den = 80.52%  $d = 1.68 \mu$   
Fine Fraction, Sintered 7 hours

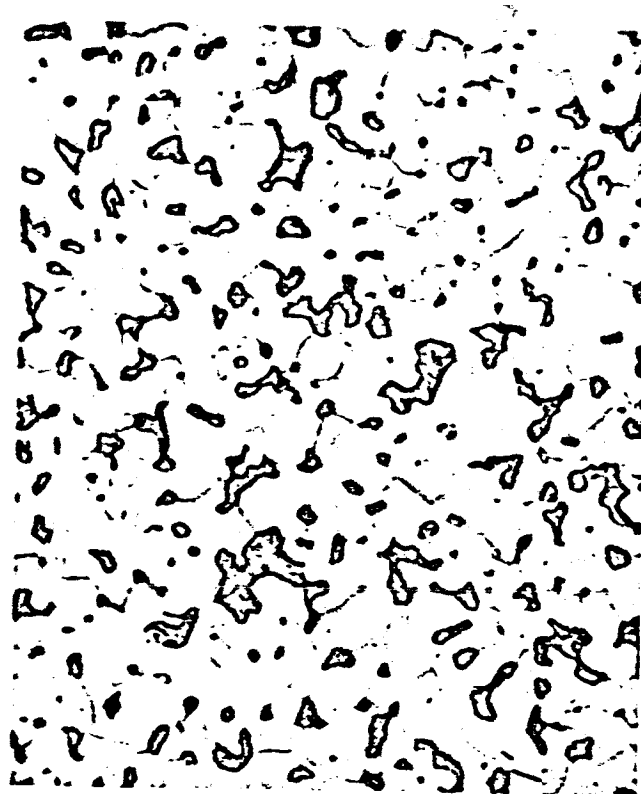


Neg. 2459  $5.78 \times 10^6$  pores/cm<sup>2</sup>  
 Den = 73.67%  $d = 2.41 \mu$   
Blended Fraction, Sintered 7 hours

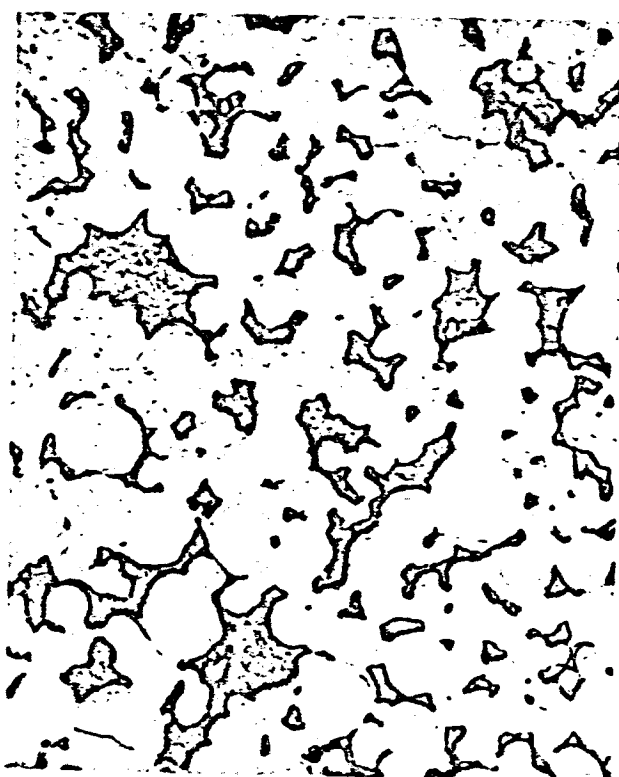


Neg. 2458  $4.24 \times 10^6$  pores/cm<sup>2</sup>  
 Den = 69.77%  $d = 3.01 \mu$   
Medium Fraction, Sintered 7 hours

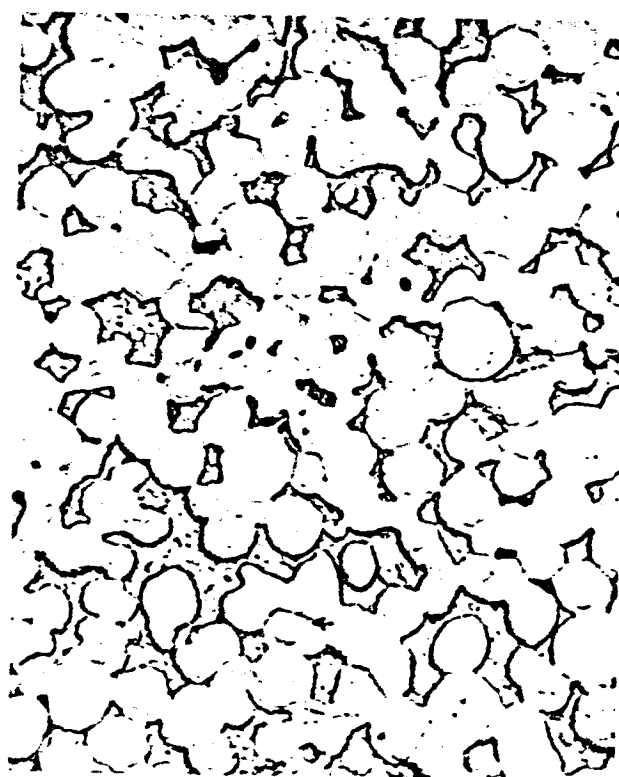
FIG. 3-11 STRUCTURES SHOWING EFFECT OF 10 W/o SUBMICRON TANTALUM ON THREE SIZE FRACTIONS OF LINDE TUNGSTEN MICROSPHERES, VACUUM SINTERED AT 1800°C (X400)



Neg. 2481  $8.10 \times 10^6$  pores/cm<sup>2</sup>  
 Den = 80.52%  $\bar{d} = 1.68 \mu$   
Fine Fraction, Sintered 7 hours



Neg. 2486  $5.78 \times 10^6$  pores/cm<sup>2</sup>  
 Den = 73.67%  $\bar{d} = 2.41 \mu$   
Blended Fraction, Sintered 7 hours



Neg. 2489  $4.24 \times 10^6$  pores/cm<sup>2</sup>  
 Den = 69.77%  $\bar{d} = 3.01 \mu$   
Medium Fraction, Sintered 7 hours

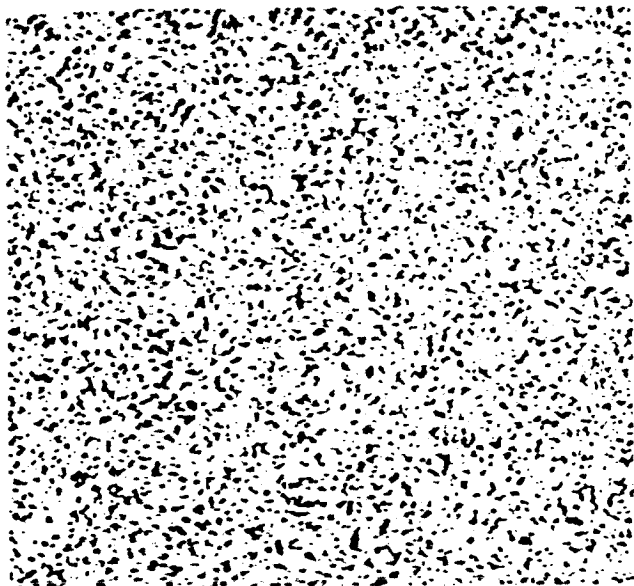
FIG. 3-12 STRUCTURES SHOWING EFFECT OF 10 W/o SUBMICRON TANTALUM ON THREE SIZE FRACTIONS OF LINDE TUNGSTEN MICROSPHERES, VACUUM SINTERED AT 1800°C (X2000)

Pellet Series	Blending		Packing Techniques (Dried Mixtures)	Pressed Density (Percent)	Microstructures	
	Vehicle	Mode			Pressed	Sintered
D	None	Ball Milling	Tapping	69.05	All contain dense Ta-rich areas, plus numerous oversized voids	Ta-rich areas no longer evident;
E	None	Ball Milling	Vibration	70.73		oversized voids fewer but larger
F	Methanol	Ball Milling	Tapping	69.62		
G	Methanol	Hi-Speed Rotor	Tapping	68.10		

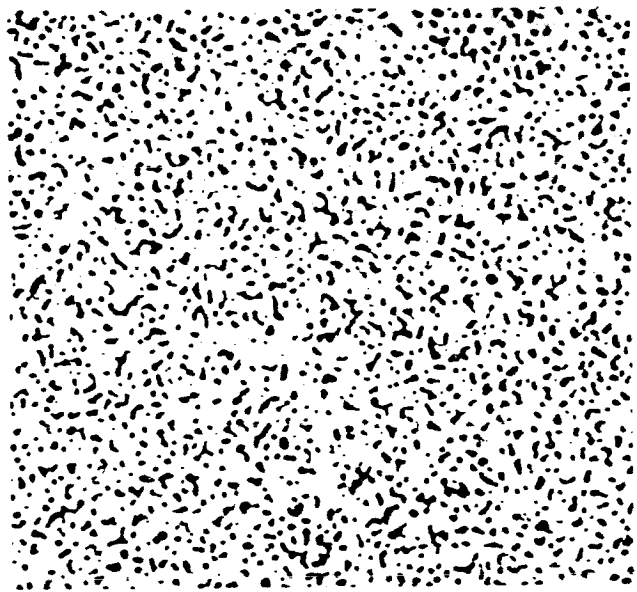
Typical microstructures, obtained before and after sintering, are shown in Fig. 3-13; the pore structure of the tungsten control is observed to be very uniform. On the other hand, the W-10Ta structure is very inhomogeneous, despite the violent slurry-blending used. Figure 3-14 photomicrographs of a W-10Ta structure before sintering, show three general types of inhomogeneities:

- Type I Oversized particles of tantalum;
- Type II Dense areas, composed of tungsten microspheres embedded in tantalum-rich matrix;
- Type III Voids, surrounded by a dense shell of tungsten microspheres embedded in a tantalum-rich matrix.

Inhomogeneities of Type I were traced to the presence of oversized tantalum particles in the starting powder, labeled "submicron" tantalum by the vendor. Upon sintering, these large tantalum particles obviously diffused into the adjacent tungsten to produce oversized voids. Inhomogeneities of Types II and III were believed to result from tantalum agglomerates in the powder blend. The agglomerates persisted despite ball milling and high-speed rotary blending of the W-Ta-methanol slurries. At this point it became apparent that deagglomeration of fine angular tantalum required the application of a large force, and that only when these agglomerates were broken apart could uniform blending with tungsten be achieved.

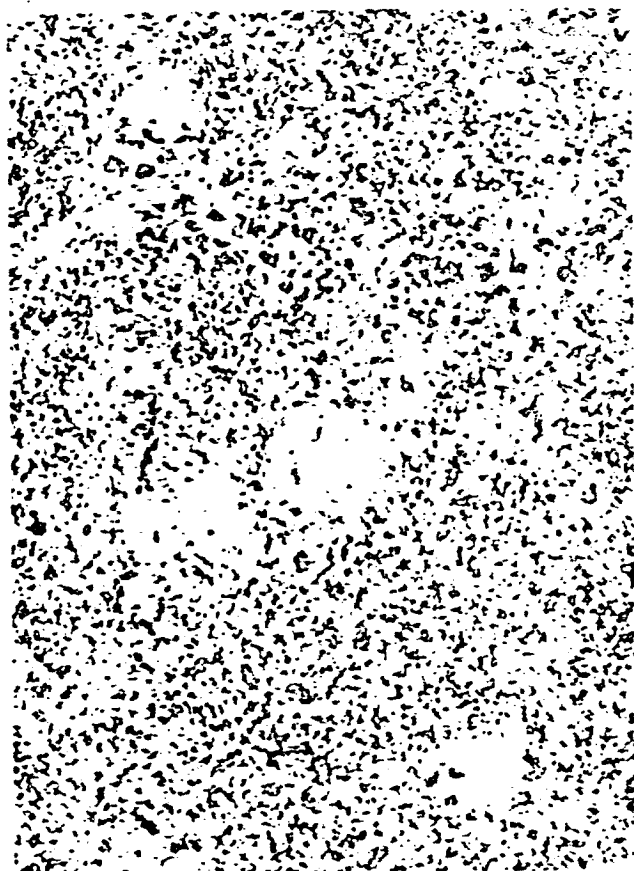


Neg. 2585 Before sintering  $\rho = 69.0\%$

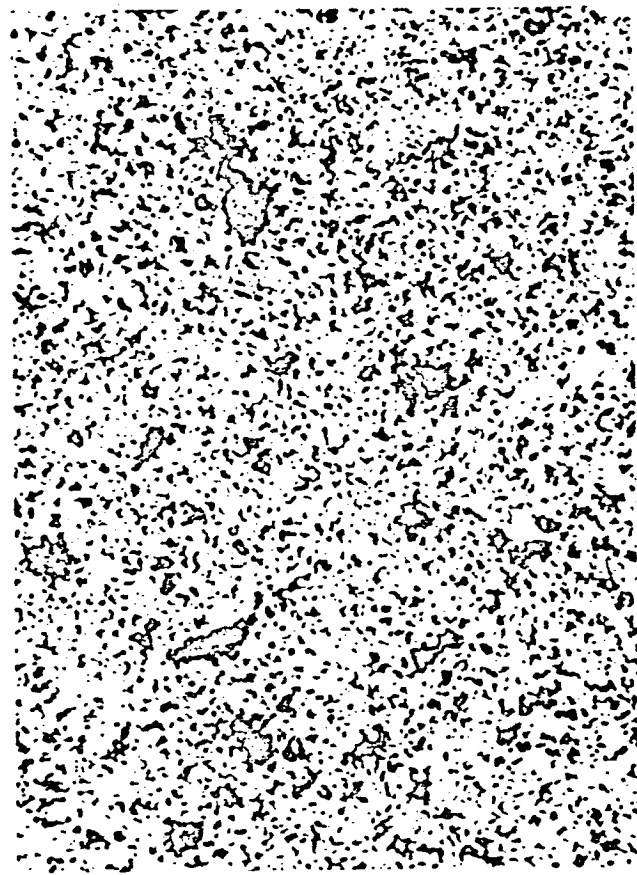


Neg. 2582 After sintering  $\rho = 83.8\%$

TUNGSTEN  
Ball milled dry and packed by vibration



Neg. 2601 Before sintering  $\rho = 68.1\%$

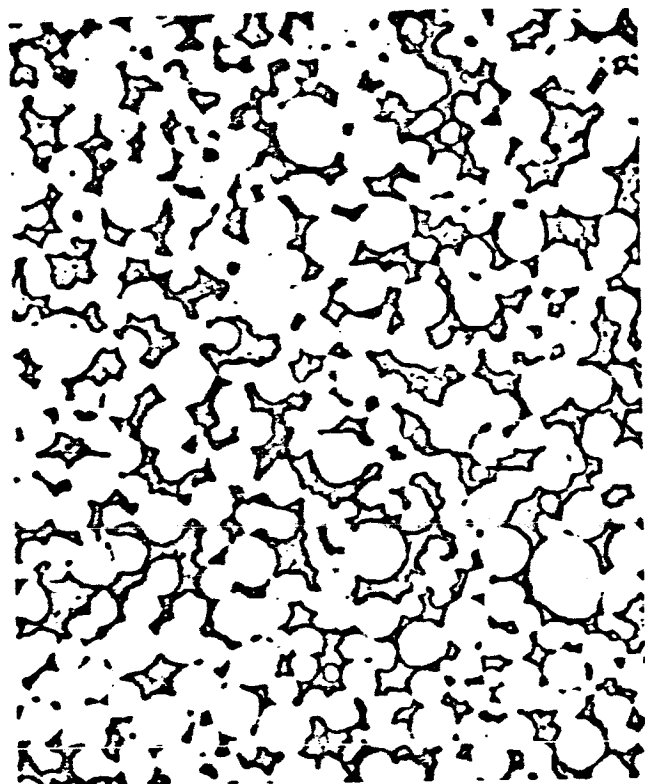


Neg. 2600 After sintering  $\rho = 73.7\%$

W-10W/oTa  
Waring blended in methanol and packed by tapping

FIG. 3-13 INFILTRATED STRUCTURES OF  $(1-4\mu)W$  AND  $(1-4\mu)W-10Ta$ , BEFORE AND AFTER VACUUM SINTERING (Inhomogeneity of the W-10Ta illustrates detriment of oversized Ta particles and of Ta agglomeration.) (X400)

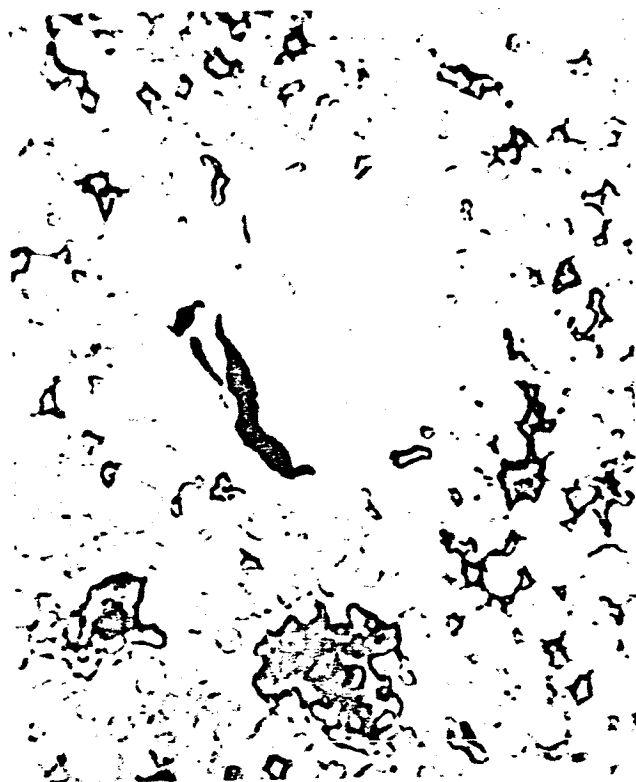




Neg. 2596

Pressed  $p = 69.0\%$

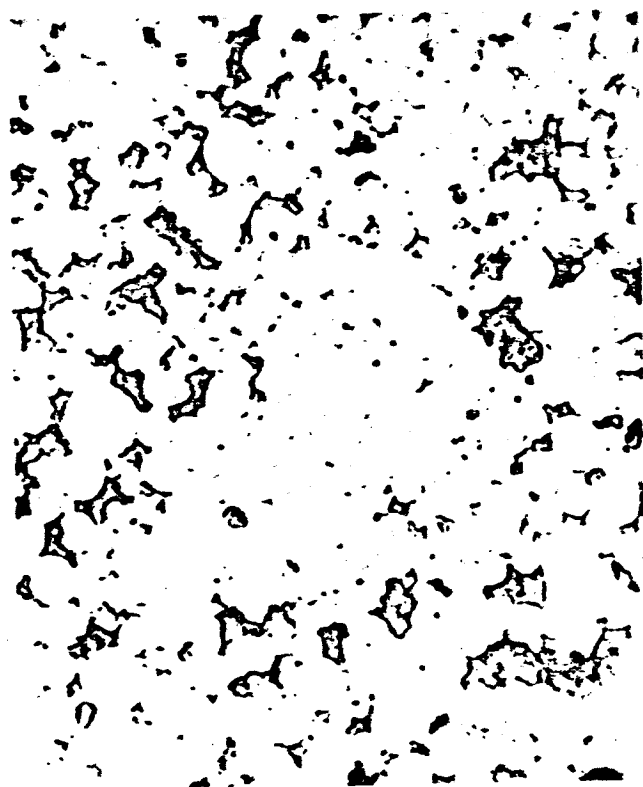
Tungsten



Neg. 2588

W-10W/oTa

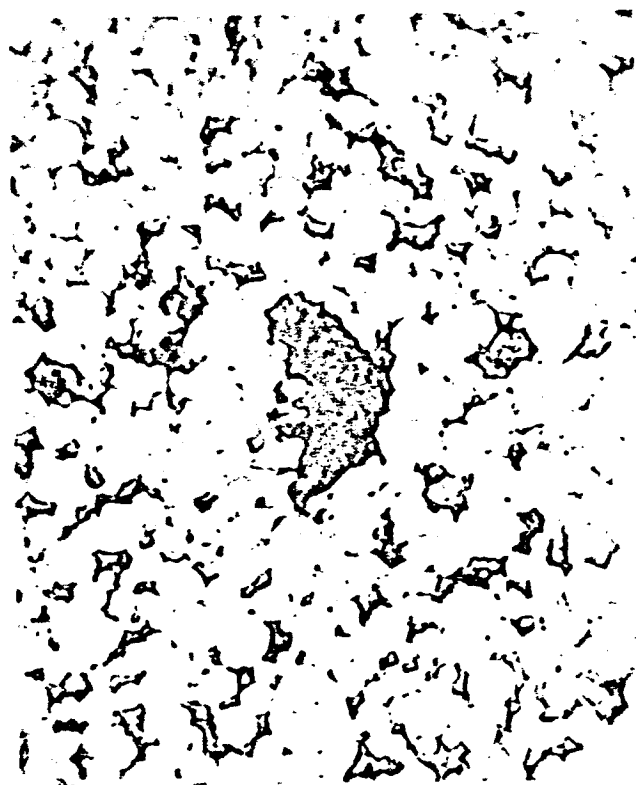
Type I



Neg. 2598

W-10W/oTa

Type II



Neg. 2599

W-10W/oTa

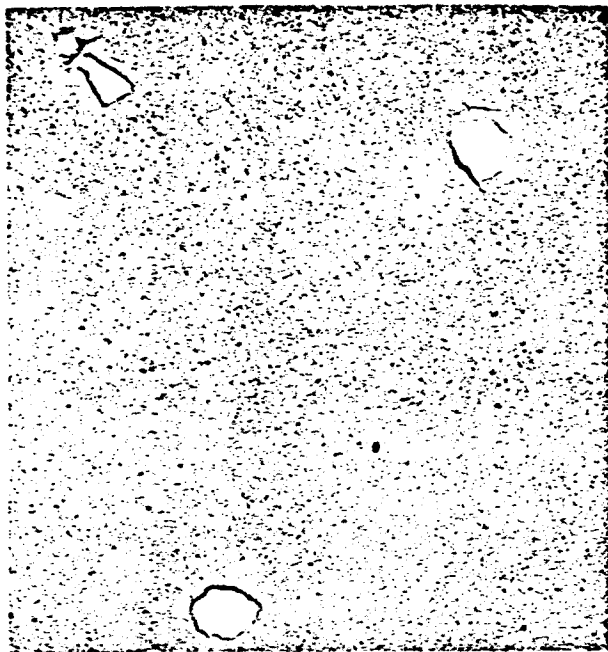
Type III

FIG. 3-14 INFILTRATED STRUCTURES OF  $(1-4\mu)W$  AND  $(1-4\mu)W-10Ta$ , BEFORE VACUUM SINTERING, SHOWING 3 TYPES OF INHOMOGENEITIES (W-10Ta mixture ball milled in methanol) (X2000)

Still another attempt to improve the blending technique and ionizer homogeneity was made. NRC Grade SQ-4 tantalum (sedimentation sized to a maximum particle diameter of  $2\mu$ ) and  $1-4\mu$  tungsten microspheres were used. A W-10W/oTa mixture was submerged in benzyl alcohol, agitated in a liquid blender for 5 minutes, separated by filtration, dried, compacted, sintered (to 77.1 percent density) and infiltrated. Use of the relatively viscous benzyl vehicle, instead of the methanol used previously, apparently increased the forces of liquid shear. As a result, the general pore structure appeared more uniform than any W-Ta composition fabricated to date. Micrographs of the sintered structure are shown in Fig. 3-15 at magnifications of X16, X100 and X400. However, the structure is seen to contain porous occlusions, the density of which is higher than that of the surrounding matrix. Further, the micrographs show that these occlusions shrank away from the matrix during sintering. The following mechanism explains formation of such occlusions.

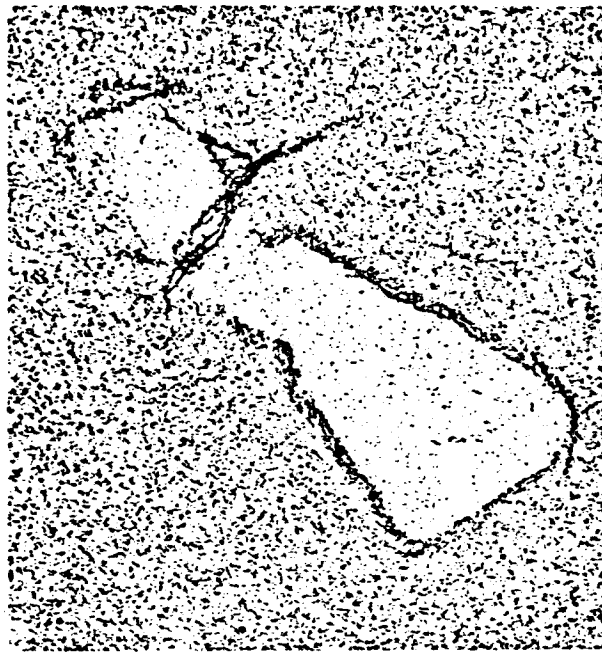
Whenever metal powders are suspended in liquid, permitted to settle, and subsequently dried, packing density of the particles is increased. In other words, the powder forms a "cake". If then the powder cake is not completely broken apart prior to compaction, residual masses of densely packed cake sinter more rapidly than uncaked particles (explaining the higher-density occlusions in Fig. 3-15). It therefore became apparent that, subsequent to slurry blending, it would be necessary to ball mill the dry powder mixtures as the final step, preceding their compaction.

Briefly, the foregoing experiments demonstrated these important requisites to achieving homogeneous structures from multi-component powder mixtures: (1) the additive or minor constituent must contain no particles significantly larger than the largest particles of the base powder, (2) the additive particles must be completely dispersed and intimately blended with the base particles,



Neg. 2739

X16



Neg. 2738

X100



Neg. 2737

X400

Neg. 2736

X400

FIG. 3-15 SINTERED W-10W/oTa CONTAINING RELATIVELY-DENSE OCCLUSIONS

and (3) the final powder mixture must be of uniform texture, free of cakes and masses which differ in density from the bulk, and as dry as as possible prior to compaction.

### 3.3 Ionizers from Fine Linde Tungsten Microspheres With Binary (Ta) and Ternary (Ta+Re) Additions

A 7-composition pellet series was fabricated, using Linde tungsten microspheres (Lot PTf), having 78.1 percent by count of 0.25-2.5 $\mu$  particles. The tantalum additive powder was obtained by gravity sedimentation of NRC Grade SGQ-4 powder. Sedimentation was performed in benzyl alcohol for a time calculated by Stoke's Law to allow settling-out of all particles greater than 3 $\mu$  in diameter. The rhenium additive was obtained by cyclonic air classification of -200 mesh powder (99.9+ percent purity) from Chase Brass and Copper. Electron micrographs of both the tantalum and rhenium powders are shown in Appendix A (Sloan Report). Best efforts to disperse the agglomerations of Ta and Re were unsuccessful, so that particle-size distributions could not be determined.

The constituents described in the foregoing paragraph were accurately weighed to form master mixtures of W-20W/oTa and W-20W/oRe. These mixtures were each suspended in benzyl alcohol, agitated in a liquid (Waring) blender at the "high-speed" setting for 15 minutes, filtered in a Buchner-type funnel, dried in vacuo, and finally ball-milled. The master mixtures (and base tungsten) were then weighed in proportions calculated to yield the compositions:

W-5Ta  
W-5Ta-5Re  
W-5Ta-10Re  
W-10Ta  
W-10Ta-5Re  
W-10Ta-10Re

The powder mixtures were then dry-box loaded into standard 5/8-inch-diameter rubber tubes, and pressed hydrostatically at 50,000 psi. Sintering was performed at 1800°C in the  $10^{-5}$  torr range as indicated in Table 3-II, where sintering conditions and sintered densities are given. Note that sintering was continued only to the low 70 percent density range, since previous pellets having a fine microsphere base could not be infiltrated when sintered to about 80 percent density. It is interesting to note in Table 3-II that the tungsten control, composed entirely of microspheres had the highest pressed density. Trends of decreasing pressed densities were induced by additions of Re to both the W-5Ta and W-10Ta mixtures.

The sintered pellets of Table 3-II were infiltrated with Cu-2Fe, machined to ionizer buttons, vacuum distilled to remove the infiltrant, and evaluated for density and N<sub>2</sub> permeability. These parameters are listed in Tables B-III and B-IV of Appendix B, with average parameters summarized as follows:

Composition, wt. %	Sintering Time at 1800°C, minutes	Average Density, % of theor.	Average N <sub>2</sub> Permeability, gm·cm <sup>-1</sup> ·sec <sup>-1</sup> ·torr <sup>-1</sup>
W (control)	30	71.7	$0.941 \times 10^{-6}$
W-5Ta	30	75.9	$0.124 \times 10^{-6}$
W-5Ta-5Re	30	76.4	$0.095 \times 10^{-6}$
W-5Ta-10Re	30	71.9	$0.209 \times 10^{-6}$
W-10Ta	105	77.3	$0.096 \times 10^{-6}$
W-10Ta-5Re	105	73.5	$0.191 \times 10^{-6}$
W-10Ta-10Re	105	74.4	$0.131 \times 10^{-6}$

It is apparent from the longer sintering time necessary to bring the above 10Ta-containing alloys to target density that these have greater thermal stability than the 5Ta alloys. It is also apparent

TABLE 3-II

SINTERING DATA FOR IONIZER PELLETS, MADE FROM  
0.25-2.5 $\mu$  TUNGSTEN MICROSPHERES,<sup>(a)</sup> WITH  
ADDITIONS OF FINE TANTALUM<sup>(b)</sup> AND/OR FINE RHENIUM<sup>(c)</sup> POWDERS

Pellet Identity	Composition, wt%	Wt, gm	Volume, cm <sup>3</sup>	Density	
				gm/cm <sup>3</sup>	% theor.

As-Pressed Hydrostatically at 50 ksi

IC	W(control)	36.2988	2.8578	12.70	65.80
IVT	W-5Ta	37.2664	2.9612	12.58	65.66
IVTVR	W-5Ta-5Re	36.8531	2.9692	12.41	64.47
IVTXR	W-5Ta-10Re	36.1934	2.9600	12.23	63.27
IXT	W-10Ta	37.7812	3.0210	12.51	65.74
IXTVR	W-10Ta-5Re	37.2778	3.0375	12.27	64.21
IXTXR	W-10Ta-10Re	29.7642	2.4846	11.98	62.40

Sintered at 1800°C for 30 min

IC	W(control)	35.3960	2.6057	13.58	70.36(d)
IVT	W-5Ta	36.2303	2.6243	13.81	72.08(d)
IVTVR	W-5Ta-5Re	35.9285	2.5416	14.14	73.45(d)
IVTXR	W-5Ta-10Re	34.9836	2.4554	14.25	73.72(d)
IXT	W-10Ta	37.2336	3.0666	12.14	63.79
IXTVR	W-10Ta-5Re	36.4645	2.9509	12.36	64.68
IXTXR	W-10Ta-10Re	29.0510	2.3459	12.38	64.48

Sintered at 1800°C for 105 min

IXT	W-10Ta	37.2051	2.8161	13.21	69.42(d)
IXTVR	W-10Ta-5Re	36.4448	2.6774	13.61	71.22(d)
IXTXR	W-10Ta-10Re	29.0380	2.1211	13.69	71.30(d)

- (a) Lot PTf tungsten with 78.1% by count of 0.25-2.5 $\mu$  microspheres.  
 (b) NRC Grade SGQ-4 tantalum, classified by gravity sedimentation - see X5000 electron micrographs of Appendix A.  
 (c) Chase Lot 449 Re, classified by cyclonic air - see X5000 electron micrographs of Appendix A.  
 (d) Infiltrated with Cu-2Fe alloy at juncture indicated.

that addition of 5 and 10W/o of tantalum particles greatly reduces permeability of the pore networks. In the following table, the data have been rearranged to more clearly indicate the trend of lower permeability with higher density.

Composition, wt. %	Sintering Time at 1800°C, minutes	Average Density, of theor.	Average N <sub>2</sub> Permeability, gm·cm <sup>-1</sup> ·sec <sup>-1</sup> ·torr <sup>-1</sup>
W (control)	30	71.7	0.941 x 10 <sup>-6</sup>
W-5Ta-10Re	30	71.9	0.209 x 10 <sup>-6</sup>
W-10Ta-5Re	105	73.5	0.191 x 10 <sup>-6</sup>
W-10Ta-10Re	105	74.4	0.131 x 10 <sup>-6</sup>
W-5Ta	30	75.9	0.124 x 10 <sup>-6</sup>
W-10Ta	105	77.3	0.096 x 10 <sup>-6</sup>
W-5Ta-5Re	30	76.4	0.095 x 10 <sup>-6</sup>

Pore parameters of the foregoing alloy series were determined, using both the pore-intercept and pore-counting methods described in Subsection 2.3.4. These parameters are given in Table 3-III, with formulae for their calculation indicated in subheadings. In addition to the spherical-base compositions, parameters for an angular W-8Cu composition are listed for comparison.

Average parameter values of Table 3-III are retabulated in Table 3-IV to facilitate comparison. Pore structures of both the W-8Cu and spherical W (control) are indicated to be relatively and comparably coarse. Pore structures of the W-5Ta, W-5Ta-5Re, and W-5Ta-10Re are extremely fine, in fact the finest measured to date. Pore structures of the W-10Ta, W-10Ta-5Re, and W-10Ta-10Re, while finer than previously measured, are somewhat coarser than those of the W-5Ta, W-5Ta-5Re, and W-5Ta-10Re alloys.

TABLE 3 - III  
Pore Parameters for Various Ionizer Compositions

Composition, Wt. %	Sample Identification	Photo Magnification	Av Intercepted Length of		Av Pore Spacing, $\mu$	Diam. of Av Equiv. Cylindrical Pore, $\mu$	Pores <sub>2</sub> per cm <sup>2</sup> at 1X
			Pores, $\mu$	Solid, $\mu$			
			(p)	(s)	(p+s)	$(2\sqrt{ps/\pi})$	$10^6/(p+s)^2$
W-8Cu*	1P3-13	X4027	1.772	3.759	5.53	3.33	$3.27 \times 10^6$
	-14	X4033	1.808	3.514	5.32	3.50	$3.53 \times 10^6$
	-15	X4033	1.656	3.924	5.58	3.43	$3.21 \times 10^6$
	Av				5.40	3.49	$3.34 \times 10^6$
Sph. W (Control)**	1C-13	X4037	1.623	4.492	6.12	3.56	$2.67 \times 10^6$
	-14	X4037	1.718	5.354	7.07	3.93	$2.00 \times 10^6$
	-15	X4027	1.621	5.229	6.85	3.76	$2.13 \times 10^6$
	Av				6.68	3.75	$2.27 \times 10^6$
			Photo Magnification	Pores Counted in 390 cm <sup>2</sup> area(a)	Av Pore Spacing, $\mu$	Diam. of Av Equiv. Cylindrical Pore, $\mu$	Pores <sub>2</sub> per cm <sup>2</sup> at 1X
			(p)	(n)	$10^4 \sqrt{nm^2/a}$	2***	$nm^2/a$
W-5Ta**	1VT-13	X4033		287	2.92	1.66	$11.79 \times 10^6$
	-14	X4033		302	2.85	1.62	$12.41 \times 10^6$
	-15	X4033		290	2.90	1.65	$11.91 \times 10^6$
	Av				2.89	1.64	$12.04 \times 10^6$
W-5Ta-5Re**	1VTB-13	X4037		338	2.68	1.37	$13.91 \times 10^6$
	-14	X4033		348	2.65	1.35	$14.30 \times 10^6$
	-15	X4040		324	2.74	1.40	$13.35 \times 10^6$
	Av				2.69	1.37	$13.85 \times 10^6$
W-5Ta-10Re**	1VTB-13	X4023		275	2.99	1.63	$11.34 \times 10^6$
	-14	X4037		305	2.82	1.54	$12.55 \times 10^6$
	-15	X4033		296	2.87	1.57	$12.16 \times 10^6$
	Av				2.89	1.58	$11.98 \times 10^6$
W-10Ta**	1XT-13	X4040		240	3.19	1.84	$9.89 \times 10^6$
	-14	X4033		240	3.19	1.84	$9.86 \times 10^6$
	-15	X4033		221	3.32	1.92	$9.08 \times 10^6$
	Av				3.23	1.87	$9.61 \times 10^6$
W-10Ta-5Re**	1XTB-13	X4033		278	2.96	1.66	$11.42 \times 10^6$
	-14	X4030		256	3.09	1.73	$10.50 \times 10^6$
	-15	X4033		258	2.88	1.72	$10.60 \times 10^6$
	Av				3.04	1.70	$10.84 \times 10^6$
W-10Ta-10Re**	1XTB-10	X4027		224	3.31	1.79	$9.17 \times 10^6$
	-11	X4030		232	3.25	1.76	$9.51 \times 10^6$
	-12	X4037		240	3.19	1.73	$9.88 \times 10^6$
	Av				3.25	1.76	$9.52 \times 10^6$

\* Tungsten powder base; 0.8u H<sub>2</sub>-reduced, with addition of fine Cu flakes

\*\* Tungsten powder base; 0.25-2.5u microspheres, with additions of finer Ta and Re

\*\*\* Values of  $\bar{r}$  calculated from  $\left(\frac{1128}{n}\right) \sqrt{\frac{(Vol. \text{ of pores } \times 10^6)}{a}}$



TABLE 3-IV  
SUMMARY OF PORE PARAMETERS FOR EIGHT IONIZER COMPOSITIONS  
(Average values for 3 microsections of each composition at  $\sim X4000$ )

Composition, wt. %	Determination Method	No. of Pores per $\text{cm}^2$	Av. Pore Spacing, $\mu$	(c) Diam. of Av. Equiv. Cylindrical Pore, $\mu$
W-8Cu (a)	Intercept	$3.34 \times 10^6$	5.48	3.49
Sph. W (control) (b)	"	$2.27 \times 10^6$	6.68	3.75
W-5Ta (b)	Counting	$12.04 \times 10^6$	2.89	1.64
W-5Ta-5Re (b)	"	$13.85 \times 10^6$	2.69	1.37
W-5Ta-10Re (b)	"	$11.98 \times 10^6$	2.89	1.58
W-10Ta (b)	"	$9.61 \times 10^6$	3.23	1.87
W-10Ta-5Re (b)	"	$10.84 \times 10^6$	3.04	1.70
W-10Ta-10Re (b)	"	$9.52 \times 10^6$	3.25	1.76

(a) W Powder Base:  $0.8\mu$   $\text{H}_2$ -reduced, with addition of fine Cu flake

(b) W Powder Base:  $0.25$ - $2.5\mu$  microspheres, with additions of finer Ta and Re

(c) Center-to-center distance for (square) grid arrangement of pores, as standard with intercept method.

Microstructures of this ionizer series are shown in Fig. 3-16 at X400, and in Fig. 3-17 at X2000; all of these pore structures are very uniform. Certainly, the gross inhomogeneities, noted in the earlier binary ionizers, are no longer present. Structures of the 5Ta series exceed one important goal of the research, namely  $>1 \times 10^7$  pores/cm<sup>2</sup>; structures of the 10Ta series closely approach the goal.

Chemical analysis data for this spherical-tungsten-base series are listed in Table 3-V. The analyses were performed by the Materials Testing Lab of Magniflux. Values for the W-5Ta-5Re and W-10Ta-5Re alloys were obtained by interpolation (where trends permitted) between adjacent compositions in the series. In a few instances, the lower alloy contained more impurity than did the higher alloy (e.g., 200 ppm Cr in W-5Ta; 30 ppm Cr in W-5Ta-10Re). Where impurity contents decreased with increasing alloy additions, interpolations were not made; in fact, such a trend indicates error in one or both of the bracketing values.

### 3.4 Delivery of Small Ionizer Samples to NASA-Lewis

In accordance with contractual requirements, samples of the following spherical-base compositions were fabricated for delivery to NASA-Lewis.

<u>Composition, Wt. %</u>	<u>Relative Sintered Density, %</u>
Spherical Tungsten*	70.26
W-5Ta	69.36
W-5Ta-5Re	70.39
W-5Ta-10Re	70.56
W-10Ta	70.15
W-10Ta-5Re	69.70
W-10Ta-10Re	71.88

Prior to fabricating this composition series, considerable preliminary work was done to determine optimum preparation techniques (Ref. Sections 3.1 and 3.2). All alloy ionizers prepared during the

\* Control composition, made from 0.25-2.5 $\mu$  tungsten microspheres

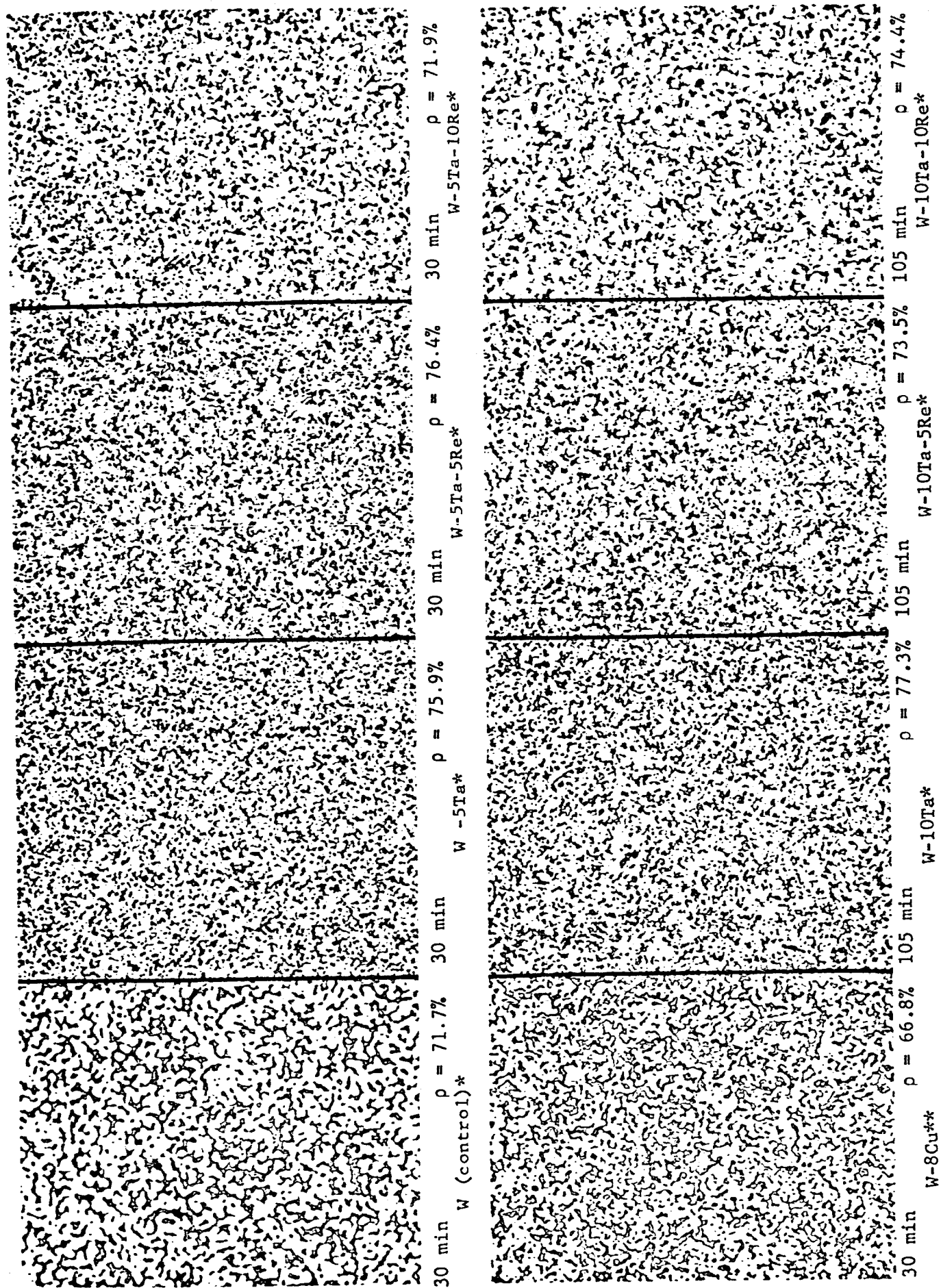


FIG. 3-16 MICROSTRUCTURES OF IONIZERS, MADE FROM VARIOUS POWDER MIXTURES, AND SINTERED AT 1800°C

FOR TIMES NOTED (X400)

\*Made from 0.25-2.5 $\mu$  Tungsten microspheres plus finer angular Ta and Re

\*\*Made from 0.8 $\mu$  H<sub>2</sub>-reduced tungsten plus fine Cu flake

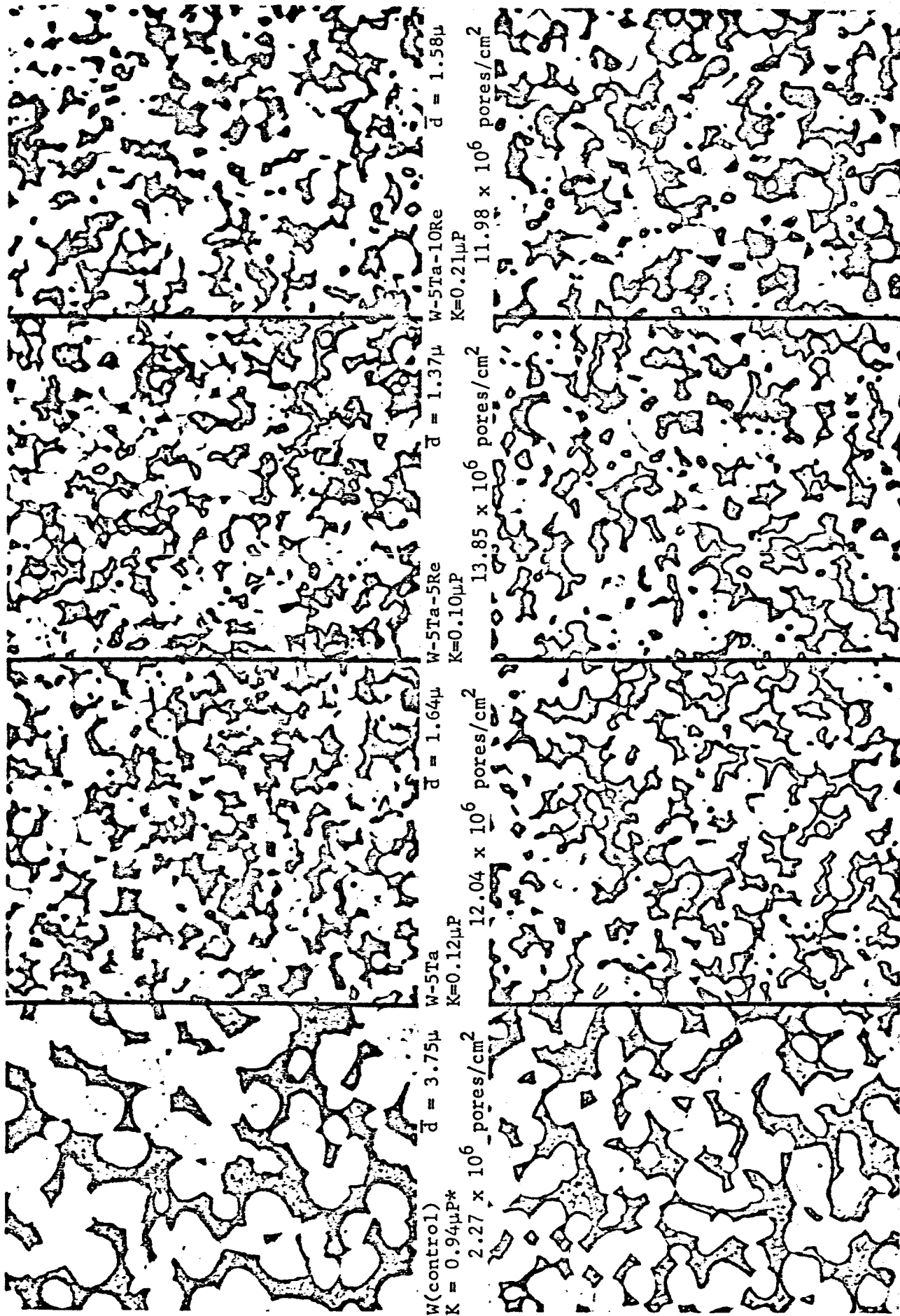


FIG. 3-17 MICROSTRUCTURES OF IONIZERS, MADE FROM VARIOUS POWDER MIXTURES, AND SINTERED AT 1800°C (X2000)

TABLE 3-V  
CHEMICAL ANALYSES DATA FOR SPHERICAL TUNGSTEN-BASE IONIZERS

(Analyzed by quantitative spectrography and  
reported as parts per million, except as noted.)

ELEMENT	UNALLOYED W(Control)	TARGET COMPOSITION, W/O					
		W-5Ta	W-5Ta-5Re	W-5Ta-10Re	W-10Ta	W-10Ta-5Re	W-10Ta-10Re
			(a)			(a)	
Ag	<1	<1	(<1)	<1	<1	(<1)	<1
Al	110	300	--	80	40	(~70)	100
B	<5	<5	(<5)	<5	<5	(<5)	<5
Ba	<3	<3	(<3)	<3	<3	(<3)	<3
Be	<1	<1	(<1)	<1	4	--	<1
Bi	<3	<3	(<3)	<3	<3	(<3)	<3
C <sup>(b)</sup>	25	19	(~32)	46	15	(~24)	48
Ca	30	30	(30)	30	30	(30)	30
Co	<3	<3	(<3)	<3	<3	(<3)	<3
Cr	50	200	--	30	30	--	<10
Cu	5	20	--	3	10	--	5
Fe	50	100	--	<30	<30	(<65)	100
Mg	10	<3	(<3)	<3	<3	(<3)	3
Mn	<3	<3	(<3)	<3	20	--	<3
Mo	100	100	(~150)	200	300	--	200
Nb	<100	<100	(<100)	<100	<100	(<100)	<100
Ni	<10	<10	(<10)	<10	100	--	<10
Pb	<10	<10	(<10)	<10	<10	(<10)	<10
Re <sup>(c)</sup>	--	--	(5+%)	(10.11%)	--	(5+%)	10.11%
Sn	<3	<3	(<3)	<3	<3	(<3)	<3
Ta <sup>(c)</sup>	--	4.56%	(4.56%)	(4.56%)	(9.52%)	(9.52%)	9.52%
Ti	60	<10	(<10)	<10	<10	(<10)	<10
V	<3	<3	(<3)	<3	<3	(<3)	<3
T.O.E. <sup>(d)</sup>	<300	<300	(<300)	<300	<300	(<300)	<300
W	Balance	Balance	Balance	Balance	Balance	Balance	Balance

- (a) Values in parentheses are interpolated from adjacent compositions.  
(b) Carbon by conductometric method  
(c) Tantalum and rhenium by ion exchange method.  
(d) Total other elements

preliminary research were sectioned for evaluation and found to be structurally inhomogeneous. Therefore, the preliminary ionizers were not duplicated for delivery to NASA. Ionizer compositions tabulated above duplicate those described in Section 3.3. They represent a compositional sequence of ionizer materials, having fine homogeneous structures and being amenable to orderly evaluation. All data determined for these ionizer compositions are submitted in detail with this report, including chemical and size analyses of starting powders, processing methods, and results of evaluation.

The preferred sample size, as specified contractually, was 5/8-inch diameter x 3/4-inch length, with 3/8-inch diameter x 1/2-inch length given as minimum. Two samples of each composition were specified. Samples of the 7 spherical-base compositions, supplied by EOS, average between 5/8-inch and 3/8-inch diameter by greater than 1 inch in length, such that each sample provides the volume equivalent of the two samples specified. The 7 "double" samples have been infiltrated with Cu-2Fe to facilitate subsequent machining and sectioning. Preparation of the larger-size samples, in lieu of 2 smaller ones, is justified technically since it provides better assurance of compositional and structural similarity.

Numerous small samples of low-density ionizer material, made from fine  $H_2$ -reduced tungsten powder by the copper flake technique, have been delivered with the large ionizer bars. Ionizers prepared from both W-8Cu and W-8Cu-2BN have been submitted. Although these samples are not cylindrical, they provide the advantage of having been fabricated with, and machined from, corresponding large ionizer bars.

#### 4. LOW-DENSITY IONIZERS MADE BY COPPER-FLAKE TECHNIQUE

A portion of the contract research effort was devoted to the development of methods for the production of uniform ionizer structures exhibiting optimum pore size, and having a density of less than 70 percent of theoretical. This effort is covered under paragraph B.1.d of the Scope of Work.

The incentive for the development of low-density ionizers having small pore diameters stems from results observed in the operation of ionizers by use of the ion microscope. It had been determined that a large fraction of the ionization phenomena took place deep within the ionizer pores. Therefore, it followed that ionizer performance should improve as the ratio of total open pore area-to-solid area of the ionizer was increased.

The geometry of the idealized minimum-density ionizer would be that of a honeycomb, wherein the hexagonal framework has a high work function, low vapor pressure, and sufficient thickness to support the structure. Unit cell diameters of such a structure should lie within the range of 1-4 $\mu$ .

Technology is not yet available for production of an idealized structure. However, such a geometry has been closely approached by the low-density structures of round or angular pores (produced under this contract) which exhibit minimum pore dimensions of the described size.

The approach investigated for the production of low-density ionizers was that of controlling the pressed density of the powdered metal compact by incorporating inert materials within the tungsten powder prior to the pressing operation. Low-density porous bodies may be produced by the addition of such volatile compounds as ammonium

carbonate, urea, and acrylic resins to the tungsten powder prior to compaction. Unfortunately, most of the volatile compounds added yielded materials exhibiting a very nonuniform microstructure. The principal reason for this nonuniformity is the void left upon evaporation of the volatile particle. Since voids left by the additive could not exceed the desired pore diameter of  $1-4\mu$ , one problem was to find inert particles having diameters within the prescribed pore size range. Another problem was that of obtaining proper blending between a low-density inert additive material, such as urea, and a high-density powder such as tungsten. Investigation of several additives indicated that flake copper, sold under the name of Copper Bronzing Powder, had extremely fine particle diameter and high specific surface area. In addition, the density of this material was sufficiently high to permit uniform blending. Flake copper was therefore selected as an ideal additive for controlling pore size and density of the pressed compacts.

#### 4.1 Procedures and Results

Flake metal powders are usually produced by milling angular metal powders with a fatty acid such as stearic. To ensure the removal of any organic film resulting from the milling operation, the flake copper was washed with a mixture of equal parts acetone and methyl alcohol. The washed powder was then vacuum dried to zero weight change.

Angular ( $0.8\mu$ ) hydrogen-reduced tungsten powder and flake copper were ball milled together to produce an intimate mixture of copper and tungsten powder. After milling, the copper-tungsten powder mixtures were placed in rubber containers and pre-pressed hydrostatically at 10,000 psi. After pre-pressing, the compacts were reground, pressed at 60,000 psi and presintered in forming gas at a temperature just below the melting point of copper. The presintering treatment was performed for the purpose of establishing interconnection or bridging between adjacent contact points of the tungsten powder. This procedure serves to freeze the pore size and configuration in the shape of the



copper powder flake so that, upon subsequent evaporation of the copper and final sintering, little change in pore size, configuration, or distribution will occur. Metallographic examination of presintered compacts, heated just below and just above the melting point of copper, indicated that the lower temperature was preferable. Higher presintering temperatures effected agglomeration of the copper flake and resulted in larger pores.

To retain low density and uniform pore structures in compacts free of stabilizing additive, it was necessary to use low temperatures and short sintering times. Since sintering temperatures are still considerably above ionizer operating temperatures, the structures obtained exhibit sufficient stability to permit exhaustive performance testing. Materials exhibiting a very high degree of thermal stability were subsequently developed and are discussed in Subsection 4.3. Powder mixtures and experimental conditions used are summarized in Table 4-I. Photomicrographs of the 13 compositions listed in Table 4-I are shown in Figs. 4-1 through 4-13, in respective order. It will be noted that the optimum structure (Fig. 4-13) was produced from mixture number 13, consisting of 92% by weight of angular tungsten and 8% of copper flake.

Using the 92W-8Cu mixture, two separate series of buttons as follows were prepared for testing:

92W-8Cu  
.8μ ANGULAR W POWDER, NO. 112 COPPER FLAKE  
NO. I SERIES

Button No.	Diam, in.	Wt, gm	Volume, cm <sup>3</sup>	Density		Δt, sec	N <sub>2</sub> Permeability, gm.cm <sup>-1</sup> .sec <sup>-1</sup> .torr <sup>-1</sup>
				g/cm <sup>3</sup>	% of theor.		
1	.2016	.2816	.02238	12.58	65.18	8.12	1.07x10 <sup>-6</sup>
2	.2015	.2711	.02210	12.27	63.57	7.03	1.23x10 <sup>-6</sup>
3	.2008	.2782	.02179	12.77	66.16	5.82	1.48x10 <sup>-6</sup>
4	.2008	.2764	.02190	12.62	65.38	6.01	1.44x10 <sup>-6</sup>
5	.2010	.2661	.02199	12.10	62.69	6.19	1.40x10 <sup>-6</sup>
6	.2014	.2636	.02156	12.23	63.36	7.32	1.15x10 <sup>-6</sup>

TABLE 4-I

SINTERING TESTS ON H<sub>2</sub>-REDUCED TUNGSTEN POWDER-COPPER FLAKE MIXTURES

No.	Mixture, % by wt	Presinter	Sinter	Density, % (Theoretical)	Remarks
1.	12 Cu Flake 88 - 0.8μ W	2 hr 1010°C	15 min-1500°C 60 min-2000°C	72.7	Small pores, quite uniform
2.	15 Cu Flake 85 - 0.8μ W	2 hr 1010°C	15 min-1500°C 60 min-2000°C	71.54	Small pores, some voids
3.	20 Cu Flake 80 - 0.8μ W	2 hr 1010°C	15 min-1500°C 60 min-2000°C	81.0	Fewer pores than No. 2, large voids
4.	25 Cu Flake 75 - 0.8μ W	2 hr 1010°C	15 min-1500°C 60 min-2000°C	78.0	Less uniform than 1, 2, or 3, large voids
5.	15 Cu Flake 8.5 Ta powder 76.5 - 0.8μ W	2 hr 1010°C	30 min-1500°C 60 min-2000°C	74.8	
6.	10 Cu Flake 4.5 Ta powder 85.5 - 0.8μ W	2 hr 1010°C	30 min-1500°C 60 min-2000°C	83.2	
7.	4 Ammonium Carbonate 96 - 0.8μ W	2 hr 1010°C	30 min-1500°C 60 min-2000°C	74.0	Large voids
8.	4 Ammonium Carbonate 9.6 Ta powder 86.5 - 0.8μ W	2 hr 1010°C	30 min-1500°C 60 min-2000°C	68.2	Large voids, closed structure
9.	15 Cu Flake 85 - 0.8μ W	2 hr 1150°C	15 min-1500°C 60 min-2000°C	80.0	Very fine structure, prepressed at 10,000 lb, reground, repressed
10.	8.1 Cu Flake 90.8 - 0.8μ W 1.1 Ni	2 hr 1040°C	15 min-1500°C 60 min-1800°C	68.9	Ni added to W powder as Ni(NO <sub>3</sub> ) <sub>2</sub> , pre-reduced before pressing, microstructure uniform, large pores
11.	15 Cu Flake 85 W (4-8μ)	2 hr 1150°C	15 min-1500°C 60 min-1800°C	61.65	4-8μ angular powder (Wah Chang), large voids, otherwise structure uniform
12.	15 Cu Flake 7 Ta powder 78 W (0.8μ)	1 hr 1150°C	15 min-1500°C 60 min-1800°C	69.1	Tantalum added as Ta <sub>2</sub> O <sub>5</sub> , excessive oxide in pores after sintering
13.	8 Cu Flake 92 W (0.8μ)	2 hr 1010°C	15 min-1500°C 15 min-1800°C	65.93	Small pores, very uniform

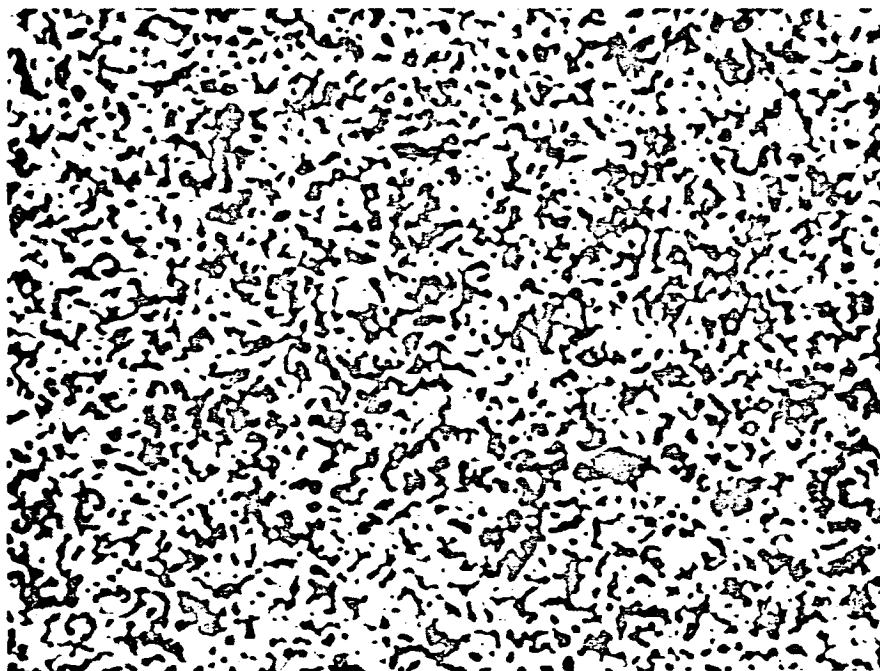


Neg. 2610

X400

FIG. 4-1 MIXTURE 1

88 Wt.% - .8 $\mu$  Angular Tungsten Powder  
 12 Wt.% - Copper Flake  
 Density - 72.7% Theoretical



Neg. 2611

X400

FIG. 4-2 MIXTURE 2

85 Wt.% - .8 $\mu$  Angular Tungsten Powder  
 15 Wt.% - Copper Flake  
 Density - 71.54% Theoretical



Neg. 2612

X400

FIG. 4-3 MIXTURE 3

30 Wt.% - .8 $\mu$  Angular Tungsten Powder  
 20 Wt.% - Copper Flake  
 Density - 81% Theoretical

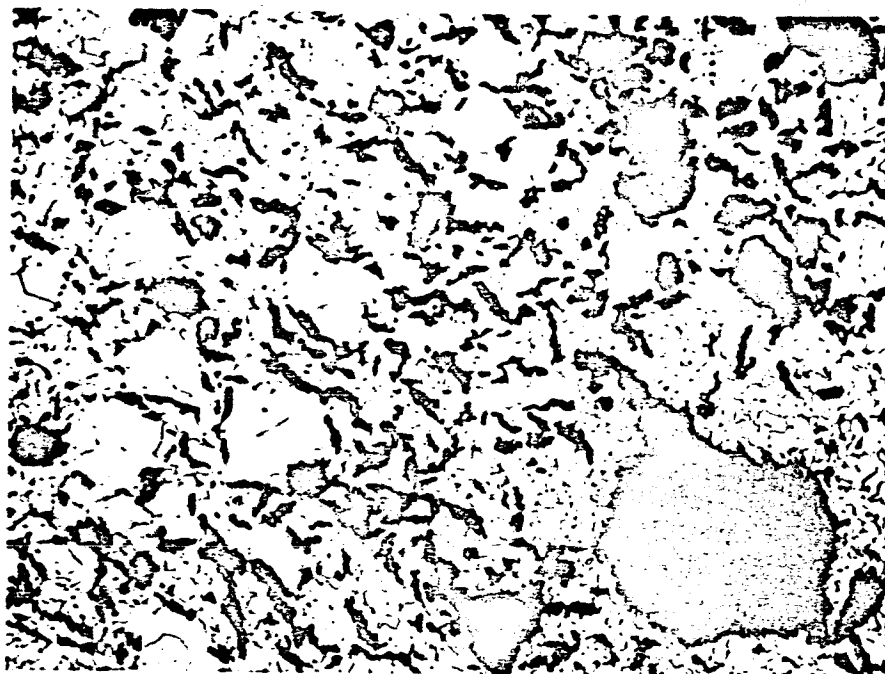


Neg. 2613

X400

FIG. 4-4 MIXTURE 4

75 Wt.% - .8 $\mu$  Angular Tungsten Powder  
 25 Wt.% - Copper Flake  
 Density - 78% Theoretical

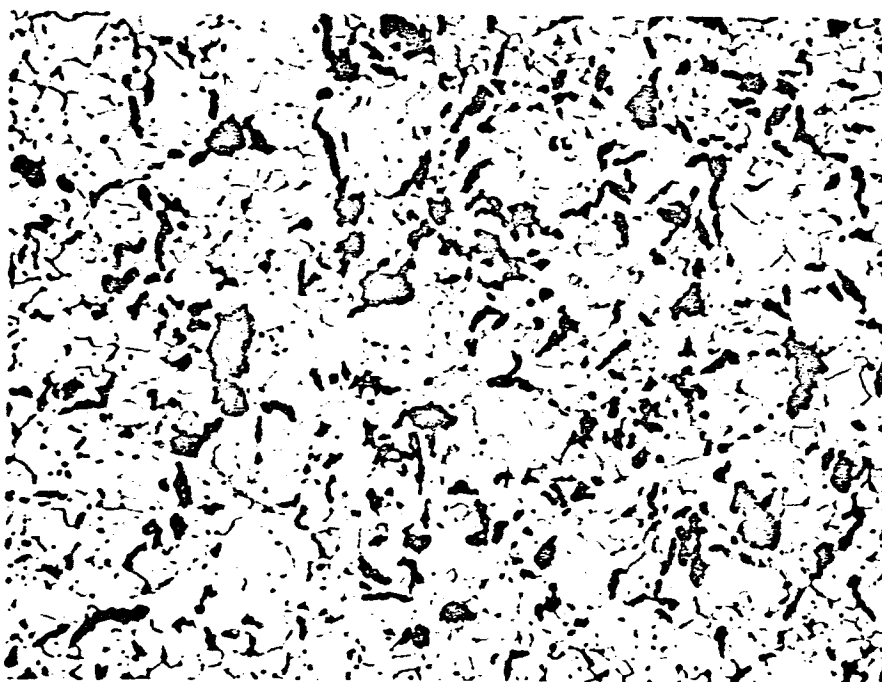


Neg. 2614

X400

FIG. 4-5 MIXTURE 5

76.5 Wt.% - .8 $\mu$  Tungsten Powder  
 8.5 Wt.% - 4 $\mu$  Tantalum Powder  
 15 Wt.% - Copper Flake  
 Density - 74% Theoretical

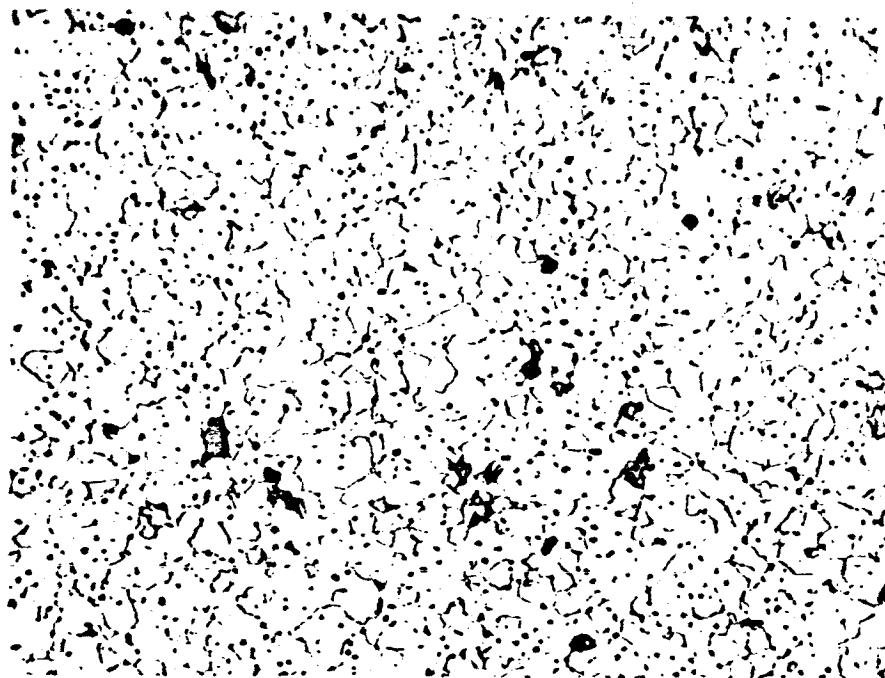


Neg. 2615

X400

FIG. 4-6 MIXTURE 6

85.5 Wt.% - .8 $\mu$  Tungsten Powder  
 4.5 Wt.% - 4 $\mu$  Tantalum Powder  
 10 Wt.% - Copper Flake  
 Density - 83.2% Theoretical

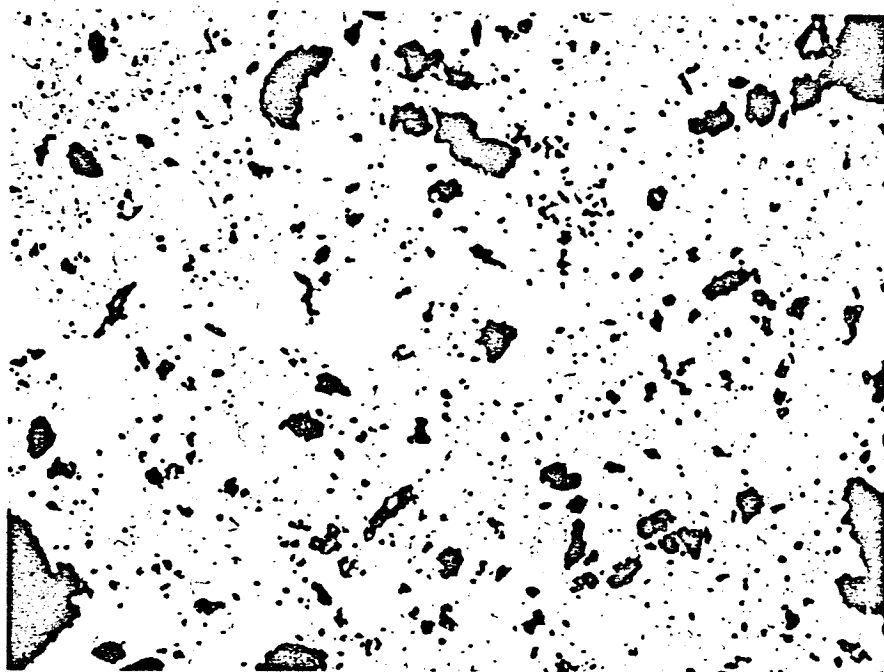


Neg. 2727

X400

FIG. 4-7 MIXTURE 7

96 Wt.% - .8 $\mu$  Angular Tungsten Powder  
 4 Wt.% - Ammonium Carbonate  
 Density - 74% Theoretical

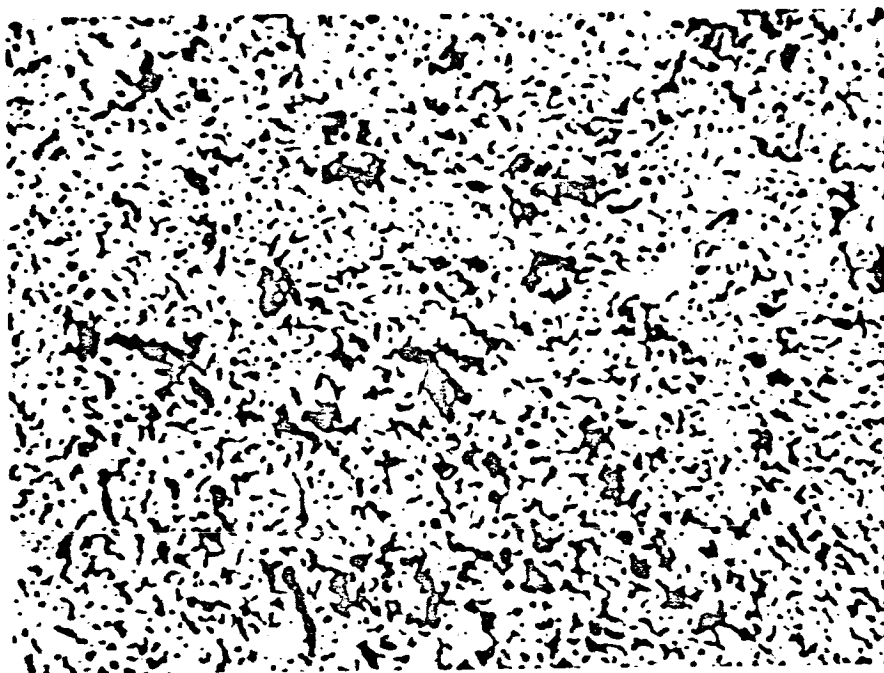


Neg. 2728

X400

FIG. 4-8 MIXTURE 8

86.5 Wt.% - .8 $\mu$  Angular Tungsten Powder  
 9.6 Wt.% - Tantalum Powder  
 4 Wt.% - Ammonium Carbonate  
 Density - 68.2% Theoretical

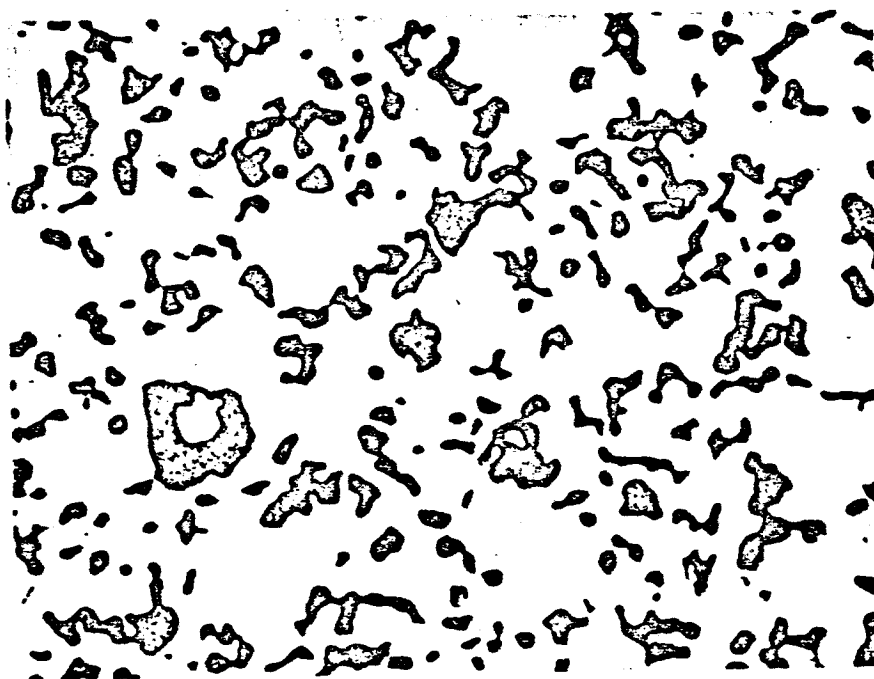


Neg. 2729

X400

FIG. 4-9 MIXTURE 9

85 Wt.% - .8 $\mu$  Tungsten Powder  
 15 Wt.% - Copper Flake  
 Density - 80% Theoretical



Neg. 2730

X400

FIG. 4-10 MIXTURE 10

90.8 Wt.% - .8 $\mu$  Tungsten Powder  
 8.1 Wt.% - Copper Flake  
 1.1 Wt.% - Nickel  
 Density - 68.9% Theoretical

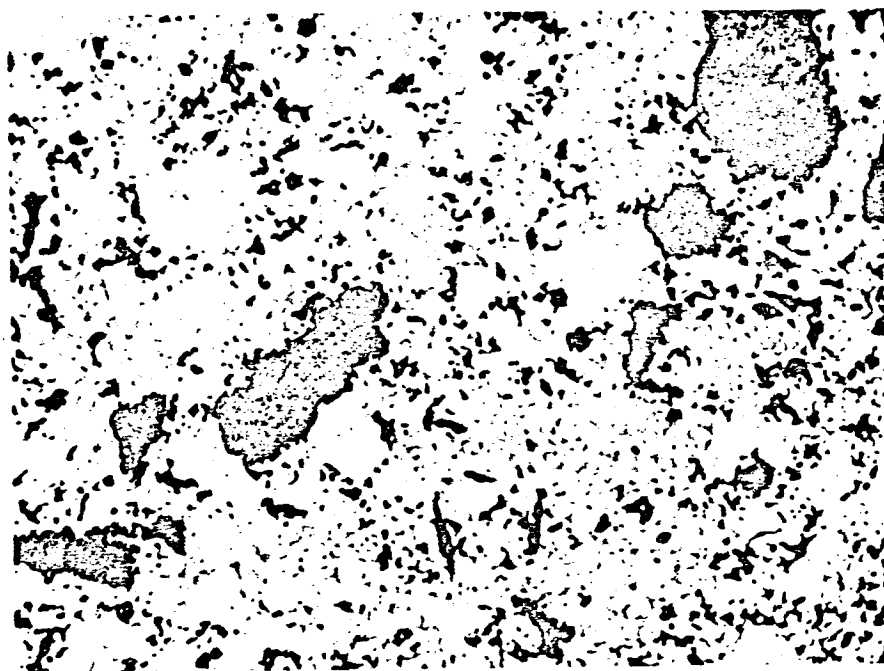


Neg. 2731

X400

FIG. 4-11 MIXTURE 11

85 Wt.% - (4-8 $\mu$ ) Tungsten Powder  
 15 Wt.% - Copper Flake  
 Density - 61.65% Theoretical



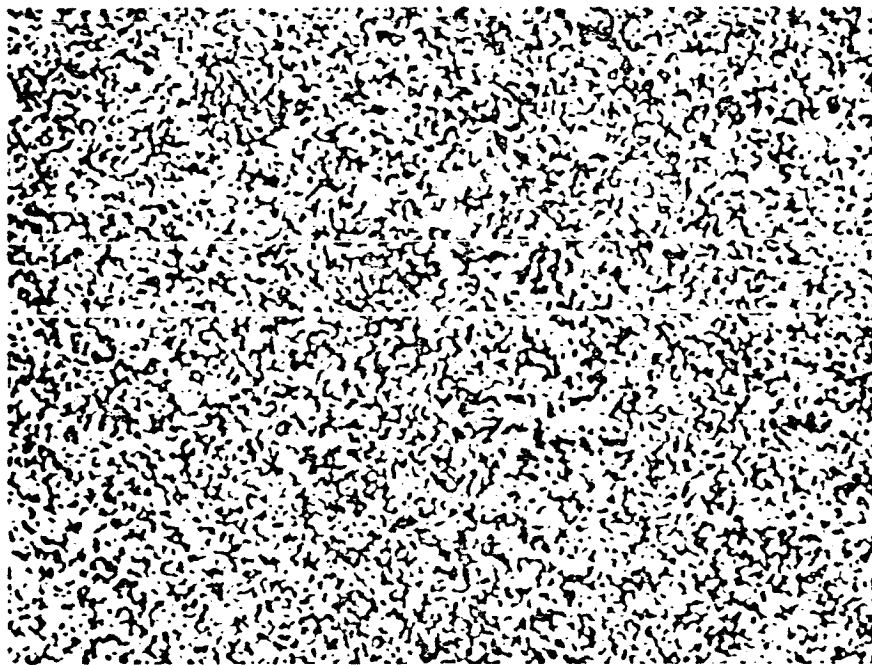
Neg. 2732

X400

FIG. 4-12 MIXTURE 12

78 Wt.% - .8 $\mu$  Tungsten Powder  
 7 Wt.% Tantalum as Ta<sub>2</sub>O<sub>5</sub>  
 15 Wt.% - Copper Flake  
 Density - 69.1% Theoretical





Neg. 2733

X400

FIG. 4-13 MIXTURE 13

92 Wt.% - .8 $\mu$  Tungsten Powder  
8 Wt.% - Copper Flake  
Density - 65.9% Theoretical

NO. II SERIES\*

Button No.	Diam, in.	Wt, gm	Volume, cm <sup>3</sup>	Density		$\Delta t$ , sec	N <sub>2</sub> Permeability, gm·cm <sup>-1</sup> ·sec <sup>-1</sup> ·torr <sup>-1</sup>
				g/cm <sup>3</sup>	% of theor.		
1	.190	.2665	.02044	13.04	67.56	7.32	1.38x10 <sup>-6</sup>
2	.190	.2566	.01998	12.84	66.53	7.47	1.32x10 <sup>-6</sup>
3	.190	.2574	.01998	12.88	66.74	7.40	1.33x10 <sup>-6</sup>

Two bars of the 92W-8Cu mixture, having dimensions of 3.89"x2.195"x.154", were prepared. Using the standard large permeability apparatus, measurements were made at 1/2-inch intervals of grid spacing over the surface of the bars. The intervals (in seconds), required for flow of 5cm<sup>3</sup> of N<sub>2</sub> under a pressure of 10" of Hg, are listed in Tables 4-II and 4-III. Readings were taken at 28 positions on both bars. It may be noted that the variation of permeability between positions is very small, indicating excellent overall uniformity.

#### 4.2 Effect of Presintering Time on Densification and Pore Structure of Low-Density Ionizers

The effect of presintering time at 1040°C on subsequent densification at 1800°C of the 92W-8Cu mixture was determined. A compact was pressed hydrostatically at 60,000 psi, and samples 1" x 1/4"

\* Spectrographic analysis in ppm:

Ca	65	Mg	26
Cu	200	Si	<30
Fe	150		

TABLE 4-II  
PERMEABILITY VARIANCE AFTER BAKEOUT  
OF 92% W + 8% Cu - BAR NO. 1  
(Density = 66.9% of Theoretical)

Posi- tion*	Time, sec.	Posi- tion	Time, sec.
1	----	17	15.0
2	20.5	18	14.0
3	21.0	19	14.5
4	----	20	16.0
5	16.0	21	16.0
6	15.5	22	14.5
7	17.0	23	15.0
8	19.5	24	16.0
9	15.0	25	17.0
10	14.5	26	15.0
11	15.0	27	14.5
12	16.0	28	16.0
13	15.5	29	----
14	14.0	30	16.5
15	14.5	31	15.5
16	16.0	32	----

\* Position Chart:

1	5	9	13	17	21	25	29
2	6	10	14	18	22	26	30
3	7	11	15	19	23	27	31
4	8	12	16	20	24	28	32

TABLE 4-III  
PERMEABILITY VARIANCE AFTER BAKEOUT  
OF 92% W + 8% Cu - BAR NO. 2  
(Density = 64.4% of Theoretical)

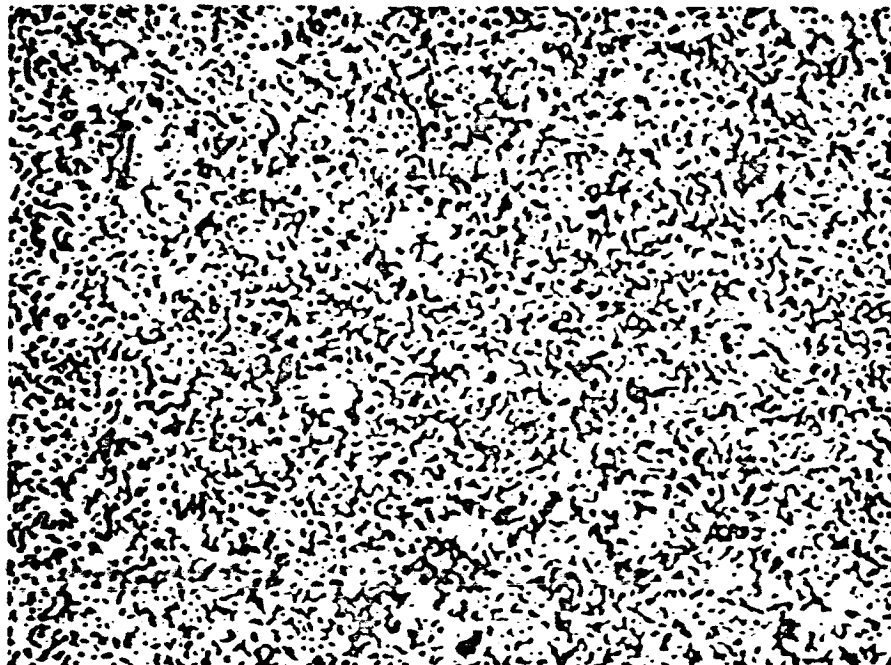
Posi- tion*	Time, sec.	Posi- tion	Time, sec.
1	-----	17	12.5
2	16.5	18	12.5
3	17.0	19	13.0
4	-----	20	13.0
5	13.0	21	13.0
6	13.0	22	13.0
7	13.0	23	13.5
8	13.0	24	13.0
9	13.0	25	14.0
10	14.0	26	14.0
11	13.0	27	14.0
12	13.0	28	14.5
13	13.0	29	-----
14	13.0	30	15.5
15	13.0	31	16.0
16	12.5	32	-----

x 1/4" were sectioned from it. One sample was presintered at 1040°C for four hours, the other for 16 hours. Both were then heated under vacuum at 1500°C for 15 minutes to evaporate the copper. Temperature was next increased to 1800°C and held for one hour. Densities of the samples were determined at this juncture to be 79.5 percent and 83.5 percent for the 4 and 16-hour presinters, respectively. After re-infiltration with copper, the samples were prepared for metallographic examination.

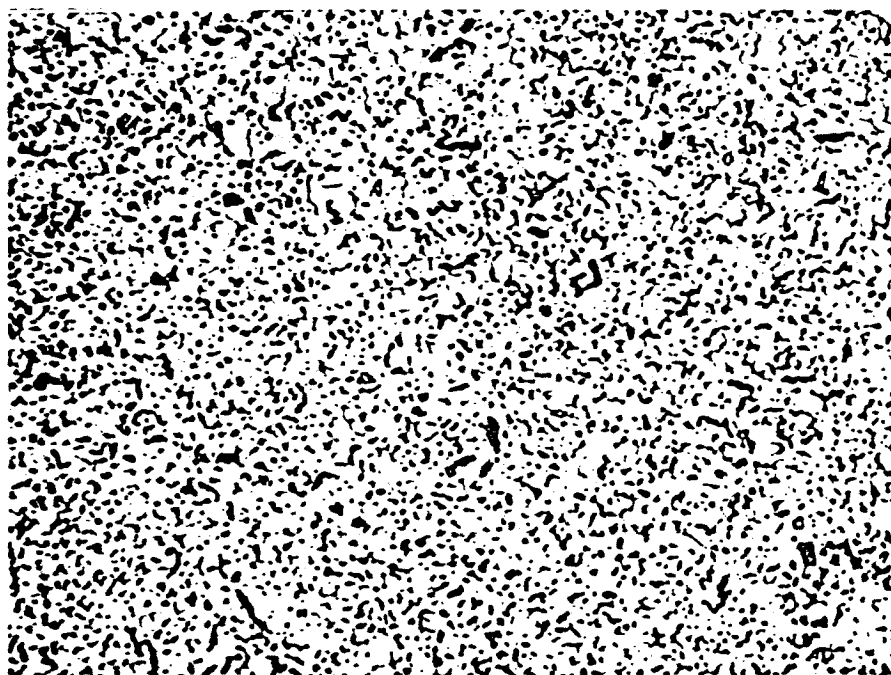
Structures of the two samples are shown in Fig. 4-14. Based on their density and structural differences, it is apparent that appreciable densification occurs at temperatures as low as 1040°C. Pore structure of the sample, presintered for 16 hours, is still quite uniform but its density is comparatively high. Based on this experiment, a presintering treatment at 1040°C for two hours was selected and used in preparing subsequent experimental samples of low density.

#### 4.3 Low-Density Ionizers Stabilized by Addition of Boron Nitride

The inherent thermal instability of ultra-fine tungsten metal powders, emphasized the need for development of a satisfactory grain-growth inhibitor other than tantalum. It was desired that such an inhibitor (1) not lower the work function of the tungsten, (2) have a low vapor pressure and (3) unlike tantalum, be readily comminuted to very fine size, allowing a uniform distribution of the inhibitor over the surface of each tungsten grain. Conventional grain-growth inhibitors, such as the oxides of thorium, zirconia and titanium, were eliminated on the basis of not fulfilling all of the above requirements. These oxides inhibit diffusion by acting as inert barriers between grains. It was reasoned that grain growth might also be inhibited by creating a tungsten compound differing in crystal structure from that of the tungsten. Since metals and metal compounds of widely differing crystal structure and lattice constants exhibit low mutual solubility, the presence of such compounds in the grain boundary should interfere with



Neg. 2876      Presintered at 1040°C for 4 hrs.    X400  
                  Sintered at 1800°C for 1 hr.  
                  Sintered Density = 79.5%

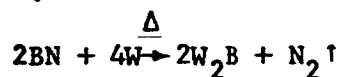


Neg. 2875      Presintered at 1040°C for 16 hrs.    X400  
                  Sintered at 1800°C for 1 hr.  
                  Sintered Density = 83.5%

FIG. 4-14 EFFECT OF PRESINTERING TIME (at 1040°C) ON SINTERED  
 STRUCTURE OF IONIZERS, MADE FROM 92 Wt.% OF H<sub>2</sub>-REDUCED  
 TUNGSTEN PLUS 8 Wt.% OF COPPER FLAKE

grain growth. The various tungsten borides differ greatly in lattice structure from body-centered-cubic tungsten. Boron was therefore investigated as a potential grain-growth inhibitor, since prior tests\* indicated that it exerted no deleterious effects on the work function of tungsten. Boron nitride was selected as the optimum boron-containing additive. This friable compound resembles graphite in crystalline structure (hexagonal), has excellent cleavage planes, and is ideal for milling to a fine state of subdivision. In addition, boron nitride is not readily oxidized during heating, as is the case with finely divided elemental boron.

Boron nitride, in intimate contact with tungsten, is believed to decompose and react at high temperature (under vacuum) in the following manner:



The nitrogen evolves as a gas and the reaction proceeds to completion. Since the tungsten is present in excess of the amount required for the formation of the higher boride, WB, it is likely that  $\text{W}_2\text{B}$  forms exclusively. It is also probable that additional vacancies are created within the pressed compact by the foregoing reaction. Such vacancies may also act as effective barriers to solid diffusion and grain growth.

The effectiveness of boron nitride in stabilizing both density and permeability is illustrated in subsequent Figs. 5-1 through 5-4. The stabilizing influence appears extremely effective at  $1800^\circ\text{C}$  (see Figs. 5-1 and 5-2) and still very effective at  $1600^\circ\text{C}$  (Figs. 5-3 and 5-4), relative to the Ta and Ta+Re additives. However, the  $1500^\circ\text{C}$  data (Fig. 5-6) indicate a faster rate of permeability decay than for three of the W-Ta-Re compositions. That permeability of the W-8Cu-4BN should decay more rapidly at  $1500^\circ\text{C}$  than at  $1600^\circ\text{C}$  is not considered normal for a temperature and time-dependent mechanism. Therefore, additional life testing of the BN-stabilized tungsten will be performed subsequently under Modification 6, which will include:

Phase I. Investigation of effects of boron nitride, boron, and nitrogen on thermal stability of fine angular tungsten.

Phase II. Determination of most advantageous level of stabilizer addition, determined as optimum under Phase I.

Phase III. Determination of relationship between stabilizer content, sintered density (40 to 75 percent range), and thermal stability.

Photomicrographs of Fig. 4-15 illustrate the changes in density and pore structure obtained by the addition of various percentages of boron nitride to W-Cu mixtures.

Procedures for the manufacture of large ionizer bars from W-Cu-BN mixtures are illustrated in the flow sheet of Fig. 7-1, Section 7.

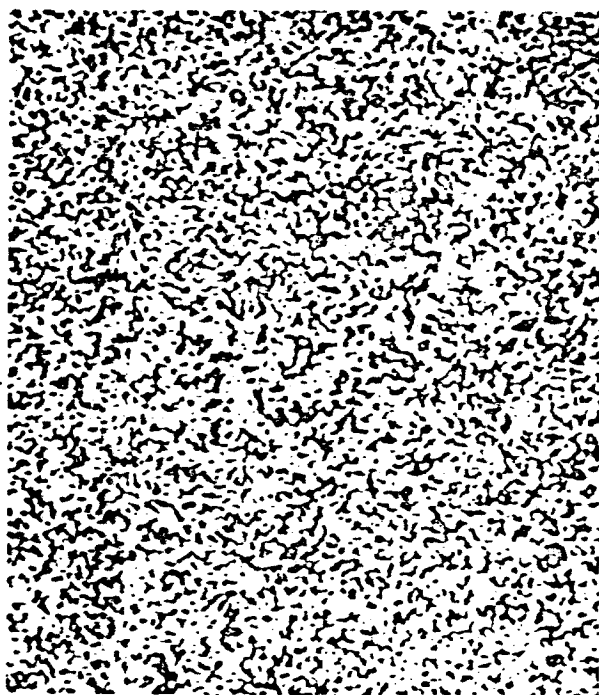
Two series of low-density boron-containing porous materials were produced and tested for ionization performance. The first compact had an average density of 47.0 percent and was produced from a mixture of W-8Cu-4BN. The ionizer button had a relative density of 47 percent and a permeability of  $2.959 \times 10^{-6}$  gm.cm.<sup>-1</sup>sec.<sup>-1</sup>torr<sup>-1</sup>. Chemical analysis of the first compact was as follows:

W-8Cu-4BN; After Copper Removal

Element	ppm	Element	ppm
Al	< 10	Fe	30
Ag	< 1	Mn	< 3
B	> 2500	Mo	200
Ba	< 3	Nb	< 100
Be	< 1	Ni	< 10
Bi	< 3	Pb	< 10
C	47	Sn	< 3
Ca	30	Ti	30
Co	< 3	V	< 3
Cr	20	Total Others	< 300
Cu	400	W	Bal.

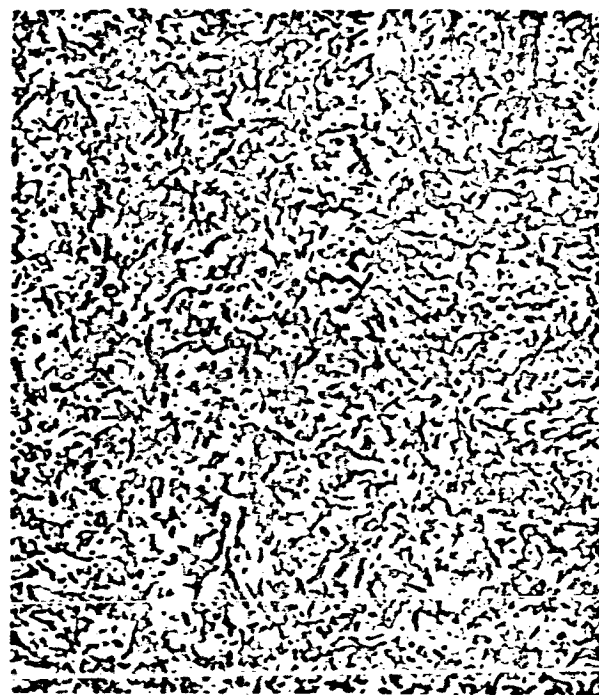
Ionization performance data for this low-density boron-containing material are presented in Section 6.





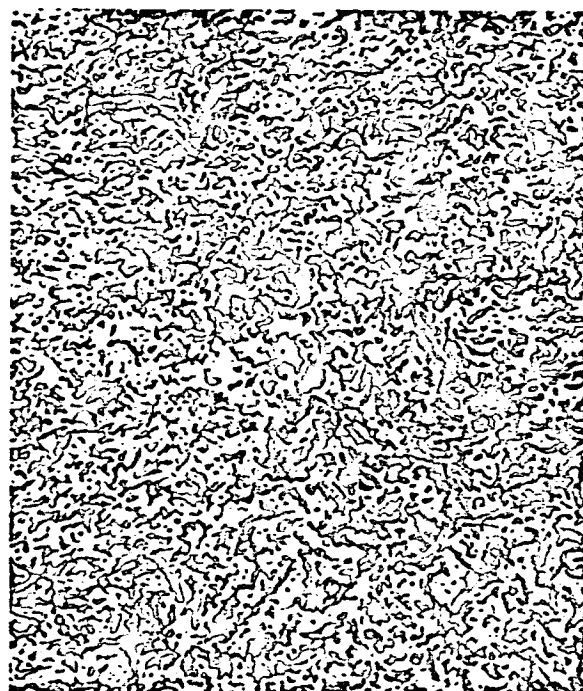
Neg. 2733

Density 70.6%  
92W-8Cu Flake



Neg. 2990

Density 63.9%  
90W-8Cu-2BN



Neg. 2989

Density 53.6%  
89W-8Cu-3BN



Neg. 2899

Density 47.5%  
88W-8Cu-4BN

FIG. 4-15 MICROSTRUCTURES OF LOW DENSITY "SHAPED CORE" IONIZER MATERIALS, SHOWING EFFECT OF BORON NITRIDE ADDITIONS. (All specimens sintered 15 minutes 1500°C plus 30 minutes at 1800°C) (X400)

Ionization performance of the 47 percent-dense, boron-containing material was inferior to that of the 67 percent-dense, pure tungsten material. To obtain performance-test comparison between the boron-containing and the boron-free material, it was necessary to produce boron-containing material having comparable density. Determinations for boron-containing mixtures indicated that a density range of 60-65 percent could be produced with the W-8Cu-2BN mixture.

Six buttons were prepared for ionization tests from W-8Cu-2BN. Data for these are as follows:

Button No.	Diam, in.	Thick, in.	Wt, gm	St, sec	Density, %	Permeability, gm.cm. <sup>-1</sup> sec. <sup>-1</sup> torr <sup>-1</sup>
1	.1876	.0407	.2160	8.11	60.73	$1.181 \times 10^{-6}$
2	.1877	.0408	.2218	8.84	62.12	$1.080 \times 10^{-6}$
3	.1879	.0406	.2168	7.47	60.88	$1.273 \times 10^{-6}$
4	.1873	.0409	.2177	7.50	61.09	$1.287 \times 10^{-6}$
5	.1869	.0407	.2159	9.20	61.14	$1.048 \times 10^{-6}$
6	.1875	.0410	.2175	8.68	60.78	$1.112 \times 10^{-6}$

Button No. 1 was selected for ionization testing. Test results for this button are discussed in Section 6. It will be noted that test results between boron-containing, and boron-free material of comparable density, indicate that boron does not exert a deleterious influence on ionization performance.

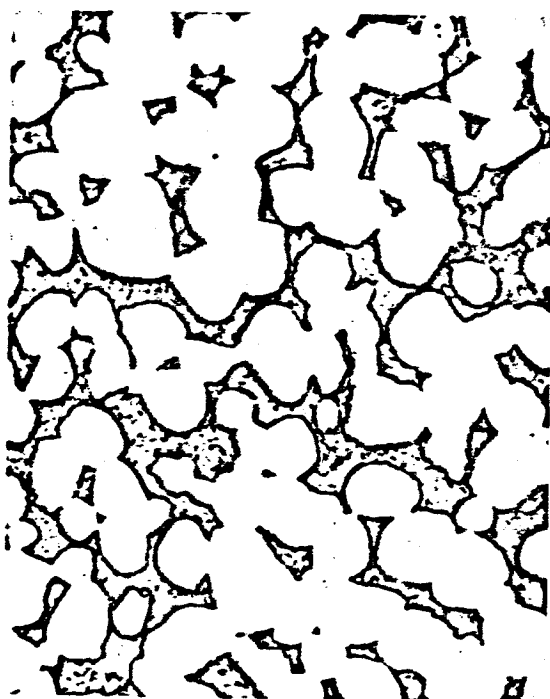
Representative microstructures of various types of ionizers are compared in Fig. 4-16.



Neg. 2974 Density = 66.8%  
W-8Cu



Neg. 3078 Density = 61.4%  
W-6Cu-2BN



Neg. 2971 Density = 71.7%  
SPH.W(0.25-2.5 $\mu$ )



Neg. 2958 Density = 71.9%  
SPH.W-5Ta-10Re

FIG. 4-16 REPRESENTATIVE MICROSTRUCTURES (X2000)

## 5. ACCELERATED LIFE TESTING OF IONIZERS

A practical technique for evaluating the thermal stability of ionizers is the accelerated or simulated life test. This consists of heating at temperatures significantly higher than those of engine operation, in order to accelerate solid diffusion and obtain measurable changes in structure-dependent parameters within feasible lengths of heating time. Under this contract, duplicate sets of ionizer buttons, representing nine ionizer compositions, were heated isothermally at 1800°C, 1600°C, and 1500°C for 8, 8, and 12 hours, respectively. The heating runs were made without cesium at  $<1 \times 10^{-5}$  torr pressure, except during heat-up when  $<1 \times 10^{-4}$  torr was maintained.

Density and  $N_2$  permeability of 18\* ionizer buttons were measured after 0\*\*, 1, 2, 4, and 8 hours at each temperature. Measurements were also taken after 12 hours at 1500°C. The density units were converted from  $gm/cm^3$  to % of maximum theoretical; the  $N_2$  permeability units from  $gm \cdot cm^{-1} \cdot sec^{-1} \cdot torr^{-1}$  to % permeability change, relative to the zero time (as-sintered) reference. Duplicate button averages of relative density, permeability, and % permeability change are given in Table 5-I for all compositions and heating periods.

The life-test data of Table 5-I are plotted as indicated in the following tabulation.

<u>Coordinates</u>	<u>For Test Temp, °C</u>	<u>Plotted in Fig.</u>
% $\rho$ vs Time	1800	5-1
% Perm. Change vs Time	1800	5-2
% $\rho$ vs Time	1600	5-3
% Perm. Change vs Time	1600	5-4
% $\rho$ vs Time	1500	5-5
% Perm. Change vs Time	1500	5-6

\* Duplicate buttons of 9 compositions

\*\* As-sintered condition used as the zero time reference

TABLE 5 - 1  
Accelerated Life-Test Data, Indicating Effect of Heating on  
Ionizer Density and Permeability (Heated under  $10^{-6}$  torr without cesium)

Ionizer Composition, Mt. %		1800°C					1600°C					1500°C						
		Hours at Temperature					Hours at Temperature					Hours at Temperature						
		0	1	2	4	8	0	1	2	4	8	0	1	2	4	8	12	
W-Bu <sup>(a)</sup>	Density, % of max. theoretical	66.07	70.44	73.34	76.66	80.55	70.16	71.50	72.31	73.81	76.14	69.23	69.82	69.85	70.26	71.64	72.52	
	H <sub>2</sub> Permeability, $\mu$ P <sup>(b)</sup>	0.988	0.667	0.413	0.287	0.087	0.704	0.577	0.522	0.451	0.350	0.645	0.580	0.564	0.560	0.468	0.401	
	Change in Perm., %	0.00	-32.49	-58.20	-70.95	-91.19	0.00	-18.04	-25.85	-35.94	-50.28	0.00	-10.08	-12.56	-16.28	-27.44	-37.83	
	Time for 50% Perm. Decrement <sup>(c)</sup>			1.62 hrs.						7.90 hrs.							17.09 hrs.	
Sph.N(control) <sup>(c)</sup>	Density, % of max. theoretical	71.30	75.37	78.34	82.23	86.82	71.76	72.52	73.01	73.97	75.21	71.37	72.15	72.39	72.83	73.89	74.61	
	H <sub>2</sub> Permeability, $\mu$ P	1.012	0.640	0.434	0.224	0.050	1.003	0.908	0.846	0.780	0.654	0.971	0.897	0.860	0.828	0.741	0.678	
	Change in Perm., %	0.00	-36.73	-57.10	-77.91	-95.06	0.00	-9.43	-15.61	-22.24	-34.81	0.00	-7.62	-11.43	-14.73	-23.69	-30.18	
	Time for 50% Perm. Decrement			1.58 hrs.						12.84 hrs.							24.22 hrs.	
W-Ta <sup>(c)</sup>	Density, % of max. theoretical	76.33	80.09	82.23	84.55	87.03	76.02	76.18	76.36	77.01	77.59	75.79	76.04	76.31	76.41	76.73	76.62	
	H <sub>2</sub> Permeability, $\mu$ P	0.115	0.063	0.035	0.016	(d)	0.122	0.116	0.112	0.106	0.096	0.127	0.123	0.122	0.120	0.114	0.113	
	Change in Perm., %	0.00	-45.22	-69.57	-86.09	--	0.00	-4.92	-8.20	-15.09	-21.31	0.00	-3.15	-3.94	-5.51	-10.24	-11.02	
	Time for 10% Perm. Decrement		0.17 hr.						2.34 hrs.								10.57 hrs.	
W-Ta-5Re <sup>(c)</sup>	Density, % of max. theoretical	76.73	80.57	82.81	85.02	87.74	75.61	76.08	76.39	77.20	77.82	76.76	76.83	76.99	77.02	77.51	77.64	
	H <sub>2</sub> Permeability, $\mu$ P	0.096	0.056	0.031	0.012	(d)	0.095	0.096	0.091	0.085	0.074	0.093	0.094	0.096	0.094	0.090	0.087	
	Change in Perm., %	0.00	-41.67	-67.71	-87.50	--	0.00	+1.05	-4.21	-10.53	-22.11	0.00	+1.08	+3.22	+1.02	-3.22	-5.15	
	Time for 10% Perm. Decrement		0.24 hr.						3.82 hrs.								16.40 hrs.	
W-Ta-10Re <sup>(c)</sup>	Density, % of max. theoretical	70.65	72.48	74.27	75.61	77.29	71.14	71.19	71.27	71.39	71.78	71.09	71.16	71.24	71.19	71.39	71.47	
	H <sub>2</sub> Permeability, $\mu$ P	0.260	0.189	0.153	0.129	0.088	0.248	0.240	0.235	0.235	0.228	0.251	0.242	0.242	0.242	0.239	0.238	
	Change in Perm., %	0.00	-27.31	-41.15	-50.38	-66.15	0.00	-3.23	-5.24	-5.24	-8.07	0.00	-3.59	-3.59	-3.59	-4.78	-5.18	
	Time for 10% Perm. Decrement		0.34 hr.								10.74 hrs.						42.26 hrs.	
W-Ta <sup>(c)</sup>	Density, % of max. theoretical	77.04	81.09	83.42	85.37	88.07	78.33	78.70	79.14	79.82	80.69	76.54	76.64	76.67	76.83	77.07	77.30	
	H <sub>2</sub> Permeability, $\mu$ P	0.099	0.053	0.030	0.012	(d)	0.099	0.096	0.093	0.085	0.069	0.095	0.092	0.095	0.096	0.094	0.090	
	Change in Perm., %	0.00	-46.46	-69.70	-87.88	--	0.00	-3.03	-6.06	-14.14	-30.30	0.00	-3.68	0.00	+0.53	-1.58	-5.26	
	Time for 10% Perm. Decrement		0.14 hr.						2.97 hrs.								16.62 hrs.	
W-Ta-5Re <sup>(c)</sup>	Density, % of max. theoretical	73.55	75.44	76.87	78.37	80.61	74.15	74.02	74.31	75.04	74.99	73.55	73.47	73.58	73.60	73.76	73.94	
	H <sub>2</sub> Permeability, $\mu$ P	0.190	0.158	0.130	0.098	0.067	0.187	0.206	0.203	0.199	0.188	0.185	0.192	0.200	0.200	0.197	0.194	
	Change in Perm., %	0.00	-16.84	-31.58	-48.42	-64.74	0.00	+10.19	+8.58	+6.70	+0.53	0.00	+3.78	+8.11	+8.11	+6.49	+4.87	
	Time for 10% Perm. Decrement		0.59 hr.							14.83 hrs.							50.21 hrs.	
W-Ta-10Re <sup>(c)</sup>	Density, % of max. theoretical	74.54	76.44	78.13	79.58	81.83	74.56	74.56	74.87	75.13	75.55	74.04	73.81	73.88	73.83	73.62	73.91	
	H <sub>2</sub> Permeability, $\mu$ P	0.148	0.143	0.114	0.087	0.057	0.146	0.177	0.173	0.169	0.159	0.099	0.126	0.129	0.161	0.169	0.166	
	Change in Perm., %	0.00	-3.38	-22.97	-41.22	-61.49	0.00	+21.23	+18.49	+15.75	+8.90	0.00	+27.27	+30.30	+62.63	+70.71	+67.68	
	Time for 10% Perm. Decrement			1.20 hrs.						18.73 hrs.							114.5 hrs.	
W-Bu-4BN <sup>(a)</sup>	Density, % of max. theoretical	49.15	50.00	50.73	51.09	52.00	47.59	47.88	47.90	47.98	48.11	49.35	49.51	49.40	49.59	49.59	49.77	
	H <sub>2</sub> Permeability, $\mu$ P	3.442	3.419	3.346	3.355	3.274	2.995	3.032	3.010	3.022	2.988	3.325	3.344	3.321	3.405	3.340	3.203	
	Change in Perm., %	0.00	-0.67	-2.79	-2.53	-4.88	0.00	+1.24	+0.50	+0.90	+0.23	0.00	+0.571	-0.120	+2.41	+0.45	-3.67	
	Time for 10% Perm. Decrement				16.39 hrs.					60.22 hrs.							17.67 hrs.	

(a) Tungsten powder base: 0.8% H<sub>2</sub>-reduced, with addition of fine Cu flake

(b) One micropore unit =  $10^{-6}$  gm.cm<sup>-1</sup>.sec<sup>-1</sup>.torr<sup>-1</sup>

(c) Tungsten powder base: 0.25-2.5% microspheres, with additions of fine Ta and Re particles

(d) Indicates apparent closure of pore network, with essentially zero permeability

(e) Times for 50 percent and 10 percent permeability decrements were obtained by interpolating or extrapolating the curves of Figs. 5-2, 5-4, and 5-6.

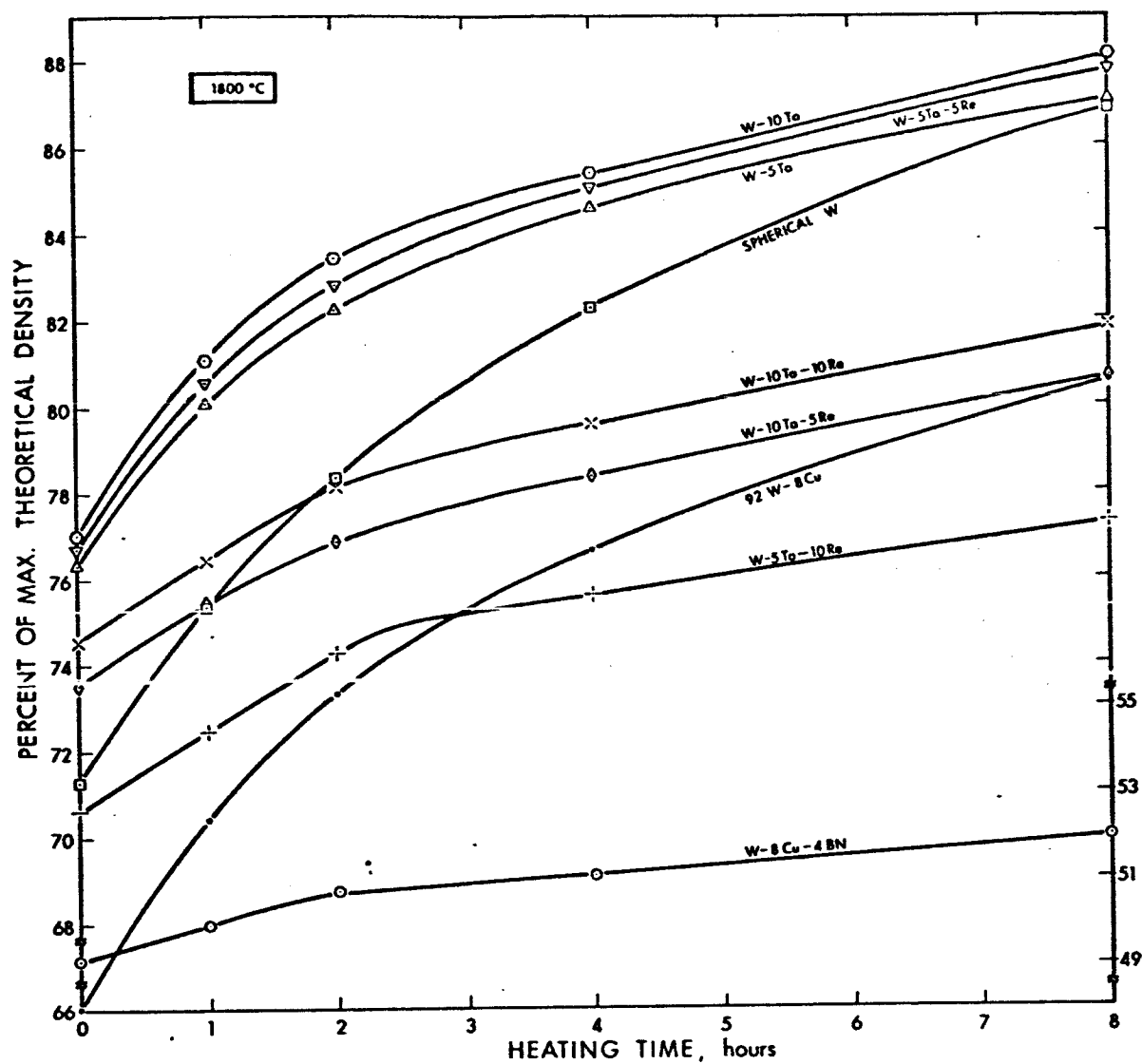


FIG. 5-1 CHANGE IN DENSITY WITH HEATING TIME AT 1800°C FOR VARIOUS TUNGSTEN BASE IONIZERS (heated in  $10^{-6}$  torr range without cesium)

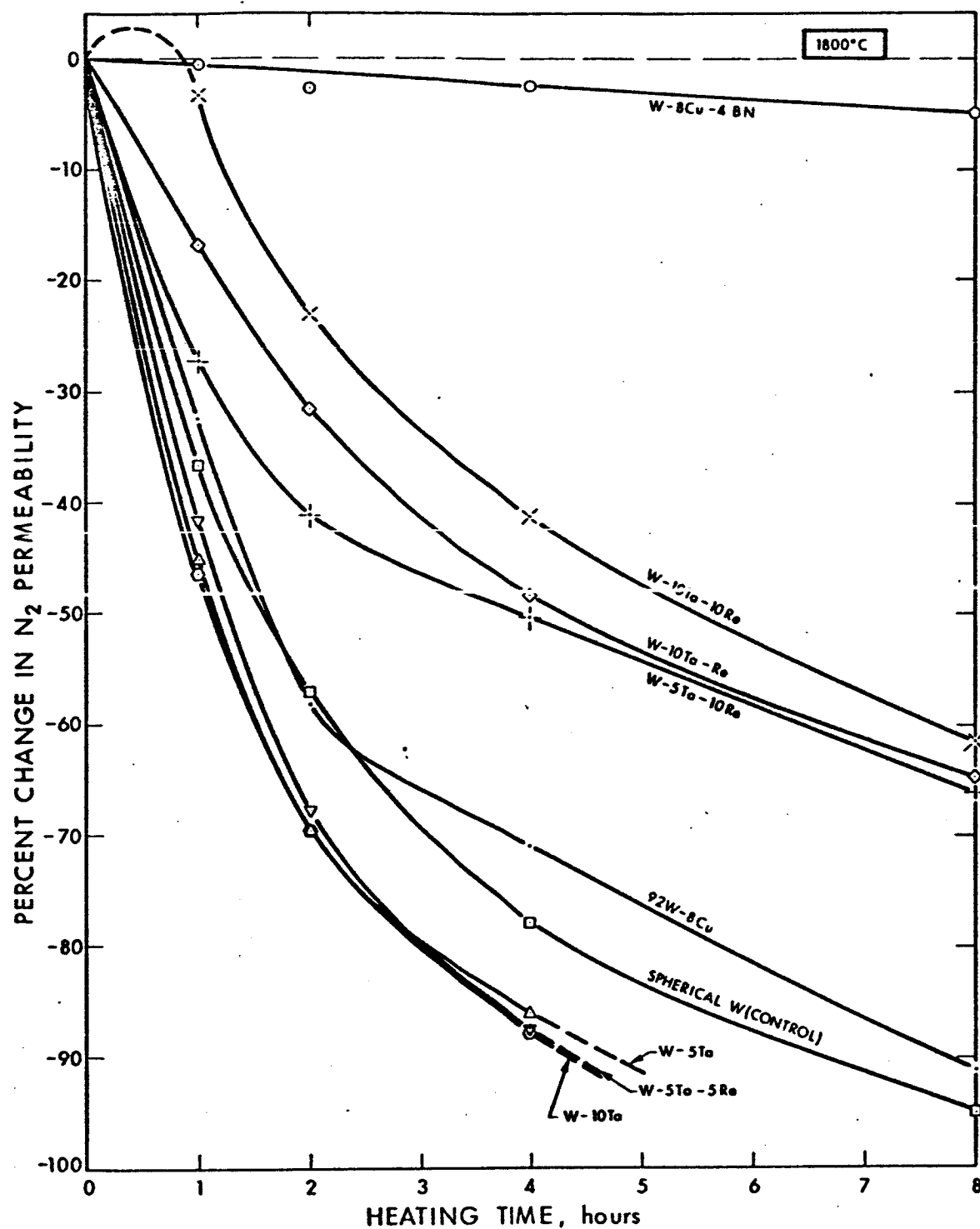


FIG. 5-2 CHANGE IN N<sub>2</sub> PERMEABILITY WITH HEATING TIME AT 1800°C FOR VARIOUS TUNGSTEN BASE IONIZERS (heated in 10<sup>-6</sup> torr range without cesium)

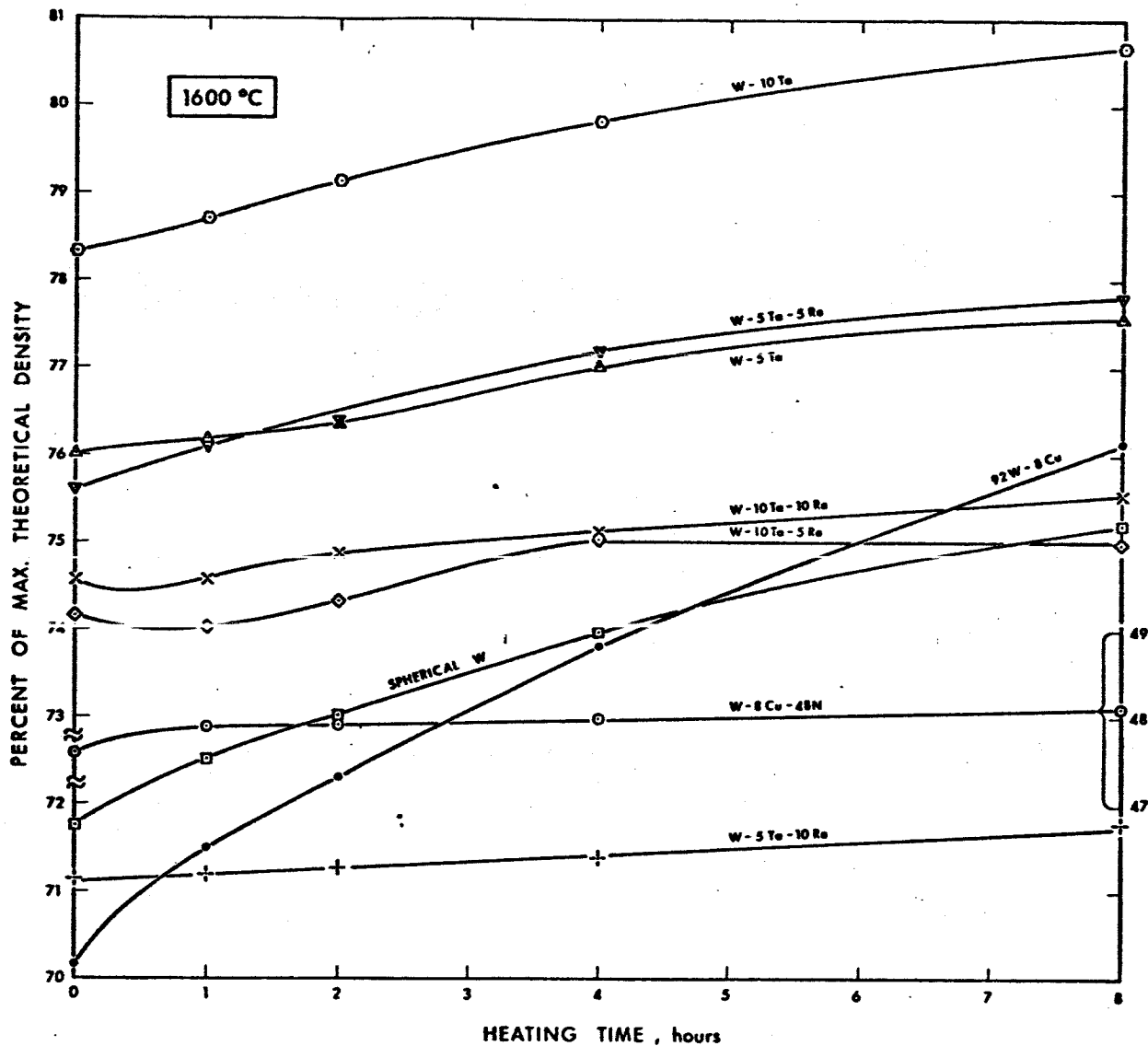


FIG. 5-3 CHANGE IN DENSITY WITH HEATING TIME AT 1600°C FOR VARIOUS TUNGSTEN-BASE IONIZERS (heated in  $10^{-6}$  torr range without cesium)



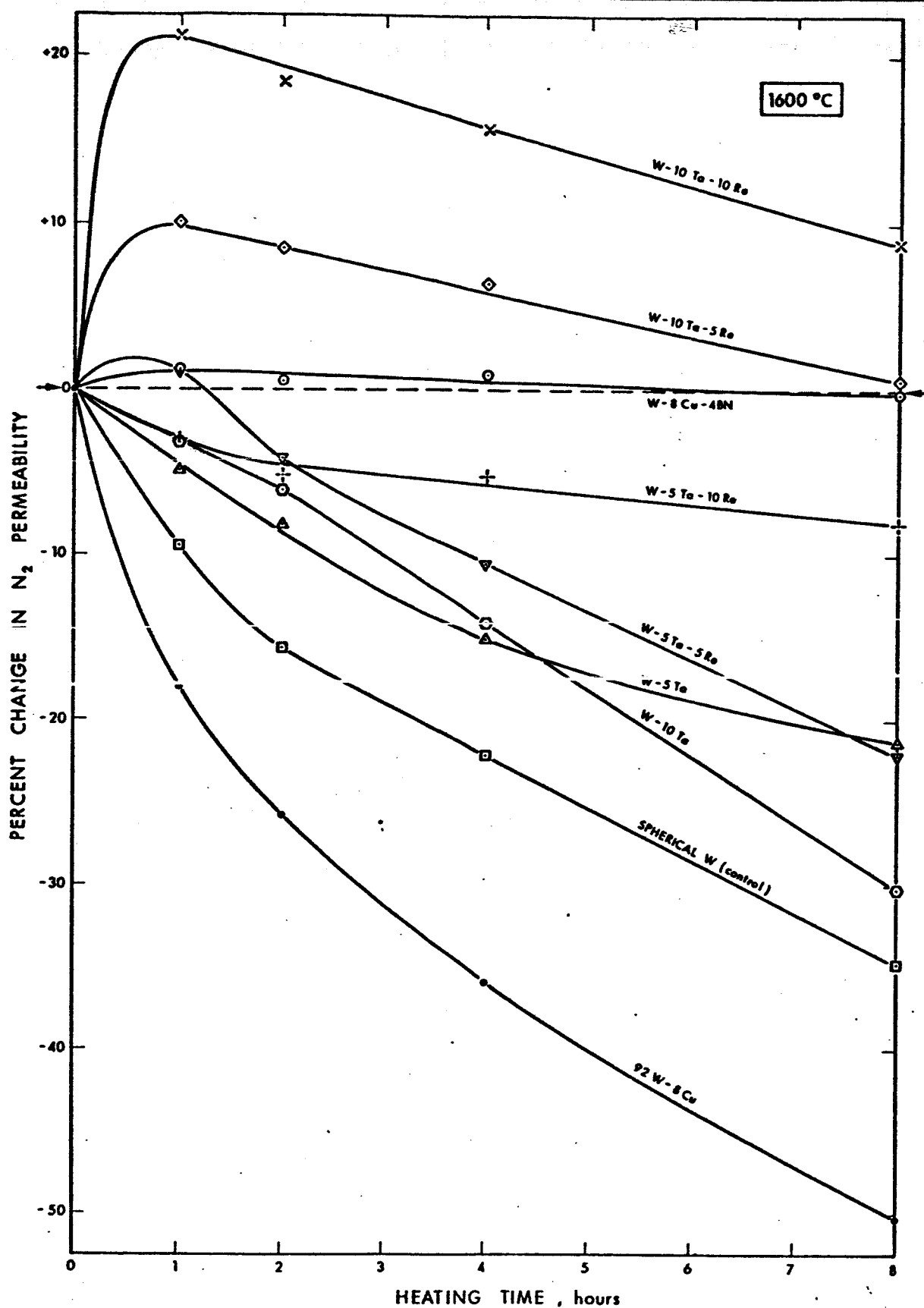


FIG. 5-4 CHANGE IN  $N_2$  PERMEABILITY WITH HEATING TIME AT 1600°C FOR VARIOUS TUNGSTEN-BASE IONIZERS (heated in  $10^{-6}$  torr range without cesium)

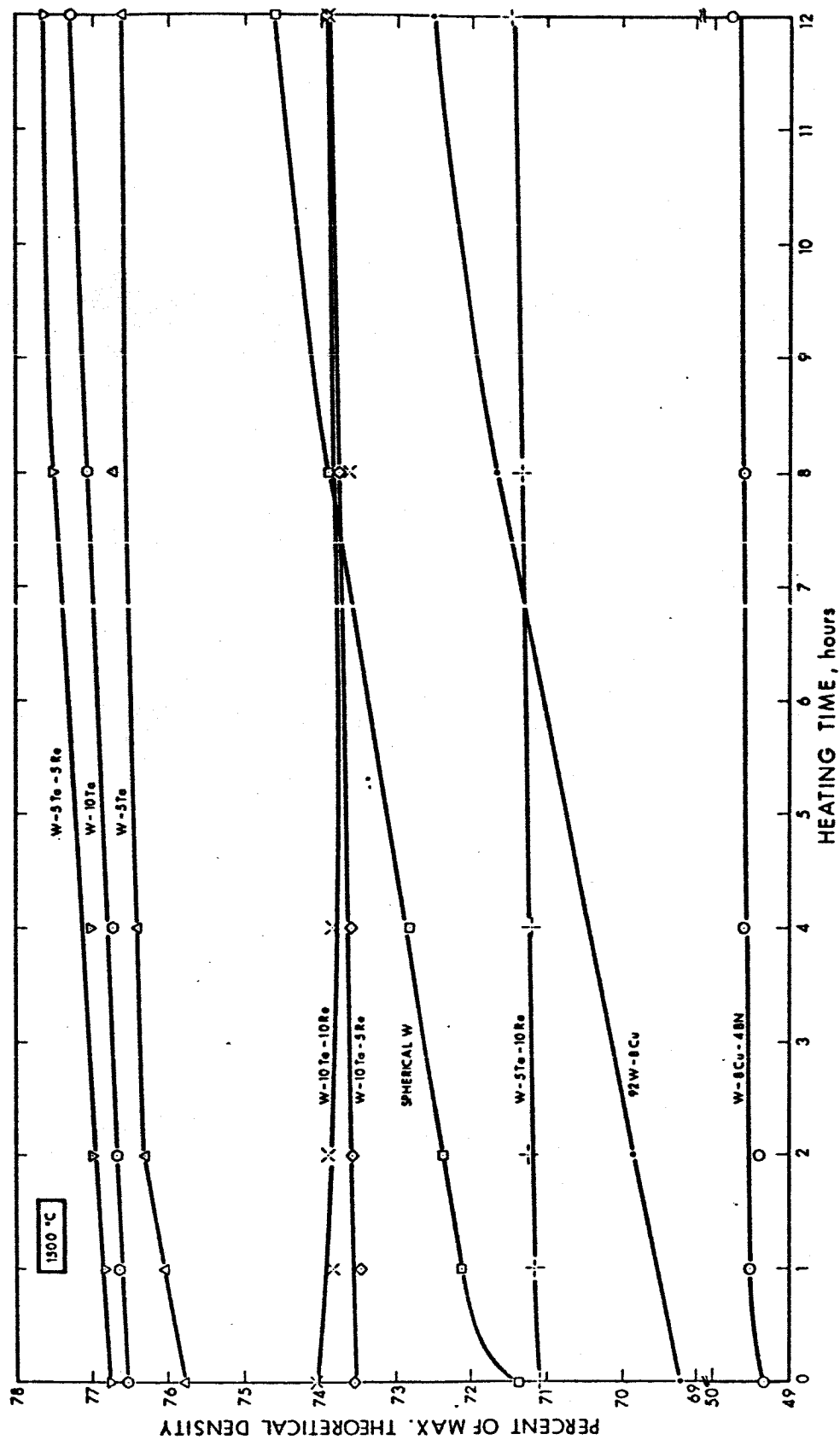


FIG. 5-5 CHANGE IN DENSITY WITH HEATING TIME AT 1500°C FOR VARIOUS TUNGSTEN BASE IONIZERS  
(heated in 10<sup>-6</sup>-torr range without cesium)

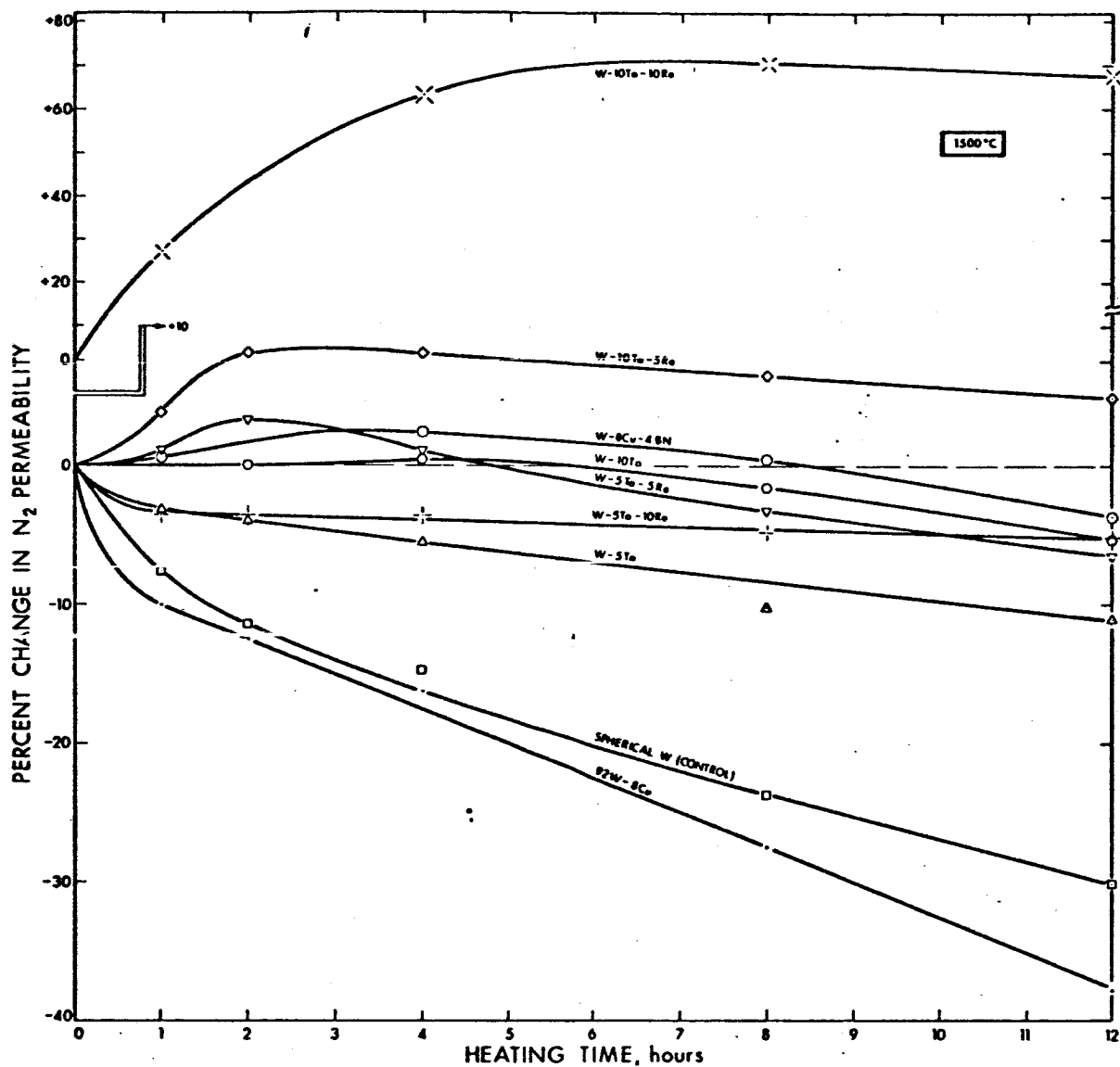


FIG. 5-6 CHANGE IN  $N_2$  PERMEABILITY WITH HEATING TIME AT 1500°C FOR VARIOUS TUNGSTEN BASE IONIZERS (heated in  $10^{-6}$ -torr range without cesium)

At 1800°C, densities increase normally and progressively with heating time, while permeabilities (except initially for W-10Ta-10Re) decrease.

At 1600°C, densities increase and permeabilities decrease more slowly than at 1800°C. However, Fig. 5-4 indicates that W-5Ta-5Re, W-10Ta-5Re, and (most markedly) W-10Ta-10Re initially increase in permeability, and (ref. Fig. 5-3) decrease initially and slightly in density.

At 1500°C, average rates of densification are still slower, as (beyond initial increases) are rates of permeability decrease. The marked tendency of W-10Ta-10Re and (to lesser degrees) W-10Ta-5Re, W-5Ta-5Re, etc., to increase in permeability during earlier stages of heating is believed to be associated with completion of homogenization by diffusion. By deduction, an initial increase in permeability reflects an opening-up or coarsening of a pore network. Such coarsening has been demonstrated to occur by diffusion and growth of one type of particle into another (adjacent) particle. Energy for driving solid diffusion can stem from (1) chemical gradients, (2) free surface energy differentials, and (3) differences in particle lattice orientation. Concerning the present compositions, it appears that W-10Ta-10Re (having highest alloy content) still retained chemical gradients in the as-sintered condition. As these gradients were eliminated during subsequent life testing, coarsening of the pore structure and attendant increase in permeability resulted. Not until the W-10Ta-10Re alloy reached chemical homogeneity did permeability begin to decay and density to increase in normal fashion.

To extrapolate the accelerated life-test data to a lower temperature range, typical of ion-engine operation, it was first necessary to decide whether to use density or permeability criteria, or both. The decision was made to use permeability-change data exclusively for the following reasons:

- (1)  $N_2$  permeability is much more sensitive to structural changes than is density.
- (2)  $N_2$  permeability can be measured much more accurately than can density.
- (3) Density levels at which different ionizer compositions become impermeable (and useless) are not only variable, but not accurately known. On the other hand, the zero value of permeability marks the absolute termination of ionizer function.

Based on the foregoing reasoning, the data of Table 5-I and curves of Figs. 5-2, 5-4, and 5-6 were used to determine the times required for specific percentages of permeability decrement at each test temperature. For the unalloyed tungsten ionizers, which decayed quite rapidly in permeability during testing, the 50% permeability decrement level was selected as being most appropriate and valid for comparison. On the other hand, since permeabilities of the spherical-base alloy ionizers decayed relatively slowly (especially at  $1500^{\circ}\text{C}$ ), a 10% permeability decrement was selected as most appropriate and valid.

The times required for either 50% or 10% permeability decrements are noted in Table 5-I for each test temperature and ionizer composition. Dividing the selected "% decrement in permeability" values by the times required to produce those decrements yielded values of "average percent decrease in permeability per hour". The latter values were plotted on a log scale versus temperature on a linear scale.

Curves of Fig. 5-7 indicate the times required at various temperature levels for the 92W-8Cu and spherical W (control) ionizers to decay 50% in permeability. As noted, data points at 1800, 1600, and  $1500^{\circ}\text{C}$  permit extrapolations down to  $1100^{\circ}\text{C}$  with reasonable confidence.

Curves of Fig. 5-8 indicate the times required at the various temperature levels for the spherical tungsten-base alloy ionizers to decay 10% in permeability. In general, data points at 1800, 1600 and

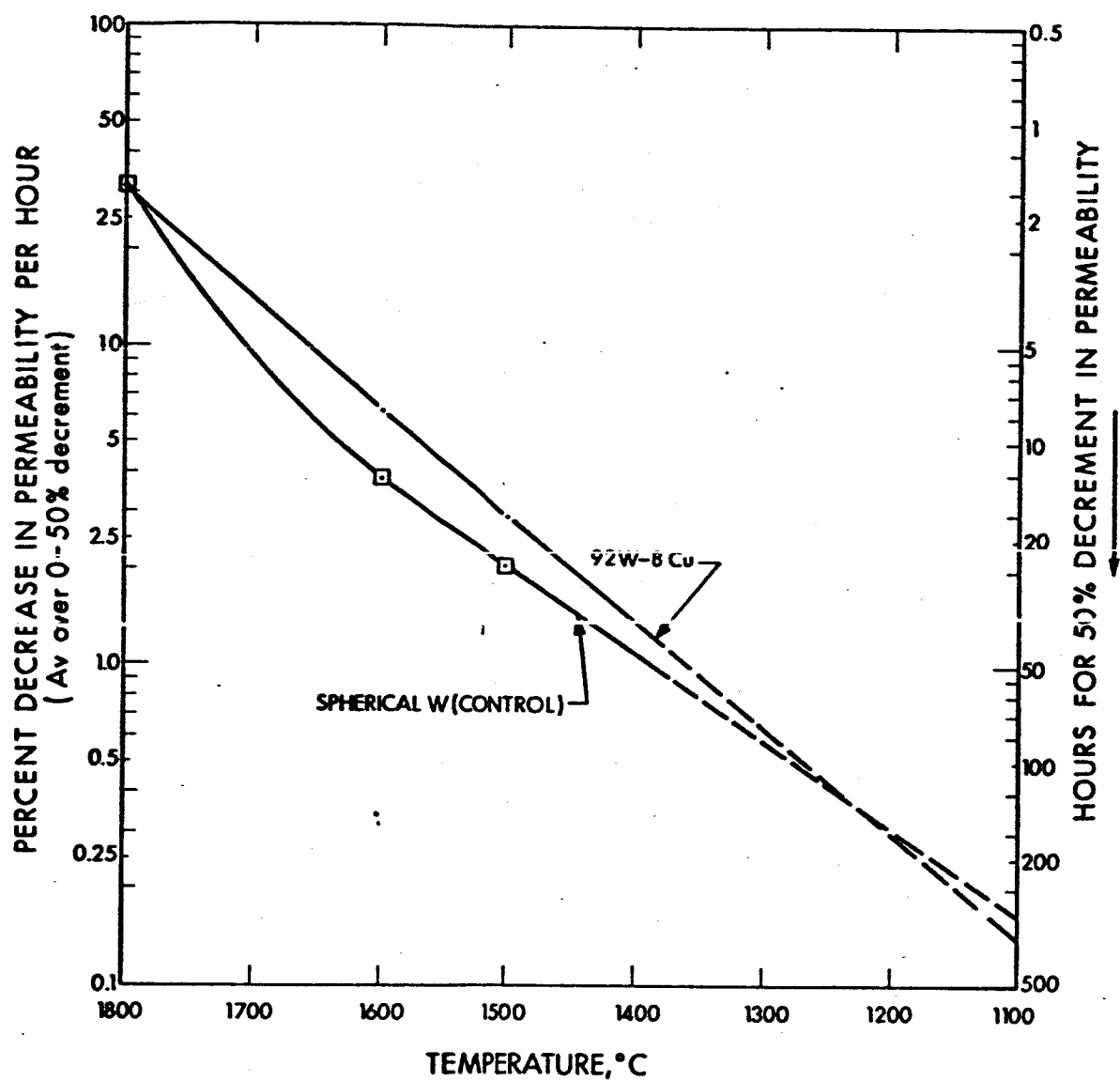


FIG. 5-7 TIME-TEMPERATURE RELATIONSHIP FOR TWO TYPES OF POROUS TUNGSTEN, INDICATING THE TIME REQUIRED AT VARIOUS TEMPERATURE LEVELS FOR A 50 PERCENT DECREMENT IN PERMEABILITY

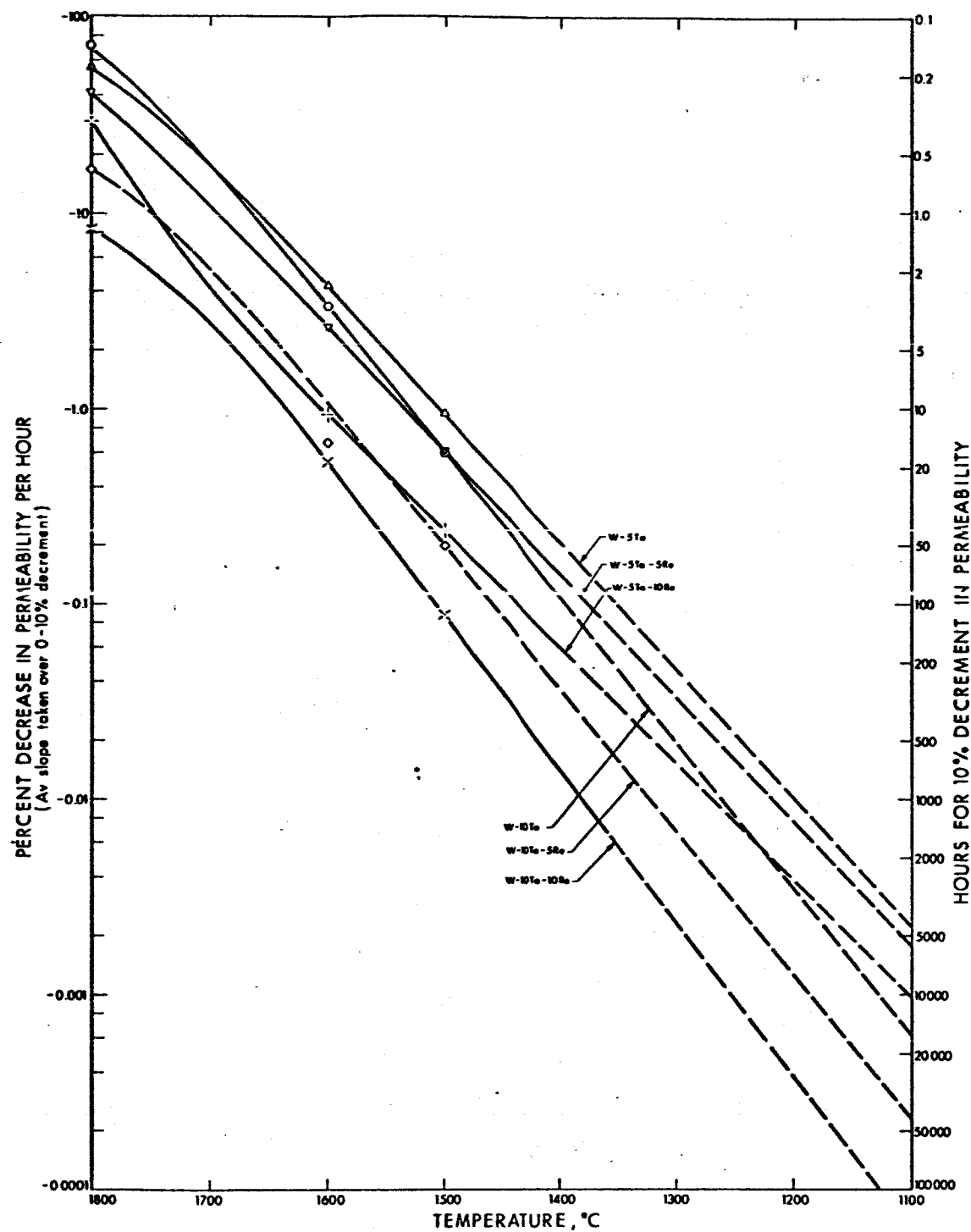


FIG. 5-8 TIME-TEMPERATURE RELATIONSHIP FOR SIX SPHERICAL -  
TUNGSTEN-BASE ALLOYS INDICATING THE TIME REQUIRED  
AT VARIOUS TEMPERATURE LEVELS FOR A 10 PERCENT  
DECREMENT IN PERMEABILITY

1500°C are in good alignment, such that extrapolations here were also made down to 1100°C. Of the 18 data points plotted in Fig. 5-8, only that for W-10Ta-5Re at 1600°C was not adhered to in drawing the curves. Therefore, the W-10Ta-5Re curve is dotted to indicate uncertainty. In general, curves for ionizers containing 5% of tantalum decline less steeply than do those containing 10% of tantalum. Such characteristic slopes serve to increase overall credibility of the data.

Time data extrapolated from Figs. 5-7 and 5-8 are summarized in Table 5-II. In general, these extrapolations indicate that the alloy additions progressively extend ionizer lifetimes.

As noted in Table 5-II, the data trend for the W-8Cu-4BN ionizer precluded extrapolation. Specifically, the permeability decay rates of this material (averaged over a decrement of 10%) were -0.610%/hr at 1800°C, -0.166%/hr at 1600°C, and -0.566%/hr at 1500°C. These data could be interpreted to mean that the material has an optimum range of thermal stability at approximately 1600°C. However, since structural and permeability changes are diffusion and temperature dependent, the presence of a stability peak at 1600°C is difficult to comprehend, much less to explain.

In summary, data presented in this section indicate that ionizers, capable of >10,000 hours of effective operation at 1100-1200°C, have been developed. The contractual design goal of 10,000 hours operation at 1100°C-1400°C (with density, permeability and pore-size changes of <1%) is still to be achieved.



TABLE 5-II

TIME REQUIRED FOR 50% OR 10% DECREMENT  
IN N<sub>2</sub> PERMEABILITY BY VARIOUS IONIZER COMPOSITIONS  
(Extrapolated from experimental data obtained at 1800°C, 1600°C, and 1500°C)

Composition, wt. %	Based on Perm. Decrement, %	Time (hrs) at Temperature, °C		
		1300	1200	1100
W-8Cu (a)	-50	7.8x10 <sup>1</sup>	1.7x10 <sup>2</sup>	3.6x10 <sup>2</sup>
Sph.W(control) (b)	-50	8.5x10 <sup>1</sup>	1.6x10 <sup>2</sup>	3.0x10 <sup>2</sup>
W-5Ta (b)	-10	2.2x10 <sup>2</sup>	9.9x10 <sup>2</sup>	4.5x10 <sup>3</sup>
W-5Ta-5Re (b)	-10	2.3x10 <sup>2</sup>	1.3x10 <sup>3</sup>	5.6x10 <sup>3</sup>
W-5Ta-10Re (b)	-10	6.6x10 <sup>2</sup>	2.6x10 <sup>3</sup>	1.0x10 <sup>4</sup>
W-10Ta (b)	-10	5.2x10 <sup>2</sup>	2.9x10 <sup>3</sup>	1.6x10 <sup>4</sup>
W-10Ta-5Re (b)	-10	1.5x10 <sup>3</sup>	8.1x10 <sup>3</sup>	4.4x10 <sup>4</sup>
W-10Ta-10Re (b)	-10	4.3x10 <sup>3</sup>	2.6x10 <sup>4</sup>	>1.0x10 <sup>5</sup>
W-8Cu-4BN (c)	-	(d)	(d)	(d)

- (a) W Powder Base: 0.8μ H<sub>2</sub>-reduced, with addition of fine Cu flake  
 (b) W Powder Base: 0.25-2.5μ microspheres, with additions of finer Ta and Re  
 (c) W Powder Base: 0.8μ H<sub>2</sub>-reduced, with additions of fine Cu flake and BN  
 (d) Indeterminate from data trend

## 6. IONIZATION PERFORMANCE TESTING OF SELECTED COMPOSITIONS

During the 5 years of continuous ionizer performance testing on NASA and AF programs, the apparatus, techniques, definitions and form of presentation of results have undergone continuous improvement. At a recent contractors meeting, the need for a complete description of the present apparatus and procedure was suggested.

### 6.1 Test Apparatus

#### 6.1.1 The Vacuum System

The vacuum system, shown in Fig. 6-1, is a 1 x 3-foot stainless-steel chamber with four six-inch window ports, a full-length cylindrical LN<sub>2</sub> shroud, and a one-bounce LN<sub>2</sub>-cooled elbow trap over a 10-inch gage valve and a 10 inch oil diffusion pump. All flanges have elastomer seals. Roughdown is done through a by-pass line with a 15-CFM two-stage mechanical pump. The elbow trap is chilled for 45 minutes, starting at a pressure of 10<sup>-4</sup> with the exhaust going through the tank shroud. The diffusion pump is turned on at a pressure in the 10<sup>-5</sup>-torr range and it takes about 30 minutes to reach 10<sup>-7</sup> torr or lower with the DC-704 silicone oil. The residual gas spectrum has a high level of hydrocarbon for the first hour or two, depending upon the previous history. The tubulated ion gage is on top of the elbow trap, looking at the cold surface. The residual gas spectrum during the early part of a typical ionizer test is shown in Fig. 6-2. The partial pressures at high ion currents decline with time as the apparatus outgasses (primarily the ion collector). The mass analyzer was placed near the collector end of the chamber.

The liquid nitrogen supply to the elbow and liner is cycled by an automatic relay valve having a temperature sensor in the exhaust line. The system is extensively interlocked to turn off all power except to the mechanical pump in case of a vacuum, source, or power supply failure.

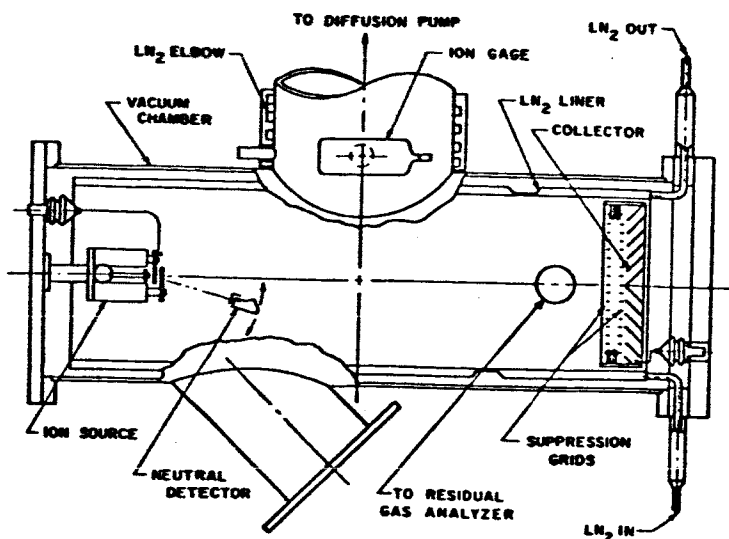
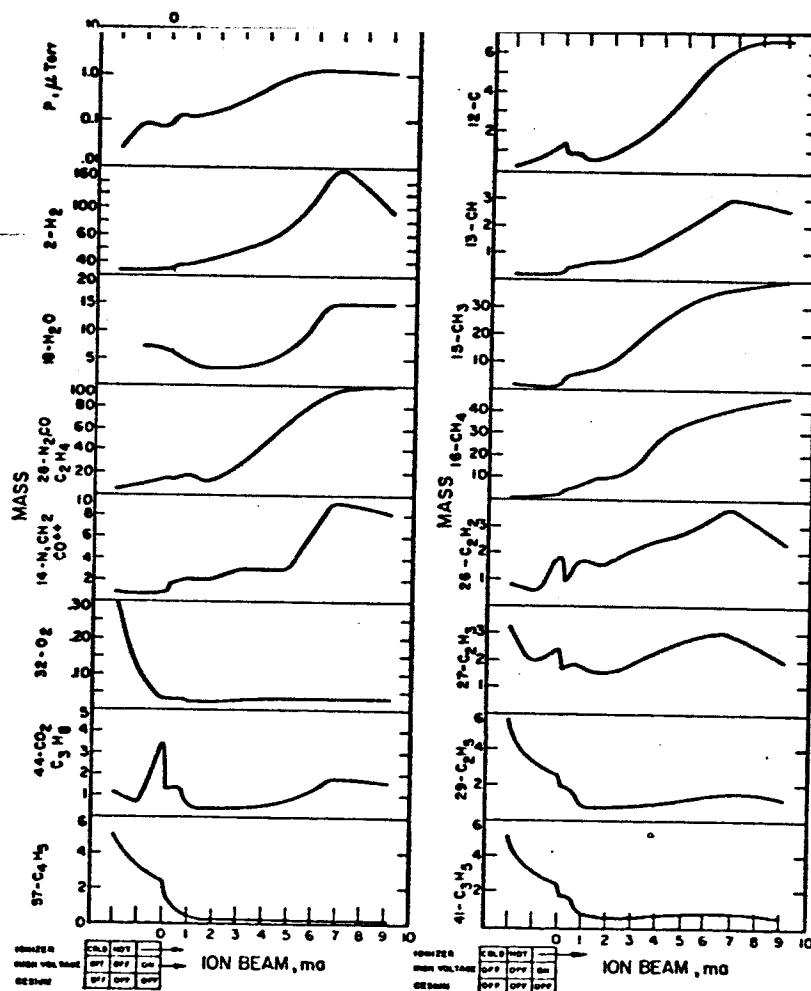


FIG. 6-1

SCHEMATIC OF VACUUM CHAMBER WITH ION SOURCE, NEUTRAL DETECTOR, ION COLLECTOR, AND RESIDUAL GAS ANALYZER

FIG. 6-2

RESIDUAL GAS ANALYSIS WITH INCREASING ION BEAM CURRENT IN DIFFUSION PUMPED SYSTEM WITH LIQUID NITROGEN LINER AND TRAP (All readings in scale divisions on a Veeco GA4 Residual Gas Analyzer)



### 6.1.2 Ion Source

The ion source has been described in two previous technical publications<sup>5,6</sup>, and has since undergone further modification. The ionizer and feed tube are electron beam welded into the Mo holder, eliminating all brazes from the high-temperature feed manifold and from areas adjacent to the porous sample. No special shielding precautions are taken during the welding, and no oxide transport of the Mo or Ta has been suspected. The re-useable ionizer and reservoir heaters are press-fitted over the respective parts (all shown in Fig. 6-3) and provide good heat transfer. The ionizer thermocouple has W-Re alloy elements, insulated by MgO in a 1/16-inch-diameter Ta sheath, located in a 0.20-inch-deep hole in the Mo holder. The reservoir thermocouple uses sheathed chromel-alumel elements, inserted into a hole in the 304 stainless-steel reservoir.

### 6.1.3 Ion Collector

The ion collector is a closed-end copper 45°-chevron with the center V section pointing toward the ionizer. All chevrons are linear and uniformly spaced. The assembly is suspended inside the LN<sub>2</sub>-cooled liner and not separately cooled. Two sets of tungsten ribbons with their edges toward the ion source are used for secondary electron suppression, with -90V on the grid closest to the collector. The outer grid and collector are at ground potential. The ion collector current (including grid current) is used for all ion current curves. These are first plotted automatically on an X-Y recorder as a function of ionizer thermocouple voltage.

### 6.1.4 Neutral Detector

The neutral detector is diagrammed in Fig. 6-4. The detector has two sets of .040"-wide collimating slits, separated by ion deflection plates, and is usually operated at 15° to the beam axis and 5 inches away from the ionizer. An electromechanical shutter permits measurement of the detector background signal. The neutral cesium atoms are ionized and repelled by an AC-heated tungsten ribbon at +45V, well

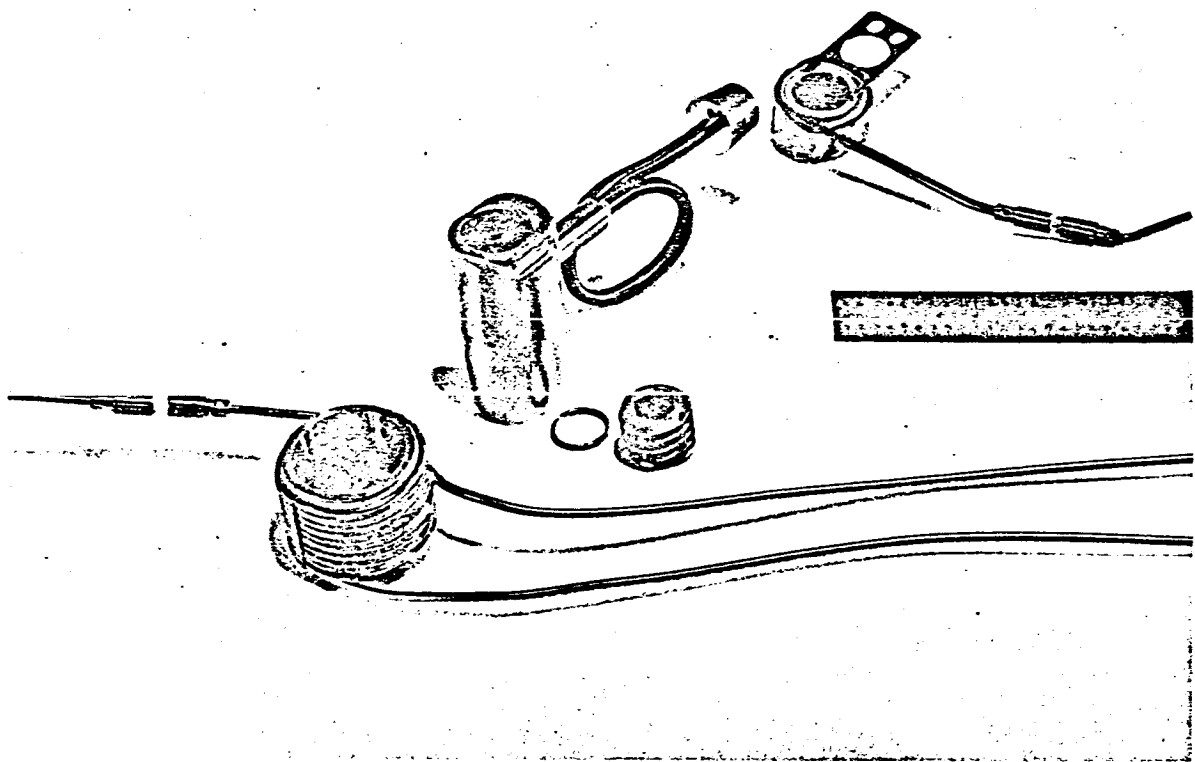


FIG. 6-3 IONIZER - RESERVOIR ASSEMBLY WITH REUSABLE HEATERS

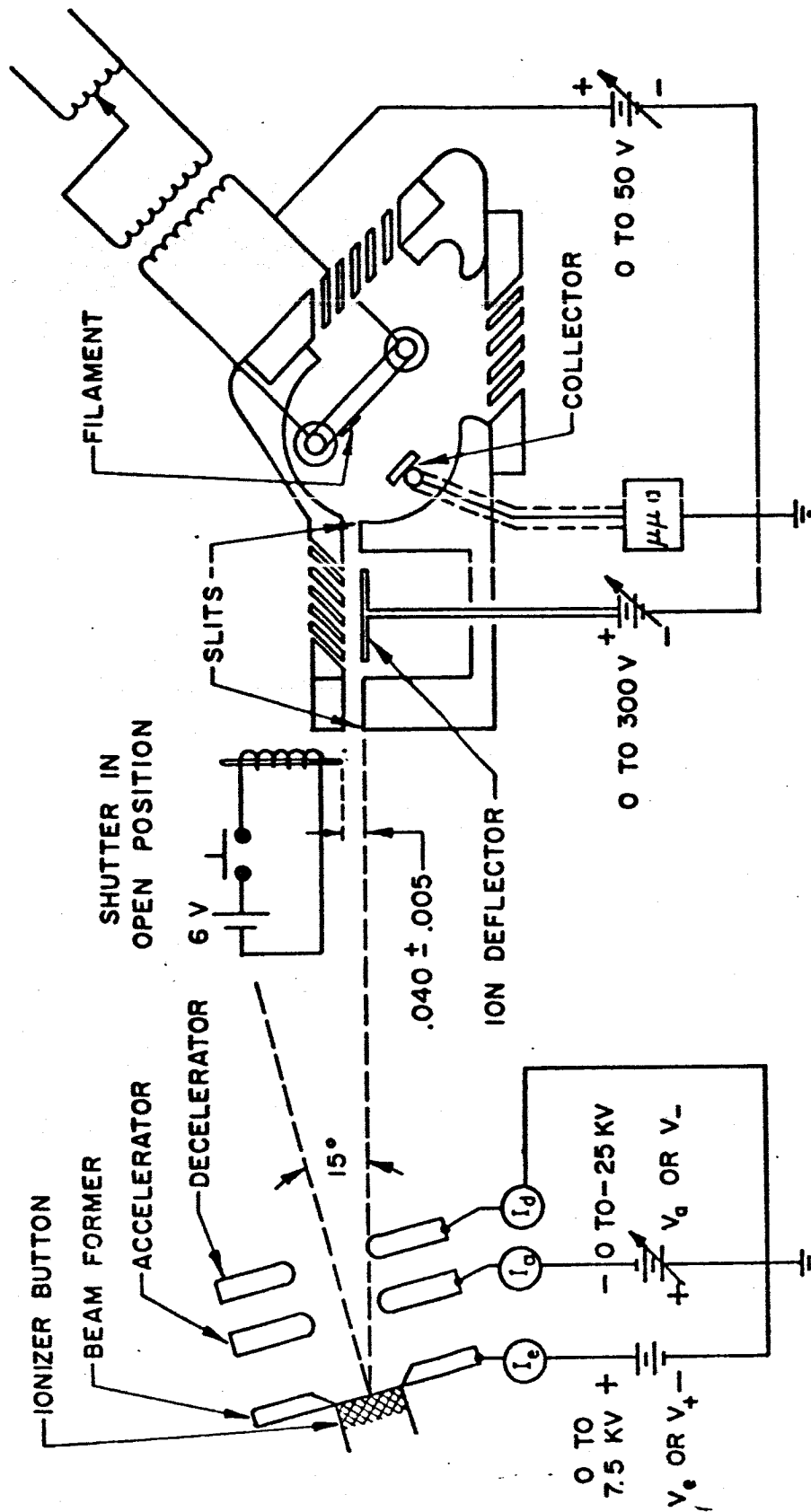


FIG. 6-4 SCHEMATIC AND CIRCUIT DIAGRAM OF ION ACCELERATOR AND NEUTRAL DETECTOR

above the space-charge limit. About half of the ions are intercepted by the vented case and the other half by the collector, both of which are at ground potential. The signal from the collector is measured by an electrometer amplifier and plotted as a function of the ionizer thermocouple voltage on another X-Y recorder. A special chopper-isolation transformer circuit is used to convert the thermocouple signals at ionizer potential to ground-potential signals.

## 6.2 Test Procedure

The porous ionizer is lathe machined with the Cu-Fe infiltrant, then finish ground. The infiltrant is removed and the ionizer's  $N_2$  permeability measured. The Ta feed tube is electron-beam welded to the Mo holder prior to attaching the ionizer. Then, after preheating the assembly to  $\sim 1000^\circ\text{C}$ , the ionizer is beam welded into the holder under a  $10^{-6}$ -torr pressure. The reservoir is then brazed on with a Ni-Cu alloy and the assembly is bubble tested in acetone. The  $N_2$  permeability is measured again and the ionizer is photographed. The porous area of the ionizer is computed from the enlarged photograph. Pore counts are not usually performed on the actual test buttons, but on representative samples from the parent compact.

The reservoir is loaded with a few grams of cesium in an argon-atmosphere dry box after several evacuations and argon flushes. The reservoir plug is sealed with a metal gasket and the assembly is handled in air during installation in the ion source and vacuum system. No serious air diffusion through the porous ionizer has been observed. Ionizers stored in air with loaded reservoir have not shown any detectable change in performance due to contamination of the cesium.

The loaded assembly is heat shielded with Ta foil, mounted in the ion source, and the accel-decel electrodes aligned with a special tool. The electric connections are checked for continuity and isolation. The system is pumped down as described previously in Subsection 6.1.1. The ionizer is heated to  $1200^\circ\text{C}$  and allowed to operate at  $5\text{ mA/cm}^2$  for several hours to outgas the hot parts, condition the insulators, and

effect a stable, reproducible surface condition. During the conditioning period, the ionizer and reservoir temperature, the neutral detector current and the ion collector currents are continuously recorded. This conditioning can be done overnight with interlocks on the ionizer heater, neutral eye, high voltage supplies, in addition to those on chamber pressure, diffusion-pump water, and  $\text{LN}_2$  supply.

The eye alignment is checked using the light beam of its filament. Electrode alignment can be checked by various methods: the neutral-detector angular scan, the glowing spot visible on the collector due to ion impingement, or by argon admission and observation of the beam.

Ion current-temperature (mV) curves and neutral detector current-temperature (mV) curves are taken on the X-Y recorders when the curves are reproducible. Total neutral reading is obtained by turning off the high voltage. The accel-electrode temperature is not controlled. No attempts to clean the surface are made by sputtering; however, the effects of admission of  $\text{O}_2$  or acetylene have been studied on occasion.

A set of curves is taken by increasing the flow rate in steps, with perveance also being tested for each voltage to insure adequacy of the voltage for emission-limited current (the neutral detector is the most sensitive indicator of adequate voltage). Frequently, these tests are continued for several days.

After the test, the apparatus is carefully examined for retention of electrode alignment and ionizer surface appearance. At times, heavy arcing causes melted surface spots. Finally, the cesium is removed from the reservoir, and the ionizer  $\text{N}_2$  permeability is again measured. A record of the reservoir temperature versus ion current is, of course, available to detect if cesium permeability changed during the test.

### 6.3 Performance Indicator Definition

The most important indicators of ionizer performance are the neutral fraction and the transition temperature as a function of ion current density and ionizer structure (i.e., pore density, pore size,



pore shape and distribution). These parameters are representative of the ionization (propellant utilization) efficiency and ion generation efficiency (with emissivity neglected) respectively, and are related to the ion engine performance parameters, accelerator lifetime and power efficiency. They are treated in detail by Kuskevics<sup>7</sup>.

The common measurements of surface ionization give the ion current density and neutral efflux as a function of ionizer temperature for various cesium flow rates. A typical set of curves for porous tungsten, normally taken with decreasing temperature, is shown in Fig. 6-5 in order to define the various regions of operation. As temperature is decreased, ion current density does not remain constant in the low cesium-coverage region, because of a change in both ionization efficiency and cesium permeability. The "transition temperature" characterizes the portion of the curve denoted as the transition region, where a rapid change in slope occurs as the various parts of the surface change from a low to a high cesium coverage (characterized by low ionization efficiency and high neutral efflux). When the transition is very discontinuous, as for uniform solid surfaces, one can speak of the upper and lower transition temperatures, one with increasing  $T_e$  and the other with decreasing  $T_e$ . For porous ionizers, there is usually no sharp discontinuity, and various definitions for transition temperature have been used by different investigators. The one definite temperature point, designated  $T_\alpha$ , is that at which neutral fraction,  $\alpha$ , reaches a minimum (if it does). This point is sensitive to surface conditions. Curves at high current densities frequently do not reach a minimum at an ionizer temperature below 1400°C, as shown in Fig. 6-22. Another definition of transition temperature, designated  $T_{CI}$ , is the temperature at which the ion current declines by 5 percent (two times the minimum detectable current change). This latter temperature depends somewhat on its definition, and may be less sensitive to surface conditions. For porous ionizers, it is best to use the actual  $j$ - $T_e$  and  $\alpha$ - $T_e$  curves; rather than the transition temperature plots.

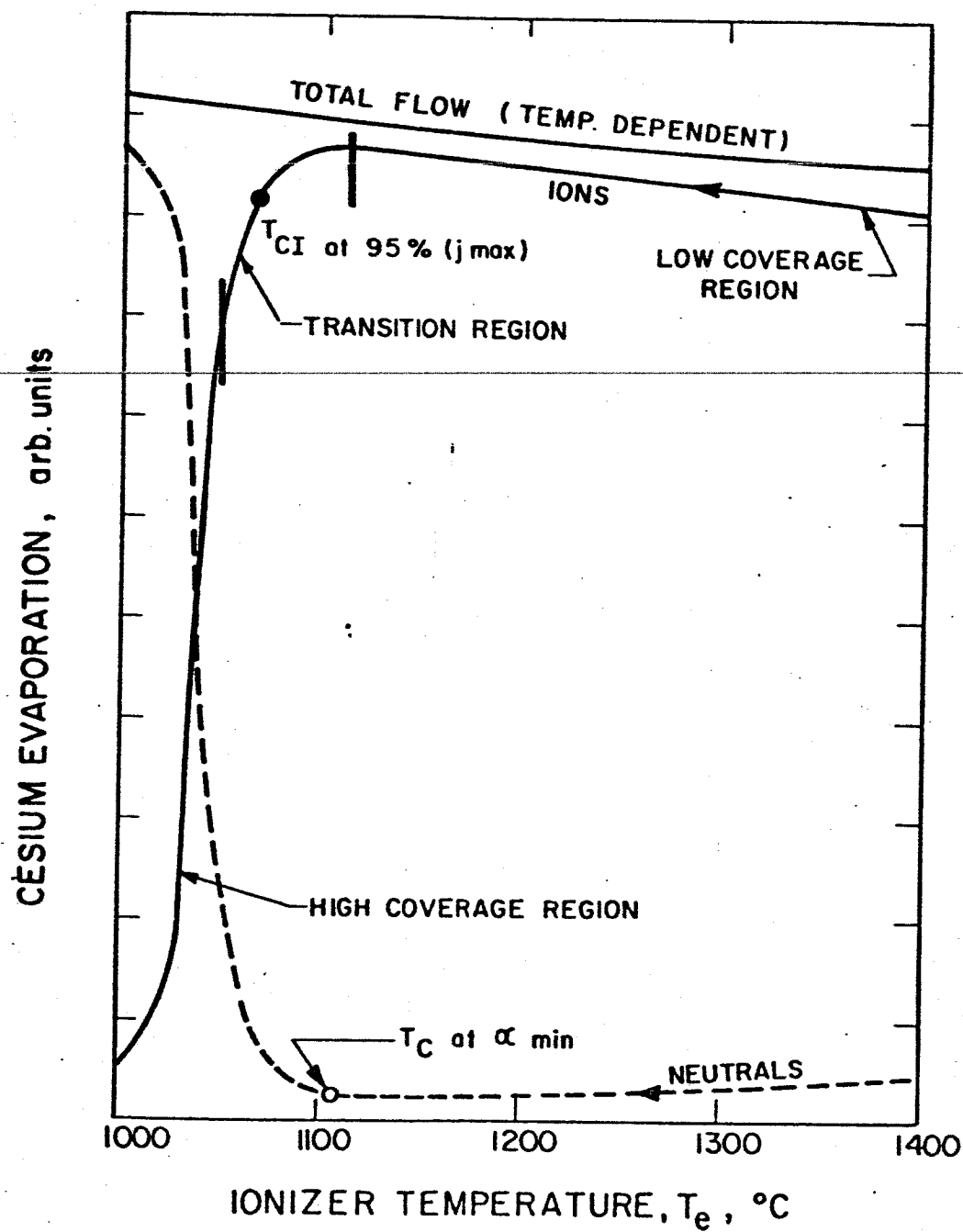


FIG. 6-5 ION CURRENT, NEUTRAL EFFLUX AND TOTAL FLOW  
VERSUS IONIZER TEMPERATURE FOR POROUS TUNGSTEN

The optimum temperature for operation of ion thrusters lies in the relatively small range between the lower  $T_{CI}$  and the higher  $T_{\alpha}$ . The sum of the ion and equivalent atom currents shows that total flow rate decreases about 3.5 percent per 100°C.

#### 6.4 Performance of Ternary Alloy Ionizers

A series of ionizers was made from 0.25-2.5 $\mu$  tungsten microspheres, with additions of tantalum and rhenium (ref. Subsection 3.3). A W-5wt%Ta-10wt%Re composition was selected for testing, because of its very high pore density, coupled with very long projected lifetime. The first sample evaluated showed excellent performance characteristics during preliminary testing. Damage to this ionizer during handling prevented verification of performance, and therefore a second ionizer was tested. Similar results were obtained from both samples. Metallurgical characteristics are listed on LeRC sheets of Appendix C, and are summarized as follows:

Ionizer No.	Density, N <sub>2</sub> %	Permeability, $\mu P^*$	Av Pore Diam, $\mu$	Av No. of pores/cm <sup>2</sup>	Av Pore Spacing, $\mu$
IVTXR-10	68.6	.28	1.58**	12.0x10 <sup>6</sup> **	2.9**
IVTXR-11	75.3	.12			

\*  $\mu P$  unit defined as  $10^{-6}$  gm/cm<sup>2</sup>·sec·torr

\*\* Measured at 72% relative density

The IVTXR-10 ionizer showed excellent performance, comparable to 60-70% dense ionizers, made by the copper-flake technique. The ion current transition temperature (Fig. 6-6) equaled the Langmuir data above 10 mA/cm<sup>2</sup>, but was 40° higher than the Langmuir data at 4 mA/cm<sup>2</sup>.

The neutral fraction versus ionizer temperature curves (Fig. 6-7) had a deep minimum below 10 mA/cm<sup>2</sup>, and had a shallow minimum even above 20 mA/cm<sup>2</sup>. The work function decreased slowly with ion current density from 5.0 eV at 5 mA/cm<sup>2</sup> to above 4.9 eV at 20 mA/cm<sup>2</sup>. The high

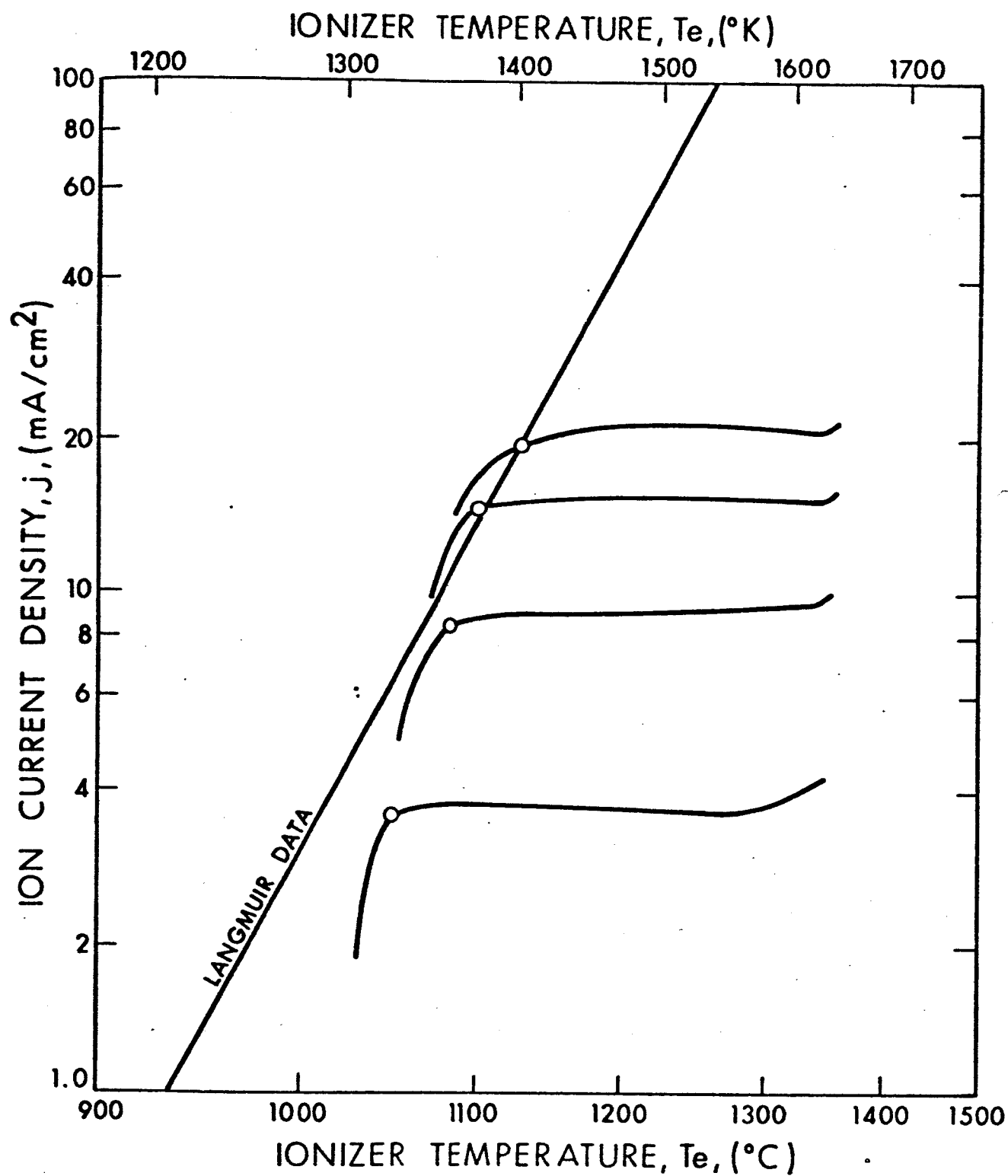


FIG. 6-6 ION CURRENT DENSITY VERSUS IONIZER TEMPERATURE FOR W-5  
TA-10Re ALLOY IONIZER, IVTXR-10

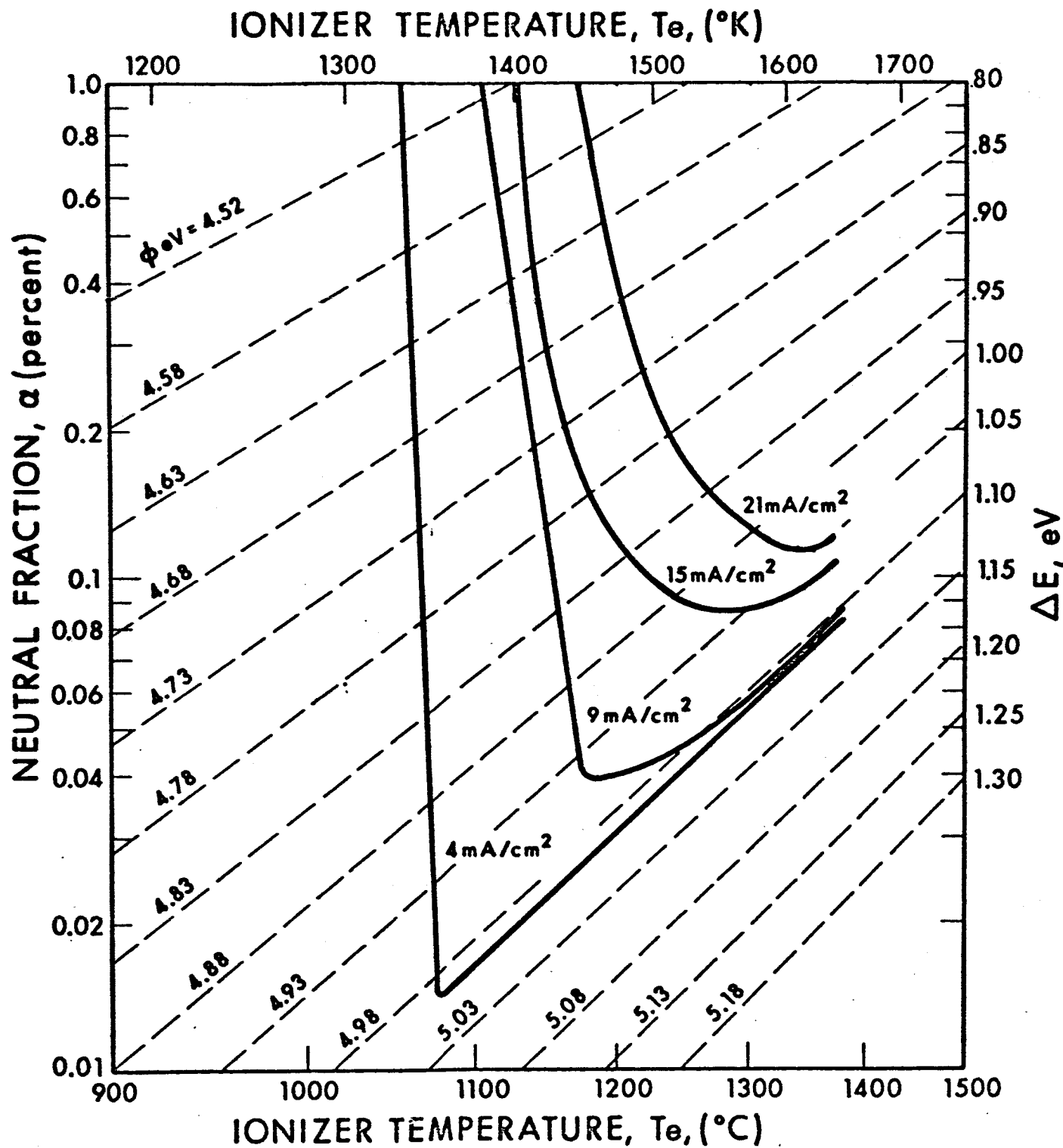


FIG. 6-7 NEUTRAL FRACTION VERSUS IONIZER TEMPERATURE FOR W-5 Ta-10Re ALLOY IONIZER, IVTXR-10

work function, coupled with a deep  $\alpha$  versus  $T_e$  minimum, resulted in a very low neutral fraction, 10X lower than E3 (1-4 $\mu$ ) spherical tungsten at 5 mA/cm<sup>2</sup> and 5X lower at 20 mA/cm<sup>2</sup>, as shown in Fig. 6-8.

The IVTXR-11 ionizer confirmed the performance of this type of ionizer material. The ion current transition temperatures were near the Langmuir data, as shown in Fig. 6-9. The neutral fraction versus ionizer temperature curves (Fig. 6-10) were very favorable at low ion current densities (below 12 mA/cm<sup>2</sup>), with a deep minimum corresponding to 4.95-5.00 eV work function. At higher ion current densities (above 20 mA/cm<sup>2</sup>), there was no shallow minimum in the curves below 1350°C. This characteristic led to a neutral fraction somewhat higher than for the other sample, especially at higher ion current densities. This may be due to the difference in final sintered density of the two samples (the lower neutral fraction came from the lower density sample). Nevertheless, neutral fraction was still superior to the E3 (1-4 $\mu$ ) spherical tungsten, as shown in Fig. 6-11.

Both of these ternary ionizers exhibited a strong Cs-flow dependence on the ionizer temperature and the rate of change of temperature at low ion current densities. Upon rapidly lowering the ionizer heater power at high temperature (1400°C), the ion current would quickly drop as much as 40% before leveling out with further temperature decline (see Figs. 6-6 and 6-9). This effect was not voltage dependent (since flow varied identically with voltage off) and did not effect the ionization efficiency. Similar behavior has been observed in many other tantalum-containing ionizers. The W-102<sup>0</sup>Ata ionizers, tested previously, all showed this phenomena to a similar degree, whereas the effect was observed to be small in the W-10%Ta ionizers. Several pure tantalum ionizers possessed such a strongly temperature-dependent Cs permeability that it was not possible to directly measure ionization efficiency as a function of ionizer temperature.

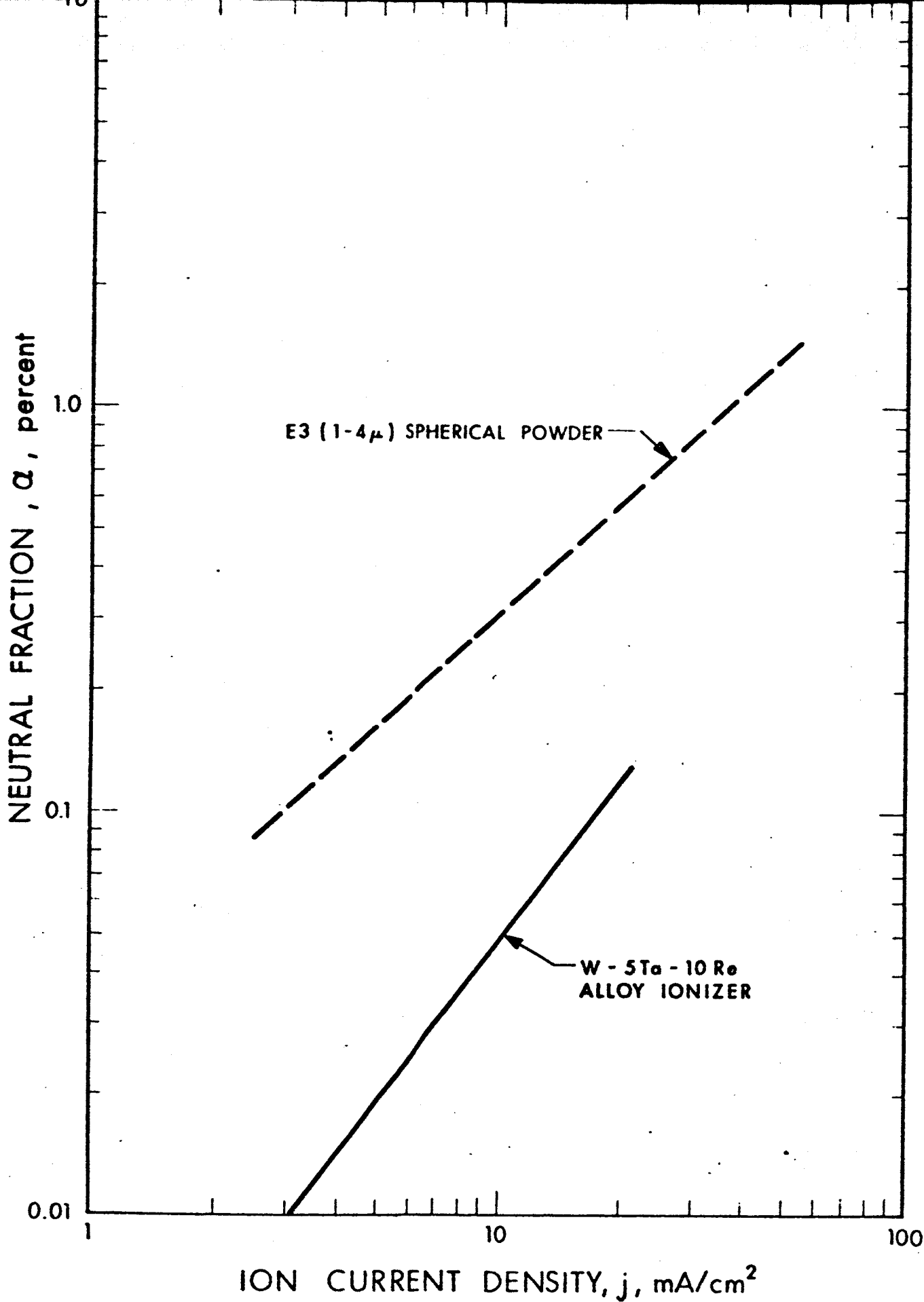


FIG. 6-8 NEUTRAL FRACTION VERSUS ION CURRENT DENSITY FOR W-5Ta-10Re ALLOY IONIZER IVTXR-10, COMPARED WITH THE E3 (1-4 $\mu$ ) SPHERICAL POWDER TUNGSTEN IONIZERS

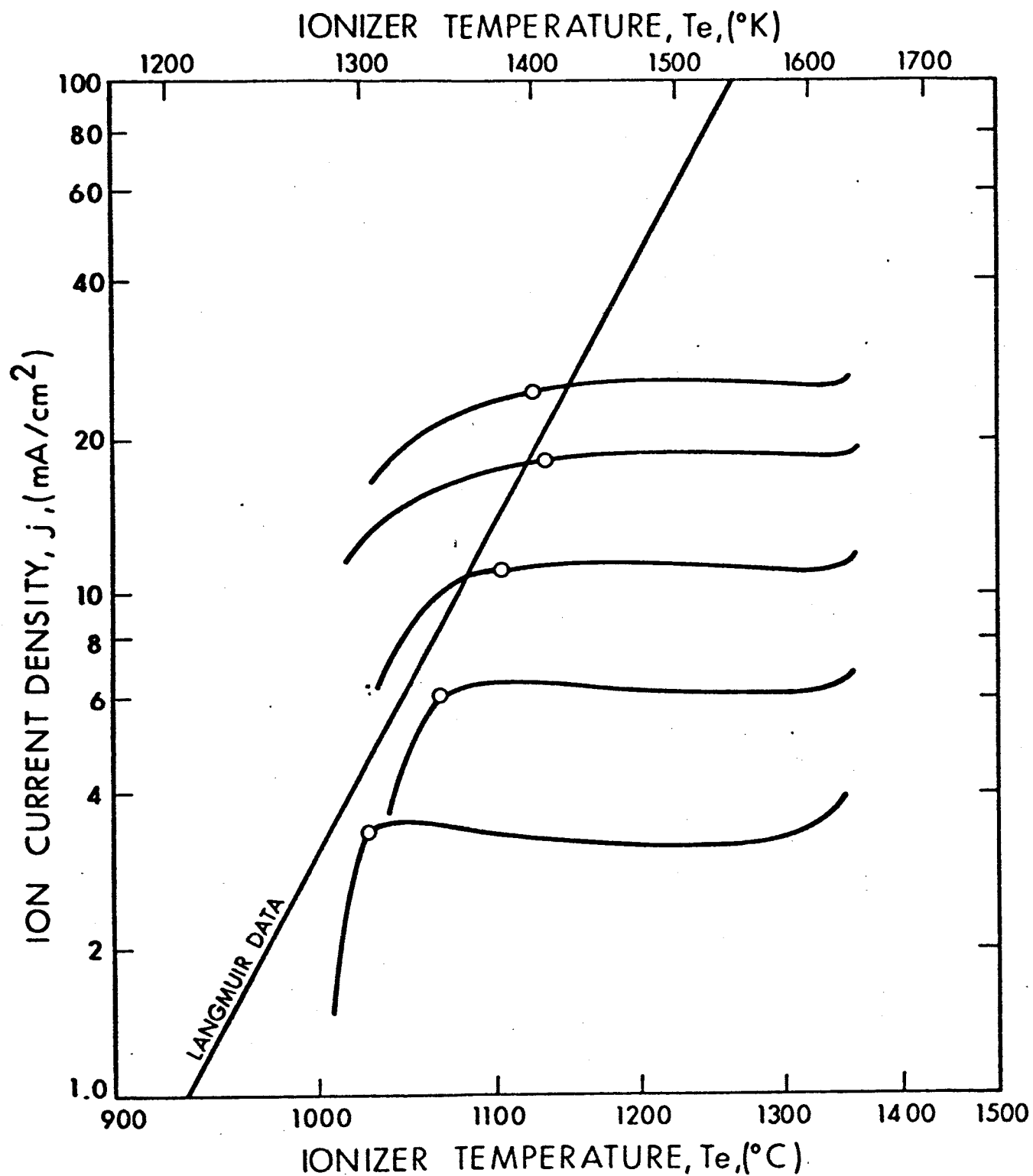


FIG. 6-9 ION CURRENT DENSITY VERSUS IONIZER TEMPERATURE FOR W-5 Ta-10Re ALLOY IONIZER, IVTXR-11



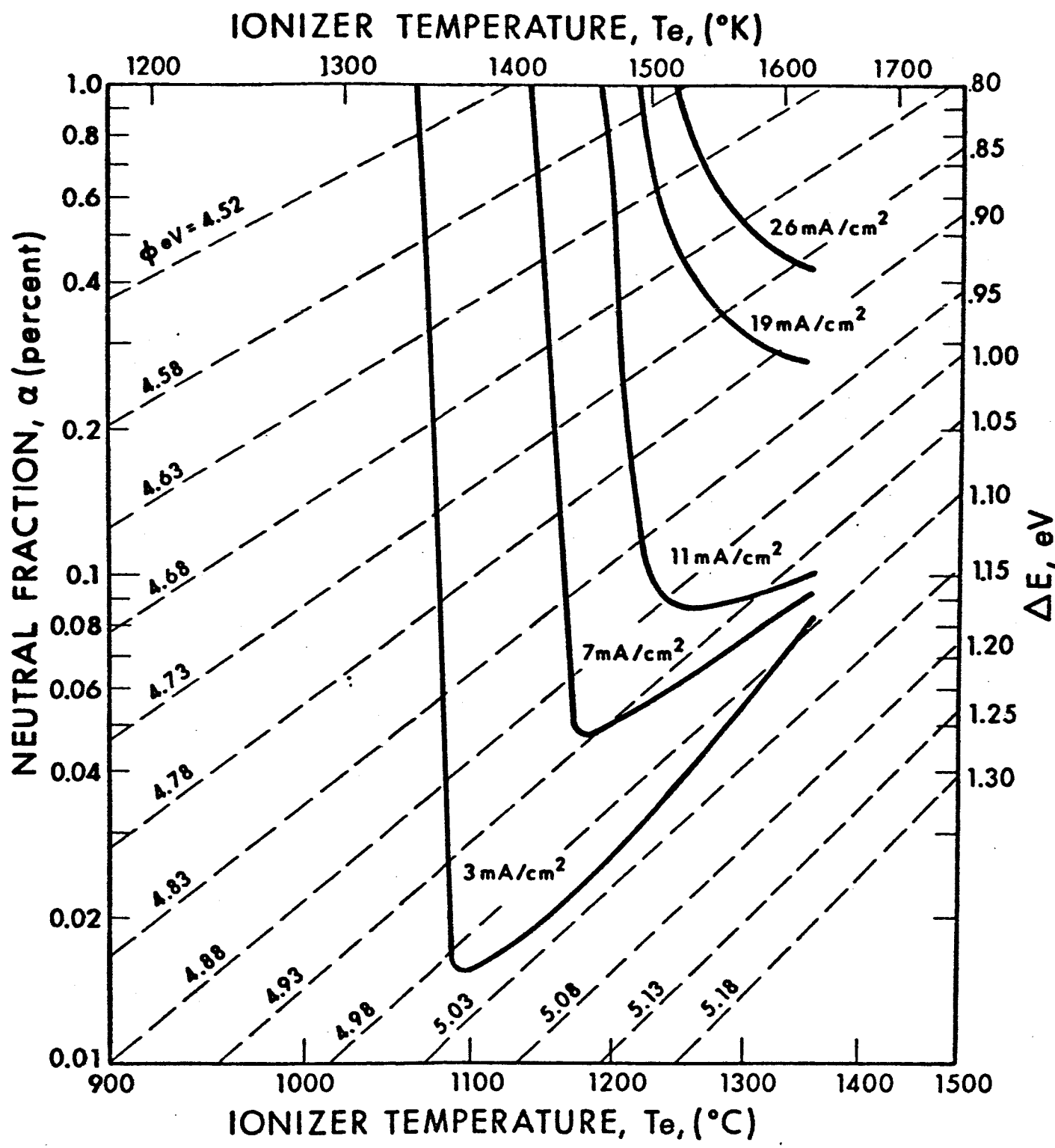


FIG. 6-10 NEUTRAL FRACTION VERSUS IONIZER TEMPERATURE FOR W-5Ta-10Re ALLOY IONIZER, IVTXR-11

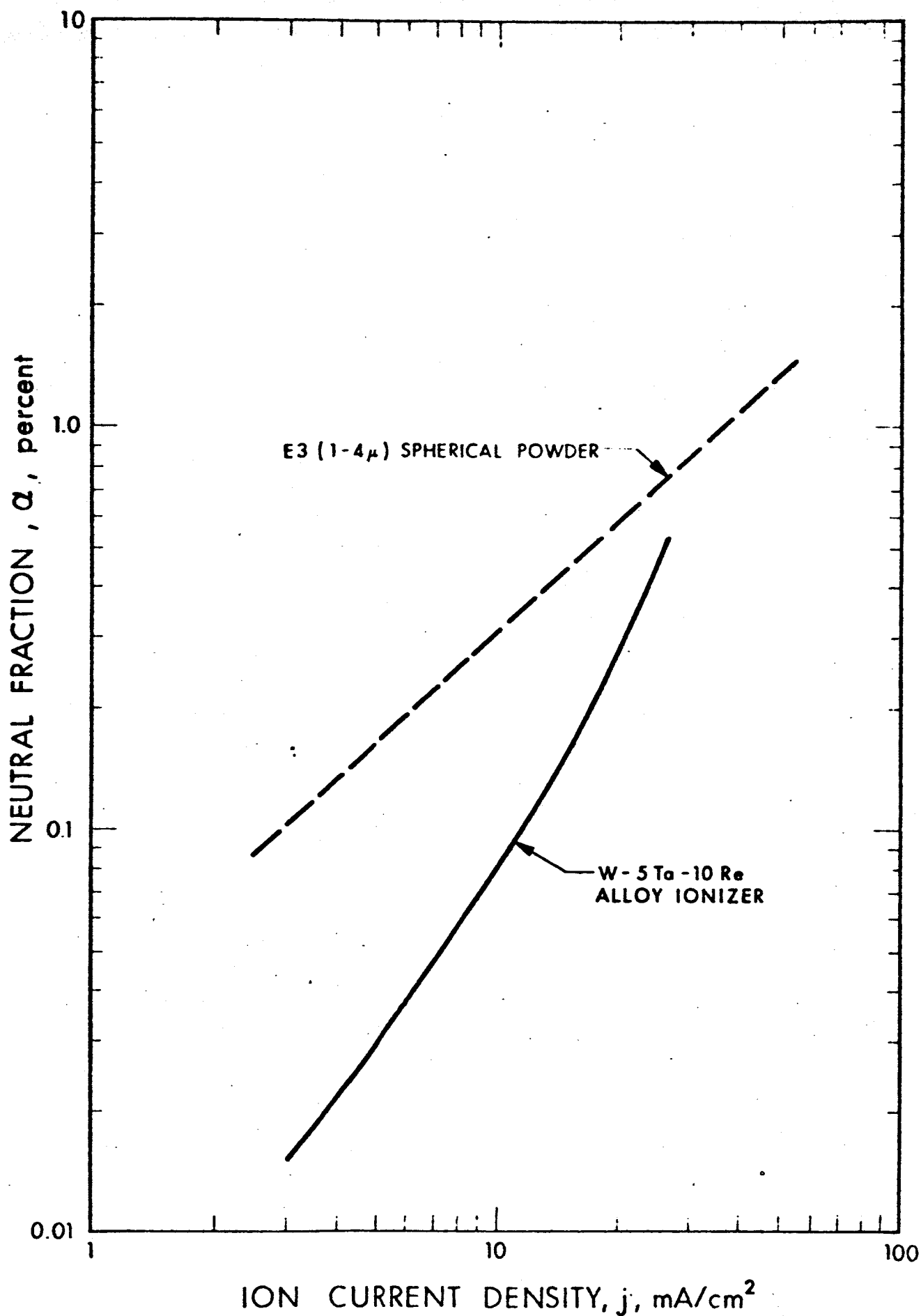


FIG. 6-11 NEUTRAL FRACTION VERSUS ION CURRENT DENSITY FOR W-5Ta-10Re ALLOY IONIZER IVTXR-11, COMPARED WITH THE E3 (1-4 $\mu$ ) SPHERICAL POWDER TUNGSTEN IONIZERS.

The magnitude of this effect (while bothersome in experimental testing due to rapid temperature cycling) is not large enough in these ternary alloy ionizers to cause any problems in ion engine control systems. Any temperature cycling in large ion engines occurs over a narrow operating range, and has long time constants due to the large thermal mass and good thermal insulation.

#### 6.5 Performance of Low-Density Ionizers

A series of ionizers, made from a fine ( $0.8\mu$ ) hydrogen-reduced tungsten powder + 8wt% copper flake mixture, were tested. Metallurgical parameters are listed on LeRC sheets of Appendix C, and are summarized in the following tabulation:

Ionizer No.	Stabilizer	Density, %	$N_2$ Permea- bility, $\mu P$	Av Pore Diam, $\mu$	Av No. of Pores/cm <sup>2</sup>	Av Pore Spacing, $\mu$
I-5	None	67.7	1.27	3.86	$1.71 \times 10^6$	7.65
II-2	None	66.5	1.32			
VIB-1	4wt%BN	47.0	2.96	Indeterminate	Indeterminate	
57WBCu-1*	2wt%BN	60.7	1.18			

\*Produced under this contract; tested under Air Force Contract.

The prime objective was to see if useful ionizers could be made from low-cost powders, using the copper flake technique, and to determine the effects of material density and boron stabilization upon ionization performance. It was found that not only could useful ionizers be made, but that ionization performance was better than that of any other ionizer previously produced. Ionizers made by the copper-flake technique are referred to in subsequent Section 6 figures as "shaped-pore" ionizers.

The first test of these low-density ionizers was made on the 68%-dense I-5 ionizer. The superiority of this ionizer, coupled with short testing time, suggested another sample be tested to verify

performance. Confirmation was achieved through testing of the 67%-dense II-2 sample. To improve the sintering stability of this type of ionizer, 4 W/oBN was added to the W-Cu flake mixture, and a resulting 47%-dense ionizer was tested. The neutral fraction was over a decade greater than for the first series. To determine if this difference was due to the density, structure, or addition of BN stabilizer, an intermediate 61%-dense ionizer with 2W/oBN was tested. Its neutral fraction was comparable to the original 68%-dense unstabilized ionizers, while its minimum neutral fraction was at a lower temperature.

The significant improvement in ionization performance to be gained with the low-density ionizers was revealed during testing of the 68%-dense I-5 ionizer. Ion current transition temperatures, which were about  $60^{\circ}\text{C}$  above the Langmuir data for solid tungsten below  $10\text{ mA/cm}^2$ , did not increase with the ion current density, and were about  $20^{\circ}\text{C}$  below the Langmuir data above  $20\text{ mA/cm}^2$  (Fig. 6-12). Nevertheless, at low ion current densities, the transitions were very sharp. Just a few degrees above the transition temperature, the neutral fraction was very low, compensating for the moderately higher transition temperature. Above  $15\text{ mA/cm}^2$ , there was no minimum in the  $\alpha$  versus  $T_e$  curves, although the neutral fraction was still low (5X lower than E3 [1-4 $\mu$ ] spherical-powder tungsten at  $15\text{ mA/cm}^2$ ) as shown in Figs. 6-13 and 6-14.

Similar performance was recorded for the 67%-dense II-2 ionizer. The ion current transition temperatures were about  $20^{\circ}\text{C}$  above the Langmuir data at  $30\text{ mA/cm}^2$ , but were only  $30^{\circ}\text{C}$  lower at  $7\text{ mA/cm}^2$  (Fig. 6-15). The neutral fraction was slightly lower for this ionizer than for the I-5 ionizer, although the  $\alpha$  versus  $T_e$  curves had no minimum below  $1300^{\circ}\text{C}$  for ion current densities above  $5\text{ mA/cm}^2$  (Fig. 6-16). This ionizer test was foreshortened by a facility breakdown during unattended operation, and before the interlock protection was completed. The trend of the data, as initially reported, was determined from relatively little data; it was distorted by several

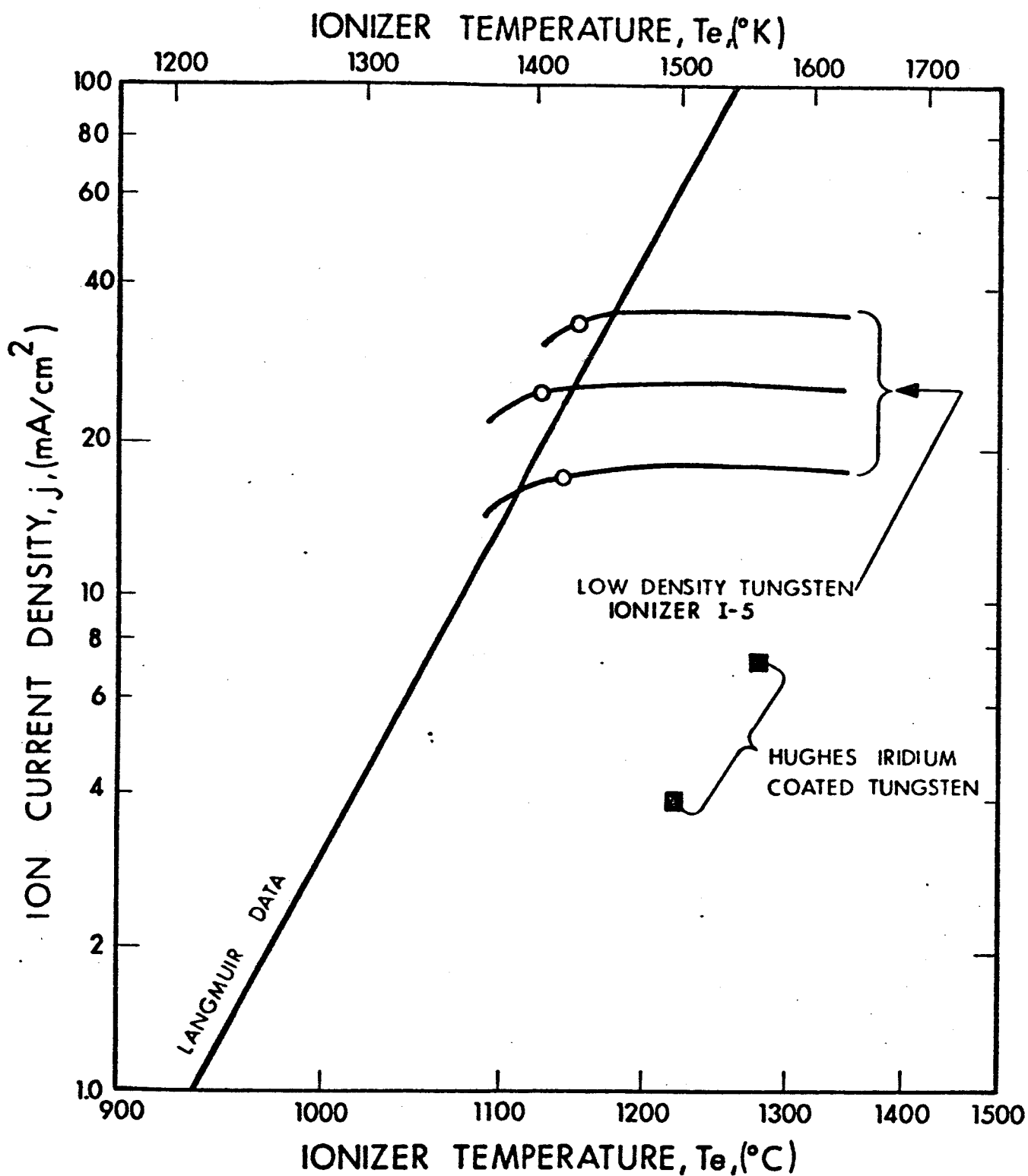


FIG. 6-12 ION CURRENT DENSITY VS IONIZER TEMPERATURE FOR A 68%-DENSE SHAPED-PORE TUNGSTEN IONIZER (I-5), COMPARED WITH HUGHES IRIIDIUM COATED TUNGSTEN IONIZER

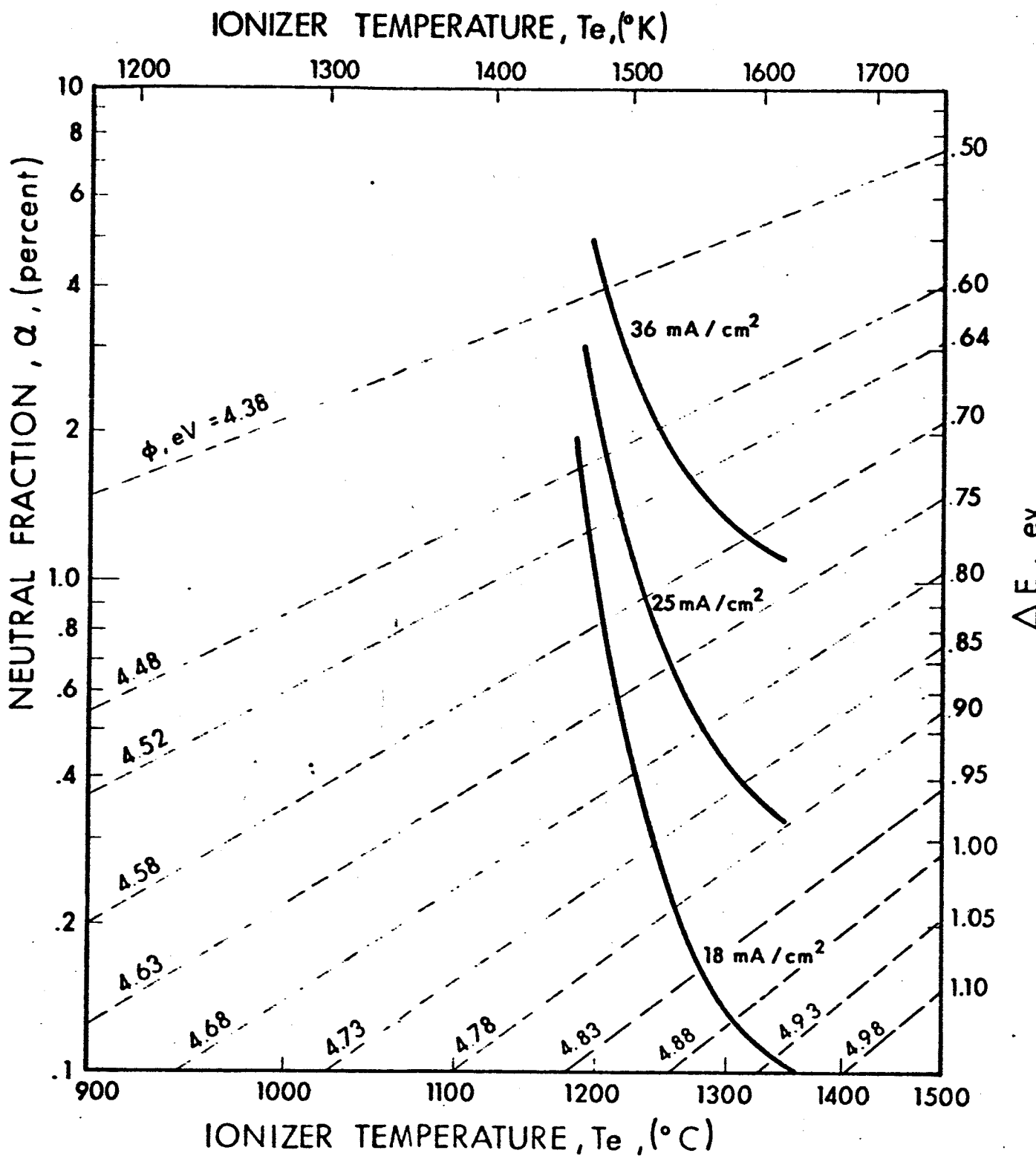


FIG. 6-13 NEUTRAL FRACTION VS IONIZER TEMPERATURE FOR A 68%-DENSE SHAPED-PORE TUNGSTEN IONIZER (I-5)

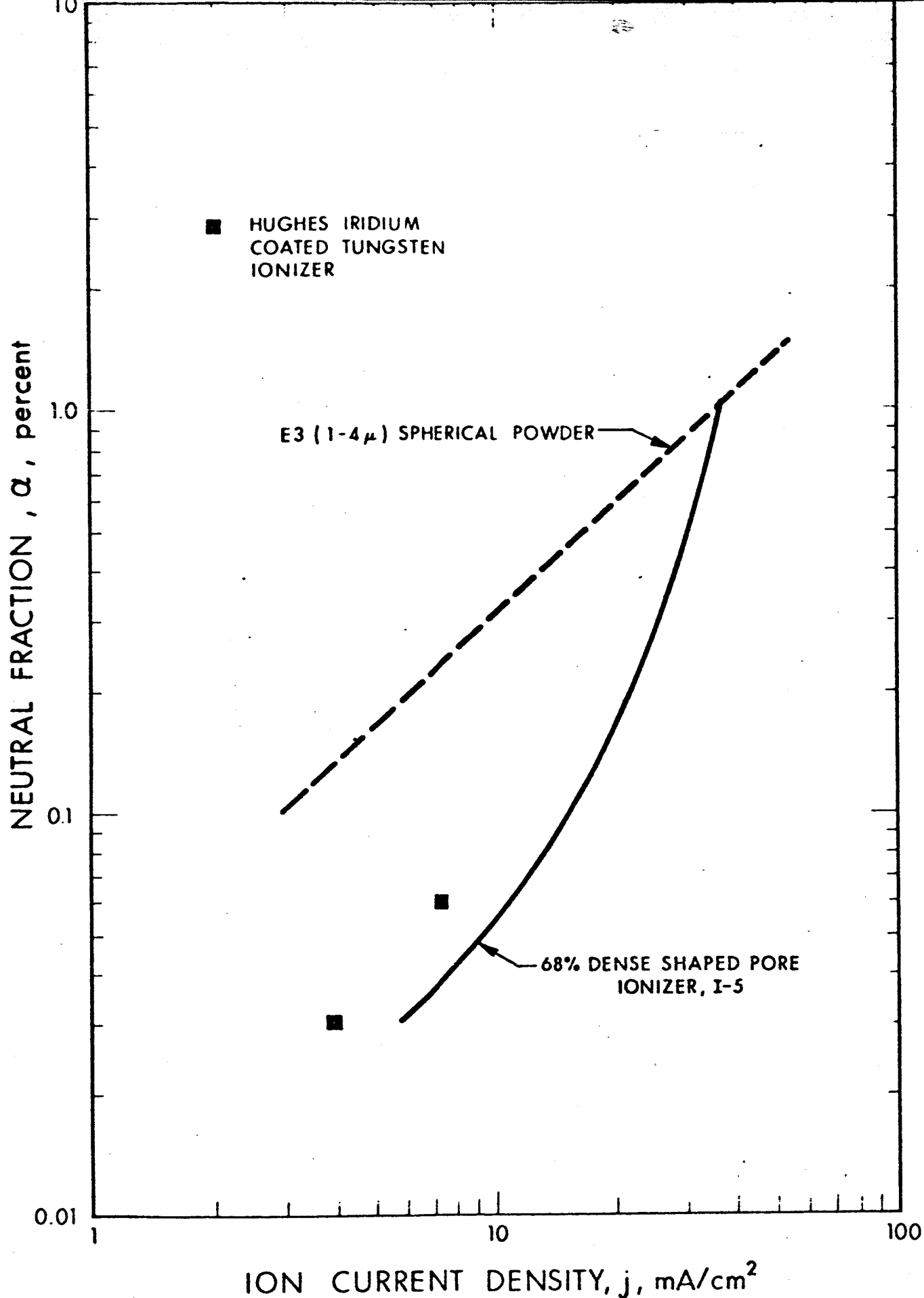


FIG. 6-14 NEUTRAL FRACTION VS ION CURRENT DENSITY FOR 68% DENSE SHAPED-PORE TUNGSTEN IONIZER I-5, COMPARED WITH THE E3 (1-4 $\mu$ ) SPHERICAL POWDER TUNGSTEN IONIZERS, AND THE HUGHES IRIIDIUM COATED TUNGSTEN IONIZER

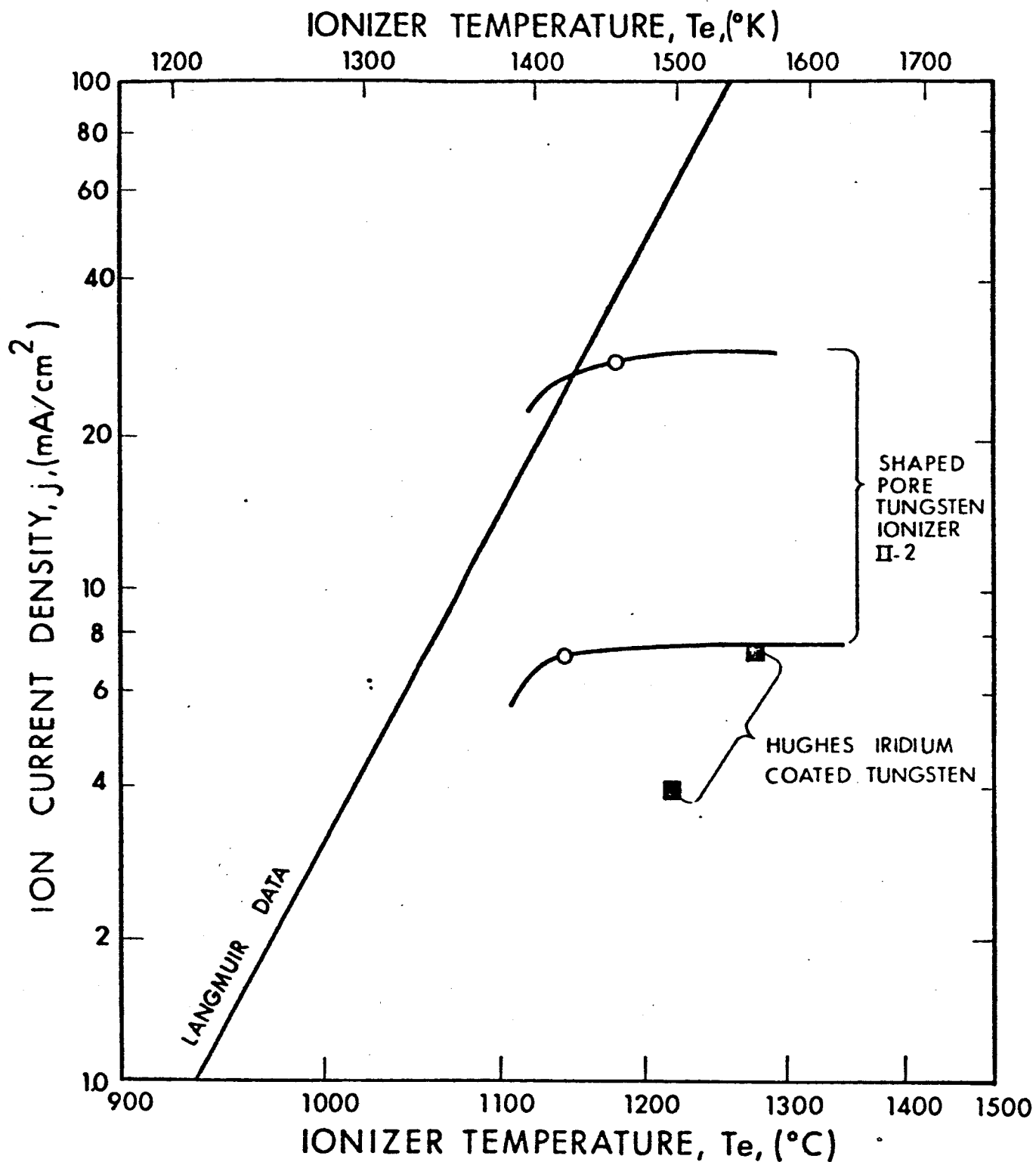


FIG. 6-15 ION CURRENT DENSITY VS IONIZER TEMPERATURE FOR 67% DENSE SHAPED-PORE TUNGSTEN IONIZER II-2, COMPARED WITH HUGHES IRIIDIUM COATED TUNGSTEN IONIZER



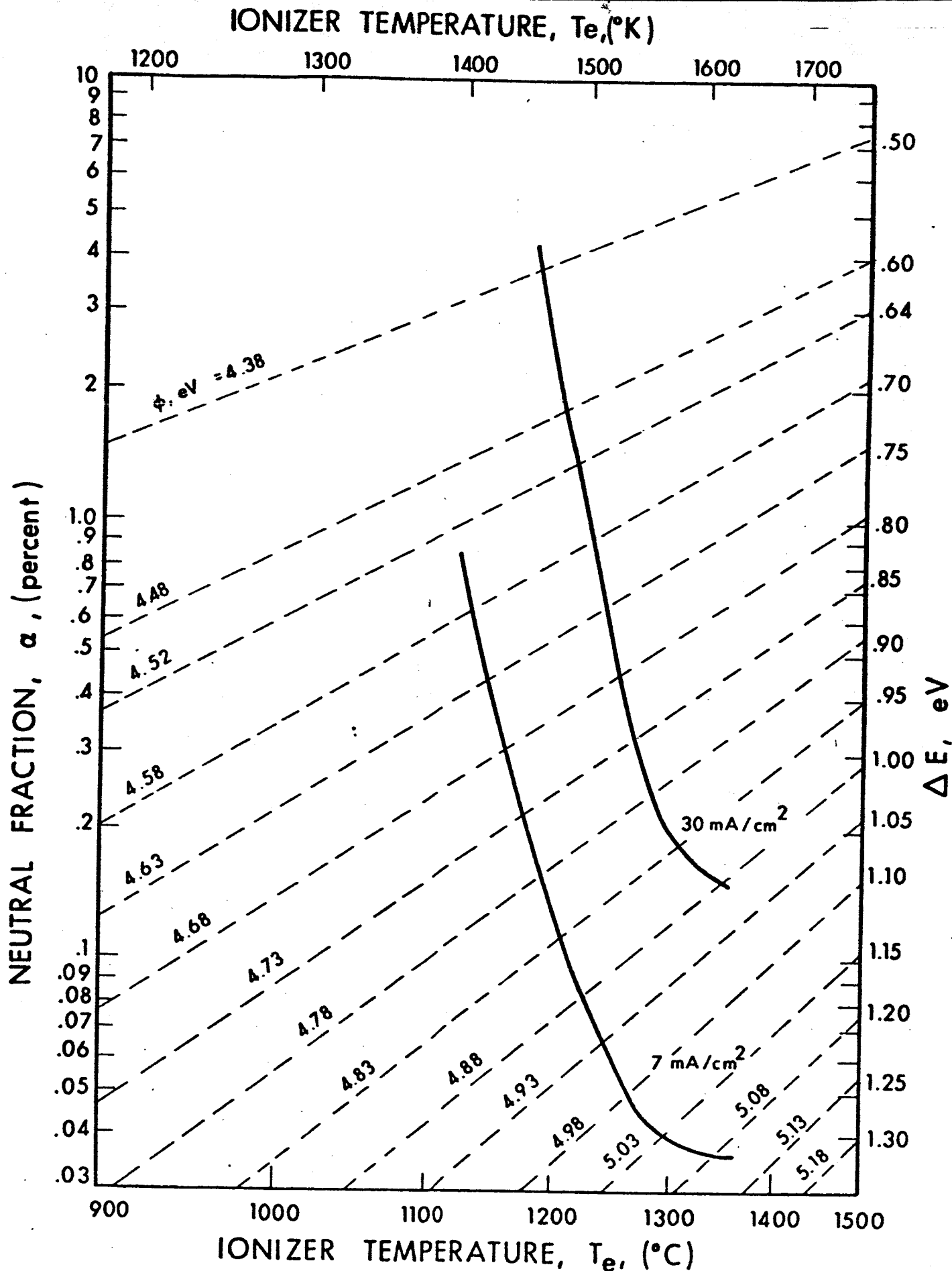


FIG. 6-16 NEUTRAL FRACTION VS IONIZER TEMPERATURE FOR 67% DENSE SHAPED-PORE TUNGSTEN IONIZER, II-2

data points at low current densities, which points were erroneously computed or now considered unreliable. Consequently, the neutral fraction at low ion current density, while still very low, is somewhat higher than previously reported. In Fig. 6-17, the corrected data are compared with the E3 (1-4 $\mu$ ) spherical tungsten ionizers which have a 6X higher neutral fraction.

Performance of the 47%-dense ionizer, VIB-1, stabilized with 4wt%BN was disappointing. The ion current transition temperatures were 15 $^{\circ}$ C below the Langmuir data at 4 mA/cm $^2$ , as shown in Fig. 6-18. The  $\alpha$  versus  $T_e$  curves had a broad minimum about 100 $^{\circ}$ C above the ion current transition temperature (Fig. 6-19) but the work function was not high, being 4.6 eV at 7 mA/cm $^2$ . The neutral fraction was consequently greater than other high-performance ionizers, being 3X greater at 5 mA/cm $^2$ , and 6X greater at 15 mA/cm $^2$  than the E3 (1-4 $\mu$ ) spherical tungsten ionizers (Fig. 6-20).

The poor performance of the 47%-dense ionizer with 4wt%BN stabilizer, after the excellent performance of the unstabilized 67%-dense ionizers, led to development of an intermediate ionizer having a 61% density and 2% of BN stabilizer. One sample of this material, No. 57WBCu-1, was tested under Air Force contract and found to be the best composition developed to date. The ion current transitions were very sharp, as shown in Fig. 6-21, and averaged 20 $^{\circ}$ C below the Langmuir data. The neutral fraction versus temperature curves had very deep minimum even at 20 mA/cm $^2$  (Fig. 6-22). The work function, as determined from the Saha-Langmuir equation, declined very slowly from 5.0 eV at 5 mA/cm $^2$  to 4.9 at 20 mA/cm $^2$ . While other ionizers (i.e., the 68%-dense low-density ionizers) have shown higher work functions, the No. 57WBCu-1 ionizer actually had a lower neutral fraction because the work function did not begin to increase until temperature had declined to a value near the ion current transition temperature. Many high work-function ionizers decline rapidly in  $\phi$

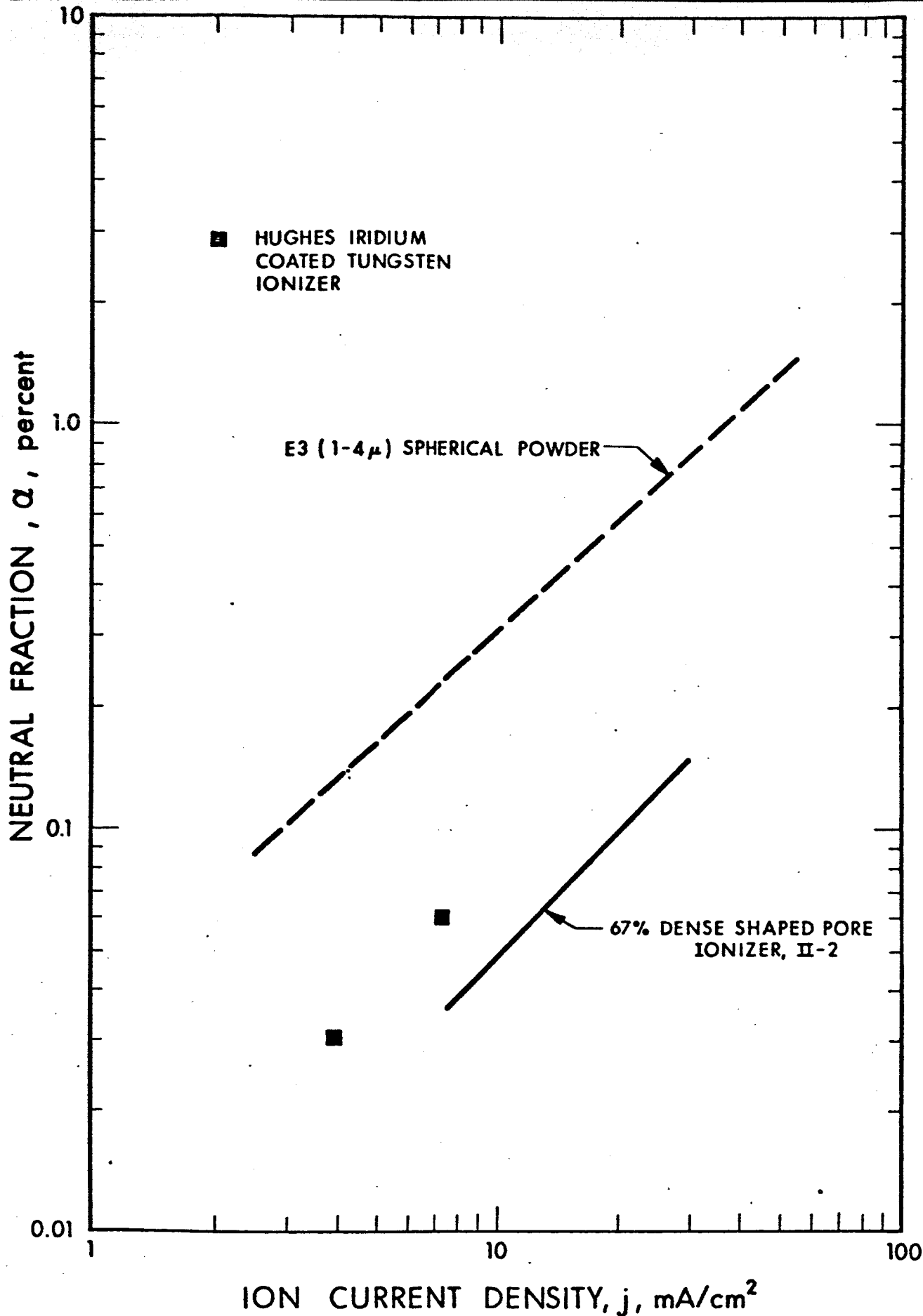


FIG. 6-17 NEUTRAL FRACTION VS ION CURRENT DENSITY FOR 67% DENSE SHAPED-PORE TUNGSTEN IONIZER II-2, COMPARED WITH THE E3 (1-4 $\mu$ ) SPHERICAL POWDER TUNGSTEN IONIZERS, AND THE HUGHES IRIIDIUM COATED TUNGSTEN IONIZER

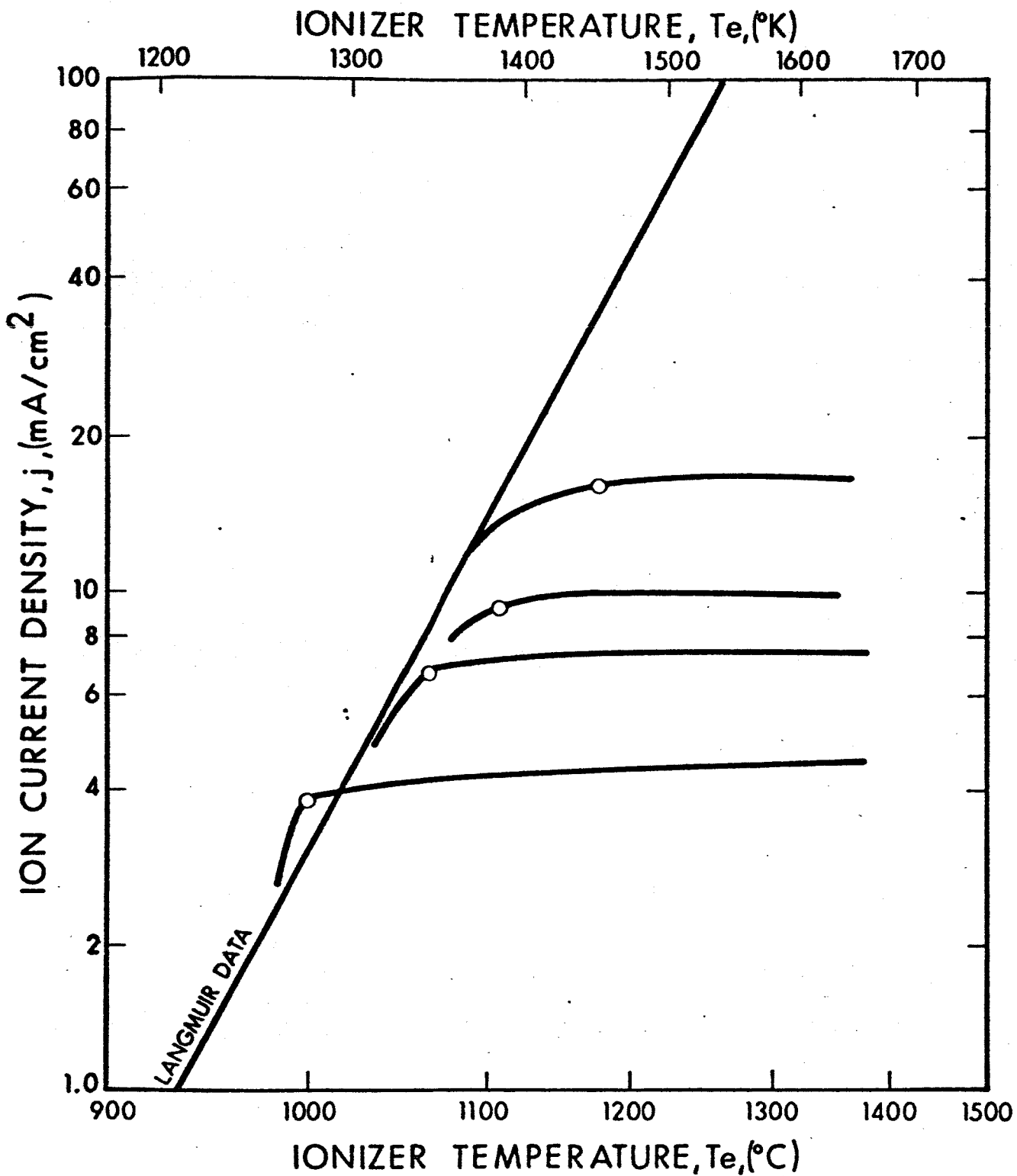


FIG. 6-18 ION CURRENT DENSITY VS IONIZER TEMPERATURE FOR 47% DENSE STABILIZED SHAPED-PORE TUNGSTEN IONIZER, VI B-1

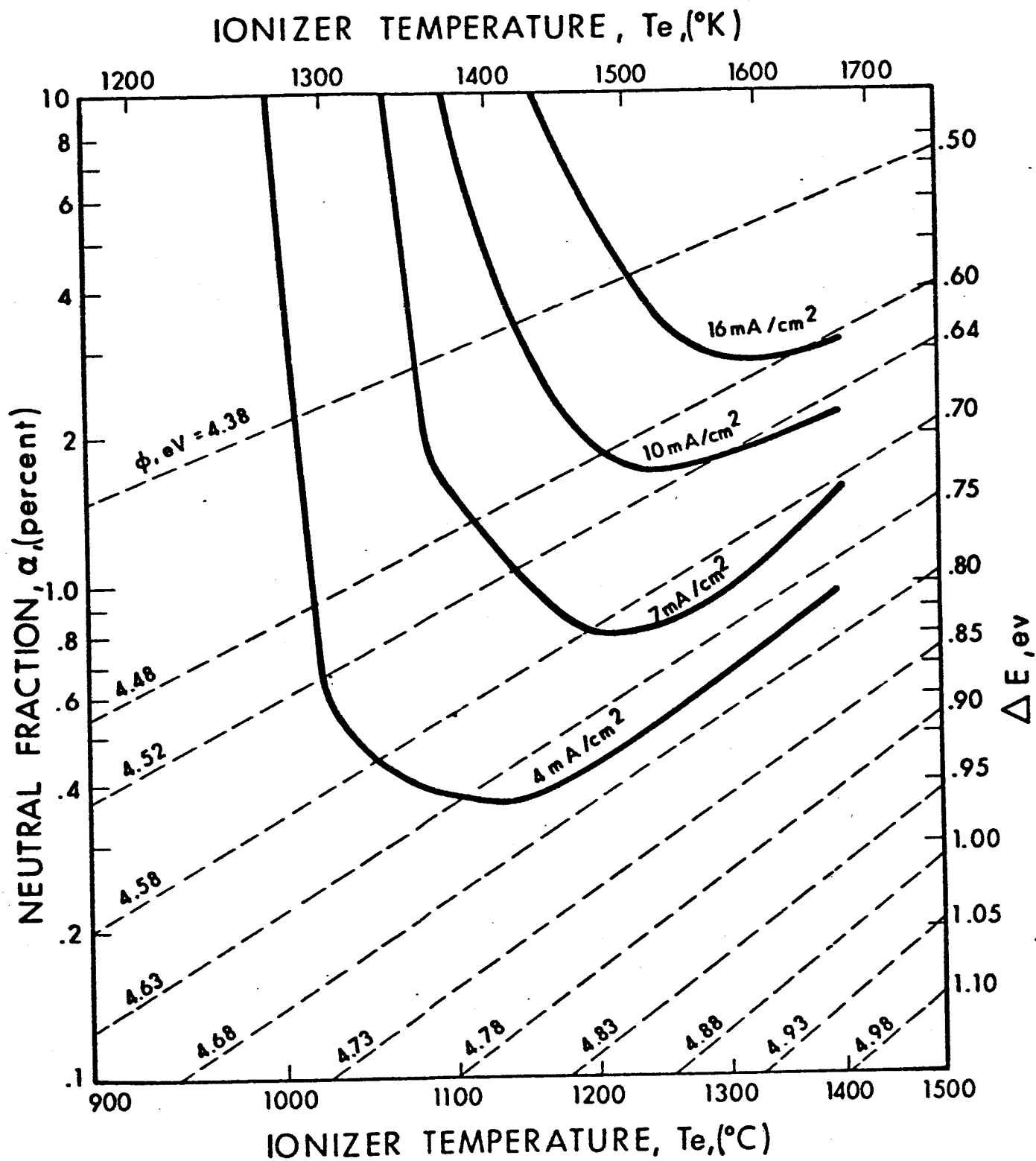


FIG. 6-19 NEUTRAL FRACTION VS IONIZER TEMPERATURE FOR 47% DENSE STABILIZED SHAPED-PORE TUNGSTEN IONIZER, VI B-1

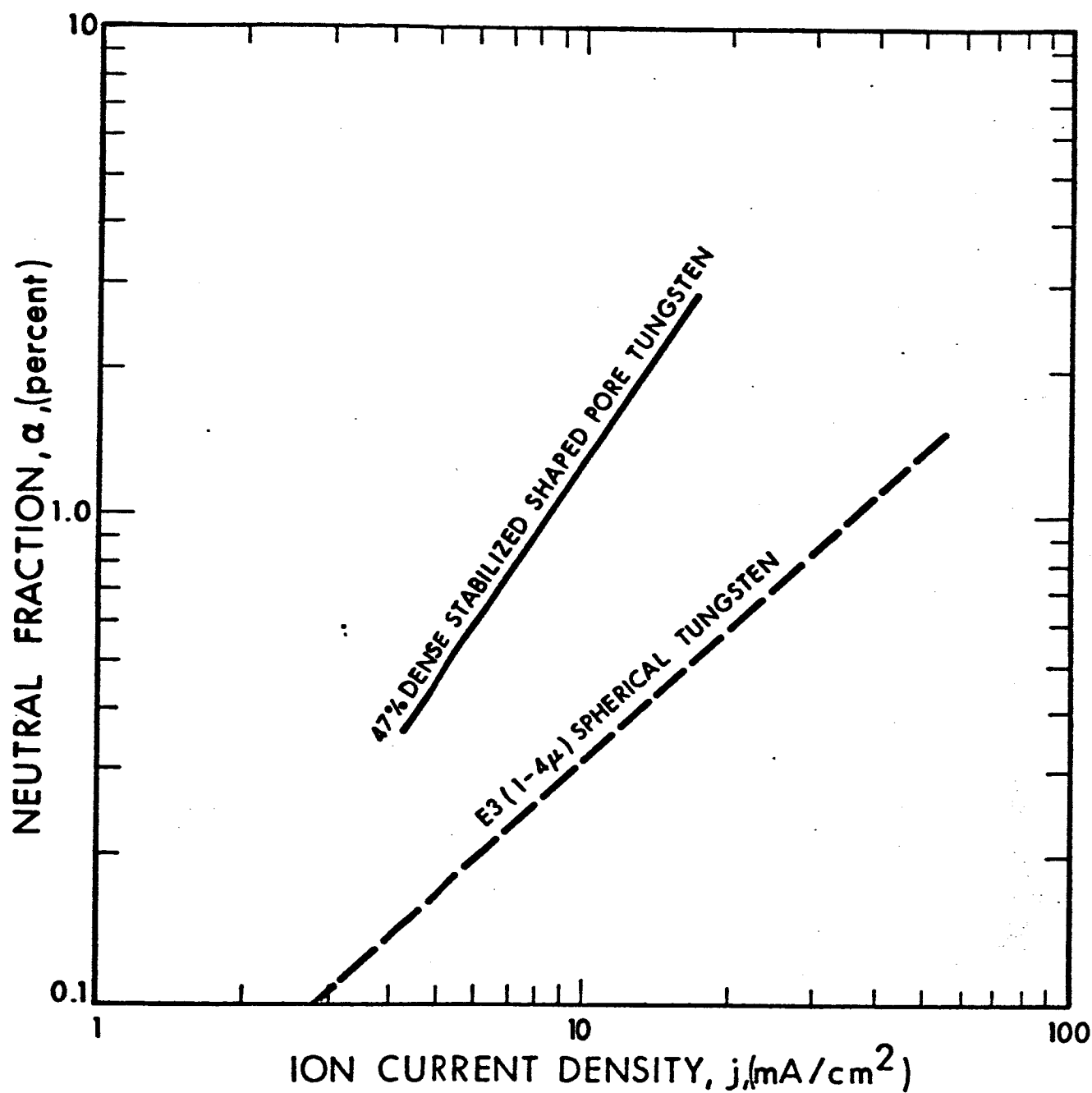


FIG. 6-20 NEUTRAL FRACTION VS ION CURRENT DENSITY FOR 47% DENSE STABILIZED SHAPED-PORE TUNGSTEN IONIZER, VI B-1, COMPARED WITH THE E3 (1-4 $\mu$ ) SPHERICAL POWDER TUNGSTEN IONIZERS

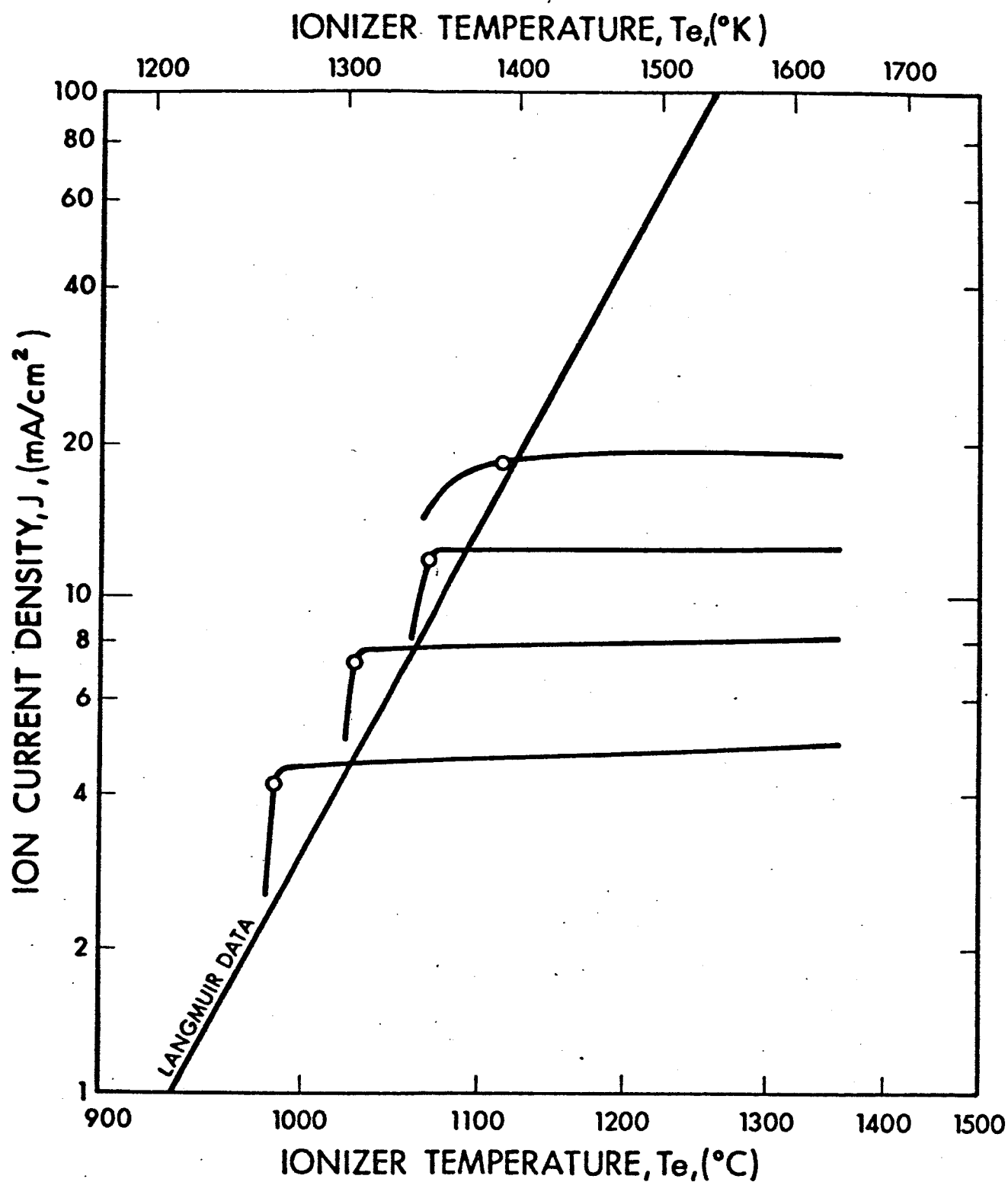


FIG. 6-21 ION CURRENT DENSITY VS IONIZER TEMPERATURE FOR 61% DENSE STABILIZED SHAPED-PORE TUNGSTEN IONIZER, #57 WB Cu-1

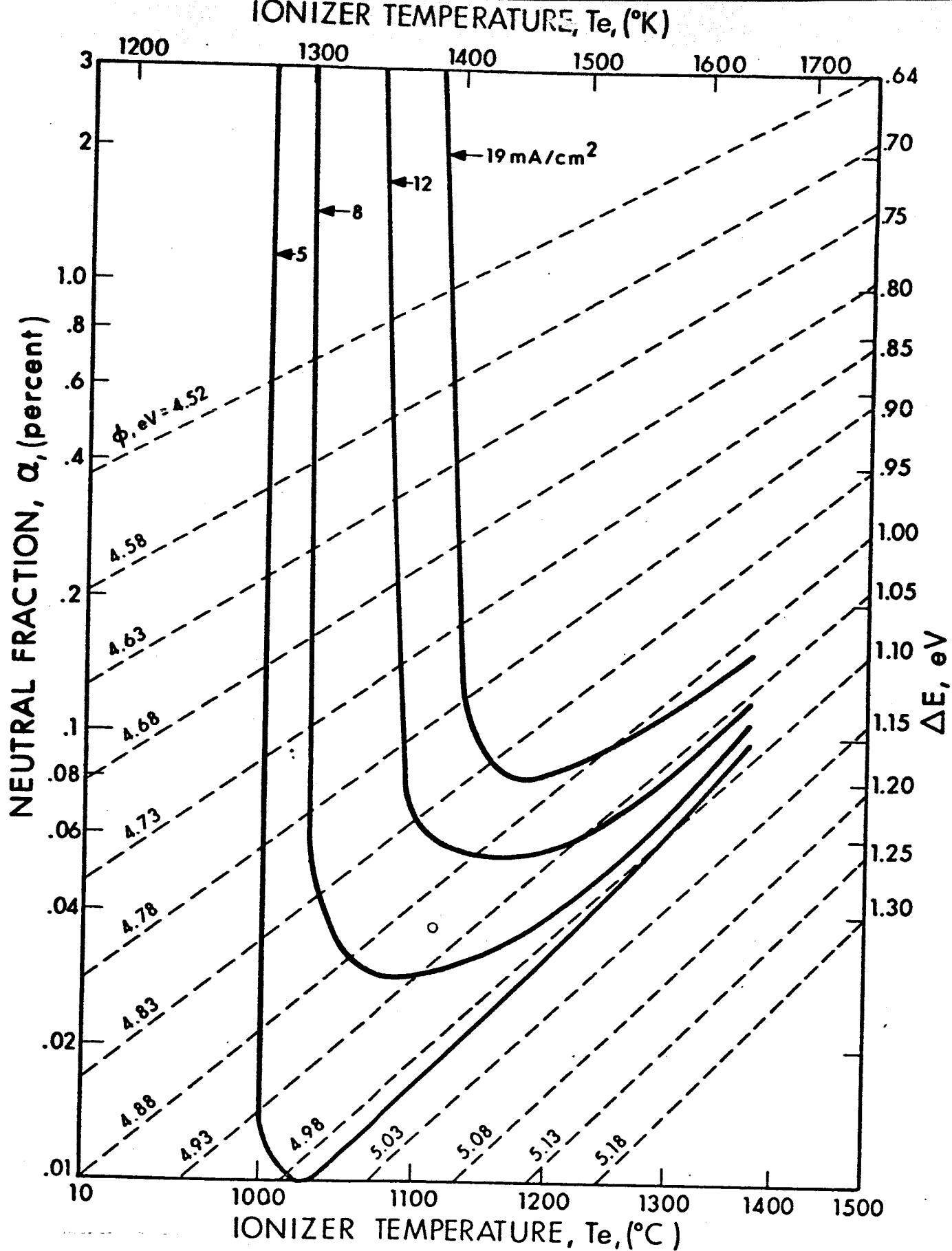


FIG. 6-22 NEUTRAL FRACTION VS IONIZER TEMPERATURE FOR 61% DENSE STABILIZED SHAPED-PORE TUNGSTEN IONIZER, #57, WB Cu-1



as the temperature declines, so that the very low neutral fractions are recorded at temperatures between 1300-1400°C. Figure 6-23 compares the minimum neutral fraction versus ion current density of the E3 (1-4μ) spherical tungsten ionizers with the No. 57WBCu-1 ionizer, which has a neutral fraction 10X lower at 10 mA/cm<sup>2</sup>.

Due to operation over widely varying performance conditions, surface damage in an experimental ion source is much more common than in large engines. The normal result of a particularly heavy arc or discharge on the ionizer surface is to melt a spot on the surface which seals that area. On small buttons, this causes a small decrease in permeability and a small increase in neutral efflux. Two small areas on a 68%-dense shaped-pore ionizer were damaged in this way. However, on the 61%-dense stabilized shaped-pore ionizer, a discharge occurred which caused the surface to melt and shrivel away, leaving a rough depression surrounded by a mildly eroded area, both of which were still porous. This damage caused a decade increase in the gross neutral fraction of the ionizer. Further experience will be needed to determine the probability of this serious damage mode occurring in ion engines, which operate under more conservative conditions.

It is not clear why the low-density (<70%) ionizers perform so well. Since their pore density is low and pore diameters large, the improved performance must be due to a larger ion emission area, mostly from within the pores. Thus ionization performance appears to be determined by a combination of pore density, pore size, and pore spacing (i.e., material density). There should be an optimum combination of pore parameters. Among these, pore shape and size distribution should also be important. The 68%-dense unstabilized ionizers have a very homogeneous structure, composed of a multitude of elongated pores in a solid matrix. The 47%-dense stabilized ionizer on the other hand, has a very open network with a solid web-like structure in a void matrix. This structure has poor homogeneity (compared with the 68%-dense ionizers) and has numerous large pores, as well as many small

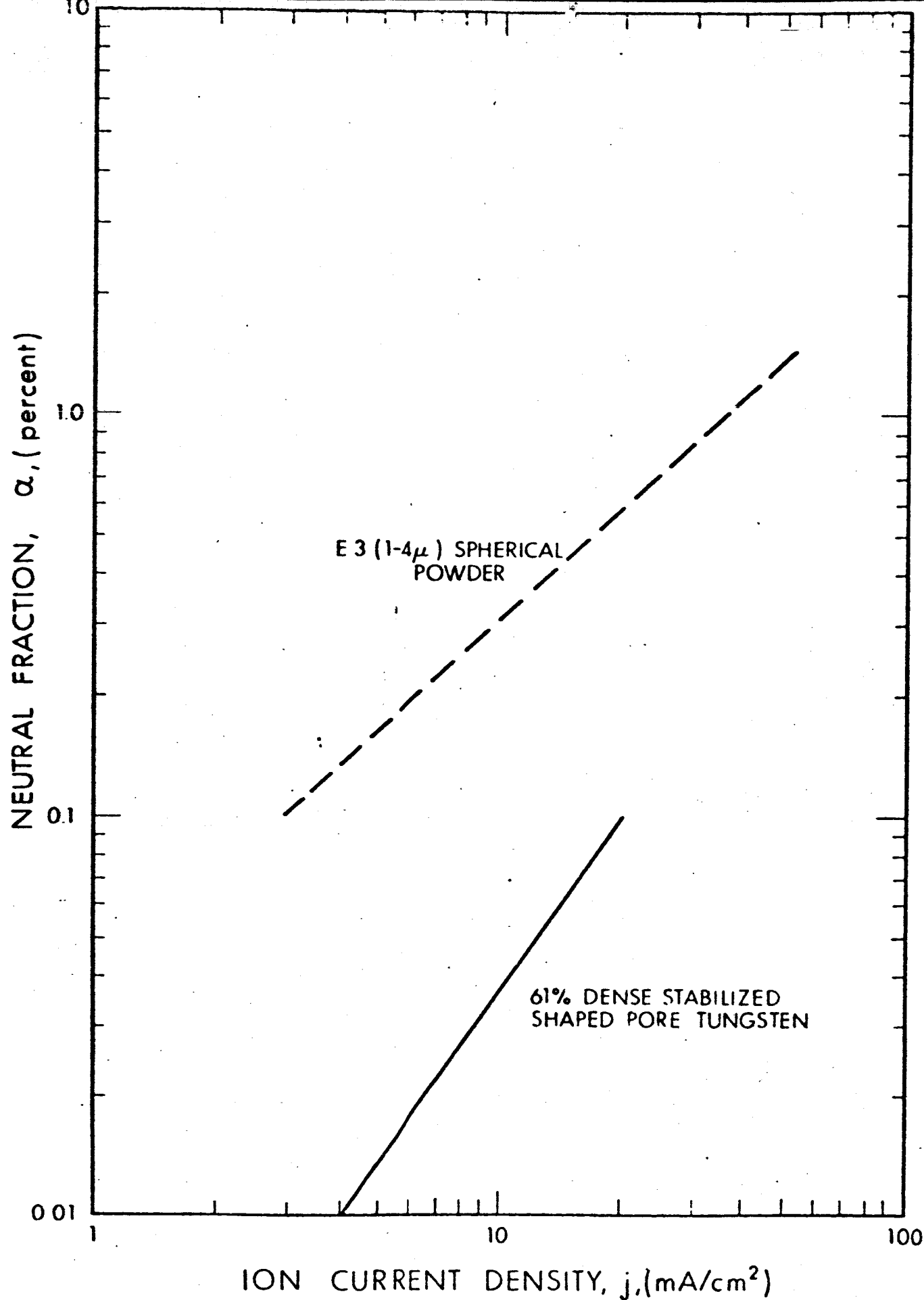


FIG. 6-23 NEUTRAL FRACTION VS ION CURRENT DENSITY FOR 61% DENSE STABILIZED SHAPED PORE IONIZER, #57 WB Cu-1, COMPARED WITH THE E3 (1-4 $\mu$ ) SPHERICAL POWDER TUNGSTEN IONIZERS

pores. Why the 61%-dense stabilized ionizer, which has a structure intermediate to the 47%-dense and 68%-dense ionizers in both homogeneity and character of porosity should have the best performance is not understood. Nor can the effects of the low-density structural characteristics and material density upon performance be delineated at this time. It appears, however, that the boron nitride stabilizing addition does not poison the ionizer surface at concentrations up to 2wt%BN, due to the lower work function of boron. The effect of larger concentrations of boron upon performance and lifetime remains to be determined under Modification 6 of this contract.

## 7. TECHNIQUES AND PROCEDURES DEVELOPED FOR PRODUCING LARGE IONIZER BARS

Before ionizer bars, large enough to conform to the LeRC specification, could be produced, certain modification and improvements in fabrication methods were made. These modifications were necessitated by the relatively low apparent density of the  $0.8\mu$  angular tungsten powder and copper flake, as well as by the limited 6-1/2" working diameter of the pressing chamber. The compaction ratios ("loose-powder" to "pressed-bar" volumes) were so much higher for the angular-tungsten plus copper-flake mixtures, compared to tungsten microspheres, that it was not possible (within the available isostatic chamber) to press a billet large enough to be machined into a LeRC ionizer bar. The principal development consisted of pre-pressing the blended powders, followed by re-milling to increase the apparent density of the powder mixture.

### 7.1 Fabrication Techniques and Procedures

The sequence of operations, used in fabricating large ionizer bars, is shown in the flow sheet of Fig. 7-1.

The various fabrication steps and their purpose are tabulated below:

STEP	OPERATION	PURPOSE
1.	Blending	Homogenize powder mixture
2.	Pre-pressing	Increase apparent density of powder in preparation for next step
3.	Re-milling	
4.	Final Pressing	Consolidate powder
5.	Pre-sintering	Increase mechanical strength
6.	Final Sintering	Establish solid bond and desired density
7.	First Infiltration	Permit machining
8.	First Machining	Form test bar
9.	De-infiltration	Permit permeability testing.
10.	Permeability Test	Determine permeance and uniformity of same
11.	Re-infiltration	Permit final machining
12.	Final Machining	Obtain bar of LeRC dimensions

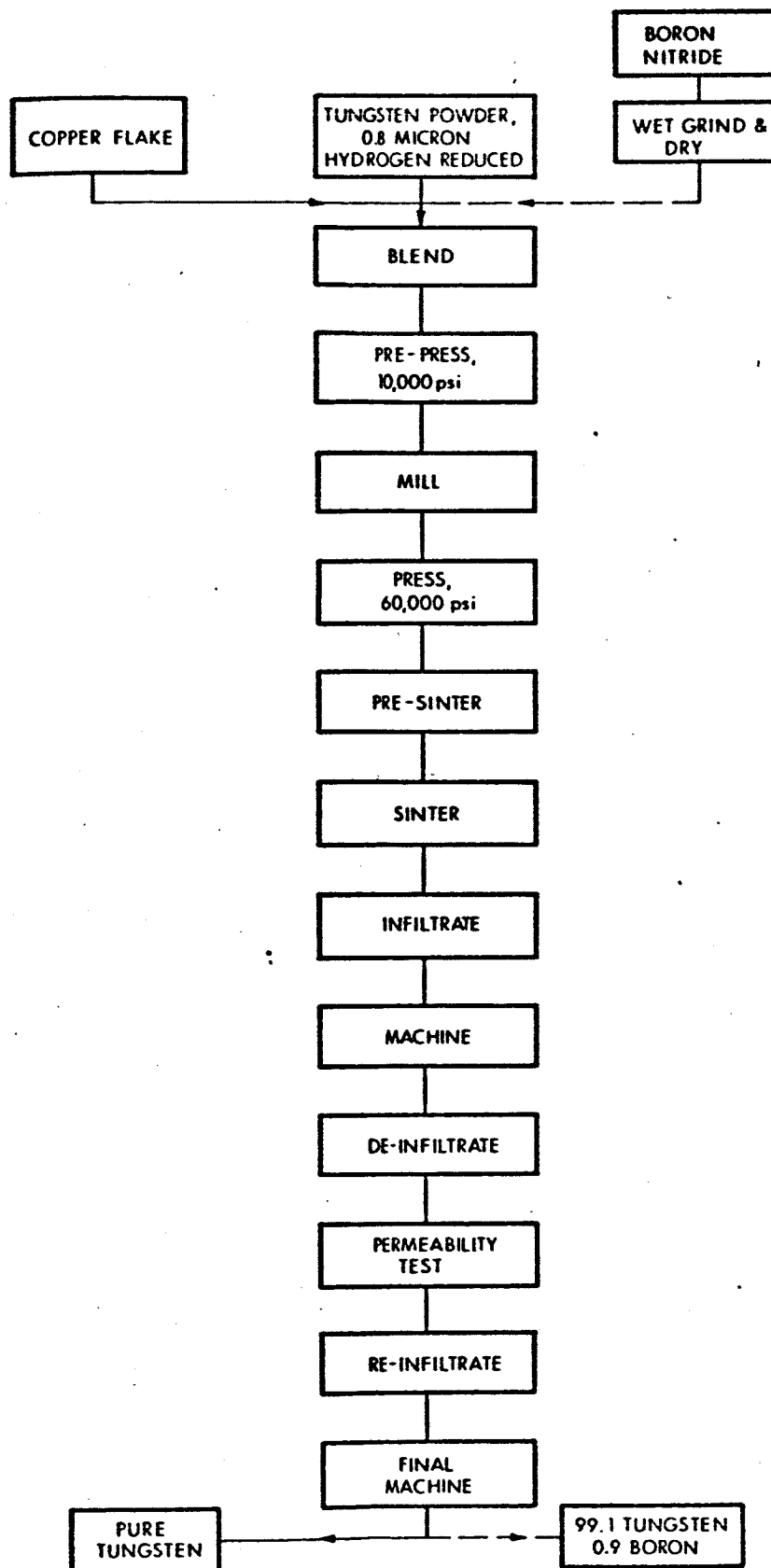


FIG. 7-1 IONIZER TEST-BAR MANUFACTURING PROCESS FLOWSHEET

### Step 1. Blending of Powder Mixtures

Ionizer bars were manufactured from two powder mixtures: (1) 92W/o of 0.8 $\mu$  angular H<sub>2</sub>-reduced tungsten plus 8W/o of copper flake; (2) 90W/o tungsten, 8W/o copper flake, plus 2W/o boron nitride. The copper was essentially all removed during subsequent sintering, resulting in bars of (1) high-purity tungsten, and (2) 99.13W/oW - 0.87W/oB. When boron nitride is added, as in mixture (2), the nitrogen is believed to be expelled during vacuum sintering, while the boron diffuses into the tungsten.

The raw materials used in the powder mixtures were as follows:

Tungsten Powder, 0.70-0.99 $\mu$  angular, H<sub>2</sub>-reduced  
Copper Flake, Cres-lite copper leaf #112  
Boron Nitride, Carborundum HPF grade

Tungsten and copper were used in the as-received condition. The boron nitride was wet ball-milled for 18 hours in a benzene medium, with hardened steel balls included to assist in breaking-up the agglomerates. After being ball-milled, the boron nitride was dried in air.

The components of the powder mixtures (92W-8Cu and 90W-8Cu-2BN) were weighed, ball-milled for two hours in benzene, and air dried.

### Step 2. Pre-pressing of Powder Mixtures

The blended mixtures were too fluffy to permit isostatic compaction of large bars within the available pressing chamber. Therefore, it was necessary to pre-press the mixtures to increase apparent density of the powder. For this operation, the powder mixtures were loaded into amber-rubber envelopes, hermetically sealed, and pressed isostatically. The most suitable pressure was found to be 10,000 psi. Pre-pressing at higher levels results in high-density agglomerates and non-uniform final pore structures, while lower pressures do not provide sufficient apparent density.

### Step 3. Re-milling of Powder Mixtures

The pre-pressed powder mixtures were broken up in a mortar, passed through a 60-mesh screen, and ball-milled for two hours under dry conditions.

### Step 4. Final Pressing of Powder Mixtures

The powder mixtures were loaded into rectangular amber-rubber envelopes, hermetically sealed, and pressed at 60,000 psi (isostatic). Compact weight was approximately 1200 grams.

### Step 5. Pre-sintering of Compacts

The compacts were presintered at  $1010^{\circ}\text{C}$  for 2 hours in forming gas ( $85\text{N}_2-15\text{H}_2$ ). This established initial bridging between tungsten particles, while the copper particles were still present, providing the desired pore network. It also provided the compacts with sufficient mechanical strength to withstand the thermal shock of rapid heating to final sintering temperature.

### Step 6. Final Sintering of Compacts

The compacts were heated in vacuum ( $10^{-5}$  torr range) to effect solid bonding. The copper component was lost through volatilization; nitrogen was also evolved in large volumes from the W-Cu-BN mixture. The W-Cu compacts were sintered for 15 minutes at  $1500^{\circ}\text{C}$  plus 15 minutes at  $1800^{\circ}\text{C}$ . The W-Cu-BN compacts were sintered for 15 minutes at  $1500^{\circ}\text{C}$  plus 30 minutes at  $1800^{\circ}\text{C}$ .

### Step 7. First Infiltration of Sintered Compacts

All compacts were initially infiltrated with Cu-2W/oFe alloy at  $1150^{\circ}\text{C}$  for 2 hours under forming gas.

### Step 8. First Machining of Infiltrated Compacts

The ionizer bars were machined larger than specified by the LeRC standards to allow for the slight warpage which occurred during final infiltration.

### Step 9. De-infiltration of Ionizer Bars

As an intermediate step and in order to determine permeability, it was necessary to remove the infiltrant. Copper and iron were quantitatively removed by heating in vacuum at  $1600^{\circ}\text{C}$  for 30 minutes.

#### Step 10. Permeability Testing of Ionizer Bars

Uniformity of porosity was determined by measuring permeability at 28 stations over the surface of each bar. Criterion of permeability was taken as the time required to collect 5 cm<sup>3</sup> of N<sub>2</sub>, while holding a constant pressure drop (10" Hg) across the ionizer. The N<sub>2</sub> gas was collected by a probe, held firmly against the bar face; the stations were at square-grid intervals of 1/2 inch.

#### Step 11. Re-infiltration of Ionizer Bars

The test bars were infiltrated with pure copper at 1150°C for 2 hours under a forming-gas atmosphere.

#### Step 12. Final Machining of Ionizer Bars

The re-infiltrated bars were final machined to the following LeRC standard size: 0.125", +.010"; 2.10", +.020"; 3.90", +.020". Finally, the bars were surface ground and etched with Murakami's reagent, in accordance with LeRC procedure.

### 7.2 Permeability Test Equipment and Procedures

Permeability surveys of the large ionizers were made in the following manner. Each bar was placed in a pressurized plenum, wherein the edges of the bar were sealed. During testing, a constant differential of 10"-Hg nitrogen pressure was maintained across the bar. By holding a gasketed probe firmly against the face of the bar, the transmitted nitrogen was collected and conducted into an accurately calibrated volumeter.

A block diagram of this permeability apparatus is shown in Fig. 7-2. Commercial bottled nitrogen was used as the diffusant gas. The gas was first passed through a drying unit (calcium-sulfate type) and then through a gas filter (Hoke No. 2231, 2-5μ). Pressure in the test plenum (indicated on a U-tube Hg manometer) was adjusted with a conventional two-stage diaphragm regulator on the N<sub>2</sub> tank, and maintained at 10"-Hg.



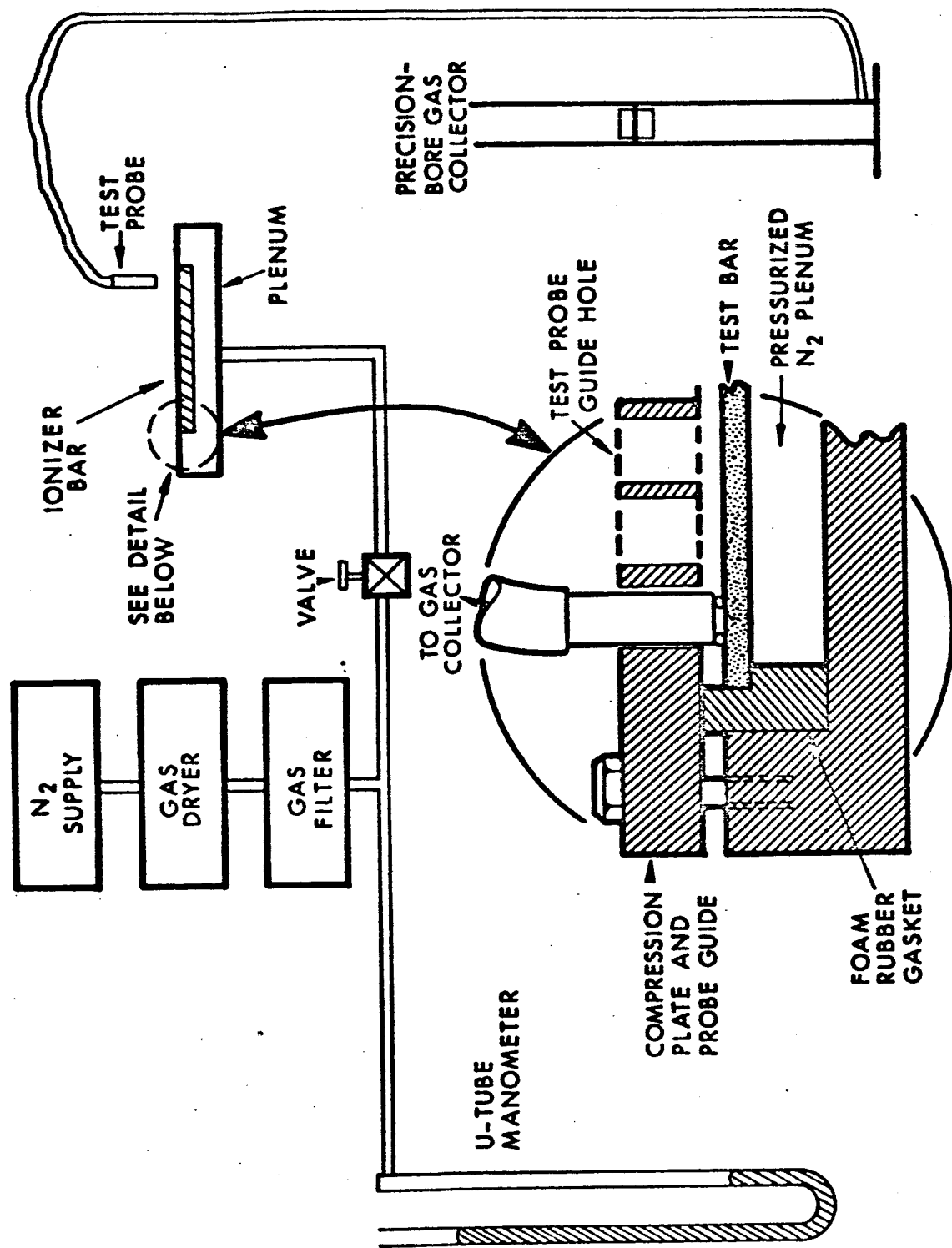


FIG. 7-2 BLOCK DIAGRAM OF PERMEABILITY APPARATUS

The test plenum is a shallow rectangular chamber, having a foam-rubber gasket around its upper periphery. The test bar rests on a shoulder of the gasket, with the outer edge of the gasket extending above the level of the plenum and the test bar. A compression plate, 1/2" thick and retained by bolts, effects sealing of the plenum. Twenty-eight through holes of 3/8" diameter guide the collector probe for the permeability survey.

The collector probe has a 3/8" O.D. x 1/4" I.D. neoprene O-ring cemented to its end. When held against the ionizer with firm hand pressure, the effluent gas is effectively collected and conducted through a Tygon tube to a Brooks volumeter (30 cm<sup>3</sup> capacity). Here, a plastic piston with a mercury seal rises as the gas enters the unit. Wall friction of the piston is negligible, with a back pressure on the order of only 0.01" Hg. The criterion of permeability is taken as the time required to collect 5 cm<sup>3</sup> of nitrogen, while the pressure drop across the ionizer bar is maintained at 10" Hg.

### 7.3 Effect of Loading Technique and Vibration on Packing Density

Investigation of vibratory packing versus static loading was performed on tungsten microspheres, before it was decided to use H<sub>2</sub>-reduced tungsten for fabricating large ionizer bars. However, results of the packing experiments are very pertinent, despite the fact that an alternate double-pressing method was subsequently developed as optimum for large-ionizer fabrication.

The objectives of vibratory packing were to improve structural uniformity, to enable pressing to closer tolerances, and, thus, to minimize waste of material. The effects of various packing techniques on apparent density were determined in a Pyrex graduate of 3/8-inch diameter. Variables of loading and packing are given in Table 7-I, together with the apparent densities derived. The lowest packing density (45.3 percent of theoretical) was obtained with damp powder, which was merely poured into the graduate. Density was increased slightly to 47.8 percent by tamping manually with a rod. When the

TABLE 7-I

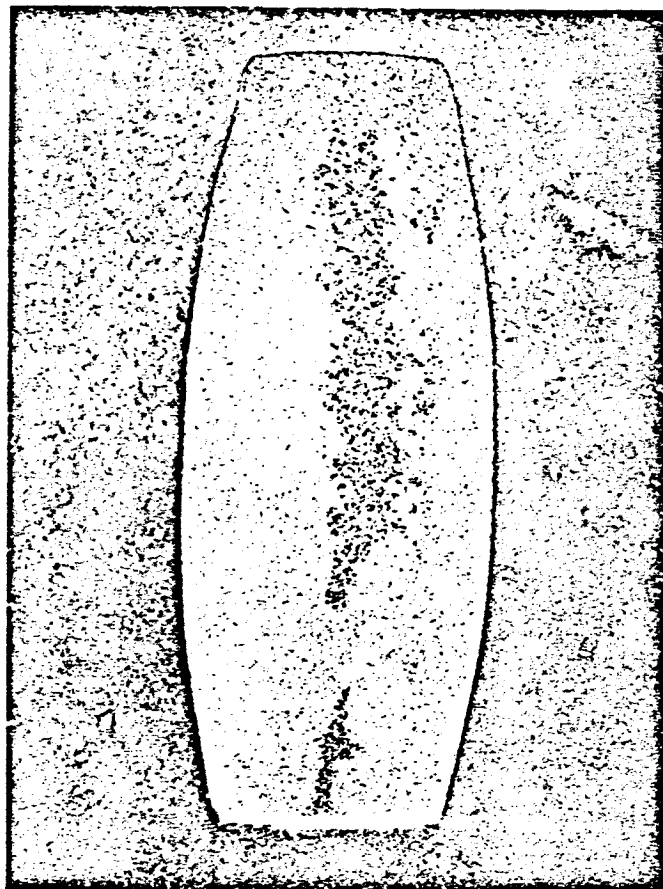
EFFECT OF VARIOUS PACKING TECHNIQUES ON APPARENT  
DENSITY OF 2.5-10 $\mu$  DIAMETER TUNGSTEN MICROSPHERES

Test No.	Powder Condition	Technique Used for Loading Graduate	Powder		Density	
			Wt, gm	Vol, cm <sup>3</sup>	gm/cm <sup>3</sup>	% of theor.
1	As-Rc'd (damp)	Poured directly	19.935	2.28	8.74	45.3
2	Dried by Desiccation	Poured directly	20.450	2.28	8.97	46.5
3	As Rc'd (damp)	Tamped manually with rod	20.681	2.24	9.23	47.8
4	Dried by Desiccation	Tamped manually with rod	21.707	2.28	9.52	49.3
5	Dried by Desiccation	Poured directly - Vibrated ultrasonically for 60 min	26.344	2.30	11.45	59.3
6	Submerged in benzyl alcohol	Vibrated ultrasonically for 60 min	26.351	2.28	11.56	59.9
		Vibrated ultrasonically for 90 min	26.351	2.26	11.66	60.4
		Vibrated ultrasonically for 120 min	26.351	2.25	11.71	60.7
7	Submerged in benzyl alcohol	Evacuated 1 hr@ $\approx$ 1 torr	25.294	2.60	9.73	50.4
		Vibrated ultrasonically for 5 min	25.294	2.30	11.00	57.0
		Vibrated ultrasonically for 65 min	25.294	2.10	12.04	62.4
		Vibrated ultrasonically for 125 min	25.294	2.10	12.04	62.4

powder was dried first and then poured into the graduate, density was increased slightly to 46.5 percent. A large increase in apparent density to 59.3 percent was effected by vibrating the dry powder at 40 kc/sec for 60 minutes. Apparent density was increased even further to 62.4 percent by submerging the powder under benzyl alcohol and vibrating at 40 kc/sec for 65 minutes. Vibrating the submerged powder for an additional 60 minutes effected no further increase in apparent density.

The foregoing results would seem to indicate that packing of tungsten microspheres by submerging in benzyl alcohol and vibrating ultrasonically was the best technique tested, since it produced the highest apparent density. However, the high-frequency vibration continuously liberated vapor bubbles, which bubbles tended to be trapped within the tungsten powder. This effect was even more pronounced when water and methyl-alcohol vehicles (both having higher vapor pressures than benzyl alcohol) were used. It is concluded, therefore, that use of a liquid vehicle in conjunction with ultrasonic vibration is not practical, due to the formation of relatively large void occlusions.

It may be noted in Table 7-I that vibrating in the dry condition yielded an apparent density of 59.3 percent, not much lower than the 62.4 percent obtained by vibrating under benzyl. A barrel-shaped compact ( $\approx 1/4$ -inch diameter x  $3/4$ -inch length) was prepared from the 2.5-10 $\mu$  microspheres by vibrating the dry microspheres at 40 kc/sec for 60 minutes, hydrostatic compaction, vacuum sintering, and copper infiltration. The infiltrated compact was sectioned longitudinally, polished, and examined microscopically. Examination revealed a core region which was much denser than the surrounding structure (see Fig. 7-3). This could occur only if (1) the core region was compacted to a higher density than the surrounding region or (2) the finer particles migrated to the core region during vibration, with subsequent rapid densification. Of these, (2) appears to be most probable. Since homogeneity of ionizer pore structure is required, and since vibratory packing is indicated to segregate the finer particles, use of this technique is not recommended.



Neg. 2767

X5

FIG. 7-3 DENSE REGIONS IN SINTERED PELLET, MADE FROM 2.5-10 $\mu$  TUNGSTEN MICROSPHERES WHICH WERE PACKED INTO RUBBER MOLD BY VIBRATING AT 40 kc/sec FOR 60 MINUTES (dense areas appear dark due to oblique lighting used in photography)

## 8. CONCLUSIONS AND RECOMMENDATIONS

Development work, described in this report, has provided greatly improved tungsten-base ionizers of two general structural types, made from: (1) small tungsten microspheres with additions of small angular Ta and Ta+Re particles, and (2) small angular tungsten particles with additions of finely ground boron nitride. Relative characteristics of the two types are summarized below:

	TYPE 1 Spherical Tung.-Base With Ta & Ta+Re	TYPE 2 Angular Tung.-Base With Boron Nitride
Absolute Density } Pore Density }	High	Low
Open Pore Volume } N <sub>2</sub> Permeability }	Low	High
Pore Diameter } Pore Spacing }	Small	Large
Lifetime at 1100-1300°C	Very Good	Indeterminate
Ionization Performance	Excellent	Excellent
Powder Cost	High	Low

The spherical tungsten-base ionizers had up to  $1.4 \times 10^7$  pores/cm<sup>2</sup>, good thermal stability, and excellent ionization performance. Neutral fractions of W-5Ta-10Re ionizers were lower than for the finest-structured ionizer (W+102Å Ta) tested previously by factors of  $\sim 1/4X$  at 5 mA/cm<sup>2</sup> and  $\sim 2/3X$  at 20 mA/cm<sup>2</sup>. Transition temperatures were approximately equivalent to those of W+102Å Ta over the 5-20 mA/cm<sup>2</sup> range. Further refinement of pore structure and improvement of ionization performance would necessitate (1) the use of an inert separator powder, such as copper flake, and/or (2) further developments by powder technologists to provide and classify tungsten microspheres finer than the diameter range 0.25-2.5μ.

The angular tungsten material with addition of boron nitride stabilizer was prepared by the copper-flake technique. This low-density, high-permeance material is a new EOS concept having great potential. Despite the fact that a relatively short time was spent in development, its ionization performance was excellent. Neutral fractions for the 61%-dense W-8Cu-2BN ionizer were lower than those of W+102Å Ta by factors of  $\sim 1/7X$  at  $5 \text{ mA/cm}^2$  and  $\sim 1/3X$  at  $20 \text{ mA/cm}^2$ . In addition, transition temperature was  $60^\circ\text{C}$  lower at  $5 \text{ mA/cm}^2$  than that of W+102Å Ta.

Further study of the high-permeance ionizers is needed (1) to optimize pore structure, density level, stabilizer content, etc., and (2) to determine the mechanism by which boron nitride provides structural stability at elevated temperatures. Optimization of pore structure and composition is expected to improve performance by a significant degree. Therefore, advanced development work on this new ionizer concept was proposed and initiated as Modification 6 of this contract.

#### REFERENCES

1. M. LaChance and G. Kuskevics, "Ionizer-Reservoir Development Studies", Electro-Optical Systems, Inc. 2150-Final Report, May 1963.
2. M. LaChance, G. Kuskevics, and B. Thompson, "Porous Ionizer Development and Testing", Electro-Optical Systems, Inc. 3720-Final Report, May 1964.
3. M. LaChance, B. Thompson, H. Todd, and G. Kuskevics, "Development of Composite Ionizer Materials", Electro-Optical Systems, Inc. 4971-Final Report, April 1965.
4. P. C. Carman, "Flow of Gases Through Porous Media", Butterworth, London, 1949.
5. G. Kuskevics and B. Thompson, "Comparison of Commercial, Spherical Powder, and Wire Bundle Tungsten Ionizers", AIAA Jour., 2, 2, 284-294 (1964).
6. G. Kuskevics and B. Thompson, "Surface Ionization Ion Source", Acc'd for Pub. in Rev. of Sci. In.
7. G. Kuskevics, "Criteria and a Graphical Method for Optimization of Cesium Surface Ionizer Materials", EOS Res. Rpt. RR-3, Jan. 1962.



**APPENDIX A**

**PARTICLE SIZE ANALYSIS REPORTS**  
**by Sloan Research Industries, Inc.**



## Introduction

On April 20, 1965, a sample of tungsten powder designated S/M No. E2143 was received for particle size studies by electron microscopic techniques. It was requested that the counting increments be such that the % by number of particles in the .5-2.5  $\mu$  range be determined. The following report is the result of the studies and is hereby respectfully submitted.

## Sample Preparation and Study Techniques

The sample preparation technique which proved to be most suitable with respect to agglomeration and particle dispersal is described as follows:

A representative portion of the sample was dusted on to a parlodian film microscope viewing grid. The excess material was removed from the grid and the specimen was placed in a vacuum chamber. Carbon was evaporated vertically on to the grid, thus effectively sandwiching the particles between the parlodian layer and the carbon film. This provided a stable sample substrate and effectively immobilized the particles. The grids were viewed in a Norelco EM 100 electron microscope capable of resolving 14 Å. The microscope was accurately calibrated to  $\pm 60$  Å, by using 2640 Å Dow calibration latex spheres (standard deviation = .0060).

The particle size counts and distribution data were performed by the equivalent circle technique which is described in detail in a following section.

## Electron Micrographs

In the lower right hand corner of each of the micrographs contained in this report a pair of black marks may be seen. The distance between the inner edges of these marks represents a distance of one micron on the surface of the micrograph. A stamp has been placed on the back of each micrograph in this report which contains information as to the identity of the sample from which the micrograph was made and the conditions under which the micrograph was taken.

## Discussion of Electron Micrographs

In general, the tungsten particles are quite spherical in nature with relatively few particles showing any crystallographic faces or other non-spherical forms. The largest particle found during preliminary visual scanning with the electron microscope was  $5.8 \mu$  in diameter. As this particle was well beyond the range of the other particles in the sample, it was considered to be atypical. Some tendency of preferred grouping of the fine particles about the surfaces of the larger particles was found to be present. These  $0.25 - 0.5 \mu$  particles were counted when visible, but undoubtedly many were spread over the top and bottom surfaces of the larger particles and could not be counted. Very little contaminating material is present in the sample.

## Discussion of Particle Size Data

At the end of this section will be found the particle size data in tabular form. The counts were taken from five representative electron micrographs and a total of 941 particles were counted. The numerical data are plotted on graphs in order that the reader may conveniently observe the general trends of the data.

Figure No. 1 is a simple histogram displaying the frequency of the actual counts of each incremental step. The conversion of this data into a percentage basis relating the incremental particle diameters to the total count is presented in figure No. 2. Cumulative data is plotted in Figure No. 3 as a Percentage Greater Than curve.

The curves show the particle count to follow a unimodal modified log-normal distribution. The cumulative plot, Figure No. 3, shows the modification to be of limited growth where  $M_0 \neq 0$  and  $M_\infty \neq \infty$ . This modification is typical of sample processing effects where limitation techniques are introduced to cause an artificial distribution. The asymptotic deviation of the Greater Than curve shows  $M_\infty = 5\mu$  as an upper limit. Some of the modification in the fine region may be due to the increasing difficulty in accurately sizing the smaller particles in this magnification range.

The Greater Than curve also shows that 50% of the particles have a diameter of  $1.5 \mu$  or more. This is the value which would be expected of a symmetrical curve limited between 0.5 and 2.5 microns.

The percentage value of any particular interval can be easily obtained by making a summation of the data for that range as found in the Incremental Percent Count column of the data table. The percent of the particles occurring in the  $0.5$  to  $2.5 \mu$  interval is 68.4%.

DETAILED DESCRIPTION FOR EQUIVALENT CIRCLE TECHNIQUEOF PARTICLE SIZE ANALYSISRequired:

1. A circle template with 10 or more circles in the range of 1/16 inch to 1 1/2 inch.
2. A micrograph taken at a magnification which brings the particles of interest in the range of 1/16 inch to 1 1/2 inch.

Assumed:

1. Particle cross sections are symmetrical, and can be easily approximated by an equivalent circle.
2. The cross section micrograph is of a truly representative area.
3. Particle volume is symmetrical, and the micrograph represents a random particle orientation.

Procedure:

The following is a step-by-step procedure for circle equivalent particle size analysis.

1. Find the largest particle present and find an equivalent circle to match its cross-sectional area. With a contrast color pen, circle the grain and count one.
2. Identify, circle and count each particle which can be represented by this largest equivalent circle.
3. Using each selected smaller size circle, mark, count and accumulate equivalent circle data.
4. When the count has been completed, no free grain should remain uncircled unless:
  - a. the particle touches the outer boundary of the area selected for analysis.
  - b. the boundary of the particle is not sufficiently well delineated to define an equivalent circle.
  - c. the particle is below the size of the smallest equivalent circle.
5. Take the sum of all counts.
6. Unitize the equivalent circle count, and express individual values as percent total population.
7. Taking the arithmetic mean between equivalent circle sizes, describe each individual particle size range.
8. REPORT AND PLOT PERCENT TOTAL POPULATION VS. EQUIVALENT CIRCLE SIZE OR EQUIVALENT PARTICLE RANGE.
9. Take the product of the cube of the equivalent circle diameter, and the individual count for that equivalent circle size -- unitize as in steps 5 and 6.
10. REPORT AND PLOT PERCENT TOTAL PARTICLE VOLUME OCCUPIED VS. DIAMETER OR EQUIVALENT PARTICLE SIZE RANGE.

COMPUTED FACTORS FOR PARTICLE SIZE ANALYSIS

FOR SAMPLE S/M NO. E2143

Particle Size - $\mu$	Particle Count	Incr. % Count	% Greater
0- .24	0	0	0
.25- .49	119	12.6	87.4
.5 - .74	122	13.0	74.4
.75- .99	125	13.3	61.1
1.0 -1.24	81	8.61	52.5
1.25-1.49	80	8.50	44.0
1.5 -1.74	82	8.71	35.30
1.75-1.99	58	6.16	29.12
2.0 -2.24	48	5.10	24.02
2.25-2.49	48	5.10	18.92
2.5 -2.74	36	3.82	15.10
2.75-2.99	35	3.72	11.38
3.0 -3.24	35	3.72	7.66
3.25-3.49	34	3.61	4.05
3.5 -3.74	17	1.81	2.24
3.75-3.99	7	.74	1.50
4.0 -4.24	6	.64	.86
4.25-4.49	6	.64	.22
4.5 -4.74	1	.11	.11
4.75-4.99	1	.11	0

200

FIGURE NO. 1

HISTOGRAM FOR PARTICLE FREQUENCY  
OF SAMPLE S/M NO. E2143

125

100

50

Diameter

0

1.0

2.0

3.0

4.0  $\mu$

FIGURE 2 FREQUENCY DISTRIBUTION FOR  
 SAMPLE S/M NO. E2143  
 INCREMENTAL % COUNT VS. PARTICLE SIZE

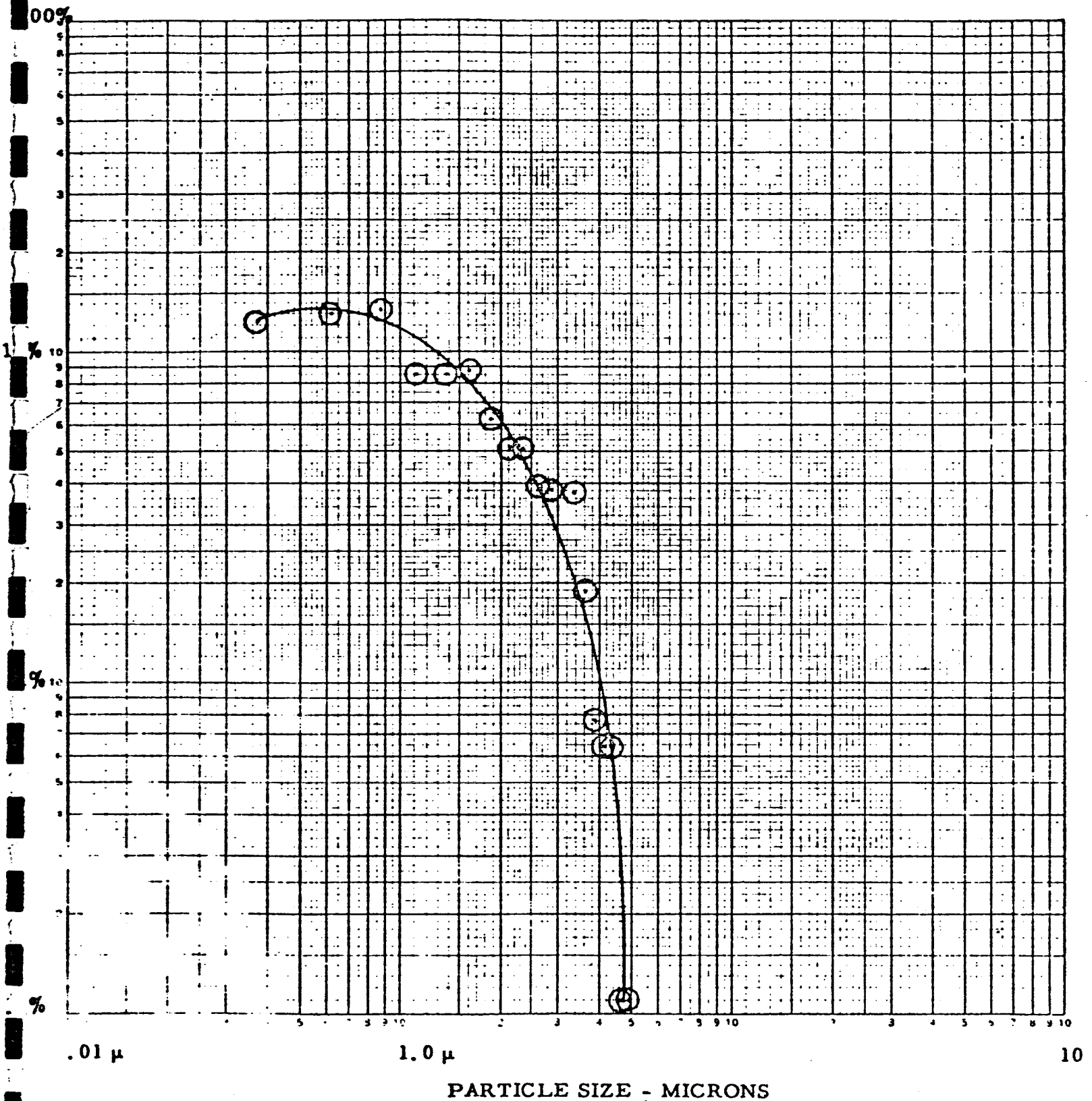
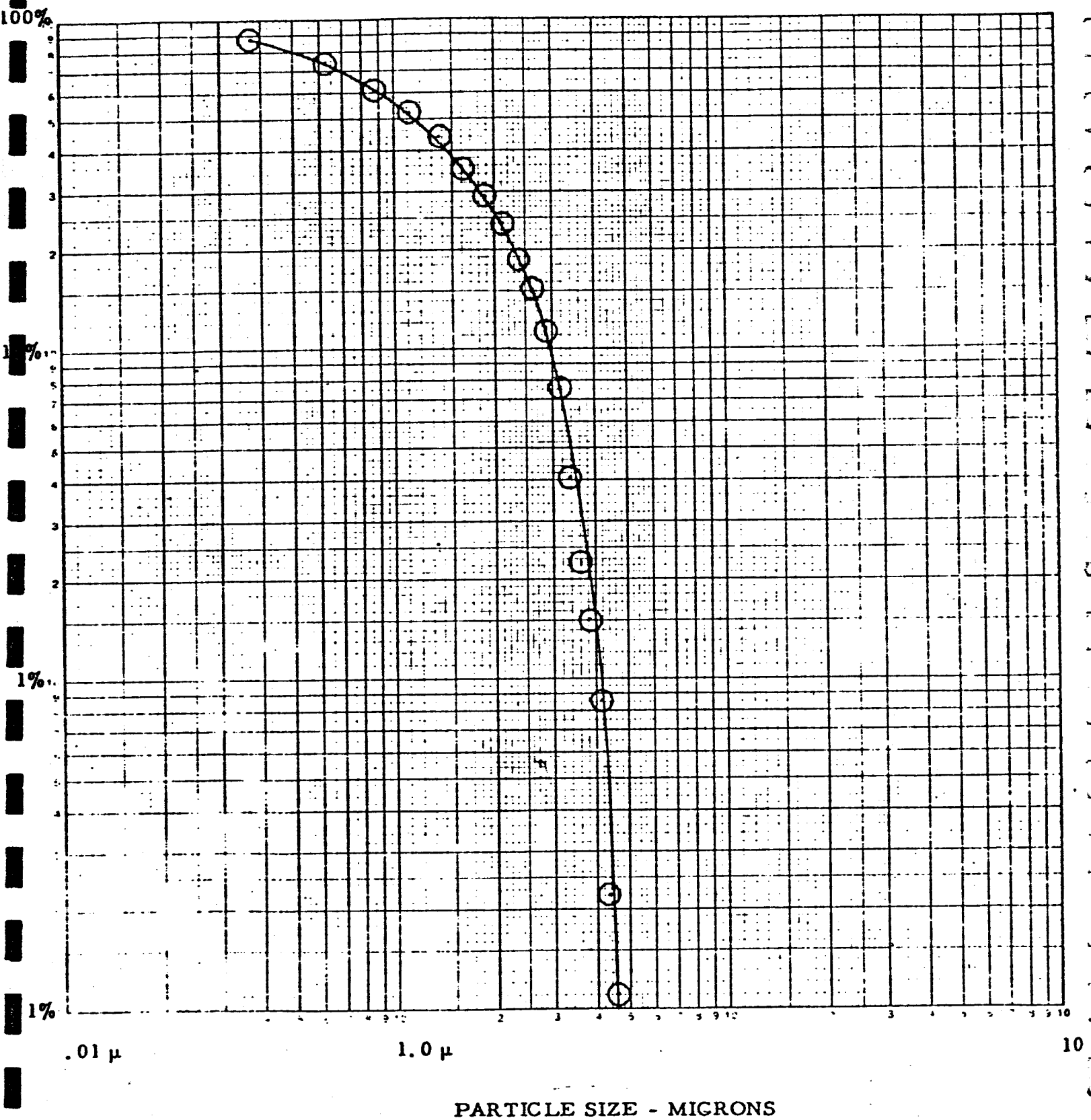
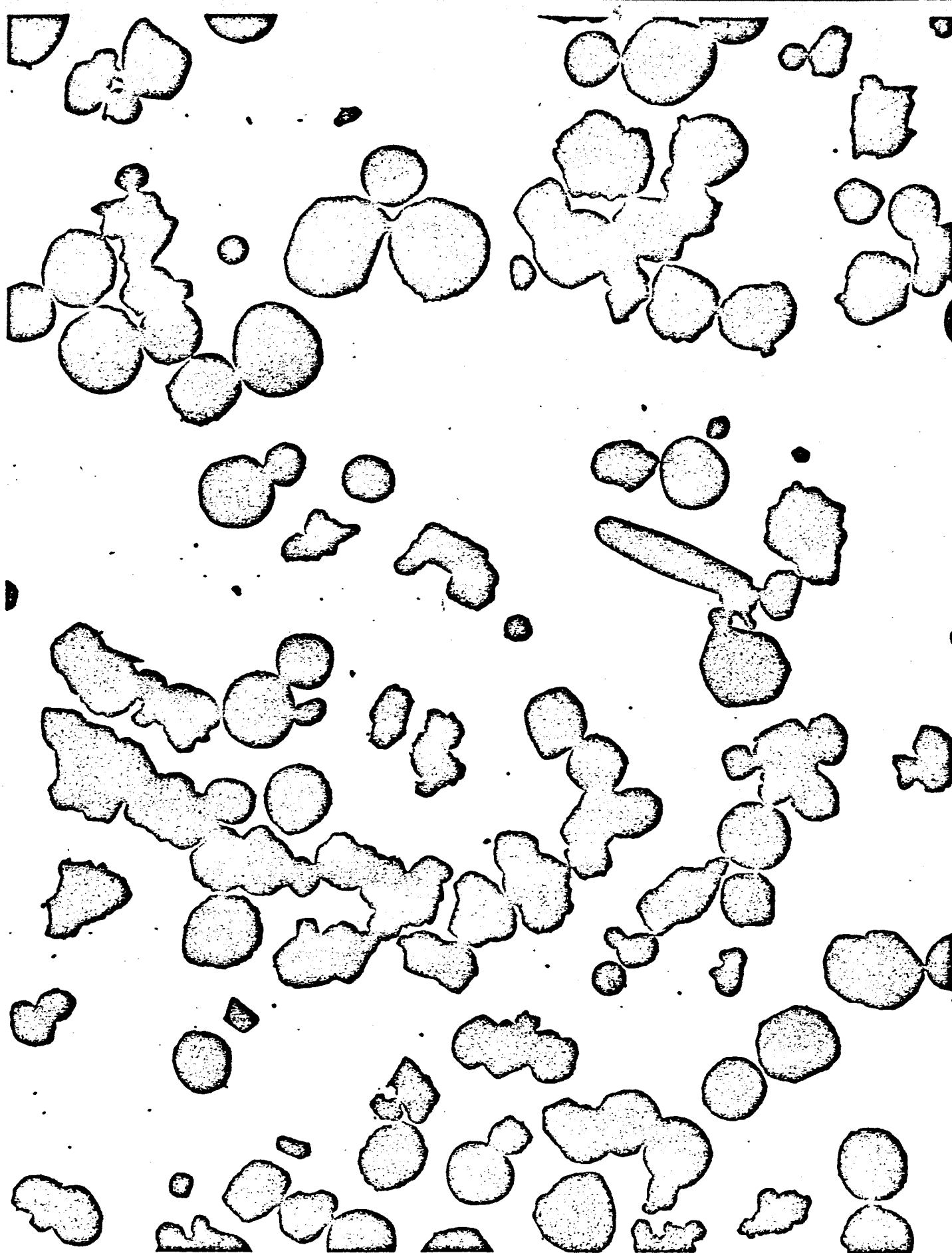
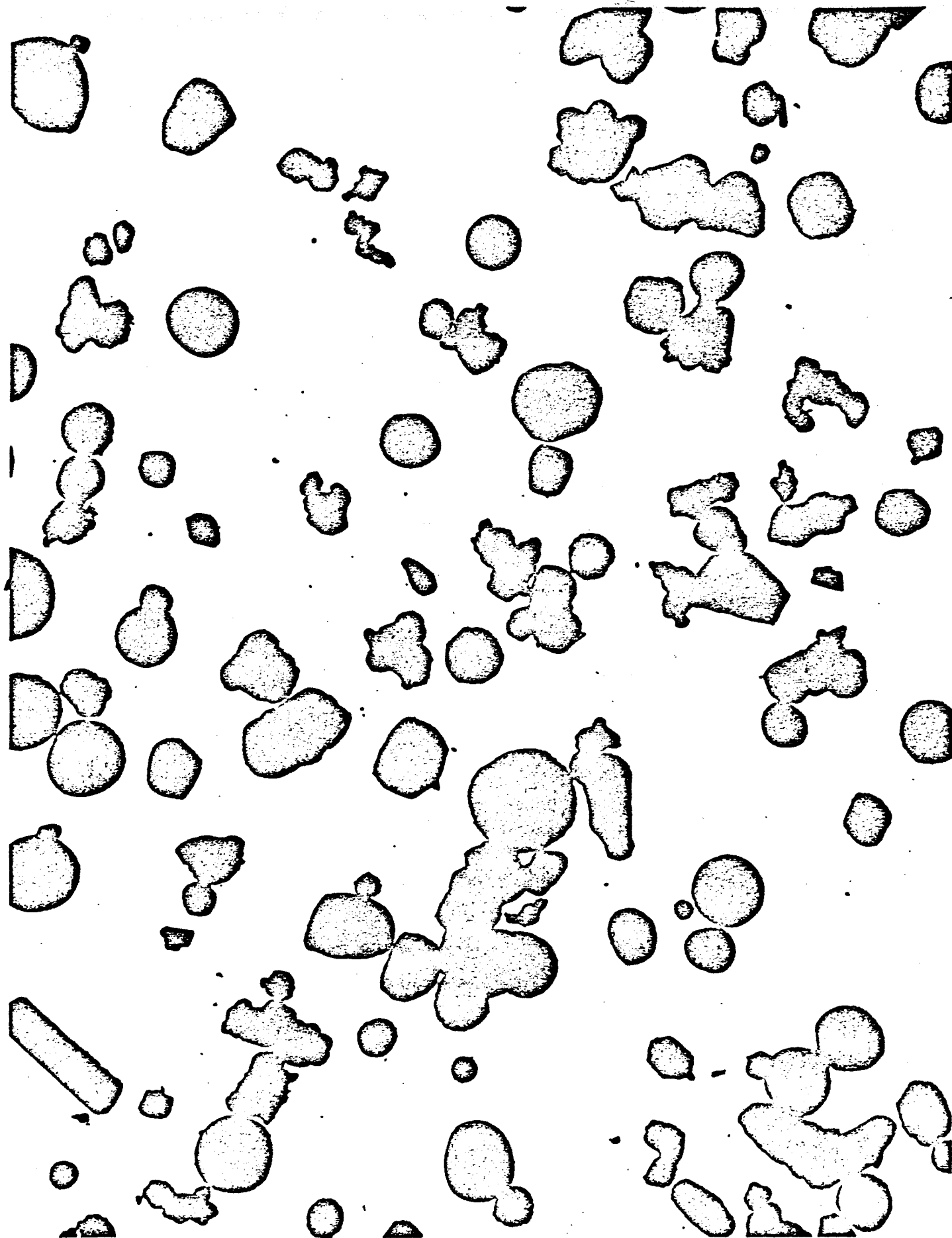


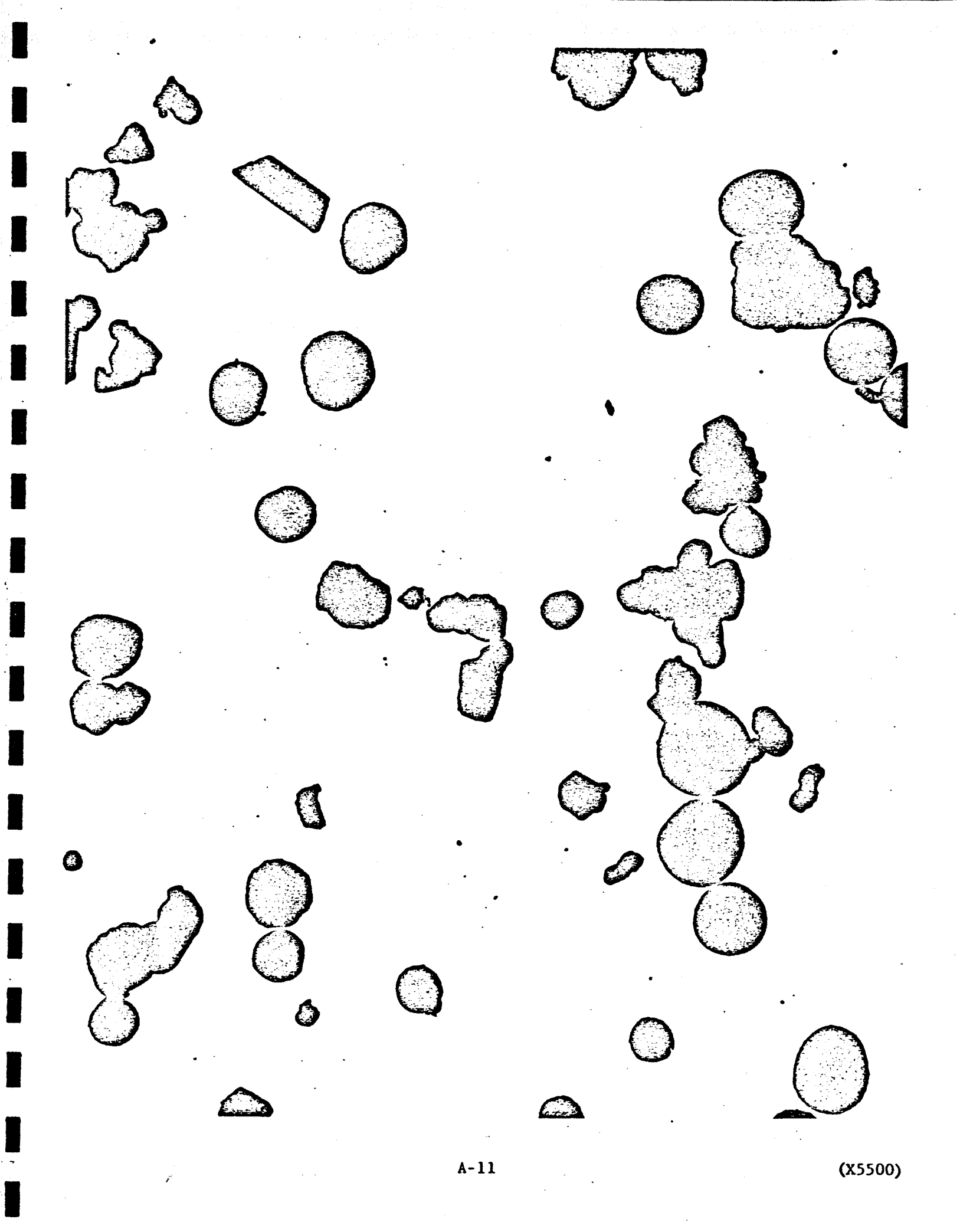


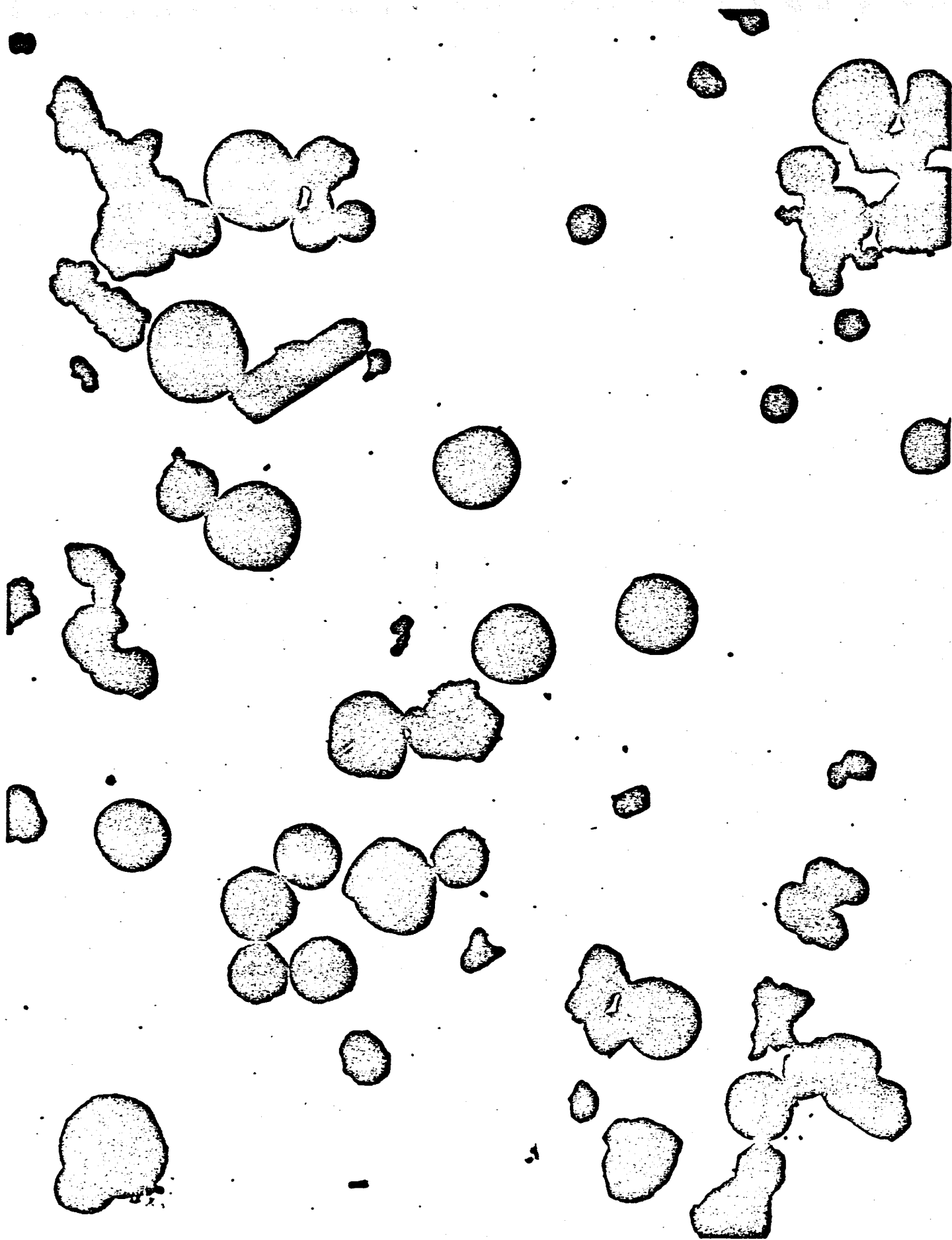
FIGURE 3 CUMULATIVE DISTRIBUTION FOR  
SAMPLE S/M NO. E2143  
% GREATER THAN VS. PARTICLE SIZE

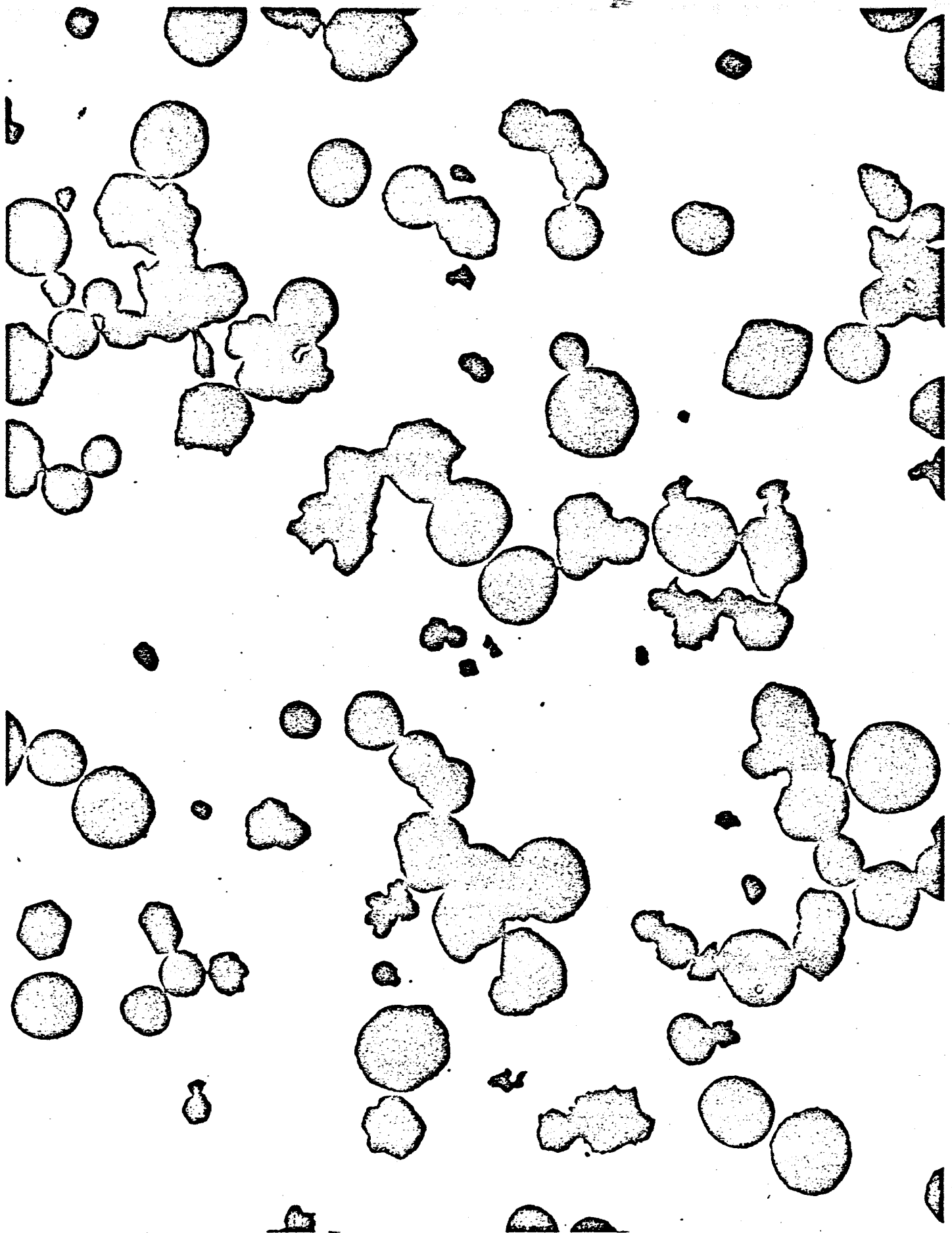












ELECTRON MICROSCOPIC PARTICLE SIZE ANALYSIS

OF EOS LOT PTF TUNGSTEN MICROSPHERES

(Classified from Linde Powder)

## Introduction

On October 8, 1965, one sample of tungsten microspheres EOS Lot PTF, Purchase Order No. 58639, was received in the laboratory for particle size studies by electron microscopic methods. It was requested that the study techniques be similar to those used in SRI Report No. 566240. The following report is the result of the studies and is hereby respectfully submitted.

## Sample Preparation and Study Techniques

A somewhat different method of sample preparation was used, which we believe should assure a more uniform sampling and still produce an adequate dispersion of the studies. This method is described as follows. An aliquot of the sample was mixed in a small vial with high purity hexane and then exposed to a 50,000 cps high intensity ultrasonic agitation for about two hours. Carbon filmed viewing grids were dipped into the dispersion immediately after removal of the sound power and allowed to dry. Viewing was accomplished in a Norelco EM 100B electron microscope, capable of resolving 14 Å. Accurate calibration of the magnification was made by using .26μ polystyrene latex calibration spheres having a standard deviation of .0060μ. The particle size counts were performed in a .25 increment by the equivalent circle technique which was discussed in detail in SRI Report No. 566240.

## Electron Micrographs

In the lower right corner of each of the micrographs contained in this report, a pair of black marks may be seen. This distance between the inner edges of these marks represents a distance of one micron on the surface of the micrograph.

A stamp has been placed on the back of each micrograph in this report, which contains information as to the identity of the sample from which the micrograph was made and the conditions under which the micrograph was taken.

The particles in this sample were found to be more uniform in shape than those observed in SRI Report No. 566240. No elongated particles were found to be present in this sample. The particles are in general quite spherical, with a small percentage (occurring mostly in the smaller size ranges) exhibiting flattened crystal-like faces. No



extremely large atypical particles were found to occur in this sample. Many more of the very fine particles could be clearly distinguished in this sample. This may be partially due to the slightly higher magnification and the different method of sample processing which was used.

#### Discussion of the Particle Size Data

The counts and distribution data were taken from six representative micrographs of the sample, containing a total of 771 particles.

For your information, a more complete statistical analysis has been made to give additional particle parameters. The calculated data and graphs will be found at the end of this section.

The histogram (Figure 1) and the frequency distribution (Figure 2) would seem to indicate a bimodal distribution, which would mean that two sources or mechanisms are responsible for the particles. The greatest deviation from the log - normal distribution that should be expected is due to the unusually high contribution of the very fine particles from the 0 - .24 $\mu$  range. Micrograph 2 shows a group in the lower center which is literally covered with .1 - .2 $\mu$  particles. These were not counted as they were considered to be an atypical grouping. To determine if these fine particles were due to some other sample contaminating material, a quick check was made using X-ray diffraction methods but no tungsten oxide formation or other crystallographic contaminants were found to be present. The Cumulative Distribution Graph (Figure 3) shows the particles again to have the limiting modification in the larger particle size range as the curve is asymptotic to 4 $\mu$ . The deviation from the straight line slope on the upper portion of the curve is greatly emphasized by the above normal accumulation of the very fine particles. This curve shows that 50% of the particles in the sample are larger than .8 $\mu$  in diameter.

As can be seen on the included data table, the arithmetical mean particle diameter has been calculated to be 1.17 $\mu$ .

Using the interval summation values from the incremental % count data, the percent of the particles occurring in the .5 - 2.5  $\mu$  range is calculated to be 63.8%.

TABLE 1

## COMPUTED FACTORS FOR PARTICLE SIZE ANALYSIS

## EOS LOT PTF SAMPLE

Particle Size - $\mu$	Count	Incr. % Count	% Greater	nd - $\mu$	nd <sup>2</sup> - $\mu^2$	nd <sup>3</sup> - $\mu^3$	Inc. % Volume	% Vol. Below
0 - .24	98	12.71	87.29	12.25	1.53	.20	.006	0
.25 - .49	85	11.02	76.27	31.88	11.45	4.48	.13	.006
.5 - .74	103	13.36	62.91	64.38	40.23	25.15	.71	.14
.75 - .99	108	14.01	48.90	94.50	82.69	72.36	2.04	.85
1.0 - 1.24	85	11.02	37.88	95.63	101.88	121.04	3.41	2.89
1.25 - 1.49	61	7.91	29.97	83.88	115.33	158.60	4.46	6.30
1.5 - 1.74	59	7.65	22.32	99.13	155.80	254.17	7.15	10.76
1.75 - 1.99	45	5.84	16.47	84.38	158.20	296.64	8.35	17.91
2.0 - 2.24	31	4.02	12.45	65.88	139.98	297.48	8.37	26.26
2.25 - 2.49	25	3.24	9.21	59.37	141.02	334.93	9.42	35.63
2.5 - 2.74	22	2.85	6.36	57.76	151.59	397.94	11.20	44.05
2.75 - 2.99	19	2.46	3.90	54.63	157.05	437.00	12.29	55.25
3.0 - 3.24	16	2.08	1.82	50.0	156.25	488.29	13.74	67.54
3.25 - 3.49	6	.78	1.04	20.25	68.34	230.66	6.49	81.28
3.5 - 3.74	4	.52	.52	14.50	52.56	190.54	5.36	87.77
3.75 - 3.99	3	.39	.13	11.63	45.05	174.56	4.91	93.13
4.0 - 4.24	1	.13	0	4.13	17.02	70.19	1.97	98.04
771-----TOTALS-----	771			904.18	1596.47	3554.23		

TABLE 2  
STATISTICAL VALUES COMPUTED FROM  
PARTICLE SIZE ANALYSIS FOR EOS LOT PTF

ARITHMETICAL MEAN DIAMETER

$$d_n = \frac{\sum nd}{N}$$

$$d_n = 1.173\mu$$

MEAN SURFACE DIAMETER

$$d_A = \frac{\sum nd^3}{\sum nd^2}$$

$$d_A = 2.23\mu$$

TOTAL E. M. SURFACE AREA

$$M^2/\text{gm.} = \frac{6}{\rho d_A(\mu)}$$

$$.14 M^2/\text{gm.}$$

NOTES:

n = number of particles of diameter, d

N = total number of particles counted

$\rho$  = density (tungsten 19.3)

$M^2/\text{gm.}$  = surface area as measured in square meters per gram.

Count

200

150

100

50

Diameter

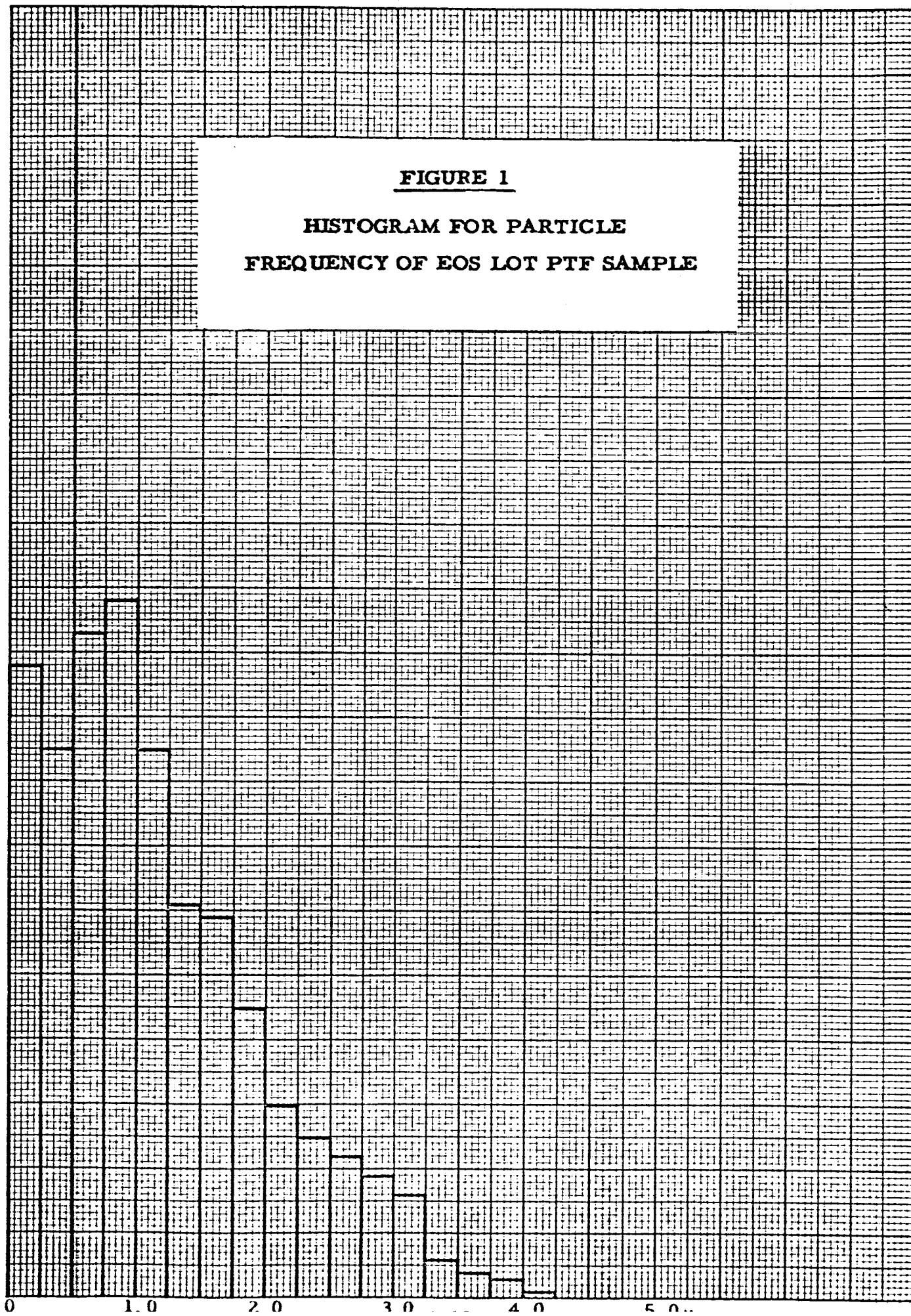


FIGURE 2

FREQUENCY DISTRIBUTION CURVE

INCREMENTAL % COUNT VS. PARTICLE SIZE FOR EOS LOT PTF

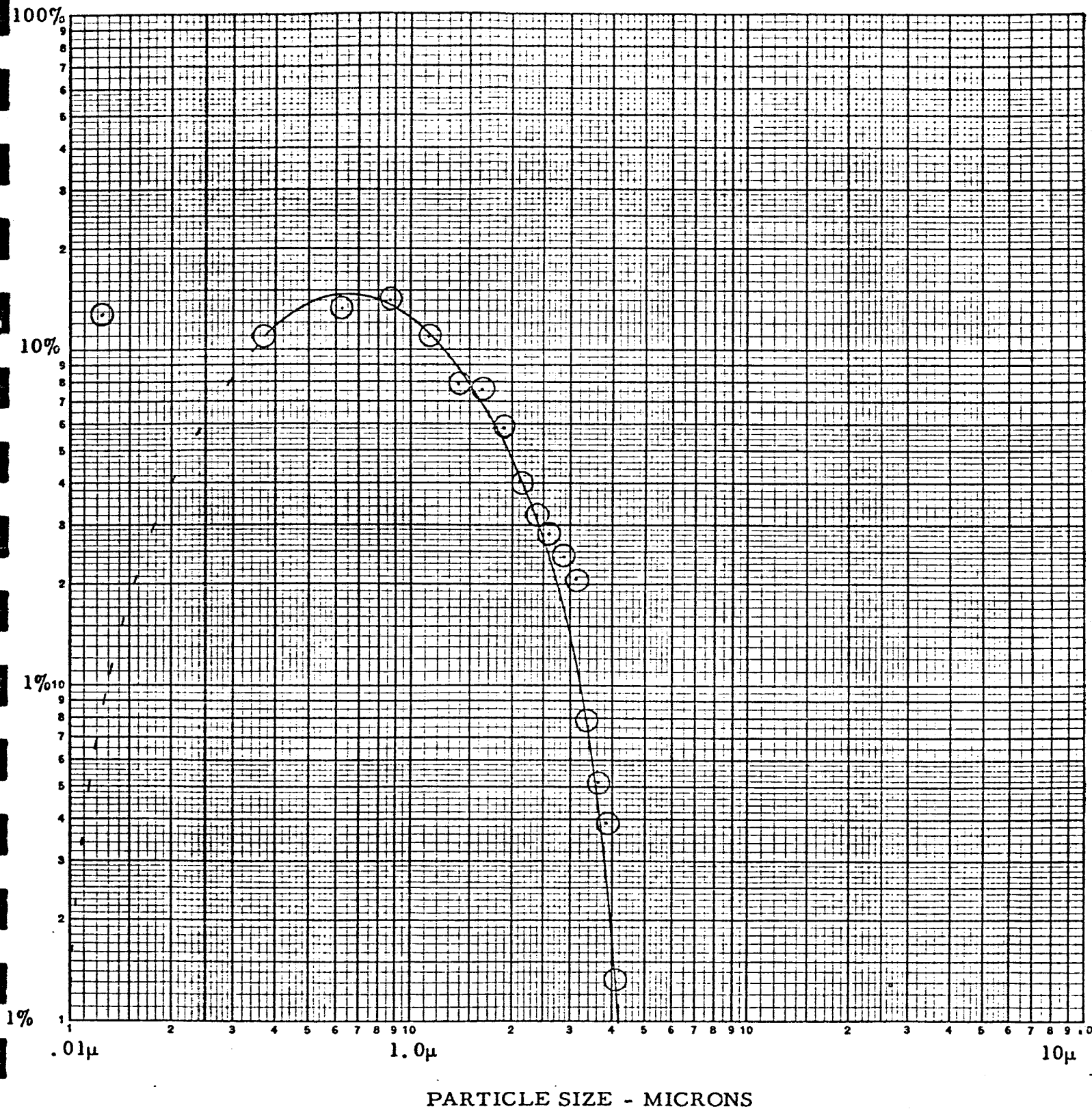
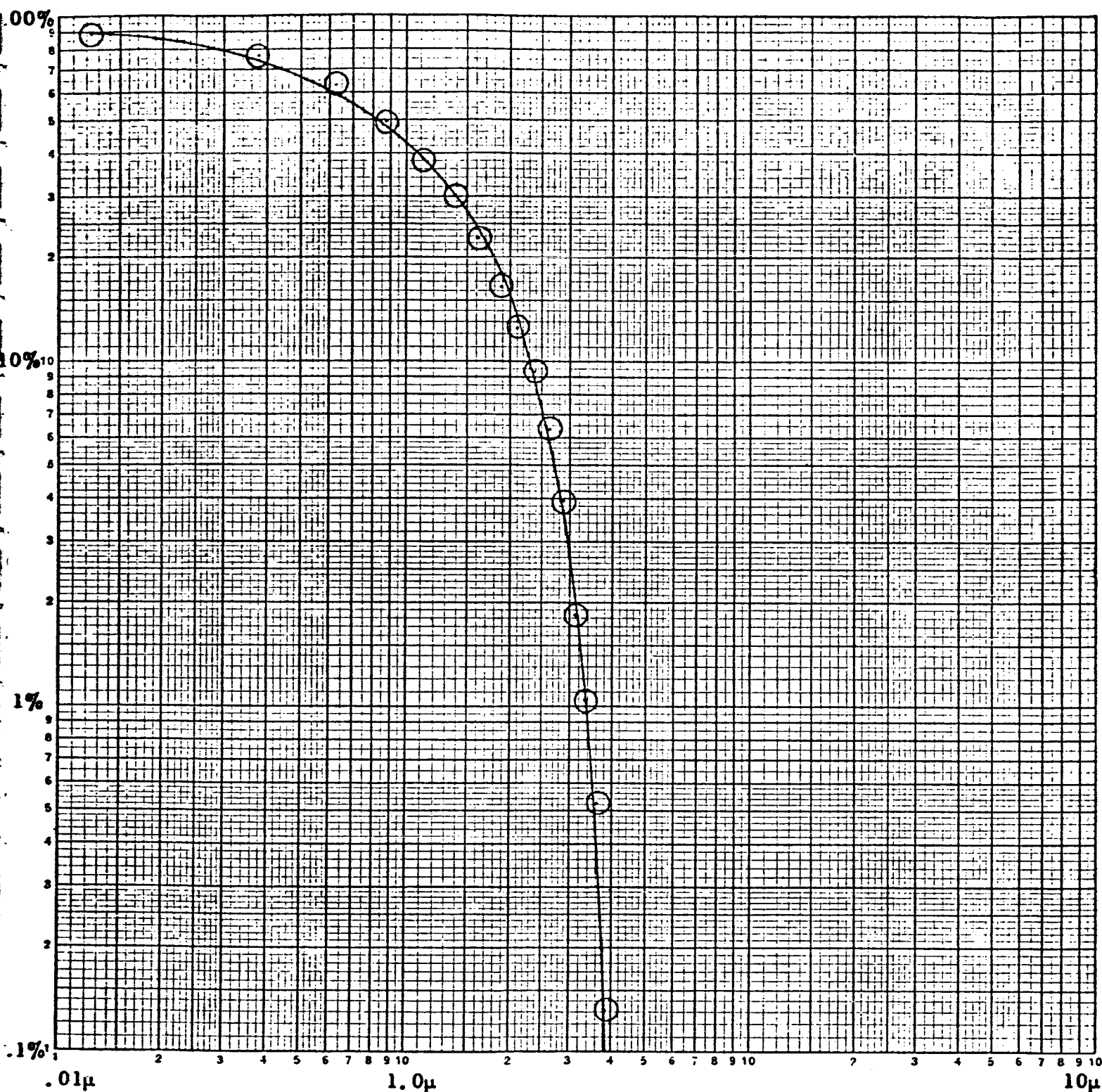


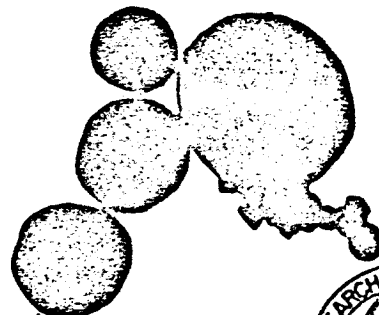
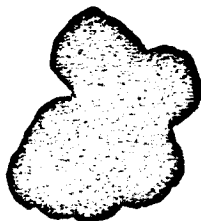
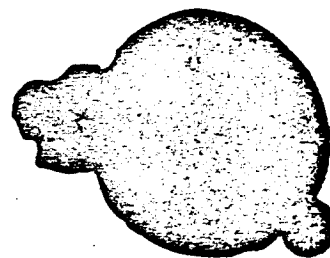
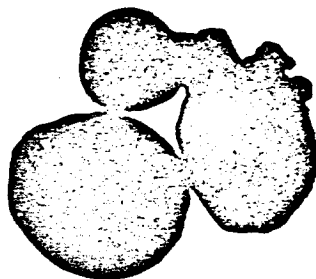
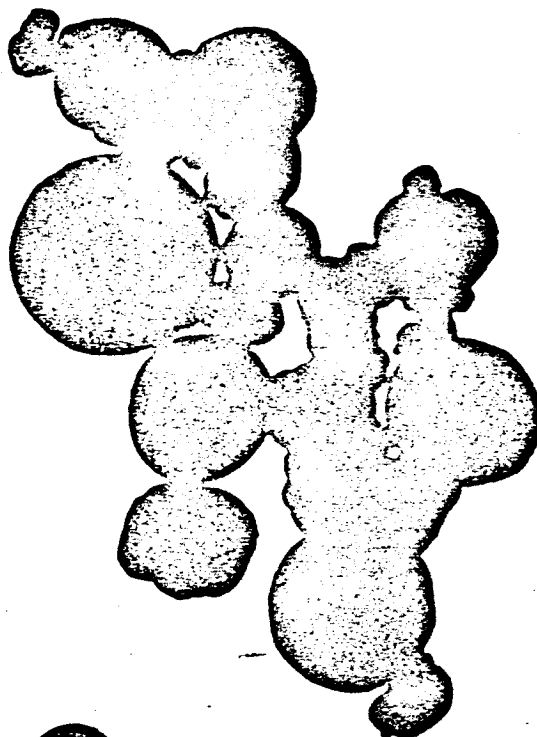
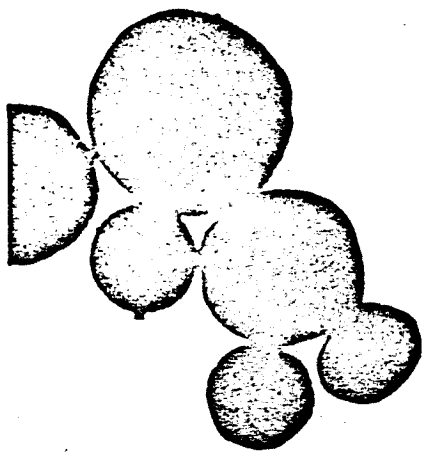
FIGURE 3

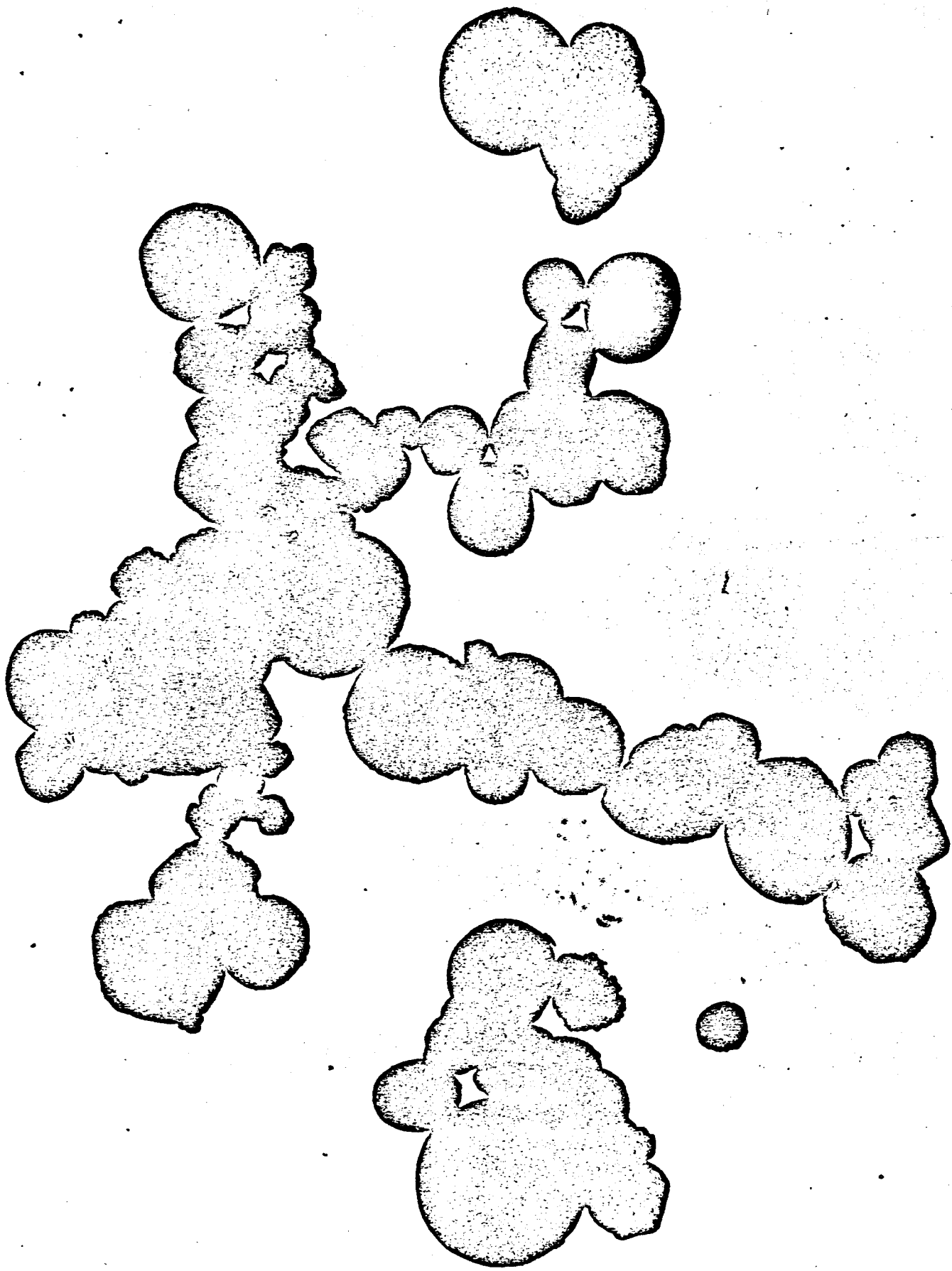
CUMULATIVE DISTRIBUTION CURVE

% GREATER THAN VS. PARTICLE SIZE FOR EOS LOT PTF

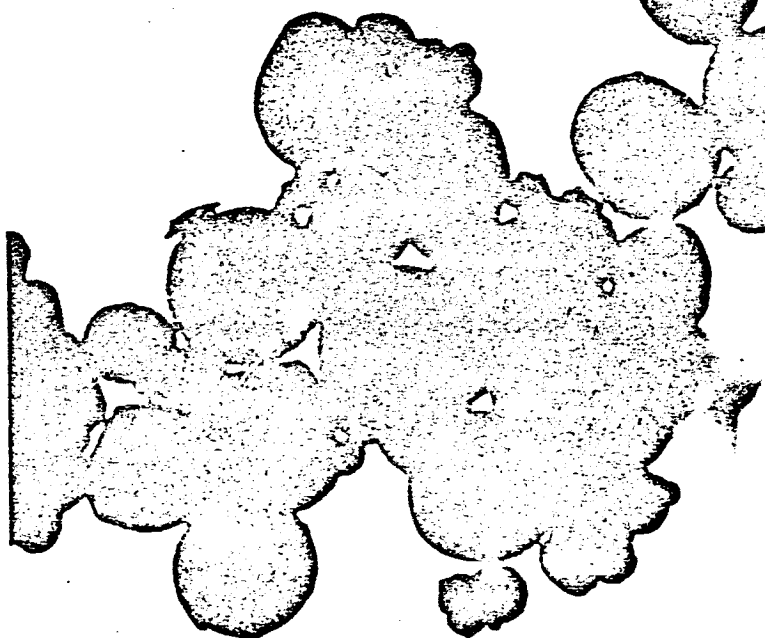
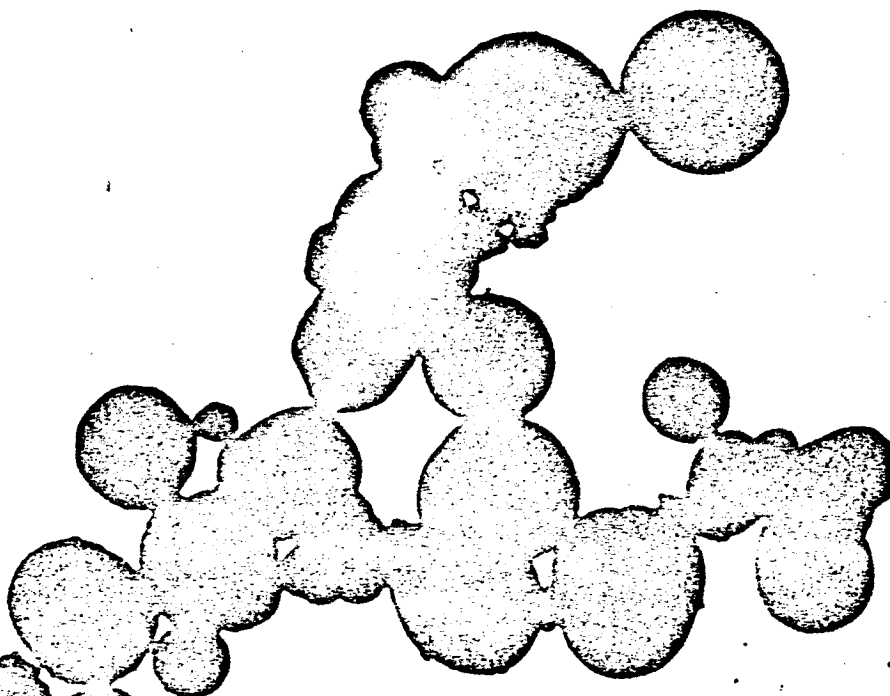
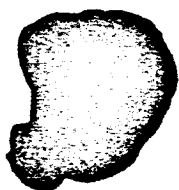
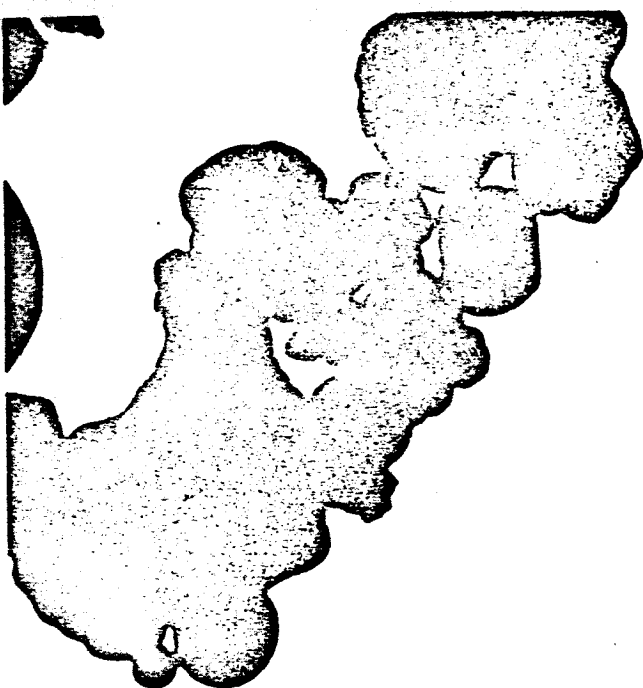


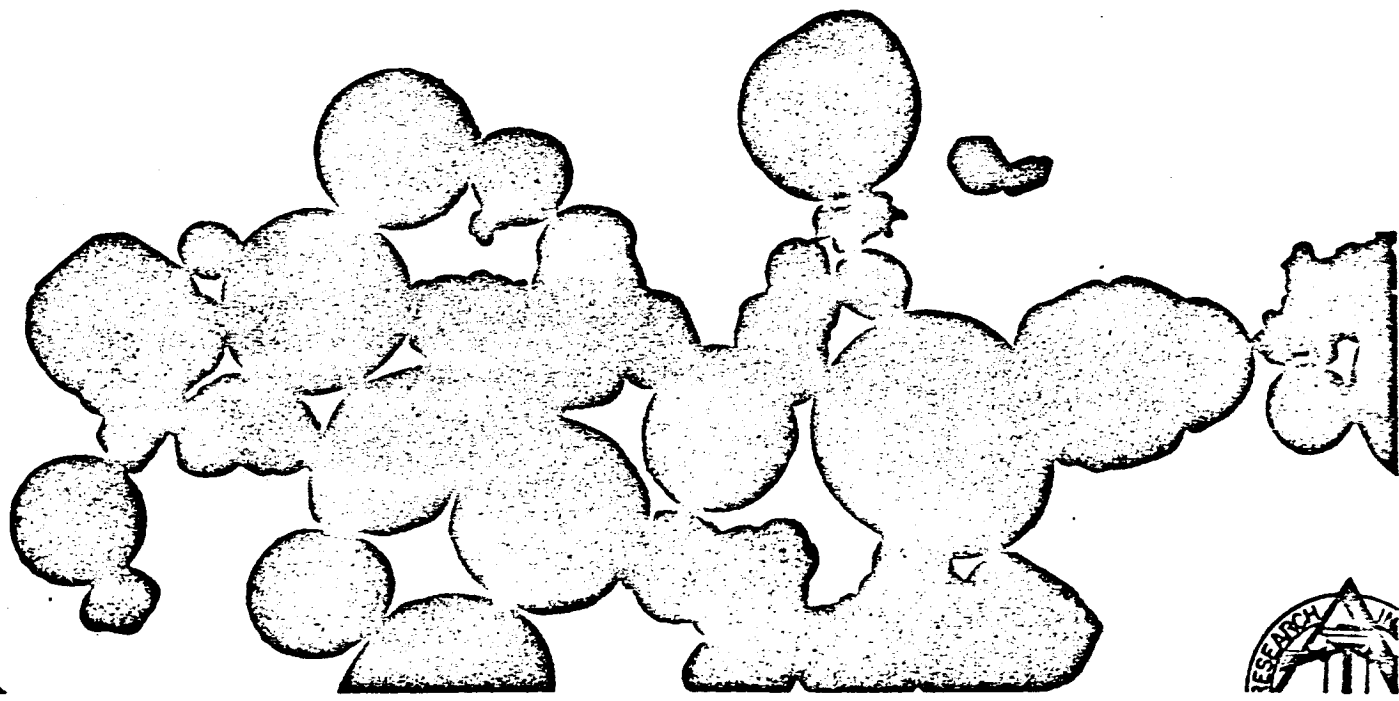
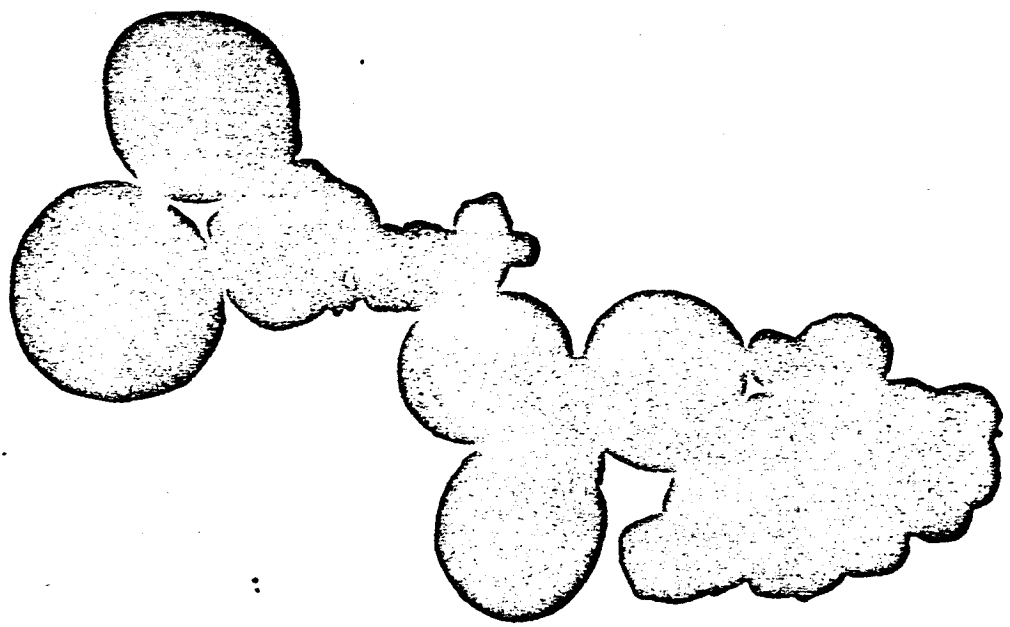
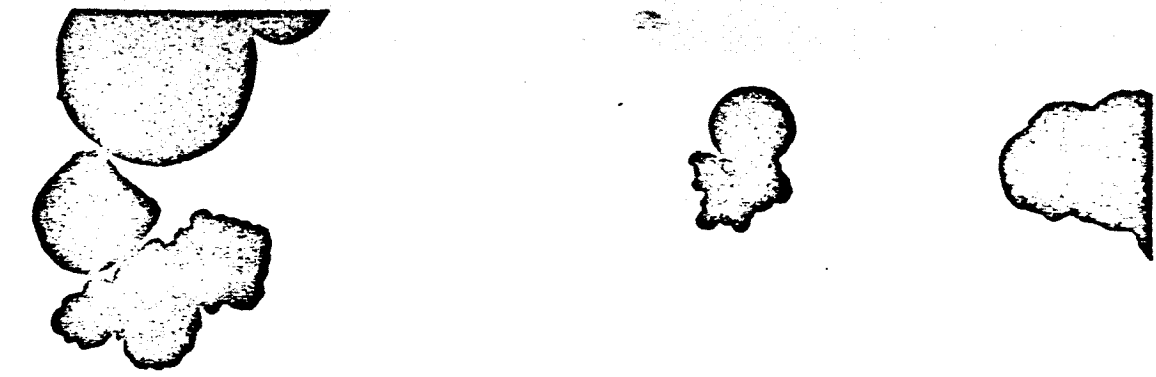
PARTICLE SIZE - MICRONS

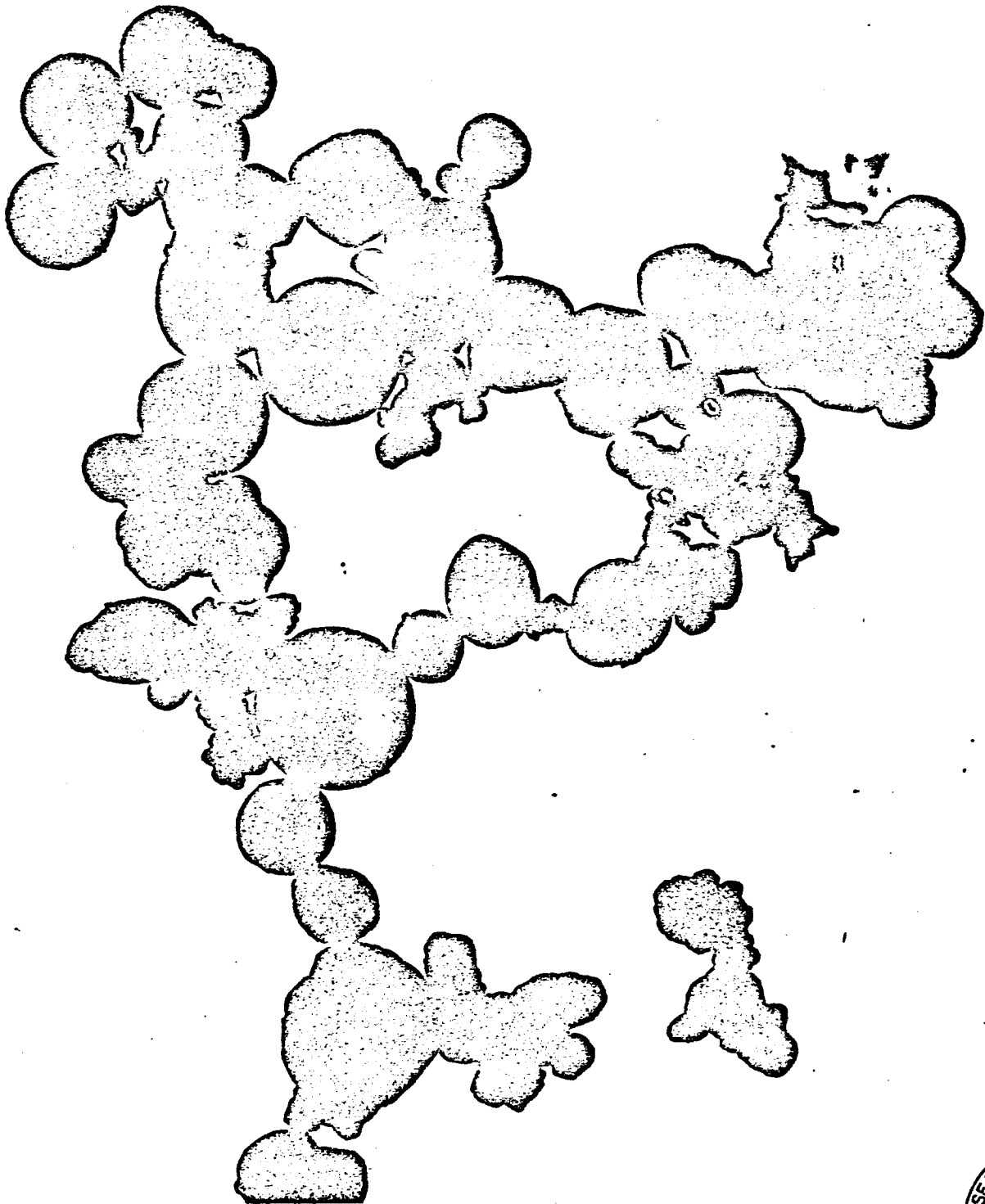
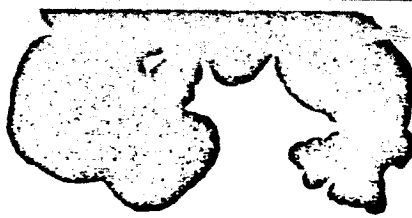












THE ELECTRON MICROSCOPIC EXAMINATION OF  
TANTALUM AND RHENIUM MICROPARTICLES TO  
DETERMINE THE PARTICLE SIZE DISTRIBUTION

## INTRODUCTION

On December 22, 1965, a sample of rhenium and a sample of tantalum microparticles were received in the laboratory for the determination of the particle size distribution by electron microscopic methods. The following report is the result of the study and is hereby respectfully submitted.

## SAMPLES

The following samples were received:

Classified SGQ-4 Ta less than  $3\mu$  Sediment  
Classified Rhenium, Fraction No. 1.

## SAMPLE PREPARATION

Several methods for particle dispersion were tried and evaluated to attempt to break-up the serious agglomeration which was encountered with these samples. These methods included aerosol techniques and ultrasonic agitation in liquids of various densities. Additions of various surfactants were also tried. The method chosen for the study was comprised of suspending the particles in high purity hexane and exposing this mixture to high intensity ultrasonic agitation for a period of 1 1/2 hours. A small amount of the suspension was allowed to evaporate on carbon filmed viewing grids. Representative viewing grids prepared by the above method were also shadowed by vacuum evaporating germanium metal onto the grid from a filament arranged in such a way so that the germanium is deposited onto the sample at an angle of  $45^\circ$ . This technique effectively shows the third-dimension contour shadow. The viewing grids were then examined in a Norelco EM 100B electron microscope capable of resolving 14 A.

## ELECTRON MICROGRAPHS

In the lower right corner of each of the micrographs contained in this report, a pair of black marks may be seen. This distance between the inner edges of these marks represents a distance of one micron on the surface of the micrograph.

A stamp has been placed on the back of each micrograph in this report which contains information as to the identity of the sample from which the micrograph was made and the conditions under which the micrograph was taken.

## DISCUSSION OF THE ELECTRON MICROGRAPHS

Classified SGQ-4 Ta less than 3 $\mu$   
Sediment

Electron Micrographs 1 - 5

Of the two samples the tantalum was found to have a higher degree of particulate dispersion, although there was still almost no separation of the very fine particles from the surfaces of the larger particles. The shadowed portion of the sample (Micrographs 1 and 2) illustrates the three-dimensional nature of the particles. The particles appear to be randomly shaped bulk particles. A few flat, flake-like particles are also present. The edges of most of the particles are sharp rather than rounded. The agglomeration is three-dimensional in nature with particles lying on top of each other as well as side by side.

The particle size in general extends to about 4 $\mu$  in diameter. A few particles ranged as high as 7 1/2 $\mu$  but they were not considered to be typical. Although the majority of the small particles cannot be seen distinctly due to the severe agglomeration which is present, a few can be seen projecting from the surfaces of the larger particles and are found to range below 1/10 $\mu$  in diameter.

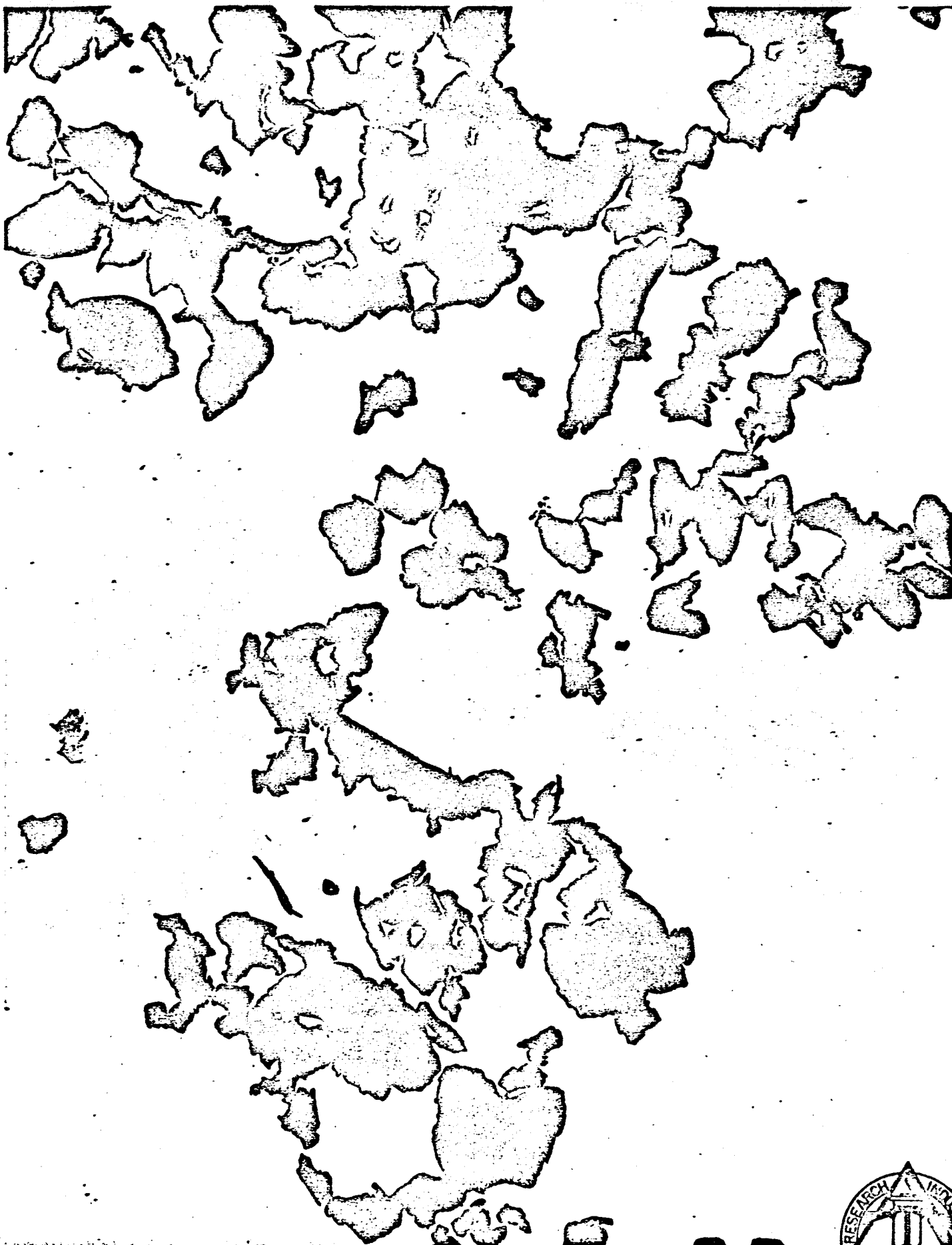
The rhenium particles appear distinctly different when compared with the tantalum particles previously discussed. This difference is exhibited by the rounded edges of the particles. The agglomerations occur in much larger masses and are firmly attached to each other as though they had been fused together. Further evidence of this hypothesis is presented by the fact that several of the dispersion techniques which were tried out approximated the same degree of particle deagglomeration as that shown in the micrographs. This may indicate that the particles are physically attached to each other rather than possessing the normal agglomeration due only to surface attractive forces. It is possible in the electron microscope to increase the beam current to the extent that the carbon filmed cellulose nitrate substrate rolls up due to differential thermal expansion. When this was done, the rhenium agglomeration remained intact as the substrate rolled up. There was no movement of particles within the agglomerations. Although the shadowed micrographs (Micrographs 9, 10 and 11) show the particles themselves to be three-dimensional, the agglomerations tend to be more two-dimensional in nature. This fact was also observed as the substrate rolled up, and tumbled the flat agglomerations on edge.

There do not appear to be as many very fine particles in this sample (although again there is evidence that the majority of the fines are hidden on the surfaces of the larger particles). It was found that the particles of this sample also ranged down to less than  $1/10\mu$  in diameter. The particles ranged to about  $5\mu$  in the other direction.

## PARTICLE SIZE DISTRIBUTION

"Best efforts" attempts were made by this laboratory to adequately disperse the particles in such a manner that the full distribution range could be observed and studied. However as the micrographs show, this was not possible. Any attempts to make a particle size distribution analysis by counting the particulate material, as displayed on these micrographs, would be greatly biased in favor of the larger particles due to the agglomeration problem. This problem complicates the matter in two ways -- as agglomerates can be easily confused with single particles and the smaller particles cannot be differentiated.





Classified NRC Ta



(X5000)

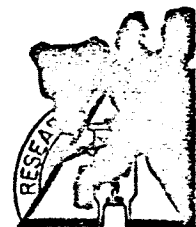


Classified NRC Ta

(X5000)



Classified NRC Ta

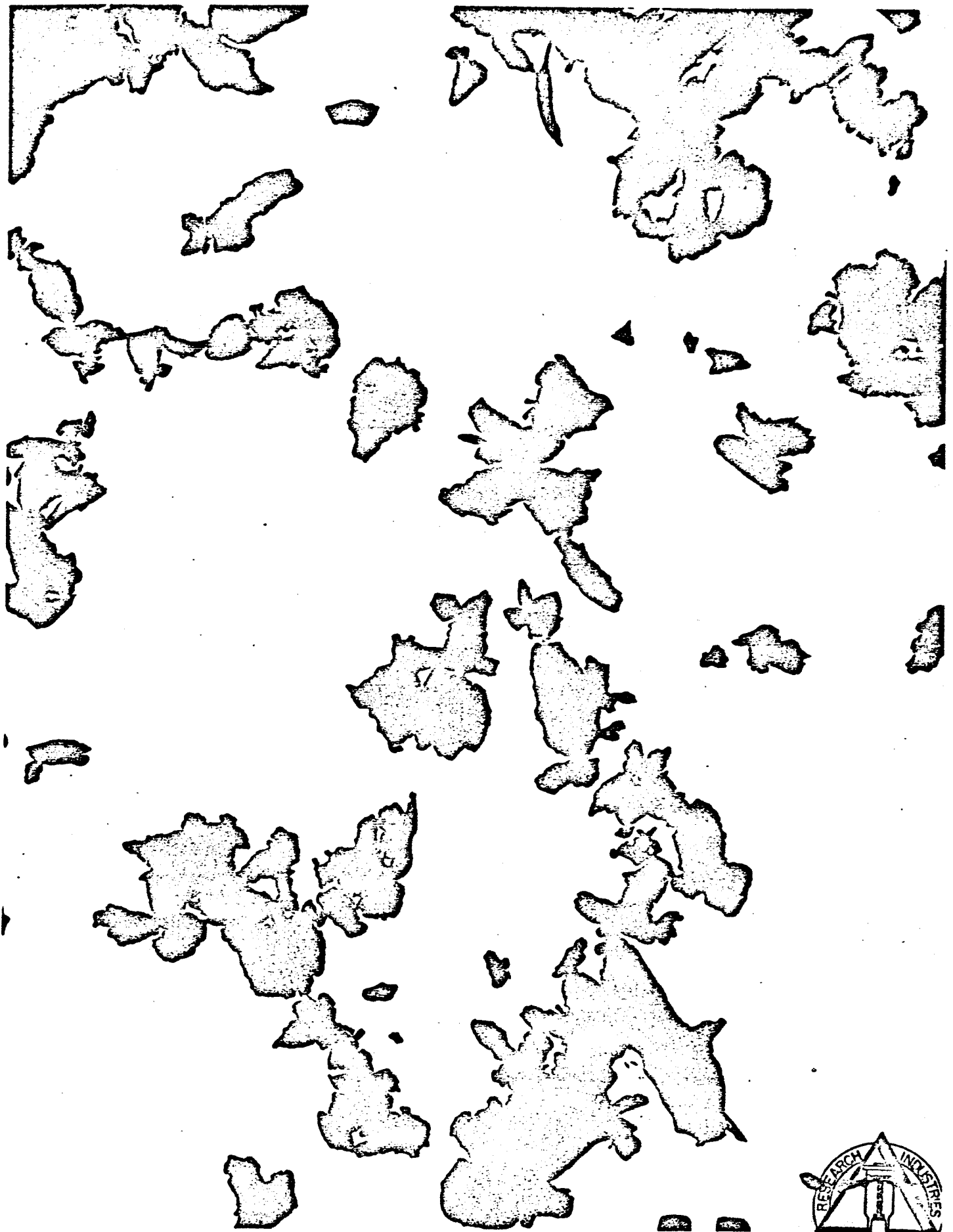


(X5000)



Classified NRC Ta

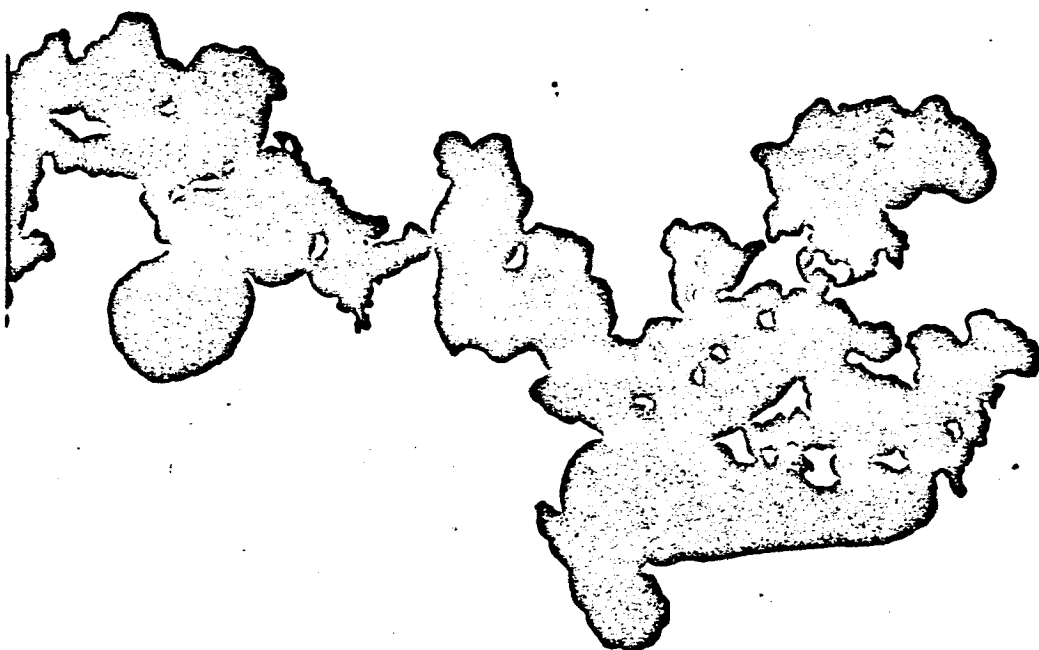
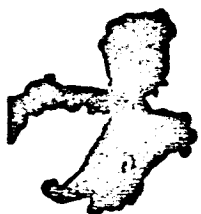
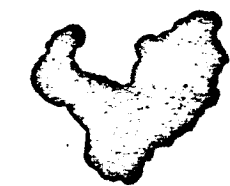
(X5000)



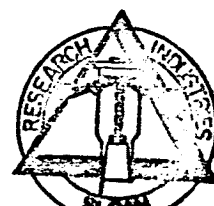
Classified NRC Ta



(X5000)



Classified Chase Re



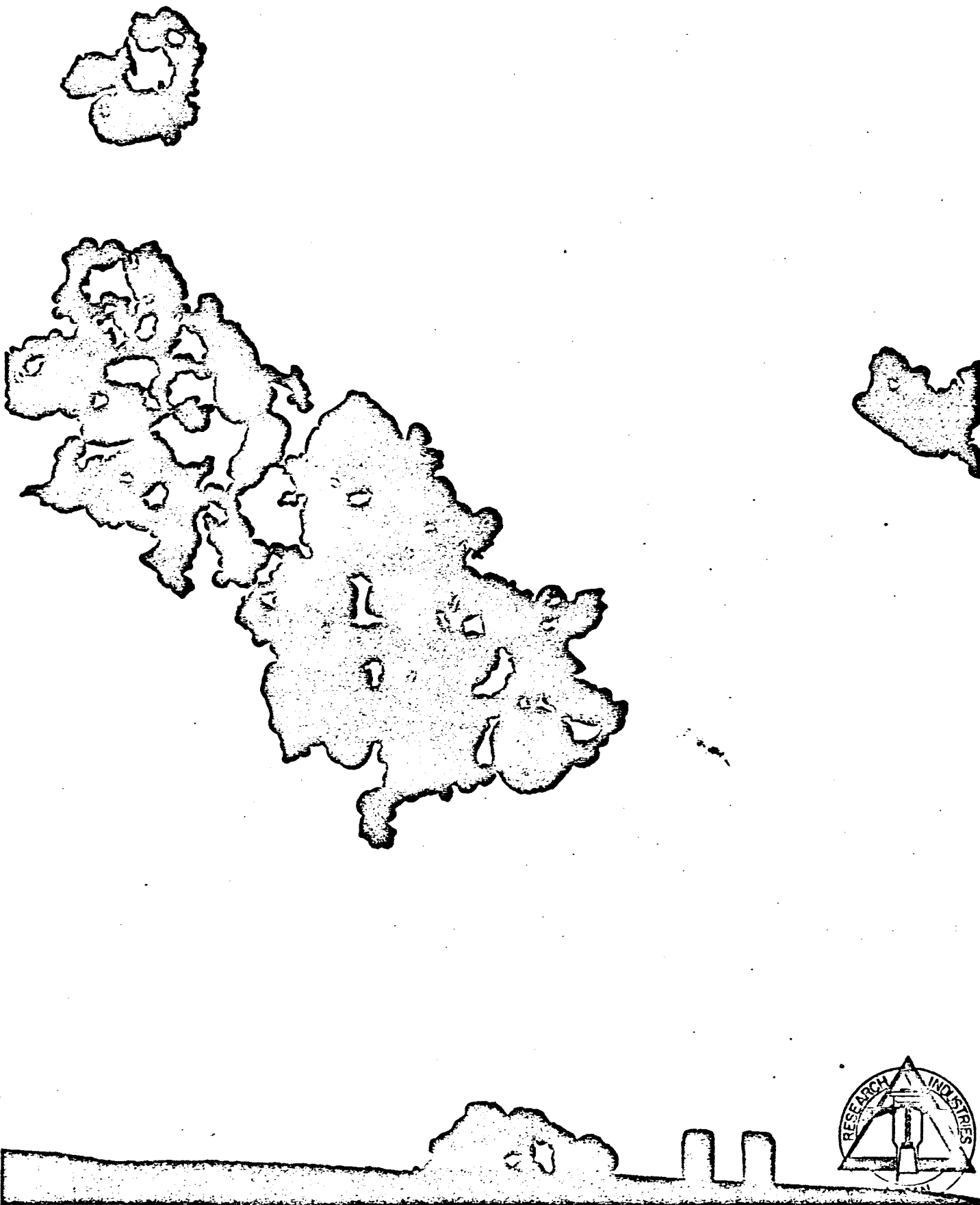
(X5000)



Classified Chase Re



(X5000)



Classified Chase Re

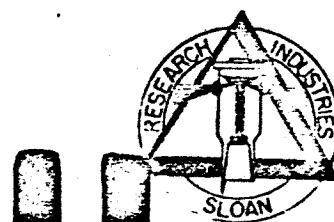
(X5000)



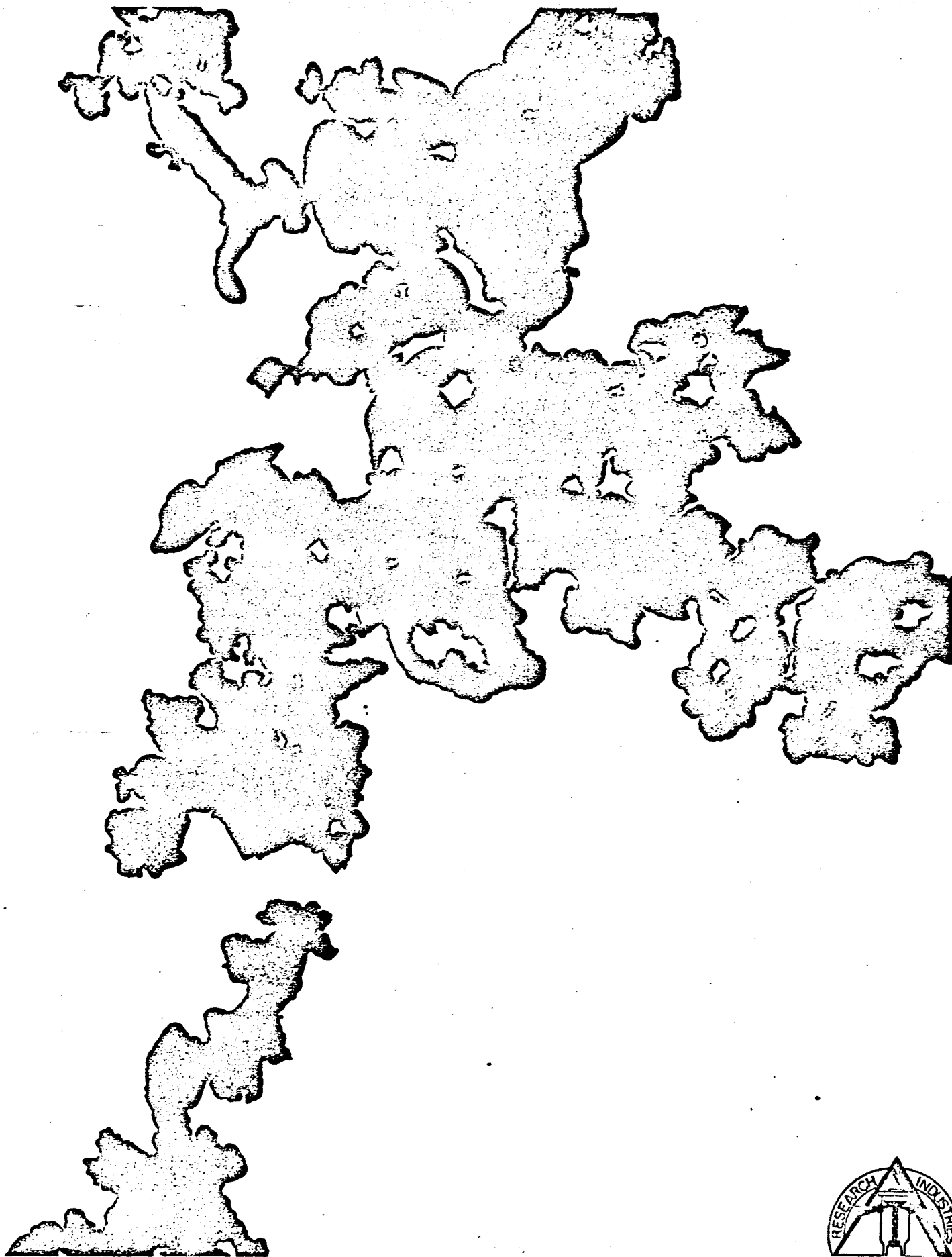


Classified Chase Re

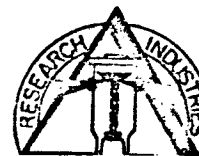
A-41



(X5000)



Classified Chase Re



(X5000)

APPENDIX B

DENSITY AND  $N_2$  PERMEABILITY DATA  
FOR EXPERIMENTAL IONIZER BUTTONS

TABLE B-I

PERMEABILITY AND DENSITY DATA FOR IONIZERS MADE FROM  
0.25-2.5 $\mu$  TUNGSTEN MICROSPHERES, WITH ADDITIONS OF Ta, Ir, AND Re  
(Vacuum Sintered at 1800°C for 7 hours. Series A)

Ionizer No.	Diam., in.	Weight, gm	Volume, cm <sup>3</sup>	Density,		$\delta t$ , sec.	N <sub>2</sub> Permeability, gm·cm <sup>-1</sup> ·sec <sup>-1</sup> ·torr <sup>-1</sup>
				gm/cm <sup>3</sup>	% theor.		
Ampro (0.25-2.5μ) Tung. Control							
UCA-1	.1869	.2364	.01758	13.45	69.69	5.54	1.673x10 <sup>-6</sup> ,
-2	.1876	.2316	.01735	13.35	69.17	4.83	1.865
-3	.1874	.2359	.01767	13.35	69.17	5.54	1.664
-4	.1873	.2323	.01738	13.37	69.27	5.57	1.631
-5	.1874	.2326	.01735	13.41	69.48	5.01	1.807
-6	.1878	.2350	.01779	13.21	68.45	5.39	1.707
-7	.1874	.2324	.01744	13.33	69.07	4.82	1.888
-8	.1872	.2391	.01741	13.73	71.14	7.96	1.146
			Av	= 13.40	69.43		1.673x10 <sup>-6</sup>
-9	.2204	.3172	.02400	13.22	68.50	4.15	1.577x10 <sup>-6</sup>
-10	.2203	.3194	.02423	13.18	68.29	4.55	1.455
-11	.2204	.3260	.02438	13.37	69.27	4.09	1.625
-12	.2207	.3384	.02476	13.67	70.83	6.37	1.054
			Av	= 13.36	69.22		1.428x10 <sup>-6</sup>
(0.25-2.5μ) W-10W/o Ta							
UTA-1	.1867	.2566	.01740	14.75	77.67	64.90	0.142x10 <sup>-6</sup>
-2	.1869	.2503	.01776	14.09	74.20	105.34	0.089
-3	.1869	.2602	.01771	14.69	77.36	63.40	0.147
-4	.1869	.2578	.01771	14.56	76.67	77.66	0.120
-5	.1868	.2612	.01765	14.80	77.94	70.09	0.133
-6	.1874	.2637	.01776	14.85	78.20	101.92	0.091
			Av	= 14.62	76.99		0.120x10 <sup>-6</sup>
-7	.2201	.3611	.02456	14.70	77.41	66.86	0.101x10 <sup>-6</sup>
-8	.2200	.3558	.02460	14.46	76.15	46.35	0.146
-9	.2198	.3504	.02419	14.49	76.30	48.49	0.137
-10	.2203	.3448	.02448	14.08	74.14	51.18	0.131
			Av	= 14.43	75.99		0.129x10 <sup>-6</sup>

TABLE B-I  
(Continued)

Ionizer No.	Diam., in.	Weight, gm	Volume, cm <sup>3</sup>	Density,		$\delta t$ , sec.	N <sub>2</sub> Permeability, gm·cm <sup>-1</sup> ·sec <sup>-1</sup> ·torr <sup>-1</sup>
				gm/cm <sup>3</sup>	% theor.		
(0.25-2.5μ) W-5W/o Ir							
UIA-1	.1881	.2494	.01803	13.83	71.14	5.28	1.755x10 <sup>-6</sup>
-2	.1878	.2603	.01802	14.45	74.33	10.18	0.916
-3	.1877	.2549	.01800	14.16	72.84	5.57	1.675
-4	.1878	.2445	.01783	13.71	70.52	4.57	2.019
-5	.1877	.2628	.01750	15.02	77.26	12.02	0.755
			Av =	14.23	73.20		1.424x10 <sup>-6</sup>
-6	.2206	.3335	.02492	13.38	68.83	3.51	1.929x10 <sup>-6</sup>
-7	.2208	.3463	.02478	13.97	71.86	4.19	1.601
-8	.2205	.3674	.02472	14.86	76.44	7.38	0.911
-9	.2202	.3431	.02471	13.89	71.45	3.87	1.747
			Av =	14.03	72.17		1.547x10 <sup>-6</sup>
(0.25-2.5μ) W-10W/o Re							
URA-1	.1873	.2357	.01810	13.02	66.87	5.19	1.823x10 <sup>-6</sup>
-2	.1884	.2366	.01827	12.95	66.51	5.89	1.584
-3	.1881	.2325	.01803	12.90	66.26	5.53	1.676
-4	.1878	.2332	.01820	12.81	65.79	5.09	1.850
-5	.1877	.2378	.01814	13.11	67.33	6.11	1.538
-6	.1872	.2326	.01813	12.83	65.90	5.36	1.772
-7	.1883	.2270	.01811	12.53	64.36	4.95	1.873
-8	.1870	.2309	.01773	13.02	66.87	6.60	1.414
-9	.1877	.2436	.01827	13.33	68.46	7.70	1.230
-10	.1874	.2332	.01807	12.91	66.31	5.03	1.875
			Av =	12.94	66.46		1.664x10 <sup>-6</sup>
-11	.2205	.3241	.02497	12.98	66.67	4.22	1.610x10 <sup>-6</sup>
-12	.2201	.3195	.02494	12.81	65.79	3.79	1.803
-13	.2206	.3192	.02518	12.68	65.13	4.18	1.636
-14	.2207	.3182	.02494	12.76	65.54	3.89	1.739
-15	.2207	.3311	.02482	13.34	68.52	5.91	1.139
			Av =	12.91	66.31		1.585x10 <sup>-6</sup>

TABLE B-II

PERMEABILITY DATA FOR IONIZERS MADE FROM 0.25-2.5 $\mu$  TUNGSTEN MICROSPHERES,  
WITH ADDITIONS OF Ta, Ir, and Re (Vacuum Sintered at 2000°C. Series B)

Ionizer No.	Diam, in	Weight, gm	Volume, cm <sup>3</sup>	Density		$\delta t$ , sec	N <sub>2</sub> Permeability, gm·cm <sup>-1</sup> ·sec <sup>-1</sup> ·torr <sup>-1</sup>
				gm/cm <sup>3</sup>	% theor.		
Ampro (0.25-2.5μ) Tung. Control							
UCB-1	.1874	.2753	.01785	15.42	79.90	18.25	0.510x10 <sup>-6</sup>
-2	.1878	.2746	.01779	15.44	80.00	19.85	0.464
-3	.1876	.2742	.01798	15.25	79.02	15.23	0.613
-4	.1877	.2842	.01795	15.83	82.02	34.46	0.270
-5	.1878	.2767	.01792	15.44	80.00	17.57	0.528
-6	.1875	.2820	.01773	15.91	82.44	35.76	0.258
-7	.1880	.2793	.01806	15.47	80.16	21.79	0.427
-8	.1877	.2761	.01805	15.30	79.27	14.74	0.634
			Av =	15.51	80.36		0.463x10 <sup>-6</sup>
-9	.2222	.3903	.02504	15.59	80.78	14.82	0.446x10 <sup>-6</sup>
-10	.2220	.3985	.02518	15.83	82.02	27.40	0.409
-11	.2222	.3765	.02523	14.92	77.31	11.20	0.594
-12	.2220	.3828	.02518	15.20	78.76	13.03	0.512
-13	.2222	.3872	.02523	15.35	79.53	11.06	0.602
			Av =	15.38	79.68		0.513x10 <sup>-6</sup>
(0.25-2.5μ) W-10 W/oTa							
UTB-1	.1873	.2751	.01838	14.97	78.67	103.19	0.093x10 <sup>-6</sup>
-2	.1879	.2735	.01836	14.90	78.30	94.03	0.101
			Av =	14.94	78.49		0.097x10 <sup>-6</sup>
-3	.2207	.3744	.02538	14.75	77.51	69.83	0.099x10 <sup>-6</sup>
-4	.2208	.3792	.02541	14.92	78.40	71.62	0.096
			Av =	14.84	77.96		0.098x10 <sup>-6</sup>

TABLE B-II  
(Continued)

Ionizer No.	Diam, in.	Weight, gm	Volume, cm <sup>3</sup>	Density		$\delta t$ , sec	N <sub>2</sub> Permeability, gm·cm <sup>-1</sup> ·sec <sup>-1</sup> ·torr <sup>-1</sup>
				gm/cm <sup>3</sup>	% theor.		
(0.25-2.5μ) W-5 W/oIr							
UIB-1	.1875	.2740	.01783	15.37	79.06	27.27	0.340x10 <sup>-6</sup>
-2	.1874	.2614	.01785	14.64	75.31	8.69	1.072
-3	.1876	.2589	.01785	14.50	74.60	6.23	1.488
-4	.1876	.2587	.01789	14.46	74.38	7.44	1.249
-5	.1875	.2738	.01787	15.32	78.81	24.54	0.377
-6	.1878	.2572	.01783	14.43	74.23	6.65	1.388
			Av =	14.79	76.08		0.986x10 <sup>-6</sup>
-7	.2221	.3655	.02488	14.69	75.57	5.85	1.125x10 <sup>-6</sup>
-8	.2221	.3819	.02513	15.20	78.20	15.87	0.419
-9	.2218	.3659	.02513	14.56	74.90	5.29	1.263
			Av =	14.82	76.23		0.936x10 <sup>-6</sup>
(0.25-2.5μ) W-10 W/oRe							
URB-1	.1886	.2817	.01803	15.62	80.23	22.15	0.414x10 <sup>-6</sup>
-2	.1887	.2712	.01796	15.10	77.56	11.08	0.823
-3	.1885	.2735	.01811	15.10	77.56	12.31	0.750
			Av =	15.27	78.43		0.662x10 <sup>-6</sup>
-4	.2227	.3862	.02515	15.36	78.89	13.00	0.506x10 <sup>-6</sup>
-5	.2227	.3763	.02425	15.52	79.71	8.91	0.712
			Av =	15.44	79.30		0.609x10 <sup>-6</sup>

TABLE B-III

PERMEABILITY AND DENSITY DATA FOR UNALLOYED TUNGSTEN IONIZERS  
MADE FROM TWO DIFFERENT TYPES OF TUNGSTEN POWDER

Ionizer No.	Diam., in.	Weight, gm	Volume, cm <sup>3</sup>	Density		$\delta t$ , sec.	N <sub>2</sub> Permeability, gm·cm <sup>-1</sup> ·sec <sup>-1</sup> ·torr <sup>-1</sup>
				gm/cm <sup>3</sup>	% theor.		
I-P3							
92W/o H <sub>2</sub> -Red. Tungsten + 8 W/o Cu Flake Mixture							
-1	.1855	.2263	.01723	13.12	67.98	14.04	0.667 x 10 <sup>-6</sup>
-2	.1864	.2258	.01753	12.88	66.74	7.53	1.240
-3	.1861	.2254	.01720	13.10	67.88	8.94	1.032
-4	.1869	.2177	.01735	12.55	65.03	5.71	1.602
-5	.1859	.2217	.01712	12.95	67.10	8.10	1.139
-6	.1856	.2144	.01729	12.40	64.25	9.94	0.943
-7	.1861	.2193	.01747	12.58	65.18	7.29	1.285
-8	.1853	.2338	.01719	12.18	63.11	15.09	0.622
-9	.1861	.2250	.01716	13.11	67.93	7.08	1.300
-10	.1853	.2194	.01613	13.60	70.47	12.88	0.683
-11	.1858	.2295	.01702	13.48	69.84	12.68	0.724
-12	.1869	.2180	.01704	12.79	66.27	4.81	1.867
Av				= 12.90	66.84		1.092 x 10 <sup>-6</sup>
Tungsten Microsphere Controls (78.1% by count of 0.25-2.5 $\mu$ particles)							
IC							
-1	.2192	.3507	.02560	13.70	70.98	7.09	1.006 x 10 <sup>-6</sup>
-2	.2194	.3501	.02534	13.82	71.61	6.92	1.017
-3	.2192	.3497	.02523	13.86	71.81	7.11	0.989
-4	.2192	.3437	.02510	13.69	70.93	7.34	0.953
-5	.2196	.3502	.02538	13.80	71.50	7.03	0.999
-6	.2193	.3517	.02531	13.90	72.02	7.00	1.006
-7	.2188	.3513	.02495	14.08	72.95	11.58	0.605
-8	.2194	.3492	.02540	13.75	71.24	6.85	1.029
-9	.2193	.3472	.02494	13.92	72.12	8.01	0.866
Av				= 13.84	71.71		0.941 x 10 <sup>-6</sup>



TABLE B-IV

PERMEABILITY AND DENSITY DATA FOR IONIZERS MADE FROM  
0.25-2.5 $\mu$  TUNGSTEN MICROSPHERES PLUS TANTALUM AND RHENIUM PARTICLES  
(Sintered at 1800°C for 105 Minutes)

Ionizer No.	Diam., in.	Weight, gm	Volume, cm <sup>3</sup>	Density, gm/cm <sup>3</sup> % theor.		δt, sec.	N <sub>2</sub> Permeability, gm·cm <sup>-1</sup> ·sec <sup>-1</sup> ·torr <sup>-1</sup>
<u>IXT</u>			<u>W-10W/oTa</u>				
-1	.2169	.3605	.02434	14.81	77.82	71.47	0.099 x 10 <sup>-6</sup>
-2	.2168	.3612	.02450	14.74	77.46	75.42	0.095
-3	.2171	.3635	.02438	14.91	78.62	72.21	0.098
-4	.2168	.3525	.02450	14.39	75.62	74.90	0.095
-5	.2169	.3583	.02422	14.79	77.72	73.33	0.096
-6	.2168	.3582	.02444	14.66	77.04	76.00	0.094
-7	.2170	.3627	.02442	14.85	78.03	71.90	0.099
-8	.2169	.3587	.02452	14.63	76.88	76.30	0.093
-9	.2168	.3519	.02426	14.51	76.25	71.27	0.099
			Av	=	14.70	77.25	0.096 x 10 <sup>-6</sup>
<u>IXTVR</u>			<u>W-10W/oTa-5W/oRe</u>				
-1	.2183	.3538	.02490	14.21	74.36	37.25	0.189 x 10 <sup>-6</sup>
-2	.2179	.3507	.02493	14.07	73.63	38.47	0.185
-3	.2182	.3502	.02494	14.04	73.47	38.38	0.184
-4	.2185	.3466	.02494	13.90	72.74	36.92	0.191
-5	.2186	.3448	.02490	13.85	72.48	34.64	0.203
-6	.2183	.3517	.02496	14.09	73.73	36.03	0.196
-7	.2178	.3537	.02491	14.20	74.31	38.06	0.187
-8	.2182	.3454	.02476	13.95	73.00	35.43	0.198
-9	.2180	.3510	.02483	14.14	73.99	38.09	0.186
			Av	=	14.05	73.52	0.191 x 10 <sup>-6</sup>
<u>IXTXR</u>			<u>W-10W/oTa-10W/oRe</u>				
-1	.2183	.3424	.02514	14.02	73.02	67.94	0.105 x 10 <sup>-6</sup>
-2	.2186	.3581	.02490	14.38	74.90	47.59	0.147
-3	.2185	.3537	.02452	14.42	75.10	47.27	0.146
-4	.2186	.3528	.02478	14.24	74.17	47.00	0.149
-5	.2183	.3597	.02496	14.41	75.05	75.66	0.093
-6	.2188	.3528	.02483	14.21	74.01	47.94	0.145
			Av	=	14.28	74.38	0.131 x 10 <sup>-6</sup>

APPENDIX C

LeRC IONIZER PELLET  
EVALUATION REPORTS

# IONIZER BUTTON EVALUATION REPORT

BUTTON CODE IVTER-10

BUTTON TYPE Sph. W-5Ta-10Re

TEST DATE April 1966

MADE BY EOS

PORES PER CM<sup>2</sup> 11.93 x 10<sup>6</sup>

AVERAGE PARTICLE SIZE of Sph. W Base=1.17μ

AVERAGE PORE SIZE 1.58 μ

PARTICLE SIZE DISTRIBUTION	
MICRON DIAMETER	PERCENT
7.5 - 5.0	0.0
5.0 - 4.0	0.1
4.0 - 3.0	3.8
3.0 - 2.0	12.6
2.0 - 1.0	32.4
<1.0	51.1

PORE SIZE DISTRIBUTION	
MICRON DIAMETER	PERCENT
>1.6	
1.2 - 1.6	
0.8 - 1.2	
0.4 - 0.8	
<0.4	

AV CENTER DISTANCE BETWEEN PORES 2.89μ

BUTTON DIAMETER (EFFECTIVE) .404 CM,

THICKNESS .1024 CM, DENSITY 68.6 PERCENT

TRANSMISSION COEFFICIENT 0.493 x 10<sup>-4</sup>

PRESSURE (Abs Chamber) 2-20 x 10<sup>-8</sup> TORR

Δp/Δt 1.49 TORR/SEC

CALCULATED TRUE DENSITY 13.25 gm/cm<sup>3</sup>

SURFACE TREATMENT Std. Wet Grinding

WORK FUNCTION Below 10 eV/cm<sup>2</sup>, 5.0, eV

SAMPLE INFORMATION Pore parameters are av. values corresponding to 71.9 % density.

Curves showing:

Ion Current Density Versus Ionizer Temperature

Neutral Fraction Versus Ionizer Temperature

Neutral Fraction Versus Ion Current Density

are included in Section 6, rather than on this format. This is necessitated by the 3-decade α values obtained on certain ionizers, whereas the format scales contained only 2 decades.

Conclusions: Data show as similar ionizer tested (IVTER-11). This material possesses

excellent performance characteristics, similar to C7, dense shaped-pore ionizers.

Neutral fraction is very low at low temp. due to sharp min. in α vs T curve. \*

Test made by E. Thompson date 4/14/66 report prepared by E. Thompson and M. LaChance

\* Transition temperature is also low, near the Langmuir data.

DISTRIBUTION LIST FOR SUMMARY REPORTS

CONTRACT NAS3-7103

<u>Addressee</u>	<u>Number of Copies</u>
1. National Aeronautics and Space Administration Washington, D. C. 20546 Attn: RNT/James Lazar	2
2. Aeronautical Systems Division Wright-Patterson Air Force Base, Ohio Attn: AFAPL (APIE)/Robert Supp	2
3. NASA-Lewis Research Center 21000 Brookpark Road Cleveland, Ohio 44135 Attn: Advance Concepts Branch W. D. Rayle M.S. 301-1 Attn: Spacecraft Technology Procurement Section M.S. 54-2 Attn: Spacecraft Technology Division C. C. Conger M.S. 54-1 D. L. Lockwood M.S. 54-3 T. J. Riley M.S. 54-3 Attn: Air Breathing Division A. E. Anglin M.S. 60-6 Attn: Technology Utilization Office, M.S. 3-19 J. Weber Attn: Office of Reliability & Quality Assurance M.S. 500-203 Attn: Neal T. Saunders M.S. 105-1 Attn: Library M.S. 60-3 Attn: Electric Propulsion Laboratory - M.S. 301-1 W. E. Moeckel Attn: Reports Control Office - M.S. 5-5	1 1 1 2 5 1 1 1 1 1 2 1 1
4. General Electric Company Cincinnati, Ohio 45215 Attn: Mr. L. P. Jahnke	1
5. Defense Materials Information Center 505 King Avenue Columbus, Ohio 43201	10
6. TRW Inc. New Products Research 7209 Platt Avenue Cleveland, Ohio 44107	1

	<u>Addressee</u>	<u>Number of Copies</u>
7.	TRW Inc. 8433 Fallbrook Avenue Canoga Park, California 91304 Attn: Mr. Milton Kirkpatrick Dr. D. Langmuir	1 1
8.	Atlantic Research Corporation Shirley Memorial Highway-Edsel Rd. Alexandria, Virginia	1
9.	United Aircraft Corporation Research Department East Hartford, Connecticut 06108 Attn: Dr. R. G. Meyerand, Jr.	1
10.	Clevite Corporation Mechanical Research Division 540 East 105th Street Cleveland, Ohio 44108 Attn: Mr. Swope	1
11.	Wah-Chang Corporation Albany, Oregon Attn: Mr. Sam Werster	1
12.	Oak Ridge Gaseous Diffusion Plant Post Office Box P Oak Ridge, Tennessee 37831 Attn: Mr. Robert Neal	1
13.	General Electric Company Lamp Metals & Components Dept. 21800 Tungsten Road Cleveland, Ohio 44117 Attn: Mr. Frank Adams	1
14.	General Electric Company Advanced Tech. Labs. Schenectady, New York Attn: Dr. D. L. Wood	1
15.	Babcock and Wilcox Company Refractories Division Old Savannah Road Augusta, Georgia 30903 Attn: Mr. R. G. Rollins	1

<u>Addressee</u>	<u>Number of Copies</u>
16. The Bendix Corporation Research Laboratories Division Southfield, Michigan Attn: Mr. C. B. Sung	1
17. Aerospace Corporation P. O. Box 95085 Los Angeles, California 90045 Attn: Dr. E. G. Kendall	1
18. Bell Aerosystems, Co. P. O. Box 2 Buffalo, New York Attn: Mr. G. F. Kappelt	1
19. National Research Corporation 70 Memorial Drive Cambridge, Massachusetts 02142 Attn: Tech. Info. Center	1
20. AFPR, Hughes Aircraft Company Florence Avenue & Teale Street Culver City, California 90232 Attn: RWRAAC-2-D, Fisher RWRAPS-9-Mr. Weldon	1 1
21. Litton Industries Electron Tube Division 960 Industrial Road San Carlos, California 94071 Attn: Dr. Rajindar Wadhwa	1
22. AFWL - Kirtland Air Force Base, New Mexico 87117 Attn: Capt. C. F. Ellis/WLPC WLIL	1 1
23. NASA-Scientific and Technical Information Facility P. O. Box 33 College Park, Maryland 20740 Attn: NASA Representative RQT-2448	6
24. Hughes Research Laboratories 3011 Malibu Canyon Road Malibu, California 90265 Attn: R. R. Turk G. Brewer W. McKee	2 1 1

<u>Addressee</u>	<u>Number of Copies</u>
25. Jet Propulsion Laboratory 4800 Oak Grove Drive Pasadena, California 91103 Attn: Mr. J. J. Paulson	1
26. General Electric Company Flight Propulsion Laboratories Cincinnati, Ohio 45215 Attn: R. N. Edwards	1
27. NASA-Langley Research Center Technical Library Langley Field, Virginia	1
28. TRW Inc. New Devices Laboratory 7209 Platt Avenue Cleveland, Ohio 44107 Attn: Dr. Park French	1
29. The Marquardt Corporation Astro Division 16555 Saticoy Street Van Nuys, California 91406	1
30. Headquarters - USAF Air Force Office of Scientific Research Washington, D. C. 20025 Attn: Dr. M. Slawsky	1
31. Aerojet-General Nucleonics Division San Ramon, California Attn: Mr. J. S. Luce	1
32. NASA-Marshall Space Flight Center Huntsville, Alabama Attn: Mr. Henry Martin Dr. E. Stuhlinger	1 1
33. Aerospace Corporation P. O. Box 95085 Los Angeles, California 90045 Attn: Library Technical Documents Group	1
34. Westinghouse Astronuclear Laboratories Electric Propulsion Laboratory Pittsburgh, Pennsylvania 15234 Attn: Mr. H. W. Szymanowski	1

<u>Addressee</u>	<u>Number of Copies</u>
35. Astro-Met Associates, Inc. 500 Glendale-Milford Road Cincinnati, Ohio 45215 Attn: John W. Graham	1
36. TRW Inc. TRW Systems Group One Space Park Redondo Beach, California 90278 Attn: Dr. Heywood Shelton	1
37. OREMET Albany, Oregon Attn: Mr. I. Vandenburg	1



# IONIZER BUTTON EVALUATION REPORT

BUTTON TYPE Shaped-Pore Button I-5

TEST DATE October 1965

MADE BY EOS

PORES PER CM<sup>2</sup>  $1.71 \times 10^6$

AVERAGE PARTICLE SIZE 0.8 $\mu$  G.E. Tungsten  
H<sub>2</sub>-Reduced

AVERAGE PORE SIZE 3.86  $\mu$

## PARTICLE SIZE DISTRIBUTION

MICRON DIAMETER	PERCENT
7.5 - 5.0	0.0
5.0 - 4.0	2.2
4.0 - 3.0	4.3
3.0 - 2.0	2.9
2.0 - 1.0	22.3
<1.0	68.3

## PORE SIZE DISTRIBUTION

MICRON DIAMETER	PERCENT
>1.6	
1.2 - 1.6	
0.8 - 1.2	
0.4 - 0.8	
<0.4	

AV CENTER DISTANCE BETWEEN PORES 1.24 $\mu$

BUTTON DIAMETER (EFFECTIVE) .442 CM,

THICKNESS .0998CM, DENSITY 37.7 PERCENT

TRANSMISSION COEFFICIENT  $2.28 \times 10^{-4}$

PRESSURE (Abs Chamber)  $<2 \times 10^{-7}$  TORR

$\Delta p/\Delta t$  7.93 TORR/SEC

CALCULATED TRUE DENSITY 13.06 gm/cm<sup>3</sup>

SURFACE TREATMENT Murakami Etch

WORK FUNCTION is high and increases

SAMPLE INFORMATION Made from "W + 8W/o copper flake" mixture with temperature to above 1350°C

Curves showing:

Ion Current Density Versus Ionizer Temperature

Neutral Fraction Versus Ionizer Temperature

Neutral Fraction Versus Ion Current Density

are included in Section 6, rather than on this format. This is necessitated by the 3-decade  $\alpha$  values obtained on certain ionizers, whereas the format scales contained only 2 decades.

Excellent performance. Neutral fraction at 15mA/cm<sup>2</sup> is 5X lower than EOS fine spherical powder tungsten. Threshold temperature near Langmuir data for ion current density above 15 mA/cm<sup>2</sup>. Since pore density is low, improved performance may be due to larger total pore area, elongated pore shape, or improved porous network.

Test made by B. Thompson  
G. Kuskevics

date 10/27-28/65 report prepared by B. Thompson and  
M. LeChance

PRECEDING PAGE BLANK NOT FILMED

# IONIZER BUTTON EVALUATION REPORT

BUTTON TYPE Shaped-Pore Button II-2

TEST DATE November 1965

MADE BY EOS

PORES PER CM<sup>2</sup>  $1.71 \times 10^6$

AVERAGE PARTICLE SIZE 0.8μ G.E. Tungsten

AVERAGE PORE SIZE 3.86 μ

PARTICLE SIZE DISTRIBUTION <sup>H<sub>2</sub>-Reduced</sup>	
MICRON DIAMETER	PERCENT
7.5 - 5.0	0.0
5.0 - 4.0	2.2
4.0 - 3.0	4.3
3.0 - 2.0	2.9
2.0 - 1.0	22.9
<1.0	68.3

PORE SIZE DISTRIBUTION	
MICRON DIAMETER	PERCENT
>1.6	
1.2 - 1.6	
0.8 - 1.2	
0.4 - 0.8	
<0.4	

AV CENTER DISTANCE BETWEEN PORES 1.24 μ

BUTTON DIAMETER (EFFECTIVE) .422 CM,

THICKNESS 1.092 CM, DENSITY 66.5 PERCENT

TRANSMISSION COEFFICIENT  $2.16 \times 10^{-4}$

PRESSURE (Abs Chamber)  $2 \times 10^{-7}$  TORR

$\Delta p / \Delta t$  6.80 TORR/SEC

CALCULATED TRUE DENSITY 12.84 gm/cm<sup>3</sup>

SURFACE TREATMENT Std. Wet Grinding

WORK FUNCTION is high and increases with temperature to above 1350°C

SAMPLE INFORMATION Made from "W + 8 W/o Copper Flake" Mixture

Curves showing:

Ion Current Density Versus Ionizer Temperature

Neutral Fraction Versus Ionizer Temperature

Neutral Fraction Versus Ion Current Density

are included in Section 6, rather than on this format. This is necessitated by the 3-decade  $\alpha$  values obtained on certain ionizers, whereas the format scales contained only 2 decades.

Conclusions: Best ionizer tested to date. Neutral fraction is 5X lower than for EOS fine spherical powder tungsten. Threshold temperatures near Langmuir data for ion current density above 25 mA/cm<sup>2</sup>. Since pore density is low, improved performance may be due to larger total pore area, elongated pore shape, or improved porous network.

Test made by B. Thompson and G. Kuskevics

date 11/23-24/65

report prepared by B. Thompson and M. LaChance

# IONIZER BUTTON EVALUATION REPORT

BUTTON TYPE Low Density Stabilized (VIB-1)

TEST DATE February 1966

MADE BY EOS

PORES PER CM<sup>2</sup> Indeterminate

AVERAGE PARTICLE SIZE 0.8 $\mu$ -G.E. Tungsten

AVERAGE PORE SIZE Indeterminate

PARTICLE SIZE DISTRIBUTION <sup>H<sub>2</sub>-reduced</sup>  
MICRON DIAMETER PERCENT

7.5 - 5.0	0.0
5.0 - 4.0	2.2
4.0 - 3.0	4.3
3.0 - 2.0	2.9
2.0 - 1.0	22.3
<1.0	68.3

PORE SIZE DISTRIBUTION  
MICRON DIAMETER PERCENT

>1.6	
1.2 - 1.6	
0.8 - 1.2	
0.4 - 0.8	
<0.4	

AV CENTER DISTANCE BETWEEN PORES Indeterminate

BUTTON DIAMETER (EFFECTIVE) .34 CM,

THICKNESS .1016CM, DENSITY 47.0 PERCENT

TRANSMISSION COEFFICIENT 5.21x10<sup>-4</sup>

PRESSURE (Abs Chamber) .8-2.0x10<sup>-7</sup> TORR

$\Delta p/\Delta t$  15.83 TORR/SEC

CALCULATED TRUE DENSITY 9.45 gm/cm<sup>3</sup>

SURFACE TREATMENT Std. Wet Grinding

WORK FUNCTION below 5mA/cm<sup>2</sup>, 4.65, eV

SAMPLE INFORMATION Made from W-8 wt% Cu flake-4 wt% BN mixture

Curves showing:

Ion Current Density Versus Ionizer Temperature

Neutral Fraction Versus Ionizer Temperature

Neutral Fraction Versus Ion Current Density

are included in Section 6, rather than on this format. This is necessitated by the 3-decade  $\alpha$  values obtained on certain ionizers, whereas the format scales contained only 2 decades.

Performance was poor by current standards. Neutral fraction was 3-5X higher than E3 (1-4 $\mu$ ) spherical powder ionizers, and a decade higher than 67% dense shaped-pore and W-5w/o Ta-10w/oRe alloy ionizers. Neutral fraction vs temperature curve has broad minimum. Transition temperature is 15° below Langmuir data at 4mA/cm<sup>2</sup>, Conclusions: and increases quickly to 70°C above Langmuir data at 15mA/cm<sup>2</sup>.

Test made by B. Thompson

date 2/9-10/66

report prepared by B. Thompson and M. LaChance